KINETICS STUDIES OF BROMINE MONOXIDE AND METHYLPEROXY FREE RADICALS BY FLASH PHOTOLYSIS

Thesis by

Stanley Paul Sander

In Partial Fulfillment of the Requirements

For the Degree of

Doctor of Philosophy

California Institute of Technology

Pasadena, California

1980

(Submitted December 6, 1979)

ACKNOWLEDGEMENTS

I wish to thank my research advisors, John Seinfeld of Caltech, and Bill DeMore and Bob Watson of the Jet Propulsion Laboratory, for their enthusiasm, guidance and the opportunities they have given me. Their encouragement and cooperation made this unusual collaborative effort between Caltech and JPL a tremendous success and one that I hope can be repeated by many other graduate students.

Many individuals at Caltech and JPL contributed to this work. In particular, I would like to thank John Brock, Roger Lewis, Gary Ray, Steve Wagner, Yuk Yung, the members, past and present, of the air pollution research groups at Caltech and JPL, and Joe Pinto of the Goddard Institute for Space Sciences. The technical skills of Herman Heyn, Bill Lattin, Jurgen Linke, Morris Patapoff and George Tennant were indispensable in the construction of the apparatus. Sharon Chapman, Susie Kulas and Barbara Paul contributed to the typing of this thesis. The financial support of JPL and NASA is gratefully acknowledged.

I am fortunate in having had a few close friends with whom to share the joys and frustrations of graduate student life. These people have had an enormous impact on me, and their sharing and support will never be forgotten.

For their lifelong encouragement and love, I gratefully dedicate this thesis to the members of my family.

ABSTRACT

A flash photolysis-ultraviolet absorption system was constructed to study the kinetics of gas-phase free radical reactions over a wide range of pressure and temperature. Because of their atmospheric importance, the reactions of methylperoxy (CH_3O_2) and bromine monoxide (BrO) radicals with themselves, and with NO and NO_2 were investigated:

$$CH_3O_2 + CH_3O_2 \rightarrow \text{products} \quad (1)$$

$$CH_3O_2 + NO \rightarrow CH_3O + NO_2 \quad (2)$$

$$CH_3O_2 + NO_2 + M \rightarrow CH_3O_2NO_2 + M \quad (3)$$

$$BrO + BrO \rightarrow 2Br + O_2 \quad (4a)$$

$$\rightarrow Br_2 + O_2 \quad (4b)$$

$$BrO + NO \rightarrow Br + NO_2 \quad (5)$$

$$BrO + NO_2 + M \rightarrow BrONO_2 + M \quad (6)$$

The rate constants for reactions 1 - 6 were determined by measuring the first-order or second-order decay rates of BrO and CH_3O_2 radicals by ultraviolet absorption spectrophotometry. The rate constants for reactions 3 and 6 were found to vary significantly with pressure, indicating the formation of a stable adduct. The pressure dependence of the rate constants was discussed in terms of the Troe theory of unimolecular reactions. Measurements of the branching ratio of reaction 4 were used to develop a detailed reaction mechanism for the disproportionation of BrO radicals. Upper limits were also obtained for the rate constants for the reactions

$$CH_3O_2 + CO \rightarrow \text{products} \quad (7)$$

$$BrO + O_3 \rightarrow Br + 2O_2 \quad (8)$$

The atmospheric implications of the rate constant measurements are discussed.

TABLE OF CONTENTS

CHAPTER I

Introduction to Free Radical Kinetics Studies by Flash Photolysis

During the last decade, the field of gas-phase kinetics has been tremendously stimulated by a renewed interest in the chemistry of the atmosphere. Concern over the effects of anthropogenic emissions of substances such as the halocarbons, nitrogen oxides and carbon dioxide have led to the development of complex models of upper atmospheric chemistry and transport.[1] Many of the same processes also pertain to the pollution of the lower atmosphere, the manifestations of which appear locally and globally. The mathematical models which have been developed to describe these processes rely heavily on accurate chemical kinetics information. These needs have resulted in tremendous improvements in both the quantity and quality of data on the reaction rates of neutral radicals of many different chemical families. This new wealth of information has also opened many new problem areas in the study of gas-phase kinetics. Such phenomena as negative activation energies,[2] vibrational enhancement of reaction rates,[3] and the formation of radical complexes,[4] once thought extremely unusual, are now common occurrences. As a result of this sudden outpouring of kinetics information, our theoretical understanding of gas-phase reactions has been outstripped, and improved techniques for applying semi-classical and quantum theories of chemical reactivity to practical kinetics problems are badly needed.

The research described in this thesis was stimulated by a number of the factors mentioned above. In seeking to maintain relevance to the problems of atmospheric chemistry, kinetics studies were conducted of reactions of proven or suspected atmospheric importance. These involve the reactions of bromine monoxide (BrO) and methylperoxy (CH_3O_2) radicals with themselves, and with NO and NO_2:

$$CH_3O_2 + CH_3O_2 \rightarrow \text{products} \quad (1)$$

$$CH_3O_2 + NO \rightarrow CH_3O + NO_2 \quad (2)$$

$$CH_3O_2 + NO_2 + M \rightarrow CH_3O_2NO_2 + M \quad (3)$$

$$BrO + BrO \rightarrow 2Br + O_2 \quad (4a)$$

$$\rightarrow Br_2 + O_2 \quad (4b)$$

$$BrO + NO \rightarrow Br + NO_2 \quad (5)$$

$$BrO + NO_2 + M \rightarrow BrONO_2 + M \quad (6)$$

These studies were conducted over ranges of pressure (50 - 760 Torr) and temperature (220 - 400K) which overlap conditions found in the atmosphere. An effort was also made to study reactions which posed interesting, if somewhat inscrutable, theoretical problems. Both the reactions of CH_3O_2 and BrO with NO_2 show a marked pressure dependence, indicating an addition channel, and provide the opportunity to make use of some recent developments in the theory of unimolecular reactions. The other reactions also posed some interesting questions which were addressed by thermochemical kinetics.

The structure of this thesis reflects the primary emphasis of this work, which was the study of reactions 1 - 6 by flash photolysis. The main body (Chapters 2 - 5) describes the results obtained in the flash photolysis studies of BrO and CH_3O_2 radicals. The Appendices contain reports of atmospheric modeling studies simulating stratospheric bromine chemistry and tropospheric SO_2 oxidation, and a paper on the reactions of chlorine atoms with some simple alkanes as studied by the technique of discharge flow-resonance fluorescence.

EXPERIMENTAL PROCEDURES

The ambient pressure in the troposphere and stratosphere varies from 760 Torr at sea level to about 1 Torr and 45 km. While no single kinetic technique can adequately cover this entire pressure range, static (or pseudo-static) methods such as flash photolysis and molecular modulation have been successfully used between 25 Torr and hundreds of atmospheres. These methods are well-suited for reactions which have pressure-dependent rate constants, particularly when the reaction is in the fall-off region between third and second-order kinetics. The fast-flow technique, while having the advantage of being a pseudo steady-state method, is limited to the 1 - 7 Torr pressure range.[5] This limitation arises from the need to achieve rapid radial diffusion of radicals to ensure that a linear relationship exists between reaction time and distance along the flow tube axis.

The direct detection of transient intermediates in kinetics experiments has been accomplished by a number of techniques including absorption and fluorescence spectroscopy induced by resonant and non-resonant sources,[6] mass spectrometry[7] and electron paramagnetic resonance.[8] Both BrO and CH_3O_2 exhibit extensive predissociation and cannot be observed using fluorescence methods. These radicals are well-suited for detection by ultraviolet spectrophotometry, however, because of their relatively strong ($\sigma > 10^{-18}$ cm^2 $molecule^{-1}$) absorption bands at wavelengths longer than 200 nm. Although the sensitivity of the uv absorption method is not ordinarily as high as that which can be achieved using fluorescence, the absorption cross-sections of both BrO and CH_3O_2 are sufficiently large that adequate sensitivity can be obtained if long path lengths are used.

The flash photolysis-uv absorption technique was the method selected for the study of reactions 1 - 6. An apparatus was constructed which incorporated many state-of-the-art features not normally found in such instruments. These include, 1) a fast-quenching 1 meter-long xenon flash lamp employing coaxial design to permit easy temperature control, 2) a long-path White optical system for the absorption cell, 3) photometric rather than photographic detection of the absorption signal, 4) use of multiple flashes in conjunction with analog signal averaging to enhance the sensitivity and, 5) a continuously flowing reagent supply system which replaces the cell contents between flashes. Detailed descriptions of these features appear in the experimental sections of Chapters 2 - 5. Figure 1 shows the flash photolysis system supported on its pneumatically isolated optical bench next to the electronics rack. Figure 2 shows the individual components of the optical system in greater detail. It is felt that the combination of the long optical path length (740 cm.) and the use of signal averaging techniques has resulted in an improvement of a factor of 10 - 50 in sensitivity over previous designs.

THEORETICAL CONSIDERATIONS

Two of the reactions studied in this work,

$$CH_3O_2 + NO_2 + M \rightarrow CH_3O_2NO_2 + M \qquad (3)$$

$$BrO + NO_2 + M \rightarrow BrONO_2 + M \qquad (6)$$

are addition reactions forming adducts which have relatively long lifetime ($t_{\frac{1}{2}} > 1$ second) at room temperature. The reverse of reactions 3 and 6 are unimolecular decompositions, a class of reactions which has received considerable theoretical attention. Since the rate constants for the forward and reverse reactions are related by the equilibrium constant,

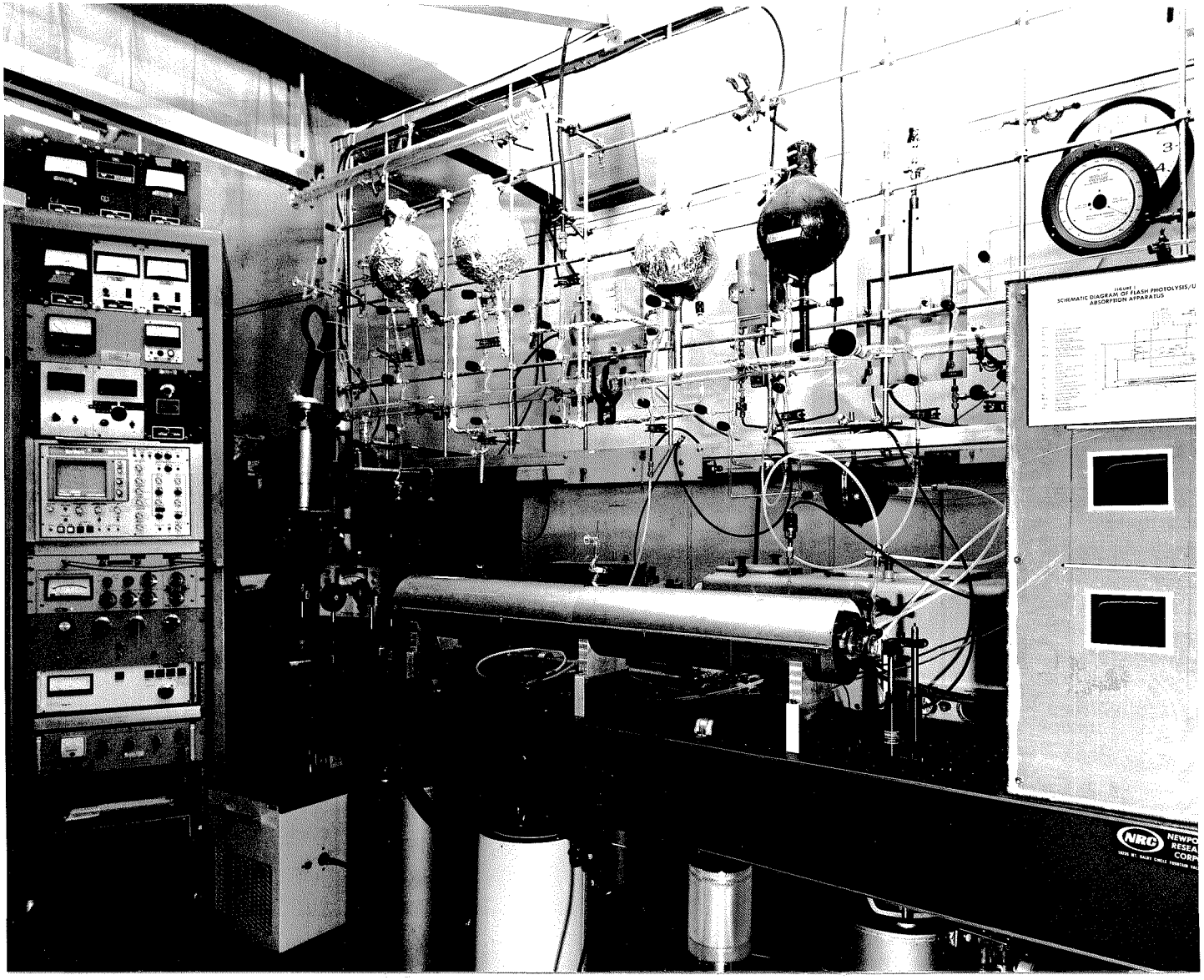

Figure 1. Photograph of the flash photolysis system. The reaction cell is in the cylindrical housing. The energy storage capacitors are in the box at the right.

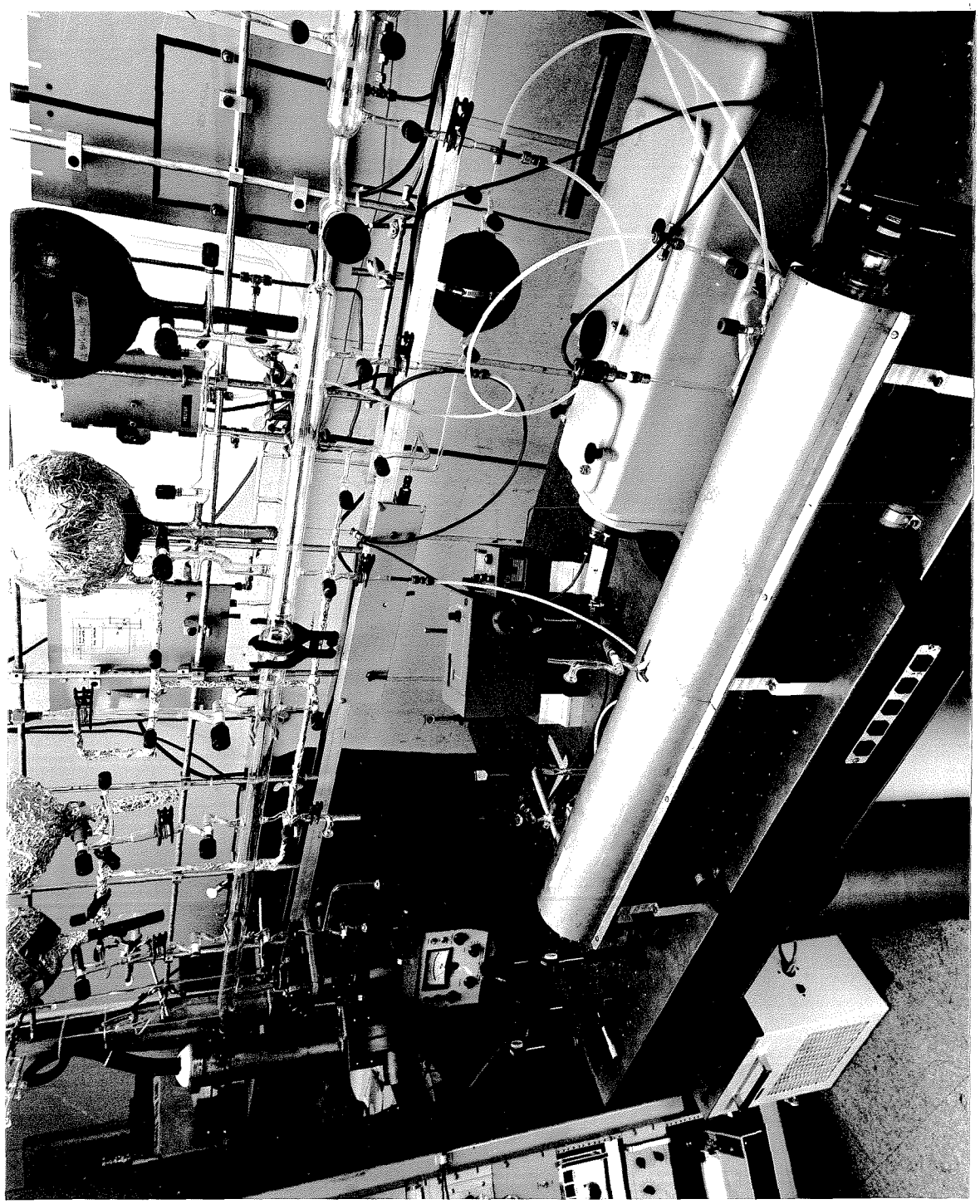

Figure 2. Photograph of the optical system showing the reaction cell, ½m. and ¼m. monochromators and the optical components.

which can be estimated from thermodynamic considerations, the theory of unimolecular decomposition is applicable to these reactions.

Elementary unimolecular reaction theory predicts that at very low pressures, the rate constant will vary linearly with pressure, approaching a constant as the pressure is increased.[9,10] In the fall-off region between these limiting cases, the simplest theory, based on the Lindemann mechanism, breaks down. The failure is caused by the simplistic assumption that the dissociation rate of the vibrationally excited intermediate is independent of its internal energy. Rice, Ramsperger and Kassel partially corrected this problem by developing a classical statistical theory to estimate the probablility that the dissociative mode will have more than the critical vibrational energy.[9] The use of their expression for the reaction probability leads to the determination of the overall rate constant for unimolecular decomposition in terms of the so-called "Kassel Integrals". A somewhat more realistic quantum version of this theory also exists. RRKM theory, the next step upward in sophistication, differs from RRK theory in several respects. The most important difference is that the rate constant for the dissociation of the excited intermediate is derived in a very general way using activated complex theory and statistical mechanics. The RRKM expression for this rate constant reduces to the RRK expression when semi-classical equations are used for the sum and density of vibrotational states in the activated complex and excited molecule. However, more accurate methods of state-counting can be used such as the Whitten-Rabinovitch approximation and the direct count method which lead to significantly more acccurate results.

The implementation of RRKM theory to the prediction of rate constant

fall-off curves is computationally somewhat involved because of the need to compute numbers of vibrotational states for each energy increment. Troe and co-workers have developed a simplified technique for computing fall-off curves that does not require extensive computation.[11,12] The method is based on the use of Kassel integrals to define the functional form of the fall-off curve but with semi-empirical correction factors added to fit the results to RRKM calculations. The shape of the curve is determined by a fitting parameter, F_c, which is itself a function of two dimensionless parameters, S_k and B_k. S_k is en "effective" number of classical oscillators, determined by evaluating the vibrational partition function for the activated complex. B_k is related to the critical energy for the decomposition. With S_k and B_k known, F_c is found from tables computed by Troe and co-workers. This method has been applied to the experimental fall-off curves obtained for reactions 3 and 6 with good agreement being obtained between theory and experiment. The exact procedure is detailed in Chapters 2 and 5.

ATMOSPHERIC IMPLICATIONS OF METHYLPEROXY AND BROMINE MONOXIDE CHEMISTRY

Both BrO and CH_3O_2 radicals are thought to play important roles in atmospheric chemistry although neither species has actually been detected in the atmosphere. Methylperoxy radicals are formed in the atmosphere by the reaction

$$CH_3 + O_2 + M \rightarrow CH_3O_2 + M \quad . \qquad (7)$$

In the "clean", i.e. non-urban, troposphere, methyl radicals originate from the attack of hydroxyl radicals on methane,

$$OH + CH_4 \rightarrow H_2O + CH_3 \quad , \qquad (8)$$

the initial step in the oxidation process which converts methane to CO_2

and other products. In urban atmospheres, other major sources of methyl radicals are the photodissociation of acetaldehyde (I) and its reaction with hydroxyl radicals (II):[13]

$$\text{(I)} \qquad CH_3CHO + h\nu \rightarrow CH_3 + HCO \qquad (9)$$

$$\text{(II)} \qquad \begin{aligned} CH_3CHO + OH &\rightarrow CH_3CO + H_2O && (10)\\ CH_3CO + O_2 + M &\rightarrow CH_3CO(O_2) + M && (11)\\ CH_3CO(O_2) + NO &\rightarrow CH_3CO_2 + NO_2 && (12)\\ CH_3CO_2 + M &\rightarrow CH_3 + CO_2 + M && (13) \end{aligned}$$

In the stratosphere, methyl radicals can be formed from the attack of atomic chlorine and excited atomic oxygen on methane as well as by reaction 8:

$$Cl + CH_4 \rightarrow HCl + CH_3 \qquad (14)$$

$$O(^1D) + CH_4 \rightarrow OH + CH_3 \qquad (15)$$

$$OH + CH_4 \rightarrow H_2O + CH_3 \ . \qquad (8)$$

The predominant loss process for CH_3O_2 is the same in the urban atmosphere and the stratosphere:

$$CH_3O_2 + NO \rightarrow CH_3O + NO_2 \ . \qquad (16)$$

The conversion of NO to NO_2 is an important process in atmospheric chemistry because photolysis of NO_2 leads to the formation of ozone:

$$NO_2 + h\nu \rightarrow NO + O \qquad (17)$$

$$O + O_2 + M \rightarrow O_3 + M \ . \qquad (18)$$

In urban atmospheres, the formation of NO_2, and therefore O_3, occurs almost entirely as a result of the reaction of peroxy radicals (HO_2, CH_3O_2, $CH_3CO(O_2)$, etc.) with NO. A question which has generated considerable controversy is whether the tropospheric ozone background of 25 ppb can be explained by photochemical processes occurring in the lower atmosphere, i.e. CH_4 oxidation, or from the transport of ozone from the

stratosphere.[14] Arguing against the photochemical explanation are the recent observations of exceedingly low background NO_x concentrations ($\simeq$100 ppt) which allow the termination processes

$$CH_3O_2 + CH_3O_2 \rightarrow \text{stable products} \qquad (19)$$

$$CH_3O_2 + HO_2 \rightarrow CH_3OOH + O_2 \qquad (20)$$

to compete with reaction 2. The picture is further complicated by reaction 3 and its reverse reaction,

$$CH_3O_2 + NO_2 + M \underset{\leftarrow}{\rightarrow} CH_3O_2NO_2 + M \ . \qquad (3,-3)$$

Methylperoxynitrate, $CH_3O_2NO_2$, may act as a temporary sink for both CH_3O_2 and NO_2 if its decomposition rate is sufficiently slow. Since reaction -3 is endothermic, and thus strongly temperature dependent, its role will be considerably different in the urban atmosphere and the clean troposphere where the temperature drops as low as 225K.

Bromine atoms are formed in the stratosphere from the photolysis of methyl bromide, used as an industrial fumigant, and the halomethanes which are employed as fire retardants and in refrigeration.[15] There are also substantial natural sources of methyl bromide, dibromomethane and bromoform, probably from the marine environment. These compounds are relatively inert in the troposphere and therefore diffuse upward into the stratosphere where photolysis can occur. Atomic bromine reacts with ozone to form the BrO radical:

$$Br + O_3 \rightarrow BrO + O_2 \ . \qquad (21)$$

Numerous reactions exist which can convert BrO back to Br including,

$$BrO + BrO \rightarrow 2Br + O_2 \qquad (4a)$$

$$\rightarrow Br_2 + O_2 \qquad (4b)$$

$$BrO + NO \rightarrow Br + NO_2 \qquad (5)$$

$$BrO + ClO \rightarrow Br + Cl + O_2 \qquad (22)$$

$$BrO + NO_2 + M \rightarrow BrONO_2 + M \qquad (6)$$

$$BrONO_2 + h\nu \rightarrow Br + NO_3 \quad . \qquad (23)$$

Except for reaction 5, these reactions, along with reaction 19, form catalytic cycles which irreversibly convert O_3 to O_2 while regenerating atomic bromine. Of course, these chain reactions are not 100% efficient; terminating processes occur which convert atomic bromine into HBr which is relatively inert. However, the chain processes are efficient enough that exceedingly small bromine concentrations (20-100 ppt) can result in a significant perturbation in the column ozone concentration in the stratosphere, particularly between 16 and 28 km. Detailed calculations on the effects of stratospheric bromine are discussed in Chapters 4 and 5 and Appendix II.

REFERENCES AND NOTES

1. (a) J. A. Logan, M. J. Prather, S. C. Wofsy and M. B. McElroy, Phil. Trans. Roy. Soc., 290, 187 (1978);
   (b) R. C. Whitten, W. J. Buruck, V. R. Watson, T. Shimazaki, H. T. Woodward, C. A. Riegel, L. A. Capone and T. Becker, NASA T.P. -1003 (1977);
   (c) J. D. Mahlman and W. J. Moxim, J. Atmos. Sci., 35, 1370 (1978).

2. (a) D. D. Davis, R. E. Huie and J. T. Herron, J. Chem. Phys., 59, 628 (1973);
   (b) M. S. Zahniser and F. Kaufman, J. Chem. Phys., 66, 3673 (1977).
   (c) J. C. Polanyi and W. H. Wong, J. Chem. Phys., 51, 1439 (1969).

3. J. C. Polanyi and W. H. Wong, J. Chem. Phys., 51, 1439 (1969).

4. (a) E. J. Hamilton, Jr., J. Chem. Phys., 63, 3682 (1975);
   (b) E. J. Hamilton, Jr. and R. R. Lii, Int. J. Chem. Kinet., 9 875 (1977).

5. (a) R. V. Poirier and R. W. Carr, Jr., J. Phys. Chem., 75, 1593 (1971);
   (b) C. J. Howard, J. Phys.Chem., 75, 1593 (1971).

6. (a) M. A. A. Clyne and H. W. Cruse, J.C.S. Faraday II, 68, 1281 (1972).
   (b) W. Braun and T. Carrington, J. Quant. Spectrosc. Radiat. Transfer, 9, 1133 (1969).
   (c) I. W. M. Smith and R. Zellner, J.C.S. Faraday II, 70, 1045 (1974);
   (d) R. J. Donovan, D. Husain and L. J. Kirsch, Trans. Faraday Soc., 66, 2251 (1970).

7. P. P. Bemand, M. A. A. Clyne and R. T. Watson, J.C.S. Faraday I, 69, 1356 (1973).

8. (a) A. A. Westenberg and N. deHaas, J. Chem. Phys., 48, 4405 (1968);
   (b) J. N. Bradley, D. A. Whytock and T. A. Zaleski, J.C.S. Faraday I, 69, 1251 (1973).

9. P. J. Robinson and K. A. Holbrook, Unimolecular Reactions, John Wiley and Sons, Inc., London (1972).

10. K. J. Laidler, Theories of Chemical Reaction Rates, McGraw-Hill, London (1969).

11. J. Troe, J. Phys. Chem., 83, 114 (1979).

12. K. Luther and J. Troe, presented at the 17th International Symposium on Combustion, Leeds (1978).

13. (a) T. A. Hecht, J. H. Seinfeld and M. C. Dodge, Environ. Sci. Technol., 8, 327 (1974).

14. (a) W. L. Chameides and J. C. G. Walker, J. Geophys. Res., 81, 413 (1976);
(b) J. Fishman and P. J. Crutzen, J. Geophys. Res., 82, 5897 (1977).

15. (a) S. C. Wofsy, M. B. McElroy and Y. L. Yung, Geophys. Res. Lett., 2, 215 (1975);
(b) R. T. Watson, "Chlorine, the Chlorine Oxides and other Halogen Species", in CIAP Monograph I, Dept. of Transportation, Washington, D. C. (1975).

CHAPTER II

KINETICS STUDIES OF THE REACTIONS OF CH_3O_2 WITH NO, NO_2 AND CH_3O_2 at 298K

S. P. Sander and R. T. Watson*

Molecular Physics and Chemistry Section

Jet Propulsion Laboratory
Pasadena, CA 91103

Abstract

The flash photolysis/ultraviolet absorption technique was used to measure the rate constants for the reactions $CH_3O_2 + NO \rightarrow CH_3O + NO_2$ (1), $CH_3O_2 + NO_2 + M \rightarrow CH_3O_2NO_2 + M$ (2) and $CH_3O_2 + CH_3O_2 \rightarrow$ products (3) at 298K over the pressure range 50-700 Torr. Values for k_1 and k_3 were determined to be $(7.1 \pm 1.4) \times 10^{-12}$ cm^3 molecule^{-1} s^{-1} and $(3.6 \pm 0.7) \times 10^{-13}$ cm^3 molecule^{-1} s^{-1}, respectively, where k_3 is defined by the relation $\frac{d[CH_3O_2]}{dt} = 2k_3[CH_3O_2]^2$. k_2 was found to vary strongly with pressure indicating that the reaction occurs primarily by addition and is in the fall-off region between second and third-order kinetics. Experimentally determined parameters describing the shape of the fall-off curve for k_2 were in reasonable agreement with those obtained using theoretical methods developed by Troe and co-workers. An upper limit of 7×10^{-18} cm^3 molecule^{-1} s^{-1} was determined for the rate constant for the reaction $CH_3O_2 + CO \rightarrow$ products.

Introduction

Recent interest in the gas-phase reactions of the methylperoxy radical, CH_3O_2, has been stimulated by its role in both atmospheric and combusion-related processes. Kinetic mechanisms describing the chemistry of urban smog, the natural and polluted troposphere and stratosphere, all include the reactions of CH_3O_2.[1] It is therefore important to elucidate as clearly as possible the reactions of this species with other atmospheric constituents.

Much of the early work on CH_3O_2 kinetics was performed using static photolysis with ratios of rate constants being measured.[2-6] The recent discovery of a strong UV absorption band of CH_3O_2 between 210 and 280nm and the detection of CH_3O_2 by mass spectroscopy[7] have provided new techniques for the direct study of CH_3O_2 kinetics. Flash photolysis/ultraviolet absorption (FP/UV),[8-12] molecular modulation ultraviolet absorption spectroscopy (MMS)[13-15] and discharge flow/mass spectroscopy (DF/MS)[7,16] have now been used to measure rate constants of CH_3O_2 reactions. These reactions include:

$$CH_3O_2 + NO \rightarrow CH_3O + NO_2 \qquad (1)$$

$$CH_3O_2 + NO_2 + M \rightarrow CH_3O_2NO_2 + M \qquad (2)$$

$$CH_3O_2 + CH_3O_2 \rightarrow 2CH_3O + O_2 \qquad (3a)$$

$$\rightarrow CH_2O + CH_3OH + O_2 \qquad (3b)$$

$$\rightarrow CH_3OOCH_3 + O_2 \qquad (3c)$$

$$CH_3O_2 + HO_2 \rightarrow CH_3OOH + O_2 \qquad (4)$$

$$CH_3O_2 + SO_2 \rightarrow CH_3O + SO_3 \qquad (5)$$

Reaction 1 is an important step in the atmospheric photochemical cycle in which NO is converted to NO_2, a process which ultimately results in the formation of ozone. This reaction has been shown to be almost as rapid as the analogous process involving HO_2[17] (unless otherwise indicated, rate constants cited in the text are from Ref. 18):

$$HO_2 + NO \rightarrow OH + NO_2 \qquad (6) \qquad k_6 = 8 \times 10^{-12} cm^3 molecule^{-1} s^{-1}$$

and has proven difficult to study due to the rapidity of the reaction and the low detection sensitivity for CH_3O_2 by all techniques. Although several studies using FP/UV, MMS and DF/MS have been published,[10,15,16] agreement has not been particularly good and in one measurement, only the lower limit to the rate constant could be measured.[11]

Reaction 2 may play a role as a sink reaction for NO_x in urban smog and atmospheric methane oxidation in a manner analogous to pernitric acid, HO_2NO_2, and peroxyacetylnitrate (PAN), $CH_3C(O)O_2NO_2$. Because these compounds have a large activation energy for thermal decomposition (20-26 kcal/mole) the position of the formation/destruction equilibrium is strongly temperature-dependent which may account for some of the unusual temperature effects observed in smog chambers.[19] In the only reported direct study of this reaction, Cox and Tyndall[15] found the rate constant to depend only very weakly on total pressure between 50 Torr of Ar/CH_4 and 540 Torr of N_2 implying that the reaction is near its high pressure limit at a relatively low pressure.

Reaction 3 may play a role in the methane oxidation process occurring in the unpolluted troposphere where NO_x levels are reasonably low. This reaction, which has three thermodynamically possible product channels, has been studied by FP/UV and MMS with good agreement being obtained for the overall rate constant.[8,9,13,14] Because it is a second-order process, however, the rate constant measurement relied upon the determination of the absolute CH_3O_2 concentration. The rate constant is then derived from the product of two experimental observables, k_3/σ and σ, where σ is the CH_3O_2 absorption cross-section. At the moment, substantial disagreement exists between measurements of σ by FP/UV and MMS. In addition, the branching ratios for channels 3a, 3b and 3c are poorly defined.

In this study, rate constants for reactions 1, 2 and 3 were measured using the FP/UV technique. Due to several improvements in the apparatus design, the disappearance of CH_3O_2 could be observed over a wide range of reactant concen-

trations and total pressure. It is shown that, contrary to previous measurements, reaction 2 is still in the fall-off region at 700 Torr and that the high pressure limit is attained only at pressures exceeding several atmospheres.

Experimental

The apparatus has been described in detail previously.[20] The flash assembly consists of four concentric tubes comprising the reaction cell, photolyzing light filter, xenon flash lamp and cooling/heating jackets. Two identical cells were constructed; one made of quartz and the other pyrex. Reagents are premixed and continuously flowed through the reaction cell (2.54cm i.d., $\sim$ 95cm long) with a residence time of 15-30s. This permits complete replacement of cell contents between flashes to minimize the photolysis and reaction of stable products from the previous flash and to ensure that the starting reagents will not be depleted. Flowmeters were individually calibrated for each gas using a bubble calibrating system (Hastings Model HBM-1). The optical train consists of a 150 watt xenon arc lamp, White 8-pass mirror system (ℓ = 720cm, pyrex cell and 769cm, quartz cell) and McPherson Model 216.5 0.5m monochromator (slit width = 300 microns, 0.6nm resolution FWHM). Dichroic mirrors are used throughout to minimize reflection losses in the 220-270nm spectral region. Proper calibration of both the flow system and the optical system was verified by comparing concentrations of NO_2 measured on the basis of partial flows and UV absorption. Agreement was typically better than 2%.

Signals from the photomultiplier tube (EMI 9659 QA) are amplified and stored in a signal averager (Tracor-Northern 570A) operating in the analog mode. Multiple flashes (30-500) are employed to improve the signal-to-noise ratio (S/N). Further improvements in S/N are obtained by treating the data with a five-point smoothing algorithm.[21] Due to scattered light from the photolysis flash, the acquisition of data was delayed for $\sim$ 50 μsec after the flash.

Methylperoxy radicals were produced either by photolysis of chlorine in

Cl_2 - CH_4 - O_2 mixtures in the quartz or pyrex cell, or by photolysis of azomethane, $(CH_3)_2N_2$, with oxygen in the quartz cell. CH_3O_2 is produced by reactions 7-9 in the Cl_2 - CH_4 - O_2 system:

$$Cl_2 + h\nu \rightarrow 2Cl \qquad (7)$$

$$Cl + CH_4 \rightarrow HCl + CH_3 \qquad (8) \quad k_8 = 1.0 \times 10^{-13} cm^3 molecule^{-1} s^{-1}$$

$$CH_3 + O_2 + M \rightarrow CH_3O_2 + M \qquad (9) \quad k_9 = 2.2 \times 10^{-14} cm^3 molecule^{-1} s^{-1}$$

and by reactions 9 and 10 in the $(CH_3)_2N_2$ - O_2 system:

$$(CH_3)_2N_2 + h\nu \rightarrow 2CH_3 + O_2 \qquad (10)$$

$$CH_3 + O_2 + M \rightarrow CH_3O_2 + M \qquad (9)$$

The ranges of reagent concentrations were (in molecule cm^{-3}):

$[Cl_2] \times 10^{-16}$: 1.1 - 7.9; $[CH_4] \times 10^{-17}$: 2.0 - 15; $[O_2] \times 10^{-17}$: 1.1 - 4.8; $[(CH_3)_2N_2] \times 10^{-15}$: 1.7 - 5.4; $[NO] \times 10^{-14}$: 4.8 - 23; $[NO_2] \times 10^{-14}$: 4.0 - 42. $[CH_3O_2]_o$ (in molecule cm^{-3}) ranged from 3.4×10^{13} to 2.0×10^{14}. For all experiments, CH_3O_2 was formed on a time scale (20 - 70 μsec, 95% formation) at least ten times shorter than its loss (> 190 μsec, 95% removal).

The photolyzing light filters on both quartz and pyrex cells were filled with absorbing gases to isolate certain spectral regions. In the CH_3O_2 + NO study, it was desirable to inhibit the formation of O_3 because of its overlapping absorption with CH_3O_2. This was accomplished by filling the filter cell with 760 Torr of SO_2 which prevented the photolysis of O_2. Since k_3 is several times smaller than k_2 at low pressures, a concerted attempt was made to minimize the photolysis of NO_2 in the CH_3O_2 + NO_2 study. For this experiment, the filter cell was filled with a Cl_2 - Br_2 mixture which, at equilibrium, contained 60 Torr BrCl and 220 Torr Cl_2. BrCl, which has an absorption band centered at 370nm intermediate in intensity between Br_2 and Cl_2, absorbs a portion of the photolysis light which would otherwise result in NO_2 photolysis. Relatively low flash energies (< 700 J per flash) were

used in these experiments. Repeated flashing of static NO_2 - He mixtures indicated that NO_2 photolysis was limited to 0.1 per cent or less per flash.

The CH_3O_2 absorption was detected at 245nm for the $CH_3O_2 + NO_2$ and $CH_3O_2 + CH_3O_2$ reactions and at 270nm for the $CH_3O_2 + NO$ and $CH_3O_2 + CH_3O_2$ reactions. The temperature of the reaction cell was maintained at 298 ± 1 K by circulating methanol through the outer cell jacket from a constant temperature circulator. Azomethane was synthesized by the method of Renaud and Leitch.[22] $NO_2 - O_2$ mixtures were made by reacting small amounts of NO (Matheson C.P. Grade, 99.0% purity) with a large excess of O_2 and allowing sufficient time for complete conversion. N_2O_4 corrections were negligible. Diluent gases had the following stated purities: He (Linde UHP Grade, 99.999%), N_2 (Linde UHP Grade, 99.999%), O_2 (Linde UHP Grade, 99.99%), SF_6 (Matheson instrument purity, 99.99%). Chlorine (Matheson research purity, 99.96%) and methane (Matheson purity, 99.99%) were used without further purification.

Results

$CH_3O_2 + NO \rightarrow CH_3O + NO_2$

The rate constant for the $CH_3O_2 + NO$ reaction was measured over a wide range of reactant concentrations and total pressure. In early experiments where CH_3O_2 was monitored at $\lambda = 245$ nm, a substantial residual absorption of the analyzing light was observed after each flash which was attributed to the formation of methyl nitrite by the reaction

$$CH_3O + NO + M \rightarrow CH_3ONO + M \qquad (11) \qquad k_{11} = 3 \times 10^{-11} cm^3 molecule^{-1} s^{-1}.$$

The identity of the product was verified by observing that the magnitude of the residual absorption could be predicted from a measurement of $[CH_3O_2]_o$ and the methyl nitrite absorption cross section.[23] Moreoever, the shape of the absorption spectrum of the product closely matched the literature spectrum of CH_3ONO. Formation of CH_3ONO, which occurs on the same time scale as the

disappearance of CH_3O_2, severely interferes with the detection of methylperoxy radicals. Correcting for this absorption is both difficult and inaccurate because the true value of I_o is not well known. For this reason, the analysis wavelength was shifted to 270 nm. Although this reduces the detection sensitivity for CH_3O_2 by a factor of two, the ratio $\sigma_{CH_3O_2}/\sigma_{CH_3ONO}$ is increased from 1.7 to 245 nm to 7.1 at 270 nm, significantly reducing the interference and simplifying the data analysis.

Methylperoxy radicals were always formed on a time scale at least ten times faster than their removal. The ratios of $[NO]_o$ to $[CH_3O_2]_o$ ranged from 7.1 to 23.4 with an average of 13.0, resulting in good pseudo-first-order conditions. Decays of CH_3O_2 were typically observed over a factor of 8-10 in concentration with a detection limit around 4×10^{12} molecule cm^{-3}. This corresponds to a minimum detectable absorption of 0.5 percent which is attained after 50 to 500 flashes. A typical first-order decay plot is shown in Fig. 1.

The values of k_1' obtained in each kinetic run were corrected for two effects; absorption of the analytical beam by the product, CH_3ONO, and minor departures from true pseudo-first-order kinetics. A correction for the small residual absorption was evaluated from both computer simulations of the complete mechanism and an analytical expression derived from a simplified mechanism. The correction amounted to a 2.9 percent effect at $\lambda = 270$ nm. The first-order rate constant was also corrected for the minor consumption of NO by reaction with CH_3O_2 (reaction 1) and CH_3O (reaction 11). The correction varied with the ratio $[NO]_o/[CH_3O_2]_o$ and averaged 4.7 percent. The correction for the bimolecular disproportionation of CH_3O_2 was negligible (< 1 percent). Removal of CH_3O_2 by other reactions, e.g.,

$$CH_3O_2 + NO_2 + M \rightarrow CH_3O_2NO_2 + M \qquad (2)$$

$$CH_3O_2 + CH_3O \rightarrow CH_2O + CH_3OOH \qquad (12)$$

$$CH_3O + O_2 \rightarrow HO_2 + HCHO \qquad (13)$$

$$CH_3O_2 + HO_2 \rightarrow CH_3OOH + O_2 \qquad (4)$$

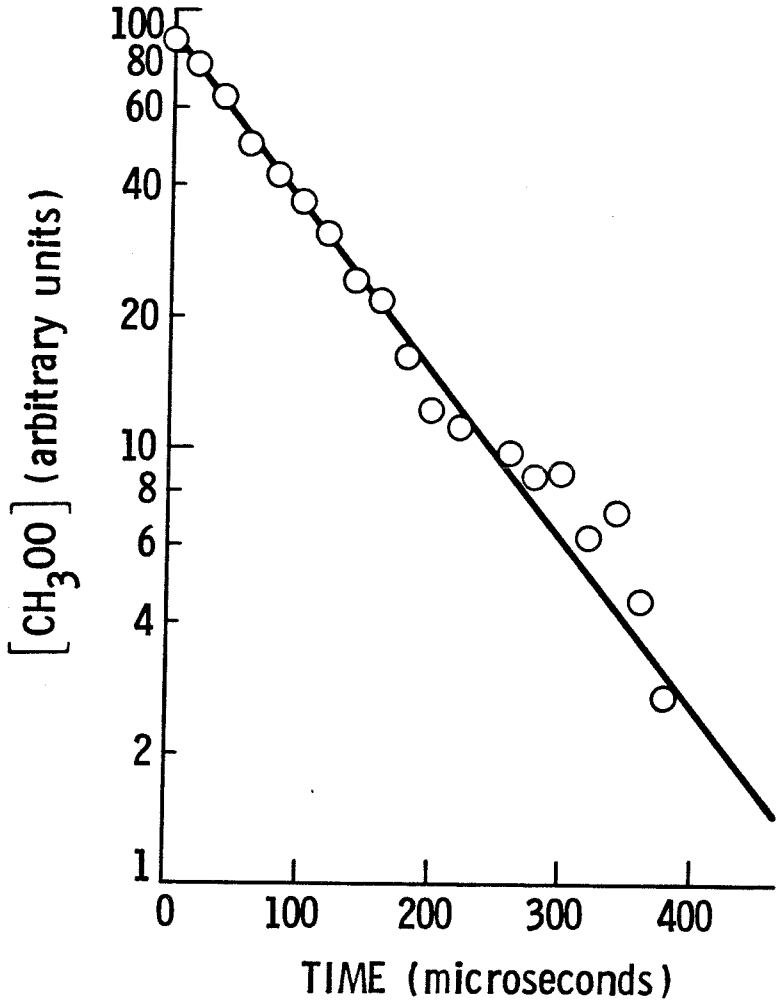

Figure 1. Pseudo-first-order decay of CH_3OO radicals reacting with NO. [NO] = 1.07×10^{15} molecule cm^{-3} and $[CH_3OO]_o \cong 1.0 \times 10^{14}$ molecule cm^{-3}.

was investigated by computer simulation and found to be insignificant.

Reaction rate data for all kinetic runs is given in Table I. A total of 47 kinetic runs were conducted at three different total pressures; 75 Torr (helium), 350 Torr (helium) and 700 Torr (helium, nitrogen). A plot of $k_1' = k_1[NO]$ vs. [NO] is given in Fig. 2 for the 19 runs at 350 Torr. Good linearity and a negligible intercept are observed further validating the assumption of first-order kinetics. Values for k_1 at each pressure were computed using two different analysis procedures; averaging the individual rate constants, and determining the least-squares slope of the k_1' vs. [NO] plot. Although small differences ($\sim$ 10 percent) exist between the rate constants derived by the two methods the preferred values are obtained from the arithmetic means. This is based on the observation that because the extrapolations to [NO] = 0 in the k_1' vs. [NO] plots are long, both the slope and y-intercept are sensitive to small changes in a few critical data points. The data in Table I indicates an increase in k_1 of about 25 percent as the total pressure is increased from 350 to 700 Torr. Although this is suggestive of a third-order component, it is not possible within the precision of the data to determine if such a process takes place. Additional studies with improved precision are required. The procedure adopted in obtaining the final rate constant, $k_1 = (7.1 \pm 1.4) \times 10^{-12}$ cm^3 molecule^{-1}s^{-1}, was to average the individual rate constants of all 47 runs.

Difficulties were encountered when azomethane was used as the source of methyl radicals. A large residual absorption was observed which could not be accounted for by any known stable reaction products. The absorber may be a product of a reaction between azomethane and other radicals in the system, or may be the result of an impurity. As a result, only $C\ell_2$-CH_4-O_2 mixtures were used to generate CH_3 radicals in the study of reaction 1.

$\underline{CH_3O_2 + NO_2 + M \rightarrow CH_3O_2NO_2 + M}$

The reaction between CH_3O_2 radicals and NO_2 was studied as a function of total pressure (50-700 Torr) and diluent gas (M = He, N_2, SF_6). Both CH_3

Table I: Reaction Rate Data for $CH_3O_2 + NO \xrightarrow{1} CH_3O + NO_2$

Flash Energy	$[Cl_2]$ x 10^{-16}	$[CH_4]$ x 10^{-17}	$[O_2]$ x 10^{-17}	$[CH_3OO]_o$ x 10^{-13}	$[NO]_o$ x 10^{-14}	k_1', meas	k_1', corr*	k_1 x 10^{12}
Joules	molecule cm^{-3}					s^{-1}		cm^3 molecule^{-1} s^{-1}
	[M] = 75 Torr, He							
608	1.6	3.8	1.7	4.6	4.84	2710	2780	5.74
691	1.6	3.8	1.7	6.2	6.39	3680	3770	5.91
608	1.6	3.8	1.6	7.1	7.65	4490	4600	6.01
680	1.9	3.8	1.7	10	10.3	6020	6170	5.99
691	2.0	4.8	1.6	11	12.3	7020	7170	5.83
691	2.3	3.8	1.7	11	12.5	6070	6190	4.96
691	2.0	4.8	1.6	11	14.9	10800	10900	7.34
691	2.4	4.8	1.6	14	19.2	11200	11300	5.90
691	2.4	4.8	1.6	14	21.0	14600	14700	7.01
691	2.4	4.8	1.6	14	23.4	14100	14200	6.06
								$\bar{k}_1$ = 6.1 ± 0.7
	[M] = 350 Torr, He							
529		5.9	2.2	3.4	3.59	1700	1740	4.85
529	1.2	6.0	2.2	4.7	5.39	3220	3280	6.09
529	1.8	5.9	2.2	6.0	6.21	4000	4100	6.60
	2.0	5.8	2.0	5.2	6.21	4830	4920	7.92
691	1.5	5.9	2.1	9.2	6.98	5090	5320	7.62
780	2.0	5.8	2.0	8.6	7.75	6000	6200	8.00
529	1.5	5.3	2.0	6.5	8.72	5250	5320	6.10
529	1.5	5.3	2.0	6.5	8.72	6070	6150	7.05
691	1.5	5.9	2.1	9.2	9.73	5480	5610	5.77
780	2.2	5.7	2.0	15	10.6	6560	6890	6.50
	1.8	5.9	2.2	13	13.2	7290	7480	5.67
691	1.5	5.9	2.1	9.2	13.7	6560	6620	4.83
780	2.2	5.7	2.0	15	14.5	7264	7480	5.16
780	2.5	5.8	2.0	15	15.4	8360	8570	5.57
780	2.0	5.8	2.0	8.6	15.5	9450	9470	6.11
	1.8	5.9	2.2	13	17.6	9850	9980	5.67
780	2.5	5.8	2.0	15	19.3	12800	13000	6.73
	1.8	5.9	2.2	13	21.9	15300	15400	7.02
780	2.5	5.8	2.0	15	22.8	14400	14500	6.37
								$\bar{k}_1$ = 6.3 ± 0.9

Table I. (Cont.)

		[M] = 700 Torr, He						
529	1.1	5.2	2.2	5.0	6.57	4300	4360	6.63
		5.2	2.3	6.5	7.46	6850	6980	9.36
531	2.0	5.6	2.1	7.0	8.13	6430	6560	8.06
	2.0	5.6	2.1	8.0	9.12	8660	8840	9.69
691	1.7	5.2	2.2	7.5	9.85	8760	8880	9.02
691	1.7	5.2	2.3	10	10.7	8840	9050	8.46
		5.2	2.3	6.5	11.8	9450	9470	8.03
691	2.2	5.2	2.2	9.0	13.1	12000	12100	9.25
		5.2	2.3	6.5	14.9	13600	13500	9.08
	2.0	5.6	2.1	13	16.2	11300	11500	7.08
	2.0	5.6	2.1	13	16.2	10500	10700	6.58
691	1.7	5.2	2.3	10	21.4	15400	15400	7.18
								$\bar{k}_1$ = 8.2 ± 1.1
		[M] = 700 Torr, N_2						
529	1.4	15	2.1	4.1	4.25	3860	3960	9.31
529	1.4	15	2.1	4.1	6.86	6130	6160	8.98
529	2.1	15	2.1	8.8	10.3	9420	9600	9.32
529	2.1	15	2.1	8.8	13.7	12500	12600	9.19
529	2.1	15	2.1	8.8	17.1	12600	12600	7.37
529	2.1	14	2.1	8.8	20.6	18600	18500	8.99
								$\bar{k}_1$ = 8.9 ± 0.7

* includes stoichiometry and CH_3ONO corrections (see text).

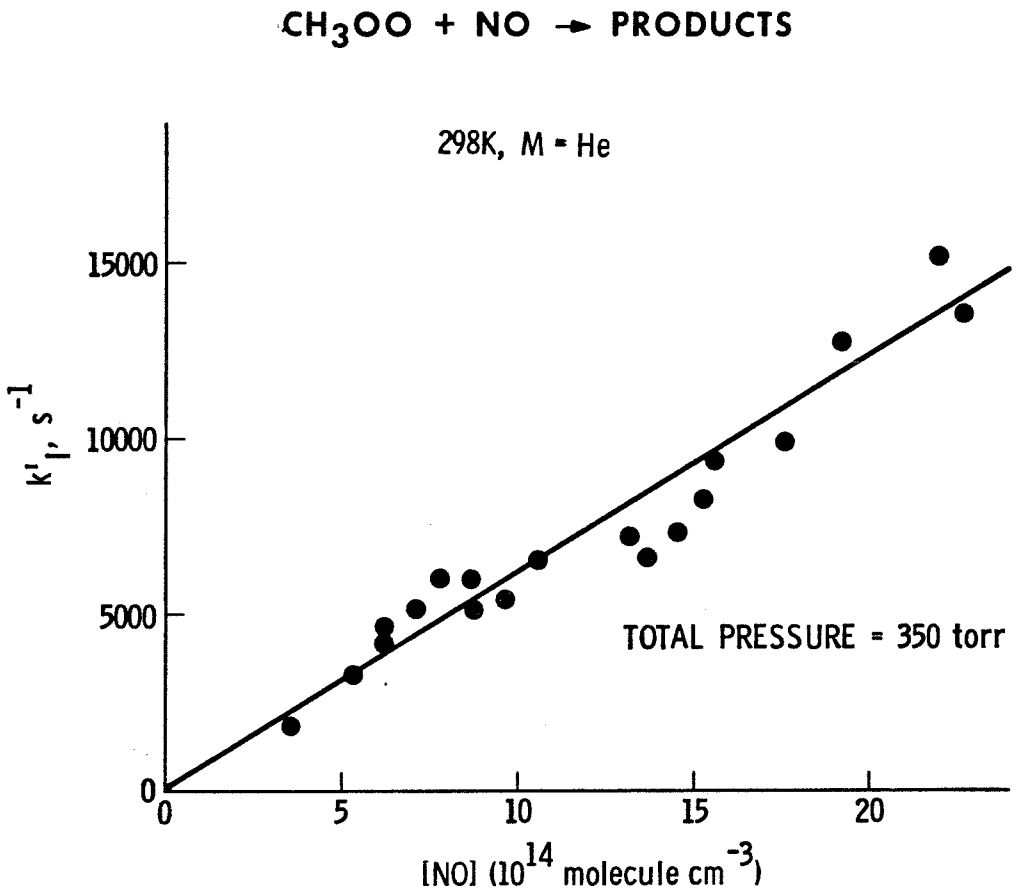

Figure 2. The reaction $CH_3OO + NO \rightarrow CH_3O + NO_2$. Variation of pseudo first-order rate constant, k_1', corrected for NO removal and CH_3ONO absorption at 298K at a total pressure of 350 Torr He.

radical sources were employed; photolysis of Cl_2-CH_4-O_2 mixtures and photolysis of $(CH_3)_2N_2$-O_2 mixtures. Experiments conducted in both quartz and pyrex cells used a BrCl filter to minimize the photolysis of NO_2. Because $k_2(CH_3O_2 + NO_2)$ is smaller than $k_1(CH_3O_2 + NO)$ in the pressure range studied, improvements in initial reactant stoichiometry over the CH_3O_2 + NO study could be realized. Values of $[NO_2]/[CH_3O_2]_o$ ranged from 20 to 40 for most runs, thus maintaining good pseudo-first-order conditions at all times. A total of 185 kinetic runs were performed at pressures of 50, 100, 225, 350, 500 and 700 Torr for each diluent gas. Reaction rate data at 350 Torr for M = He, N_2 and SF_6 are given in Table II.

A small residual absorption attributed to $CH_3O_2NO_2$ was detected in each experiment. A similar absorption feature was observed by Cox and Tyndall by molecular modulation spectroscopy.[15] The absorption cross-sections of the product were measured relative to the absorption cross-section of CH_3O_2 between 240 and 280 nm by observing the residual absorption in kinetic runs with known $[CH_3O_2]_o$ and assuming stoichiometric conversion to $CH_3O_2NO_2$. The same spectrum was measured by Cox and Tyndall[15] by the MMS technique. The two sets of results are compared in Table III. Although measured over a small wavelength range, the shape of the spectrum and the magnitude of the absorption are consistent with other structurally similar compounds such as HO_2NO_2.[24] Using the CH_3O_2 cross-sections of Hochanadel et al.,[8] the ratio $\sigma_{CH_3O_2}/\sigma_{CH_3O_2NO_2}$ was found to be about 6.8 at the analysis wavelength, 245 nm. However, it can be shown that an absorber ($CH_3O_2NO_2$) formed as an immediate product of the reaction of the species being monitored (CH_3O_2) does not interfere with the measurement of k' (see Appendix A). No correction to k_2' is therefore required to account for the presence of $CH_3O_2NO_2$.

Good linearity is observed for all k_2' vs. $[NO_2]$ plots, several of which are shown in Fig. 3. For each diluent gas, the bimolecular rate constant increases by at least a factor of three over the pressure range 50-700 Torr

Table II: Reaction Rate Data for $CH_3O_2 + NO_2 + M \xrightarrow{2} CH_3O_2NO_2 + M$ at 350 Torr

Flash Energy	$[(CH_3)_2N_2]$ x 10^{-15}	$[C\ell_2]$ x 10^{-16}	$[CH_4]$ x 10^{-17}	$[O_2]$ x 10^{-17}	$[CH_3O_2]_o$ x 10^{-13}	$[NO_2]$ x 10^{-14}	k_2'	k_2 x 10^{12}
Joules	molecule cm^{-3}						s^{-1}	cm^3 molecule$^{-1}s^{-1}$
	[M] = 350 Torr, He							
529		2.1	5.6	2.4	2.5	4.34	950	2.19
540	3.2			3.3	9.8	8.23	1710	2.19
540	4.1			3.3	10	9.30	1890	2.03
529		2.1	5.6	2.1	2.6	9.50	2530	2.67
540	3.2			2.8	9.8	11.7	2580	2.21
334	3.2			2.8	9.8	11.7	2260	1.94
529		2.1	5.6	2.8	4.0	12.7	3250	2.56
540	3.2			3.1	9.8	15.5	3880	2.50
540	4.1			3.3	10	15.7	3510	2.23
529		2.1	5.6	3.1	4.0	18.9	5060	2.68
540	3.2			3.9	9.8	23.4	4610	1.97
540	3.2			4.3	9.8	27.5	5370	1.96
	[M] = 350 Torr, N_2							
529		3.9	6.3	2.6	2.8	5.41	1720	3.18
389	4.2			1.8	3.9	5.63	1720	3.06
389	4.2			2.1	3.9	7.62	2260	2.96
389	4.2			2.2	7.0	7.85	2320	2.95
529		3.9	6.3	2.8	2.8	8.66	2640	3.04
529		5.5	9.4	3.6	5.5	10.3	2970	2.88
389	4.2			2.6	7.0	10.7	3020	2.82
529		3.9	6.3	2.9	4.6	10.9	3030	2.78
540	4.2			1.7	10	11.7	3460	2.96
540	4.2			1.8	10	14.0	4240	3.03
529		3.9	6.3	3.3	4.6	16.4	4140	2.53
540	4.2			2.2	10	19.4	6510	3.35
529		5.5	9.4	4.3	5.5	21.4	7320	3.42
529		3.9	6.3	3.6	4.6	21.8	5900	2.71
540	4.2			2.4	10	23.6	7240	3.07
	[M] = 350 Torr, SF_6							
529		2.9	6.2	2.4	5.5	5.61	1960	3.49
529		2.9	6.2	2.5	5.0	8.24	3170	3.85
529		2.9	6.2	2.7	5.0	11.0	4920	4.47
529		2.9	6.2	2.7	5.5	11.0	4255	3.87
529		2.9	6.2	3.0	5.0	16.5	6280	3.81

Table III: Summary of Rate Data for $CH_3O_2 + NO_2 + M \rightarrow CH_3O_2NO_2 + M$; Comparison Between Least-Squares Slopes of k_2 vs. $[NO_2]$ Plots and Mean Rate Constants

	M = He		M = N_2		M = SF_6	
	Slope	Mean	Slope	Mean	Slope	Mean
P, Torr	$k_2(10^{-12}$ cm^3 molecule^{-1} s^{-1})					
50	0.971 ± 0.053	0.884 ± 0.064	1.19 ± 0.11	1.15 ± 0.10	1.02 ± 0.12	1.28 ± 0.16
100	1.43 ± 0.072	1.18 ± 0.16	1.78 ± 0.059	1.58 ± 0.15	1.57 ± 0.13	1.99 ± 0.25
225	1.93 ± 0.11	1.74 ± 0.14	1.80 ± 0.19	2.22 ± 0.31	3.09 ± 0.48	3.07 ± 0.35
350	2.00 ± 0.21	2.26 ± 0.27	3.11 ± 0.19	2.98 ± 0.23	3.99 ± 0.49	3.90 ± 0.36
500	2.71 ± 0.20	2.53 ± 0.31	3.13 ± 0.097	3.67 ± 0.21	3.82 ± 0.45	4.21 ± 0.37
700	2.58 ± 0.19	2.80 ± 0.35	3.68 ± 0.10	3.94 ± 0.17	4.64 ± 1.62	4.81 ± 0.59

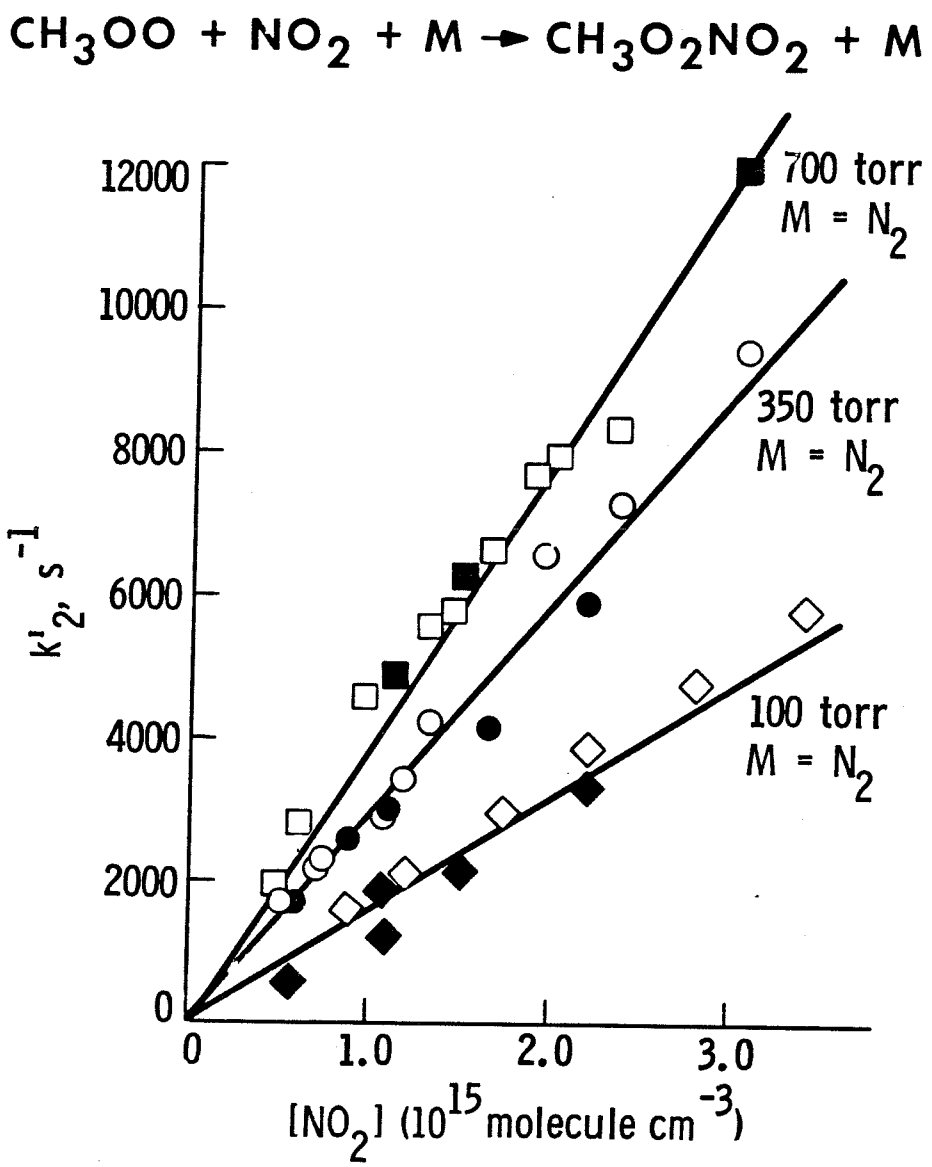

Figure 3. The reaction $CH_3OO + NO_2 + M \rightarrow CH_3O_2NO_2 + M$. Variation of first-order rate constant, k_2', at 298K at total pressures of 100, 350 and 700 Torr N_2. ■, ●, ◆, $(CH_3)_2N_2 - O_2$ system; □, ○, ◇, $Cl_2 - CH_4 - O_2$ system.

indicating that the reaction occurs primarily by addition to form $CH_3O_2NO_2$. No significant differences were observed between results obtained from the Cl_2-CH_4-O_2 system and the $(CH_3)_2N_2$ system, confirming that the measured CH_3O_2 decay rates are independent of the method of CH_3 radical production. Consequently, since the $(CH_3)_2N_2$-O_2 experiments were conducted in the quartz cell, it is confirmed that there are no adverse effects due to possible vibrational excitation of CH_3 from the photolysis of azomethane in its short wavelength (λ < 240 nm) absorption band. This possibility has been suggested by other workers.[9]

Experimental values of k_2 are listed in Table IV. The results given are the mean values for all kinetic runs at a given pressure of diluent gas and include the data for both Cl_2-CH_4-O_2 and $(CH_3)_2N_2$-O_2 systems. Slopes of k_2' vs. $[NO_2]$ plots differ on average by only 3 percent from mean values indicating that the small intercepts on these plots are not due to any systematic removal path for CH_3O_2 other than the one identified. Values of k_2 vs. total pressure for each diluent gas are plotted in Fig. 4.

Thermal decomposition of $CH_3O_2NO_2$,

$$CH_3O_2NO_2 + M \rightarrow CH_3O_2 + NO_2 + M \qquad (-2)$$

can interfere with the measurement of k_2 if it occurs on the same time scale as its formation. Such an effect, if important, would manifest itself as curvature in this first-order decay plot, i.e., regeneration of CH_3O_2, and curvature in k_2' vs. $[NO_2]$ plots, neither of which were observed. Although rate constants for the unimolecular decomposition of $CH_3O_2NO_2$ have not been measured, the decomposition rates for the analogous compound, HO_2NO_2, are applicable. At 298 K and 760 Torr N_2, this rate constant is .076 s^{-1}.[25] Over the pressure range encountered in this experiment (50-700 Torr), k_{-2} ranges from .013 s^{-1} to .073 s^{-1}. Even allowing for a slightly weaker O-N bond in $CH_3O_2NO_2$, thermal decomposition at room temperature cannot compete with the first-order formation rates of 700 to 7000 s^{-1} encountered here.

Table IV: Measured UV Absorption Cross-Sections of $CH_3O_2NO_2$

Wavelength nm	$\sigma(10^{-19}$ cm$^2)$	
	This Work	Cox and Tyndall[15]
240	6.2 ± 1.2	6.1
245	4.6 ± 0.9	5.0
250	4.0 ± 0.8	4.0
260	3.1 ± 0.6	1.8
265	2.3 ± 0.5	1.1
270	2.2 ± 0.4	1.0
280	1.7 ± 0.3	0.7

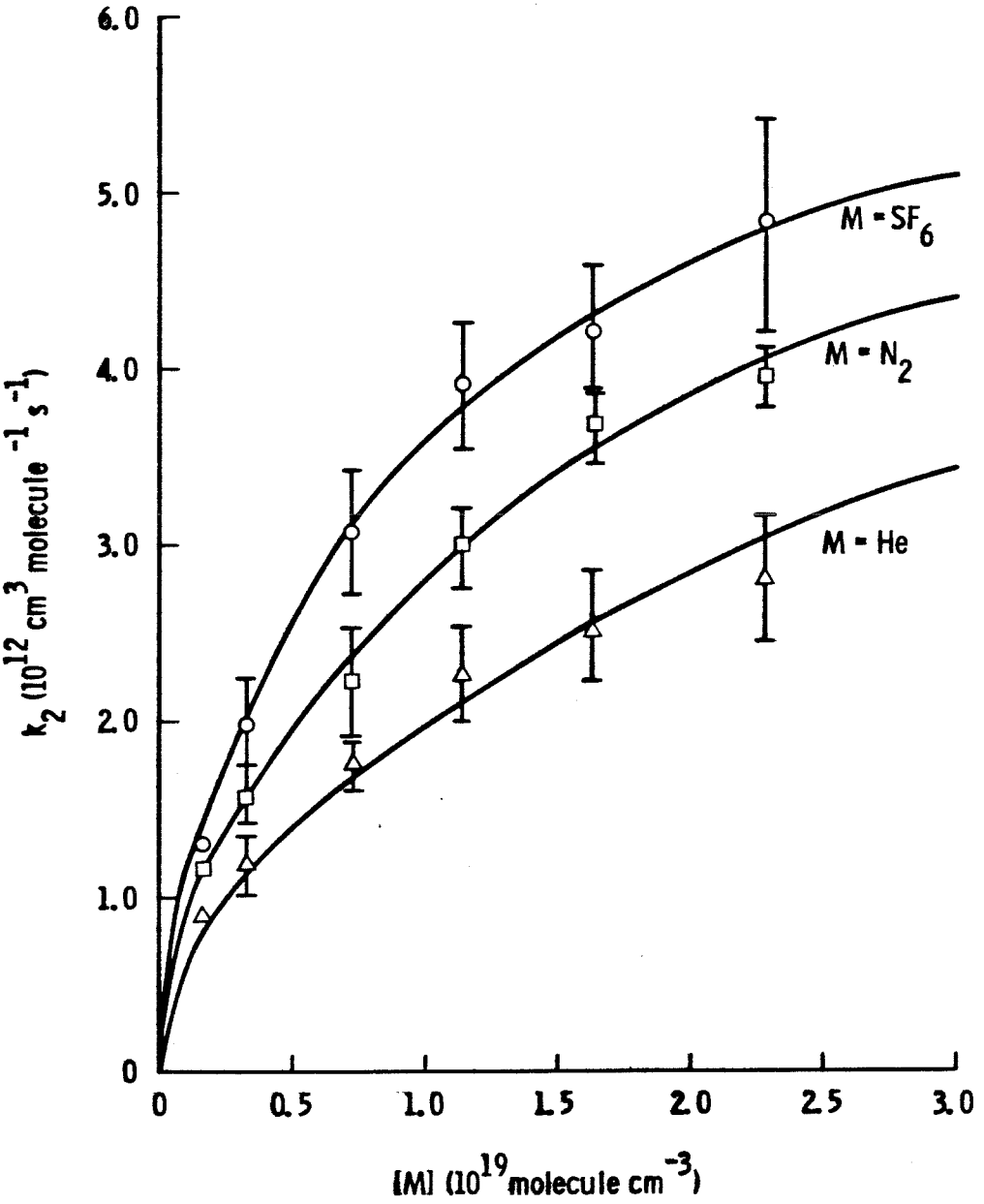

Figure 4. Variation of k_2' with total pressure for M = He, N_2 and SF_6. The solid lines are the best fit of the data to Eqn. (1).

As indicated above, photodissociation of NO_2 occurs to a small extent resulting in the formation of NO. Competition for CH_3O_2 by NO would be most important at 50 Torr where $k_{2,He} \cong 9 \times 10^{-13}$ cm^3 molecule^{-1} s^{-1} and $k_1 \cong 7 \times 10^{-12}$ cm^3 molecule^{-1} s^{-1}. However, since the amount of NO formed photolytically is small (1×10^{12} to 1×10^{13} molecule cm^{-3}) the first-order rate constant, k_1' is less than 70 s^{-1}. With these low concentrations of NO, first-order conditions do not prevail, and the true correction in the worst case would be less than 10% and typically 1-2%. For this reason, this effect can be ignored.

$CH_3O_2 + CH_3O_2 \rightarrow$ Products

Kinetic studies of the $CH_3O_2 + CH_3O_2$ reaction were conducted using the Cl_2-CH_4-O_2 system. Experiments were conducted at λ = 245 nm and 270 nm with $[CH_3O_2]_o$ varying from 2.6×10^{13} to 2.2×10^{14} molecule cm^{-3}. Total pressure was varied from 50 to 500 Torr using He, N_2 and SF_6 as diluent gases. Plots of $1/(\sigma[CH_3O_2])$ vs. time were linear over a concentration range of 10-50, however the linearity and hence the value derived for the initial slope were extremely sensitive to the choice of I_o. For example, a 0.5 percent variation in I_o resulted in a 10 percent change in the slope. For these experiments, the measurement precision of I_o was typically 0.1 percent or better. Figure 5 shows the decay plots of three kinetic runs differing only in $[CH_3O_2]_o$. The fact that the plots are parallel indicates that the rate constant is independent of $[CH_3O_2]_o$. Variation of $[O_2]$ from 2.7×10^{16} to 6.6×10^{17} molecule cm^{-3} resulted in an increase in $[CH_3O_2]_o$ of approximately 50 percent as an increasing fraction of the CH_3 reacted with O_2 instead of with other CH_3 radicals. Observed values of k_3 decreased by about 20 percent as $[O_2]$ was increased. The addition of CO as a possible scavenger of CH_3O to pressures up to 160 Torr resulted in a systematic decrease in k_3 of about 15 percent.

Results of all kinetic runs are given in Table V. For runs with a constant value of $[O_2] \cong 2.5 \times 10^{17}$ molecule cm^{-3} and no added CO, k_3/σ was found to be $(1.06 \pm 0.07) \times 10^5$ cm s^{-1} at 245 nm and $(2.84 \pm 0.36) \times 10^5$ cm s^{-1} at 270 nm.

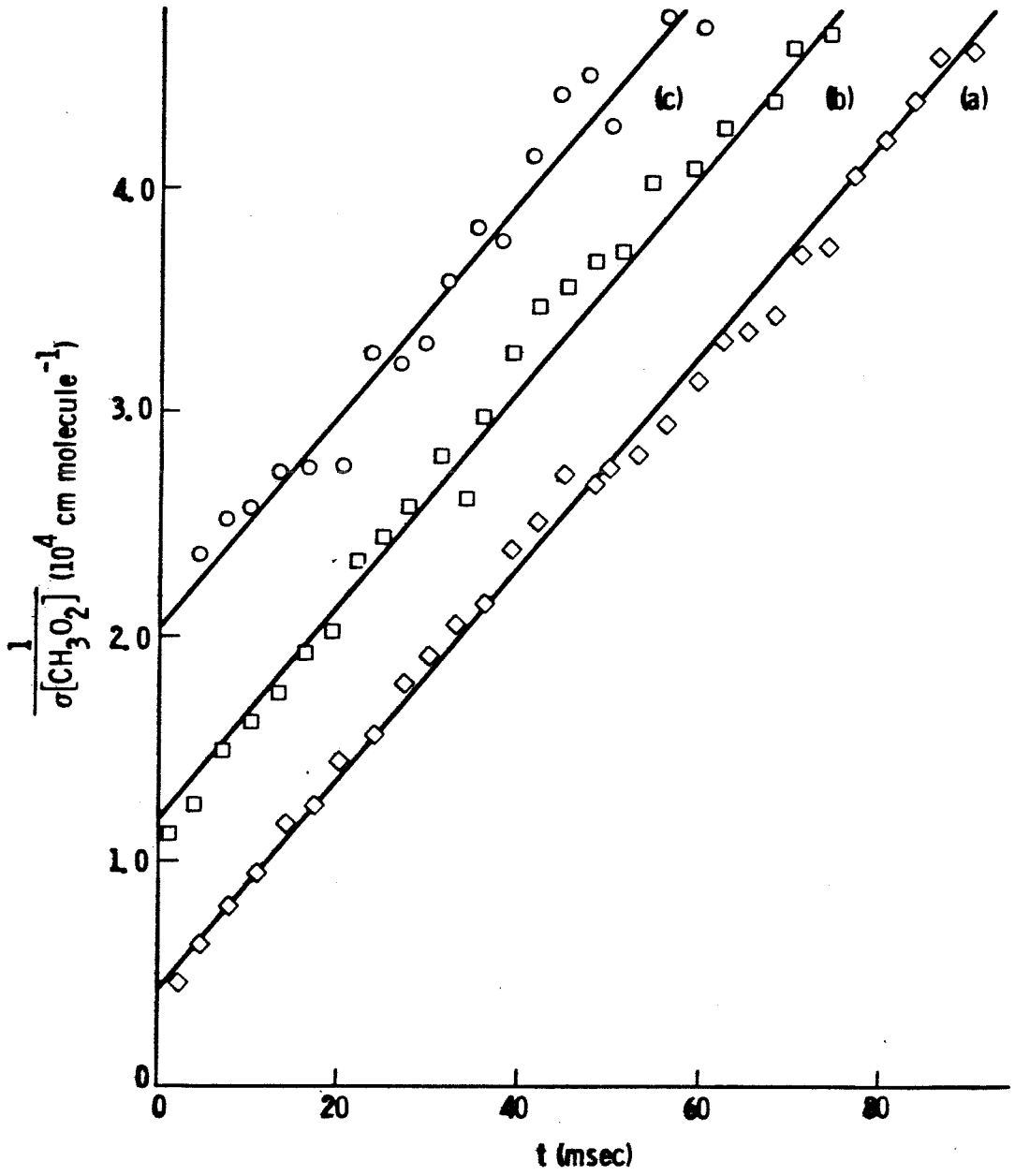

Figure 5. The reaction $CH_3OO + CH_3OO \rightarrow$ products. Second-order decays of CH_3OO for three different values of $[CH_3OO]_o$; (a) 2.2×10^{14} molecule cm^{-3}, (b) 1.0×10^{14} molecule cm^{-3}, (c) 3.3×10^{13} molecule cm^{-3}.

Table V: Reaction Rate Data for $CH_3O_2 + CH_3O_2 \xrightarrow{3}$ Products

Pressure Torr	Diluent	λ* nm	$[C\ell_2]$ x10^{-16} molecule cm^{-3}	$[CH_4]$ x10^{-17} molecule cm^{-3}	$[O_2]$ x10^{-17} molecule cm^{-3}	[CO] x10^{-18} molecule cm^{-3}	$[CH_3O_2]_o$ x10^{-13} molecule cm^{-3}	$2k_3/\sigma$ x10^{-5} cm molecule^{-1} s^{-1}	k_3 x10^{13} cm^3 molecule^{-1} s^{-1}
50	SF_6	245	3.5	3.1	1.7	0	5.2	2.26	3.41
			3.6	3.3	1.9		5.7	2.02	3.05
225	SF_6		3.4	8.6	2.3		4.4	2.28	3.44
			3.3	8.1	2.8		4.9	2.08	3.14
			3.3	8.1	2.5		7.8	1.91	2.88
500	SF_6		3.8	10	2.6		5.2	2.21	3.34
			3.2	10	2.6		4.2	2.10	3.17
350	N_2	270	3.5	12	2.2		10	4.75	3.56
			3.5	12	2.2		22	5.89	4.42
			3.5	12	2.2		6.3	5.55	4.16
			3.5	12	2.2		3.3	5.00	3.75
350	He		3.8	8.7	0.27		10	7.44	5.58
			0.69	8.7	0.31		3.0	5.70	4.28
			3.8	8.7	0.83		14	6.51	4.88
			0.69	8.7	2.1		3.2	5.31	3.99
			3.8	8.7	2.1		17	5.47	4.10
			4.1	8.2	2.1		17	6.21	4.66
			3.8	8.7	6.6		19	5.99	4.49
			4.1	7.4	1.9	1.2	16	5.73	4.30
			4.1	7.4	1.9	2.3	17	5.67	4.25
			5.6	7.0	0.25	2.6	2.6	5.35	4.01
			4.1	9.1	2.4	5.2	17	5.47	4.10

* $\sigma(245)\text{nm} = 3.0 \times 10^{-18}$ cm^2 (Ref. 8)
$\sigma(270)\text{nm} = 1.5 \times 10^{-18}$ cm^2

Using the CH_3O_2 cross sections of Hochanadel et al.[8] ($\sigma = 1.5 \times 10^{-18}$ cm^2 at 245 nm, $\sigma = 3.0 \times 10^{-18}$ cm^2 at 270 nm), $k_3 = (3.2 \pm 0.21) \times 10^{-13}$ at 245 nm and $k_3 = (4.3 \pm 0.54) \times 10^{-13}$ at 270 nm where k_3 is defined by the relation

$$\frac{-d[CH_3O_2]}{dt} = 2\, k_3[CH_3O_2]^2 \ .$$

The difference between the two values of k_3 probably reflects the experimental uncertainty in σ. Combining the data for the two wavelengths gives $k_3 = (3.65 \pm 0.67) \times 10^{-13}$ cm^3 $molecule^{-1}$ s^{-1}.

Discussion

$CH_3O_2 + NO$

The $CH_3O_2 + NO$ reaction has been studied using both indirect[2-5,26] and more recently, direct techniques.[10,11,15,16] The primary conclusion of the indirect studies, determined largely from product analysis, was that CH_3O radicals are formed from reaction 1 and that other channels, adduct formation in particular, do not proceed. The ratio k_1/k_2 was measured in two of these studies; Simonaitis and Heicklen[3] obtained a value of 2.2 at a pressure of 700 torr of CH_4 at 298 K while Cox et al.[5] obtained a lower limit of 12 at a pressure of 760 torr of N_2 at 296 K. The former value agrees favorably with the value $k_1/k_2 = 1.8 \pm 0.2$ determined in this study at 298 K in 700 torr N_2.

The results of the direct studies are summarized in Table VI. The DF/MS study of Plumb et al.[16] and the MMS study of Cox and Tyndall[15] are in excellent agreement with this study. Both studies, however, encountered difficulties with secondary chemistry due to marginal sensitivity for CH_3O_2 detection and the relatively large rate constant for reaction 1. Because of the large number of competing reactions, numerical simulation of the chemical system in conjunction with curve fitting were required to determine k_1 in the study of Cox and Tyndall. Analysis of the mechanism may have been complicated by the depletion of NO along the length of the reaction cell and removal of CH_3O_2 by reaction with NO_2. However, even though a strong absorption at 250 nm from

Table VI: Summary of Previous Work on the CH_3O_2 + NO Reaction

Reference	$k_1(10^{-12}$ cm^3 molecule^{-1}s$^{-1})$	Technique
Plumb, Ryan, Steven and Mulcahy[16]	8.0 ± 2.0	DF/MS
Cox and Tyndall[15]	6.5 ± 2.0	MM/UV
Anastasi, Parkes and Smith[11]	> 1.0	FP/UV
Adachi and Basco[10]	3.0	FP/UV
This work	7.1 ± 1.4	FP/UV

CH_3ONO was detected, the MMS technique permitted deconvolution of the methylperoxy signal.

In the study of Plumb et al., a number of secondary reactions take place which were not mentioned by the authors. These reactions, along with possibly inadequate first-order conditions, make the results of their system somewhat difficult to interpret. In their study, CH_3O_2 is formed in the following sequence of reactions:

$$O + C_2H_4 \rightarrow CH_3 + HCO \qquad (14) \quad k_{14} = 6.8 \times 10^{-13} cm^3 molecule^{-1} s^{-1}$$

$$CH_3 + O_2 + M \rightarrow CH_3O_2 + M \qquad (9) \quad k_9 = 2.6 \times 10^{-31} cm^6 molecule^{-2} s^{-1}, \; M = N_2$$

The authors considered the reactions

$$O + HCO \rightarrow CO + OH \qquad (15a) \quad k_{15a} + k_{15b} = 2.1 \times 10^{-10}$$

$$\rightarrow CO_2 + H \qquad (15b) \quad cm^3 \; molecule^{-1} \; s^{-1}$$

$$CH_3 + HCO \rightarrow CH_4 + CO \qquad (16)$$

as possible loss processes for HCO. However, with $[O_2] = 2.2 \times 10^{16}$ molecule cm^{-3} and $[O]_o \cong 4 \times 10^{12}$ molecule cm^{-3}, the reaction

$$HCO + O_2 \rightarrow HO_2 + CO \qquad (17) \quad k_{17} = 5.1 \times 10^{-12} cm^3 molecule^{-1} s^{-1}$$

will dominate the removal of HCO. This reaction was not considered in the original paper. The HO_2 formed in reaction 17 will have time to react with itself and with CH_3O_2 in the region of the flowtube before NO is injected by the reactions

$$HO_2 + HO_2 \rightarrow H_2O_2 + O_2 \qquad (18) \quad k_{18} = 7.5 \times 10^{-13} cm^3 molecule^{-1} s^{-1}$$

$$HO_2 + CH_3O_2 \rightarrow CH_3OOH + O_2 \qquad (4) \quad k_4 = 6.0 \times 10^{-12} cm^3 molecule^{-1} s^{-1}$$

In this region, CH_3O_2 will be removed by reactions 3 and 4 and CH_3 will be removed by disproportionation

$$CH_3 + CH_3 \xrightarrow{M} C_2H_6 \qquad (19) \quad k_{10} = 5.0 \times 10^{-12} cm^3 molecule^{-1} s^{-1}$$

Simulations of the reactions that occur in the flow tube, using conditions given in the paper, indicate that at the NO injection point, $[CH_3O_2]$ = (1.1 - 1.6) x 10^{12} molecule cm^{-3} and $[HO_2]$ = (1.3 - 2.0) x 10^{12} molecule cm^{-3}. After the injection point, several reactions occur which remove NO:

$$CH_3O_2 + NO \rightarrow CH_3O + NO_2 \qquad (1)$$

$$HO_2 + NO \rightarrow OH + NO_2 \qquad (6)$$

$$CH_3O + NO \overset{(M)}{\rightarrow} CH_3ONO \qquad (11)$$

HO_2 is also regenerated by

$$CH_3O + O_2 \rightarrow HO_2 + HCHO \qquad (13)\ k_{13} = 6.0 \times 10^{-16} cm^3 molecule^{-1} s^{-1}.$$

Although some ambiguity exists in the Plumb et al. paper concerning the exact NO and $O(^3P)$ concentrations used, [NO] = 8.0 x 10^{12} molecule cm^{-3} and $[O(^3P)]$ = 4.0 x 10^{12} molecule cm^{-3} are indicated as typical values. Using the concentration of $[CH_3OO]_o$, $[HO_2]_o$ and $[NO]_o$ calculated above, computer simulations of the reactions occurring after the NO injection point indicate that almost 40% of the NO is removed by reactions 1, 6 and 13 at the 1/e point for CH_3O_2. The absence of good first-order conditions would be expected to result in curvature in the plots of $\ln[CH_3O_2]$ vs. time in addition to that already attributed by the authors to a residual ion fragment at m/e = 47. Kinetic runs utilizing higher NO or lower $O(^3P)$ concentrations, if performed, would be less severely affected by NO depletion but in this example, an error of 30% would be expected in the measured rate constant. As a result, the accuracy of this study must be viewed with caution.

Two flash photolysis studies of this reaction have been reported.[10,11] Due to their low detection sensitivity for CH_3O_2, Anastasi et al.[11] could report only a lower limit, $k_1 > 1.0 \times 10^{-12}$ cm^3 $molecule^{-1}$ s^{-1} for the rate constant. The FP/UV study of Adachi and Basco suffers from complications due to secondary chemistry. Although the experimental technique and reaction mechanism are

similar to this work, there exists an important difference. In both systems, CH_3O radicals from reaction 1 will quickly react with NO to form CH_3ONO. In analyzing for CH_3O_2 at 245 nm, the technique of Adachi and Basco is susceptible to the interference caused by the formation of CH_3ONO on the same time scale as the CH_3O_2 disappearance. This has the effect of reducing the apparent CH_3O_2 loss rate, which is consistent with their much lower result for k_1. However, since their I_o value was derived from a blank cell, the CH_3ONO formation should have resulted in both non-linear first-order decay plots and a large residual absorption. Neither of these effects is mentioned by the authors and cannot be explained. As indicated above, our study circumvents the problem by analyzing for CH_3O_2 at 270 nm where CH_3ONO does not absorb strongly.

$CH_3O_2 + NO_2 + M$

The single previous direct kinetic study of this reaction is by Cox and Tyndall[15] who report $k_2 = (1.2 \pm 0.3) \times 10^{-12}$ cm^3 $molecule^{-1}$ s^{-1} at 50 Torr of Ar + CH_4, and $k_2 = (1.6 \pm 0.3) \times 10^{-12}$ cm^3 $molecule^{-1}$ s^{-1} at 540 Torr N_2. The small pressure dependence observed is used to argue that k_2 is near the second-order limit at 50 Torr total pressure. Although their measurement at 50 Torr of Ar/CH_4 is in good agreement with this study at 50 Torr N_2, the marked pressure dependence observed in Figure 4 strongly contradicts their conclusion. Due to the relatively long time scales encountered in their molecular modulation experiment, several sources of systematic error may appear which account for their results. These include depletion of NO_2 along the length of the cell and thermal decomposition of the adduct, $CH_3O_2NO_2$, in the period required for cell transit. As indicated above, because the time scale of the flash photolysis experiment is short and the cell contents are totally replaced between flashes, difficulties due to $CH_3O_2NO_2$ decomposition are avoided.

The experimental fall-off curves obtained in this study show the typical behavior expected for the formation of a stabilized adduct from a vibrationally excited intermediate. The vibrational quenching efficiency of the diluent gas,

hence the overall rate constant, increases with its size, complexity and total pressure. Recent work by Troe and co-workers[27,28] has shown that the rate constant fall-off curves of addition reactions can be described by a three-parameter equation:

$$k([M],T) = \frac{k_o(T)[M]}{1 + \frac{k_o(T)[M]}{k_\infty(T)}} \; F_c^{\{1 + [\log_{10}(k_o(T)[M]/k_\infty(T)]^2\}^{-1}} \qquad (1)$$

where $k_o(T)$ is the rate constant in the third-order regime, $k_\infty(T)$ is the rate constant in the second-order regime, and F_c is a parameter which characterizes the broadening of the fall-off curve due to the energy dependence of the rate constant for the decomposition of the vibrationally excited intermediate.[27,29]

Equation (1) is derived from a semi-empirical fit to the RRKM formalism. The utility of fitting experimental data to such an expression is that the rate constant for any value of total pressure can be determined (for the purpose of atmospheric modeling, for example) once the parameters are determined. This is much easier than computing the rate constant from a full RRKM calculation or from tables of Kassel integrals.

The parameters k_o, k_∞ and F_c were derived in this study by nonlinear least squares curve-fitting to Equation (1). For a given diluent gas (He, N_2 or SF_6) multiple sets of solutions can be obtained which give nearly the same fit to the data. However, the constraint is posed that the values of k_∞ and F_c (neglecting weak collision effects) must be the same for each diluent gas. The procedure adopted in this study was to map the entire domain of reasonable parameter values, holding k_∞ and F_c constant, and determine k_o by least squares. The parameters finally selected were the ones that resulted in overlapping regions of minimum χ^2 for all three data sets. It should be emphasized that at least two, and preferably three,

different third-body data sets are required to assign unambiguously the three parameters. This is particularly true for a reaction such as $CH_3O_2 + NO_2$ where the rate constant at the highest measured pressure is well below the high pressure limit, yet where there is significant fall-off at the lowest measured pressure. The parameters which gave the best fit to all three data sets were: $k_o = (1.19 \pm 0.06) \times 10^{-30}$ cm^6 molecule^{-2} s^{-1}, M = He; $(2.33 \pm 0.08) \times 10^{-30}$ cm^6 molecule^{-2} s^{-1}, M = N_2; $(3.94 \pm 0.13) \times 10^{-30}$ cm^6 molecule^{-2} s^{-1}, M = SF_6, $k_\infty = (8.0 \pm 1.0) \times 10^{-12}$ cm^3 molecule^{-1} s^{-1} and $F_c = 0.4 \pm 0.10$.

A procedure for the estimation of F_c from structural information about the adduct has been developed by Troe and co-workers.[27,28] F_c is given by a product of strong collision and weak collision broadening factors, F_c^{sc} and F_c^{wc},

$$F_c = F_c^{sc} F_c^{wc} \quad .$$

The overall expression for the rate constant, applicable in all pressure regimes, is then given by:

$$\frac{k}{k_\infty} = F^{LH}(k_o[M]/k_\infty) \; F_c(k_o[M]/k_\infty)$$

where F^{LH} is the Lindemann-Hinshelwood factor,

$$F^{LH}(k_o[M]/k_\infty) = \frac{k_o[M]/k_\infty}{1 + k_o[M]/k_\infty} \quad .$$

Values of F_c^{sc} have been determined by Luther and Troe[28] in tabular form as a function of the parameters S_k and B_k. S_k is given by

$$S_k = S_{eff} + 1 \text{ or } S_{eff} + 2$$

where S_{eff} is the effective number of transition state oscillators. S_{eff} can be estimated from the vibrational partition function of the adduct

molecule from the relation

$$S_{eff} = -\frac{1}{T}\frac{\partial \ln Q_v}{\partial(1/T)}$$

$$= \sum_{i=1}^{S} \frac{h\nu_i/kT}{\exp(h\nu_i/kT)-1}$$

where S = number of internal modes including hindered rotations (3N-6). The parameter B_k is given by:

$$B_k \simeq \frac{B'(S_k - 1)}{S - 1}$$

where

$$B' = \frac{E_o + a(E_o)E_Z}{kT}$$

E_o = critical energy for the unimolecular decomposition of $CH_3O_2NO_2$

E_z = zero-point energy of vibrations

$a(E_o)$ = Whitten-Rabinovitch factor.[29]

Higher-order approximations to B_k are derived by Luther and Troe.[28]

Since a complete normal-coordinate analysis of $CH_3O_2NO_2$ is lacking, vibrational frequencies were estimated by comparison with model compounds ($FONO_2$, CH_3F and N_2O). These frequencies are listed in Table VII. At 300K, $S_k \simeq 3.8$, $E_z = 41.6$ kcal mole^{-1} and $a(E_o) \simeq 1.0$. E_o is assumed to be 20 kcal mole^{-1} by analogy with HO_2NO_2 thermal decomposition.[25] The resulting value of B_k is ~ 14, and from the tables in Ref. 28, $F_c^{sc} = 0.51$.

The weak collision broadening factor, F_c^{wc}, can be approximated by a function of only one parameter, the collision efficiency factor β_c. F_c^{wc} is given by:

Table VII: Estimated Vibrational Frequencies for $CH_3O_2NO_2$

Frequency cm^{-1}	Type	Model[a]
3006	CH_3 Degen-stretch	CH_3F
2930	CH_3 Sym-stretch	CH_3F
2000	OON Sym-stretch	N_2O
1759	NO_2 Asym-stretch	$FONO_2$
1467	CH_3 Degen-Def.	CH_3F
1464	CH_3 Sym-Def.	CH_3F
1301	NO_2 Sym-stretch	$FONO_2$
1182	CH_3 Rock	CH_3F
1050	OON Asym-stretch	N_2O
1049	CO Stretch	CH_3F
928	OO Stretch	$FONO_2$
804	NO_2 Scis.	$FONO_2$
709	NO_2 Wag	$FONO_2$
633	NO_2 Stretch	$FONO_2$
455	NO_2 Rock	$FONO_2$
450	OON Bend	N_2O
303	OC Bend	$FONO_2$
120	OC Torsion	$FONO_2$

[a]Frequencies taken from Ref. 33 with minor corrections where appropriate.

$$F_c^{wc} \cong \beta_c^{0.14}$$

where

$$\beta_c \equiv \frac{k_o}{k_o^{sc}}$$

k_o^{sc} = low pressure-limiting strong collision rate constant.

k_o^{sc} can be estimated by methods derived by Troe.[28,30] Values of k_o^{sc} for several third-order reactions of atmospheric interest have recently been computed,[31] and the value for reaction 3 has been estimated to be 1.4×10^{-29} cm^6 $molecule^{-2}$ s^{-1} for $M = N_2$. From this, values of k_o^{sc} can be calculated for the other diluent gases by correcting the Lennard-Jones collision frequency. The resulting values of β_c are : 0.044 (M = He), 0.17 ($M = N_2$) and 0.39 ($M = SF_6$). Since F_c^{wc} is a relatively weak function of β_c, weak-collision effects in F_c are masked by experimental error. The average value of F_c^{wc} for the three diluent gases is 0.77. The composite broadening factor, F_c, is calculated to be 0.51 x 0.77 = 0.39 in good agreement with the value 0.40 ± 0.10 derived from the experimental data. At low temperatures (300K-600K), S_k is small relative to S, but F_c^{sc} is relatively sensitive to S_k. As a result, small errors in the estimation of S_k resulting, for example, from uncertainties in the estimation of the low-frequency vibrational modes have a large effect on F_c. Another source of error in S_k is the uncertainty in the difference between S_k and S_{eff}. The exact difference is[28]

$$S_k - S_{eff} = \frac{E_{a\infty} - E_o}{kT}$$

where $E_{a\infty}$ is the Arrhenius activation energy at the high-pressure limit. Since $E_{a\infty}$ is often experimentally unobtainable, the energy difference must be obtained from a complete RRKM calculation or by estimation, as above.

$CH_3O_2 + CH_3O_2$

Recently, a large number of studies on the $CH_3O_2 + CH_3O_2$ reaction have been published.[8,9,12-14] The results of these studies are listed in Table VIII. Although the room temperature rate constants are in remarkable agreement, the agreement is misleading. The fundamental parameter measured, k_3/σ, cannot be directly compared because most of the studies were carried out at different wavelengths. Of the three measurements of the CH_3O_2 absorption spectrum, two are in excellent agreement[8,9] while the third is scaled upward by about 50%.[14] If the measured spectrum of Hochanadel et al. is used to derive values of k_3 from all the different studies, the spread in k_3 ranges from 2.6 to 4.1 x 10^{-13} cm^3 $molecule^{-1}$ s^{-1}. The rate constant obtained in this study, (3.7 ± 0.7) x 10^{-13} cm^3 $molecule^{-1}$ s^{-1}, is in excellent agreement with the results of Kan et al.,[9] Sanhueza et al.[12] and Hochanadel et al.[8]

The interpretation of the kinetic data from this, and other studies of the $CH_3O_2 + CH_3O_2$ reaction is complicated by the possibility of a reaction branch forming CH_3O, i.e.

$$CH_3O_2 + CH_3O_2 \rightarrow 2CH_3O + O_2 \qquad (3a) \qquad \Delta H = +3.5 \text{kcal mole}^{-1}$$

In addition there are two exothermic reaction paths,

$$CH_3O_2 + CH_3O_2 \rightarrow CH_2O + CH_3OH + O_2 \qquad (3b) \qquad \Delta H = -77.4 \text{ kcal mole}^{-1}$$

$$\rightarrow CH_3O_2CH_3 + O_2 \qquad (3c) \qquad \Delta H = -42.8 \text{ kcal mole}^{-1}$$

Secondary removal of CH_3O_2 by the processes

$$CH_3O_2 + CH_3O \rightarrow CH_2O + CH_3OOH \qquad (12)$$

$$CH_3O + O_2 \rightarrow HO_2 + CH_2O \qquad (13)$$

$$CH_3O_2 + HO_2 \rightarrow CH_3O_2H + O_2 \qquad (4)$$

Table VIII: Summary of Previous Work on the CH_3O_2 + CH_3O_2 Reaction

Reference	λ nm	k_3/σ x 10^{-4} cm molecule^{-1}s^{-1}	σ^a x 10^{18} cm^2	k_3 x 10^{13} cm^{3}molecule^{-1}s^{-1}	σ^b x 10^{18} cm^2	k_3^c x 10^{13} cm^{3}molecule^{-1}s^{-1}
Parkes et al.[13]	220-290			2.2 - 4.4		
Parkes[14]	237	8.4	5.5 ± 1.0	4.6 ± 1.2	3.2	2.7 ± 0.7
Hochanadel et al.[8]	235	11	3.3	3.8 ± 0.7	3.3	3.8 ± 0.7
Anastasi et al.[11]	238	8.0	5.5, Ref. 14	4.4 ± 1.1	3.2	2.6 ± 0.6
Kan et al.[9]	265	20	2.0	4.1 ± 0.5	1.8	3.7 ± 0.4
Sanhueza et al.[12]	253.7	15	2.5, Ref. 8	3.7 ± 0.3	2.5	3.7 ± 0.3
This Work	245	11			3.0	3.2 ± 0.2
	270	28			1.5	4.3 ± 0.5

[a] CH_3O_2 cross-section used to derive k_3. Reference number given if taken from the literature.

[b] CH_3O_2 cross-section measured by Hochanadel et al. (Ref. 8);

[c] k_3 derived from measured k_3/σ and σ (Ref. 8).

occurs subsequent to the formation of methoxy radicals. Several radical termination steps also occur which reduce the probability of secondary CH_3O_2 removal. These include:

$$CH_3O + CH_3O \rightarrow \text{products} \qquad (20)$$

$$CH_3O + HO_2 \rightarrow CH_3OH + O_2 \qquad (21)$$

$$HO_2 + HO_2 \rightarrow H_2O_2 + O_2 \qquad (18)$$

Kan et al. have considered the effect of the above reactions on the overall CH_3O_2 removal rate.[9] Their conclusion, based on the assumption that

$$\frac{k_{3a}}{k_{3a} + k_{3b} + k_{3c}} = 0.33$$

was that the secondary consumption of CH_3O_2 would result in a maximum error of 12% in the determination of k_3. This is smaller than the error factor of 1.33 that would be expected if every CH_3O radical was effective in removing a CH_3O_2 radical.

The relationship between the true rate constant for CH_3O_2 disproportionation, k_1 and the observed rate constant k_1', is strongly affected by the relative and absolute rates of the secondary reactions which consume CH_3O_2,

$$CH_3O_2 + CH_3O \rightarrow CH_2O + CH_3OOH \qquad (12)$$

$$CH_3O_2 + HO_2 \rightarrow CH_3O_2H + O_2 \qquad (4)$$

the termination reactions for CH_3O and HO_2, and the rate of conversion of CH_3O to HO_2. The relative importance of these processes can be qualitatively determined by varying $[O_2]$. In the limiting cases in which reactions (12) and (4) are both extremely rapid or extremely slow compared to competing processes, varying $[O_2]$ will have no effect on k_1', and $\frac{k_1'}{k_1}$ will be $\frac{k_{1a} + k_1}{k_1}$ or 1.0, respectively. If (12) is fast and (4) is slow, increasing $[O_2]$ will reduce k_3'. If (4) is fast and (12) is slow, increasing $[O_2]$ will increase k_3'.

Parkes[14] observed no change in k_3' as $[O_2]$ was varied from 3×10^{15} to 2.5×10^{19} molecule cm^{-3}. In this study, however, k_3' decreased by about 15% as $[O_2]$ was varied from 2.7×10^{16} to 6.7×10^{17} molecule cm^{-3}.

Addition of CO to the system resulted in a slight decrease in k_3'. CO may have reacted directly with CH_3O_2 by the reaction

$$CH_3O_2 + CO \rightarrow CH_3O + CO_2 \qquad (22)$$

or with CH_3O,

$$CH_3O + CO \rightarrow CH_3 + CO_2 \qquad (23a)$$

$$\rightarrow HCHO + HCO \qquad (23b)$$

thereby competing with reaction 12. If the decrease in k_3' is attributable solely to reaction 22, one can show that $k_{22} \leq 7 \times 10^{-18}$ cm^3 $molecule^{-1}$ s^{-1}. Only one study of reaction 23 has been conducted which gave $k_{23}/k_{11} = 5 \times 10^{-14}$.[32] If this measurement is correct, the presence of CO in the concentration range $1\text{-}5 \times 10^{18}$ molecule cm^{-3} should have resulted in almost complete removal of CH_3O by this reaction. However, since neither the rate constant not the branching ratio of reaction 23 are known with certainty, little can be said about the effect of adding CO except that it suggests that CH_3O is present and that k_{3a} is probably non-zero. The same conclusion can be reached concerning the effect of varying $[O_2]$.

To date, data on the temperature dependence of reaction 1 are limited to the observation by Parkes[14] that k_3' was independent of temperature between 288 and 298K. According to the most recent evaluation of kinetic and thermochemical data on CH_3O_2,[18] reaction 3a is endothermic by 3.5 kcal/mole. Even if reaction 3a had a 3.5 kcal/mole activation energy, it would be difficult to observe a temperature dependence for k_3 over the limited range they employed. Due to the large uncertainty on the CH_3O_2 enthalpy of formation, however, reaction 3a may be thermoneutral or even slightly exothermic.

Appendix A: The Effect of Reaction Product Absorption on the Measured First-Order Rate Constant, k'.

For a reaction such as

$$CH_3O_2 + NO_2 + M \xrightarrow{k} CH_3O_2NO_2 + M$$

in which both the minor reactant species (CH_3O_2) and a product ($CH_3O_2NO_2$) absorb a fraction of the analytical light, the effect of the product absorber on k' must be considered. From Beer's law,

$$I_t = I_o \exp(-\ell(\sigma_x x + \sigma_y y)) \qquad (A\text{-}1)$$

where:

I_t = transmitted light intensity

I_o = "true" I_o, i.e. intensity of the light beam emerging from the evacuated cell.

ℓ = path length

$x = [CH_3O_2]$

$y = [CH_3O_2NO_2]$

σ_x = CH_3O_2 absorption cross-section

σ_y = $CH_3O_2NO_2$ absorption cross-section

For first-order conditions,

$$x = x_o \exp(-k't) \qquad (A\text{-}2)$$

where:

$$k' = k[NO_2]$$

and,

$$y = x_o - x \qquad (A\text{-}3)$$

Substituting for x and y in (A-1)

$$I_t = I_o \exp(-\ell x_o ((\sigma_x - \sigma_y) \exp(-k't) + \sigma_y)) \; . \qquad (A\text{-}4)$$

Under experimental conditions, I_o is usually taken to be the transmitted light intensity at the end of the reaction. However, with a stable product absorber,

this will be somewhat less than the "true" I_o, i.e.

$$I_o' = \lim_{t\to\infty} I_t = I_o \exp(-\ell x_o \sigma_y) \qquad \text{(A-5)}$$

The apparent concentration of the minor reactant, x', is then:

$$x' = \ln(I_o'/I_t)$$

$$= \ln \frac{I_o \exp[-\ell x_o \sigma_y]}{I_o \exp(-\ell x_o((\sigma_x-\sigma_y)\exp(-k't) + \sigma_2))}$$

$$= \ell x_o(\sigma_x-\sigma_y) \exp(-k't) \qquad \text{(A-6)}$$

A plot of ln x' vs. t will have slope -k', the true first-order rate constant. If x' is calculated using I_o rather than I_o', plots of ln x' vs. t will be non-linear and the rate constant thus obtained will be in error.

When the product absorber comes from the second of two consecutive first-order reactions, e.g.,

$$CH_3O_2 + NO \rightarrow CH_3O + NO_2$$
$$CH_3O + NO + M \rightarrow CH_3ONO + M$$

the rate constant and the simple relationship derived above no longer apply and the correction to the first-order rate constant must be obtained by numerical techniques.

Acknowledgements

The authors are grateful to W. B. DeMore, G. W. Ray, J. C. Brock and J. Margolis for helpful discussions and to C. Kan (Ohio State University) and M. Kalloo (Merck, Sharp and Dohme Ltd.) for assistance in the preparation of azomethane. The research described in this paper was carried out at the Jet Propulsion Laboratory, California Institute of Technology, under NASA Contract NAS7-100.

References and Notes

1. (a) T. A. Hecht, J. H. Seinfeld and M. C. Dodge, Environ. Sci. Technol., 8, 327 (1974);
   (b) J. A. Logan, M. J. Prather, S. C. Wofsy and M. B. McElroy, Phil. Trans. Roy. Soc. London A, 290, 187 (1978);
   (c) W. L. Chameides, Geophys. Res. Lett., 5, 17 (1978).

2. C. W. Spicer, A. Villa, H. A. Wiebe and J. Heicklen, J. Amer. Chem. Soc., 95, 13 (1973).

3. R. Simonaitis and J. Heicklen, J. Phys. Chem., 78, 2417 (1974).

4. C. T. Pate, B. J. Finlayson and J. N. Pitts, Jr., J. Amer. Chem. Soc., 96, 6554 (1974).

5. R. A. Cox, R. G. Derwent, P. M. Holt and J. A. Kerr, J.C.S. Faraday I, 72, 2444 (1976).

6. R. Simonaitis and J. Heicklen, J. Phys. Chem., 79, 298 (1975).

7. (a) R. Atkinson, B. J. Finlayson and J. N. Pitts, Jr., J. Amer. Chem. Soc., 96, 6554 (1974);
   (b) N. Washida and K. D. Bayes, Int. J. Chem. Kinet., 8, 777 (1976).

8. C. J. Hochanadel, J. A. Ghormley, J. W. Boyle and P. J. Ogren, J. Phys. Chem., 81, 3 (1977).

9. C. S. Kan, R. D. McQuigg, M. R. Whitbeck and J. G. Calvert, Int. J. Chem. Kinet., 11, 921 (1979).

10. H. Adachi and N. Basco, Chem. Phys. Letters, 63, 490 (1979).

11. C. Anastasi, I. W. M. Smith and D. A. Parkes, J.C.S. Faraday I, 74, 1693 (1978).

12. E. Sanhueza, R. Simonaitis and J. Heicklen, Int. J. Chem. Kinet., 11, 907 (1979).

13. D. A. Parkes, D. M. Paul, C. P. Quinn and R. C. Robson, Chem. Phys. Letters, 23, 425 (1973).

14. D. A. Parkes, Int. J. Chem. Kinet., 9, 451 (1977).

15. R. A. Cox and G. S. Tyndall, Chem. Phys. Letters, 65, 357 (1979).

16. I. C. Plumb, K. R. Ryan, J. R. Steven and M.F.R. Mulcahy, Chem. Phys. Letters, 63, 255 (1979).

17. (a) C. J. Howard and K. M. Evenson, Geophys. Res. Letters, 4, 437 (1977);
   (b) C. J. Howard, W.M.O. Symposium on the Geophysical Aspects and Consequences of Changes in the Composition of the Stratosphere, Toronto, June 1978.

18. CODATA Task Group on Chemical Kinetics, "Evaluated Kinetic and Photochemical Data for Atmospheric Chemistry", J. Phys. Chem. Ref. Data, in press.

19. W. P. L. Carter, A. M. Winer, K. R. Darnall and J. N. Pitts, Jr., Env. Sci. Technol., 13, 1094 (1979).

20. R. T. Watson, S. P. Sander and Y. L. Yung, J. Phys. Chem., in press.

21. A. Savitsky and M.J.E. Golay, Anal. Chem., 36, 1627 (1964).

22. R. Renaud and L. C. Leitch, Can. J. Chem., 32, 545 (1954).

23. J. G. Calvert and J. N. Pitts, Jr., Photochemistry, Wiley, New York, 1966.

24. R. A. Graham, A. M. Winer and J. N. Pitts, Jr., Geophys. Res. Letters, 5, 909 (1978).

25. R. A. Graham, A. M. Winer and J. N. Pitts, Jr., J. Chem. Phys., 68, 4505 (1978).

26. R. Simonaitis and J. Heicklen, Chem. Phys. Letters, 65, 362 (1979).

27. J. Troe, J. Phys. Chem., 83, 114 (1979).

28. K. Luther and J. Troe, "Weak Collision Effects in Dissociation Reactions at High Temperatures", presented at the 17th International Symposium on Combustion, Leeds, Aug., 1978.

29. P. J. Robinson and K. A. Holbrook, Unimolecular Reactions, Wiley, London, 1972.

30. J. Troe, J. Chem. Phys., 66, 4758 (1977).

31. NASA Panel for Data Evaluation, "Chemical, Kinetic and Photochemical Data for Use in Stratospheric Modelling, Evaluation No. 2", Jet Propulsion Laboratory Publication 79-27, April 1979.

32. R. F. Hampson, Jr., and D. Garvin, Eds., "Reaction Rate and Photochemical Data for Atmospheric Chemistry-1977", NBS Special Publication 513, 1978.

33. T. Shimanouchi, J. Phys. Chem. Ref. Data, 6, 993 (1977).

CHAPTER III

RATES AND MECHANISM OF THE DISPROPORTIONATION OF BrO RADICALS

S. P. Sander and R. T. Watson*

Molecular Physics and Chemistry Section

Jet Propulsion Laboratory
Pasadena, CA 91103

ABSTRACT

The flash photolysis-ultraviolet absorption technique was used to measure the rate constants for the reactions

$$BrO + BrO \rightarrow 2Br + O_2 \qquad (1a)$$

$$BrO + BrO \rightarrow Br_2 + O_2 \qquad (1b)$$

over the temperature range 223-388 K and pressure range 50-475 Torr He. Two independent techniques were used to measure the branching ratio; one dependent and the other independent of the BrO absorption cross-section with the results in excellent agreement. The rate constant $k_1 = (k_{1a} + k_{1b})$ was found to be $9.58 \times 10^{-13} \exp((255 \pm 195)/T)$ where k_1 is defined by the relation $-d[BrO]/dt = -2k_1[BrO]^2$. The branching ratio $(k_{1a}/(k_{1a} + k_{1b}))$ was found to be 0.84 ± 0.03 at 298 K. An upper limit was also determined for the rate constant for the reaction:

$$BrO + O_3 \rightarrow Br + 2O_2 \qquad (2)$$

of $k_2 \leq 4 \times 10^{-15}$ cm^3 molecule^{-1} s^{-1} at 298 K.

INTRODUCTION

The disproportionation reactions of halogen monoxide radicals are among the most often-studied and least understood processes in gas-phase kinetics. Although much of the early work on these reactions was carried out using the flash photolysis-ultraviolet absorption (FP/UV) technique,[1,2] other methods such as discharge flow-mass spectroscopy (DF/MS),[3-6] molecular modulation-ultraviolet absorption (MM/UV)[7,8] and discharge flow-ultraviolet absorption (DF/UV)[9,10] have now been used to extend the pressure range and detection capability. In spite of this attention, the mechanisms of XO + XO reactions remain highly uncertain primarily because of difficulties associated with detecting the intermediates that appear to be involved. The initial step for all these reactions is probably the formation of a transient XOOX intermediate

$$XO + XO \underset{\leftarrow}{\overset{\rightarrow}{}} [XOOX]^{\neq}$$

which can either be collisionally stabilized, undergo rearrangement or decompose

$$[XOOX]^{\neq} \begin{cases} \xrightarrow{(M)} XOOX \\ \rightarrow [X\overset{O}{\diagdown\!\!\diagup}O\!-\!O\overset{\diagdown\!\!\diagup}{}X]^{\neq} \rightarrow X_2 + O_2 \\ \rightarrow X + XOO \end{cases}$$

The XOO radical may decompose

$$XOO \rightarrow X + O_2$$

or react with an X atom

$$X + XOO \rightarrow X_2 + O_2$$

Of course, the relative importance of the above reaction steps for the particular halogen species is influenced by the thermodynamic stability of the intermediates involved. In the fluorine case, evidence from two previous studies pointed to the formation of atomic fluorine as the primary product although the formation of F_2, F_2O_2 and FOO could not be ruled out.[3,11] In the ClO + ClO reaction, reaction paths forming $Cl_2 + O_2$, Cl + ClOO and Cl + OClO have all been proposed.[1-8,12-14] In addition, Cl_2O_2 and the ClOO radical have been identified as intermediates in this reaction.[1,2,7,8] The reaction is further complicated by an apparent pressure effect, and a poorly understood effect of $[O_2]$ on the quantum yield for O_3 disappearance in $Cl_2 - O_3$ mixtures.[15] In the only quantitative study of the IO + IO reaction, Clyne and Cruse[10] interpreted their data as indicating that the reaction channel forming atomic iodine is the only pathway.

Previous work on the BrO + BrO reaction has utilized the DF/MS,[5] DF/UV[9] and FP/UV[14,16] techniques. Agreement among these studies on the overall rate constant is poor with values of the rate constant for the overall BrO disappearance ranging from 1.0×10^{-12}[14] to 5.2×10^{-12}[9] cm^3 $molecule^{-1}$ s^{-1} (where the rate constant is defined by the relation $-d[BrO]/dt = 2k[BrO]^2$). None of these studies attempted to measure accurately the relative rates of the two most probable reaction channels

$$BrO + BrO \rightarrow BrOO + Br \qquad (1a)$$

$$\rightarrow Br_2 + O_2 \qquad (1b)$$

The temperature dependence of reaction 1 was reported by both Clyne and Cruse, and Brown and Burns. However, the temperature ranges employed in these studies did not extend below room temperature. Clyne and

Watson[5] used the DF/MS technique and therefore did not need to measure σ but their study was conducted only at room temperature.

All of the halogen monoxide disproportionation reactions have potential atmosphere significance. By converting two XO radicals (where X = F, Cℓ, Br or I) into two X atoms (or into an X_2 molecule which subsequently photolyzes), XO + XO reactions can take part in catalytic cycles which destroy odd oxygen in the troposphere and stratosphere.[17,18] A recent atmospheric modeling study[17] has shown that of all the catalytic cycles involving bromine species, the most efficient in terms of ozone destruction is the one which has the mixed disproportionation reaction,

$$BrO + C\ell O \rightarrow Br + C\ell + O_2$$

as its rate-determining step. When BrX mixing ratios ([BrX] = [Br] + [BrO] + [$BrONO_2$] + [HBr]) exceed 100 parts-per-trillion (ppt), the cycle involving the BrO + BrO reaction also becomes important. It is therefore necessary to measure both the rates and branching ratios of these reactions as accurately as possible.

In this study, the flash photolysis/UV absorption technique has been used to measure the rate constant for reaction 1 over the temperature range 223-388 K. The branching ratio, $k_{1a}/(k_{1a} + k_{1b})$, was determined at 298 K using two independent methods, one dependent and the other independent of the BrO cross-section. An upper limit was also determined for the rate constant for the reaction

$$BrO + O_3 \rightarrow Br + 2O_2 \qquad (2)$$

EXPERIMENTAL SECTION

The flash photolysis/UV absorption system has been described in detail previously.[19] The flash assembly consists of four concentric tubes comprising the reaction cell, photolyzing light filter, xenon flash lamp and cooling/heating jacket. Two identical cells were used; one constructed of quartz and the other of pyrex. In contrast to other studies using this system,[19] the cell was not operated in the flowing mode. Reagents were thoroughly pre-mixed in an external 2-liter volume before being admitted into the cell. The optical system consists of a 150 watt xenon analytical lamp, 8-pass White mirror system with 740 cm path length and McPherson Model 216.5 0.5 m monochromator. The monochromator wavelength was calibrated with a low-pressure mercury line source. Signals from the photomultiplier tube (EMI 9659QA) are amplified and stored in a signal averager (Tracor-Northern 570A) operating in the analog mode. The data is punched onto paper tape for subsequent computer analysis.

BrO radicals were monitored by their absorption at 339.0 nm ($A\,^2\Pi(v' = 4) \leftarrow X\,^2\Pi(v'' = 0)$ transition).[20] The absorption spectrum of BrO consists of a series of vibrational bands on an underlying continuum which, in the 290-300 nm region, has a cross-section of $\sim 2 \times 10^{-18}$ cm^2. Since the finite monochromator resolution results in the overlap of several rotational lines within the (4-0) band, the effective cross-section was a function of the monochromator slit width and wavelength setting. A slit width of 100 μm was used resulting in a resolution of 0.09 nm FWHM as measured by scanning a mercury line source. The time-resolved absorption of O_3 was also monitored. A beam splitter reflected part of the analytical light exiting the reaction cell into a

0.25 m monochromator and EMI 9659 photomultiplier. Ozone was monitored in the 250-280 nm spectral region. Both the O_3 and BrO absorption signals were recorded simultaneously by the signal averager.

Production of BrO ($^2\Pi$) Radicals

Two chemical systems were used to produce BrO radicals. In the first, a Br_2/O_3/He mixture was photolyzed in a pyrex reaction cell to produce Br atoms which reacted with O_3 to form BrO (unless otherwise indicated, rate constants cited in the text are from Ref. 21):

$$Br_2 + h\nu(\lambda > 300 \text{ nm}) \rightarrow 2Br \qquad (3)$$

$$Br + O_3 \rightarrow BrO + O_2 \qquad (4) \qquad k_4 = 1.1 \times 10^{-12} \text{ cm}^3\text{molecule}^{-1}\text{s}^{-1}$$

In order to elucidate the mechanism of the BrO self-reaction, experiments were conducted in which either Br or O_3 was in excess over the other. At the flash energies used in this study (300-1500 Joules/flash) between 2 and 10 percent of the Br_2 is dissociated. The primary fate of the excess Br is atomic recombination,

$$Br + Br + M \rightarrow Br_2 + M \qquad (4a) \qquad k_{4a} = 3.0 \times 10^{-33} \text{ cm}^6\text{molecule}^{-2}\text{s}^{-1}$$

and, to a lesser extent, heterogeneous removal on the wall,

$$Br + \text{wall} \rightarrow \tfrac{1}{2}Br_2 \qquad (4b).$$

A small amount of O_3 photolysis was observed in the pyrex cell. Since this would have affected the results of the quantum yield studies, photolysis of O_3 was eliminated by filling the filter cell with one atmosphere of SO_2. The strong absorption band of SO_2 at 300 nm reduced the ozone photolysis to immeasurable levels without affecting the dis-

sociation of Br_2.

In the second method of BrO formation, Br_2-O_2 mixtures were photolyzed in the quartz reaction cell:

$$O_2 + h\nu(\lambda > 180 \text{ nm}) \rightarrow 2O(^3P) \quad (5)$$

$$O + Br_2 \rightarrow BrO + Br \quad (6) \quad k_6 = 1.4 \times 10^{-11} \text{ cm}^3\text{molecule}^{-1}\text{s}^{-1}$$

The photolytic dissociation of O_2 was about 0.003% at 1150 J. Other processes competing for the removal of atomic oxygen,

$$O + O_2 + M \rightarrow O_3 + M \quad (7) \quad k_7 = 5.6 \times 10^{-34} \text{ cm}^6 \text{ molecule}^{-2}\text{s}^{-1}$$

$$O + BrO \rightarrow Br + O_2 \quad (8) \quad k_8 = 3 \times 10^{-11} \text{ cm}^3 \text{ molecule}^{-1}\text{s}^{-1}$$

were negligible relative to reaction 6 under the experimental conditions of high Br_2 concentrations employed in this study. No difficulties were therefore encountered with regeneration of BrO from the reaction of Br with photolytically generated O_3.

The ranges of reagent concentrations were (in molecule cm^{-3}): $[Br_2] \times 10^{-16}$: 2.4-16 (excess Br); $[Br_2] \times 10^{-13}$: 5.6-36 (excess O_3); $[O_3] \times 10^{-13}$: 2.3-31 (excess Br); $[O_3] \times 10^{-15}$: 4.2-8.5 (excess O_3); $[O_2] \times 10^{-17}$: 2.2-30. $[BrO]_o$ (in molecule cm^{-3}) ranged from 1.3×10^{13} to 3.0×10^{14}. In all experiments, BrO was formed on a time scale ($t_{1/2} \leq$ 150 μsec) at least ten times faster than its loss ($t_{1/2} \geq 1.5$ msec). In the Br_2-O_3 system, BrO decays were obtained in a single flash since the O_3 was depleted by reaction with Br. In the Br_2-O_2 experiments, the reactants were regenerated after each flash permitting multiple BrO decays to be averaged with each filling. Ten to fifty flashes were used depending on $[BrO]_o$ and the enhancement in signal-to-noise ratio desired.

The temperature of the reaction cell was controlled by circulating methanol ($T < 298$ K) or ethylene glycol ($T \geq 298$ K) through the outer jacket from a constant temperature bath (Haake). Diluent gases with the following stated purities were used: He (Linde UHP Grade, 99.999%), O_2 (Linde UHP Grade, 99.99%). Br_2 (J.T. Baker Reagent Grade) was thoroughly de-gassed and distilled, retaining the middle fraction. O_3 was prepared by passing an electric discharge through O_2 at 77 K with subsequent purification.

RESULTS

The bimolecular disproportionation of BrO radicals can be described by a second-order rate law:

$$-\frac{d[BrO]}{dt} = 2\,k_1[BrO]^2 \quad ,$$

the solution of which is:

$$\frac{1}{[BrO]} - \frac{1}{[BrO]_o} = 2\,k_1 t \quad .$$

The BrO concentration is related to the absorption signal by Beer's Law, leading to the equation

$$\frac{\ell}{\ell n(I_o/I_t)} = \frac{2\,k_1 t}{\sigma} + \frac{\ell}{\ell n(I_o/I')}$$

where: ℓ = absorption path length

σ = BrO absorption cross-section

I_o = incident light intensity

I_t = transmitted light intensity at time t

I' = transmitted light intensity immediately after the flash.

Plots of $\ell/\ell n(I_o/I_t)$ vs. time should be linear with slope $2\ k_1/\sigma$. k_1 is therefore obtained from the product of two experimental observables, k_1/σ and σ.

Determination of σ

Spectroscopic work on the BrO absorption spectrum has indicated that the (4,0) band of $A\ ^2\Pi \rightarrow X\ ^2\Pi$ transition appears to be the strongest.[9.14,16,20] Absolute BrO absorption cross-section measurements have been made in other studies. However, since an integration over several narrow rotational lines is involved, σ is a strong function of the monochromator spectral bandwidth and wavelength setting. A separate determination of σ for this set of experimental conditions was therefore required. A wavelength for the analysis of BrO was selected within the (4,0) band (339.0 nm) that ensured that no part of the monochromator spectral response extended beyond the band head. The cross-section was measured by determining the initial light absorption due to BrO in Br_2-O_3 mixtures containing an excess of Br and a known concentration of O_3. Since $[BrO]_o = [O_3]_o$ in this system, σ could be then determined from Beer's Law, i.e.

$$\sigma = \frac{\ell n[I_o/I']}{\ell[O_3]_o}$$

The initial light absorption for each experiment was found by back-extrapolating the BrO decay plot to t = 0 to obtain the y-intercept, y_o. This back-extrapolation is valid provided that BrO is formed much more quickly than it is lost and that the duration of the flash is short compared to the time period of the extrapolation. Both these requirements are satisfied. The average ratio of the half-lives for BrO removal and formation is 132 with values ranging from 36 to 317. This

is large enough that the formation of BrO can be considered instantaneous. Similarly, the duration of the flash, $\sim$ 15 μs, is much shorter than the 1-2 msec extrapolation required to obtain y_o. Since $y_o = (\sigma[BrO])^{-1}$, a plot of y_o^{-1} vs. $[O_3]_o$ should be linear with slope σ. The results of 28 experiments are shown in Fig. 1. Good linearity is obtained indicating that stoichiometric conversion of O_3 to BrO takes place on a rapid time scale. The value of σ obtained from the slope of the least-squares line in Fig. 1 is 1.01×10^{-17} cm^2 while the value obtained by averaging the individual results is $(1.14 \pm 0.14) \times 10^{-17}$ cm^2. No physical significance is attached to the small intercept in the least-squares line, and the preferred value of σ is obtained from the simple average. The same procedure was used to derive σ at 223 K and 388 K (see Table I).

Determination of $(k_{1a} + k_{1b})/\sigma$

The quantity $(k_{1a} + k_{1b})/\sigma$ was measured using two chemical systems. In the first, Br_2-O_3 mixtures were photolyzed with conditions adjusted to give an excess of Br over O_3 ($30 \leq [Br]_o/[O_3] \leq 300$) during the time in which the decay of BrO was monitored. Under these conditions, bromine atoms formed from reaction 1a add to the pool of excess atoms produced by the photolysis flash. Since reaction 1b leads to the formation of stable products (Br_2 and O_2) the observed rate constant is the sum of the rate constants of the two channels. The same quantity, $(k_{1a} + k_{1b})/\sigma$, is also obtained in experiments conducted on Br_2-O_2 mixtures. BrO radicals formed in this system by reactions 5 and 6 disappear by both reaction channels 1a and 1b with no subsequent regeneration of BrO. Values of k_1/σ obtained using both chemical systems are given in Tables II and III. In these experiments, k_1 was invariant with $[O_2]$ ($2.2\text{-}30 \times 10^{17}$

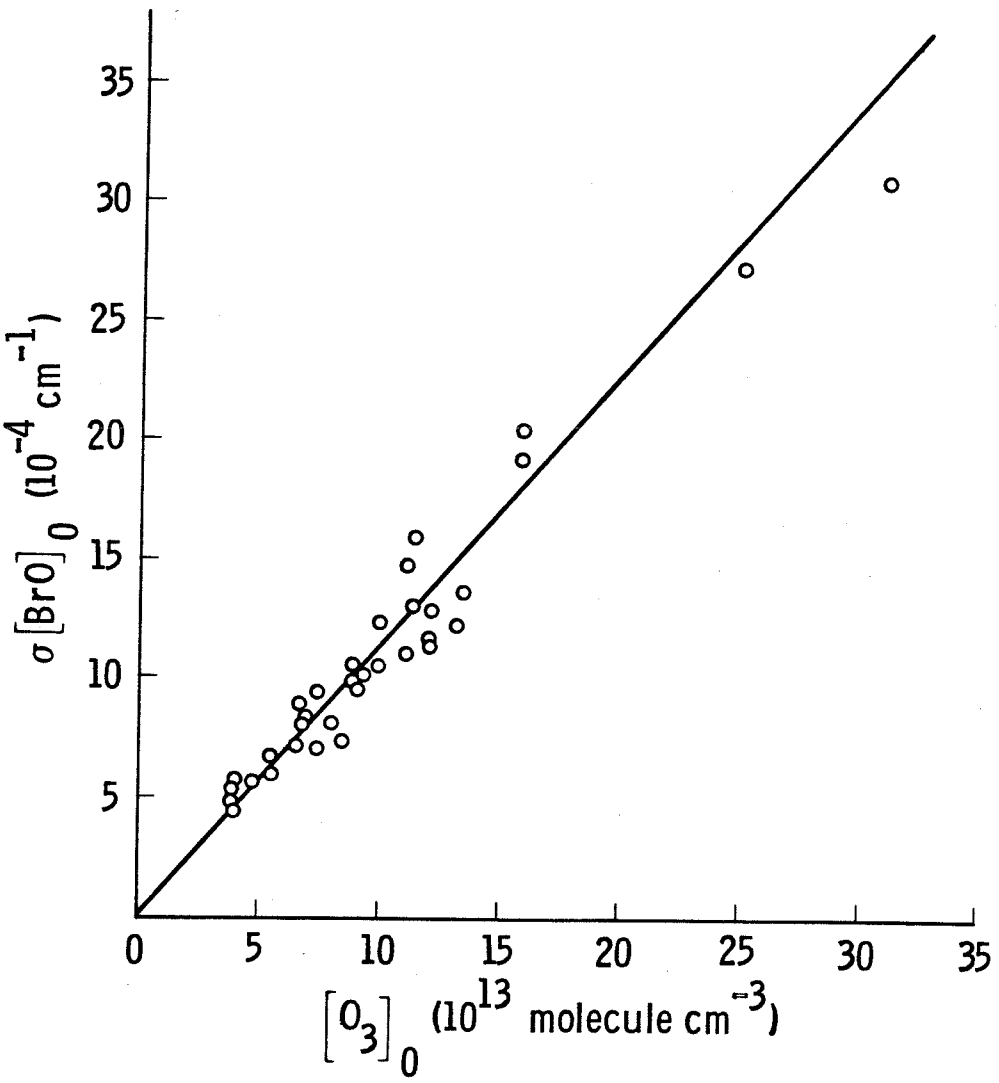

Figure 1. Variation of $\sigma[BrO]_o$ with $[O_3]_o$. The slope of the plot is determined from the mean value of the individual measurements.

Table I. Summary of Data for the BrO + BrO Reaction

T / K	σ / $\times 10^{17}$ cm^2	$2k_1/\sigma$ / $\times 10^{-5}$ cm molecule^{-1} s^{-1}	k_1 / $\times 10^{12}$ cm^3 molecule^{-1} s^{-1}
223	1.56 ± 0.14	3.88 ± 0.47	3.03 ± 0.64
298	1.14 ± 0.14	3.80 ± 0.73	2.17 ± 0.68
388	0.961 ± 0.12	3.95 ± 0.79	1.90 ± 0.62

T / K	$2k_{1b}/\sigma$ / $\times 10^{-4}$ cm molecule^{-1} s^{-1}	k_{1b} / $\times 10^{13}$ cm^3 molecule^{-1} s^{-1}	Method[a]
298	6.07 ± 0.45	3.46 ± 0.68	1
298		4.12 ± 1.99	2

Method 1: Measurement of second-order BrO decay in Br_2-O_3 (excess O_3) system.

Method 2: Measurement of quantum yield of O_3 destruction in Br_2-O_3 (excess O_3) system.

Table II. Experimental Data from the Br_2-O_3 System (excess Br).

T	p_{TOT}	Flash Energy	$[O_3]$ x 10^{-14}	$[Br_2]$ x 10^{-16}	$2k/\sigma$ x 10^{-5}	y-intercept	σ x 10^{17}	k^a x 10^{12}
K	Torr	Joules	molecule cm^{-3}		cm $molecule^{-1}$			molecule s^{-1}
298	50	800	0.91	8.2	2.10	1040	1.05	1.20
		800	1.21	8.0	2.35	775	1.07	1.34
		800	1.15	7.8	2.33	799	1.09	1.33
		800	1.31	7.8	2.46	829	0.920	1.40
		800	1.35	7.8	2.39	737	1.00	1.36
		800	0.93	8.0	2.86	984	1.09	1.63
		800	1.1	8.0	3.07	895	1.02	1.75
	125	800	3.1	8.0	4.27	325	0.993	2.43
		800	0.74	8.0	4.33	1050	1.29	2.47
		800	1.1	8.0	2.82	675	1.35	1.61
		800	0.74	8.0	3.88	1175	1.15	2.21
		800	0.39	8.0	2.97	1925	1.33	1.69
		800	0.69	8.0	3.77	1250	1.16	2.15
		800	0.39	8.0	3.46	2320	1.11	1.97
	250	800	2.5	8.0	4.18	368	1.09	2.38
		800	1.0	8.0	4.09	812	1.23	2.33
		800	0.69	8.0	4.62	1210	1.20	2.63
		800	0.23	8.0	3.75	2875	1.51	2.14
		800	0.54	8.0	3.49	1680	1.10	1.99
		800	0.46	8.0	3.77	1770	1.23	2.15
		800	1.2	8.0	3.50	862	0.967	2.00
		800	1.2	8.0	3.72	883	0.944	2.12
		1458	0.656	7.8	2.68	1385	1.10	1.53
		1458	0.803	8.0	2.65	1225	1.01	1.51
		1458	0.403	7.3	2.38	2125	1.17	1.36
		1458	0.407	8.5	2.45	1750	1.40	1.40
		875	1.33	2.45	4.80			2.74
		875	1.21	3.90	4.70			2.68
		875	0.52	15.8	3.02			1.72

Table II. (Cont.)

T	p_{TOT}	Flash Energy	$[O_3]$ x 10^{-14}	$[Br_2]$ x 10^{-16}	$2k/\sigma$ x 10^{-5}	y-intercept	σ x 10^{17}	k^a x 10^{12}
K	Torr	Joules	molecule cm^{-3}		cm $molecule^{-1}$			molecule s^{-1}
		875	1.03	16.0	3.25			1.85
		875	1.21	8.54	4.12			2.35
		875	1.37	4.15	4.35			2.48
		875	1.34	6.11	3.63			2.07
		875	1.12	10.1	3.83			2.18
		875	1.10	12.1	4.04			2.30
		875	1.10	13.8	3.13			1.78
		893	1.00	7.99	3.91			2.23
		705	0.97	8.10	3.77			2.15
		500	1.03	8.0	3.90			2.22
		300	1.09	8.0	4.67			2.66
		400	0.95	8.0	4.51			2.57
		598	0.87	8.0	4.44			2.53
		800	0.87	8.0	4.45			2.54
		1200	0.98	8.0	3.19			1.82
	475	800	1.59	8.0	4.69	487	1.29	2.67
		800	1.59	8.0	4.47	526	1.19	2.55
		800	0.885	8.0	4.33	1000	1.13	2.47
		800	0.390	8.0	3.36	2250	1.14	1.92
		800	0.542	8.0	3.64	1500	1.23	2.07
		800	3.07	8.0	4.24			2.42
223	250	1458	0.622	5.3	3.37	1080	1.49	2.63
		1458	0.610	4.6	3.71	1030	1.59	2.89
		1458	0.570	5.1	3.49	1250	1.40	2.72
		1458	0.482	5.1	3.24	1300	1.60	2.53
		1458	0.354	5.4	3.69	1925	1.47	2.88
		1458	0.506	5.1	3.27	1100	1.80	2.55
388	250	1458	0.856	8.3	3.58	1050	1.11	1.72
		1458	0.686	8.1	3.12	1800	0.831	1.50
		1458	0.470	8.2	2.90	2325	0.915	1.39
		1458	0.588	8.2	2.89	1725	0.986	1.39

[a] computed using σ values from Table I.

Table III. Experimental Data for the Br_2-O_2 System

T	P_{TOT}	Flash Energy	$[O_2]$ x 10^{-18}	$[Br_2]$ x 10^{-16}	$2k/\sigma$ x 10^{-5}	k^a x 10^{12} cm^3
K	Torr	Joules	molecule cm^{-3}		cm $molecule^{-1}$	$molecule^{-1}$ s^{-1}
298	50	1450	1.31	1.17	3.88	2.21
	75	1450	1.31	1.17	4.17	2.38
	100	1450	1.30	1.16	4.32	2.46
	250	1450	1.18	1.49	4.22	2.41
		1450	0.773	1.54	4.30	2.45
		1450	0.364	1.54	3.56	2.03
		1450	0.217	1.57	4.83	2.75
		1450	3.03	1.47	4.82	2.75
		1450	1.25	1.12	4.04	2.30
		1450	1.34	1.20	4.47	2.55
		1012	1.30	1.74	4.25	2.42
		620	1.27	1.71	4.49	2.56
		1150	1.57	7.51	4.33	2.47
		1150	1.58	5.94	3.95	2.25
		1150	1.56	4.67	4.00	2.28
		1150	1.69	1.60	4.50	2.57
		1150	1.61	8.43	3.38	1.93
		1150	1.60	6.66	3.63	2.07
		1150	1.63	1.62	4.38	2.50
		1150	1.55	5.94	3.79	2.16
		1150	1.55	3.99	4.11	2.34
		1150	1.55	3.07	4.40	2.51
		1150	1.55	14.2	2.20	1.25
		1150	1.55	10.6	2.63	1.50
		1150	1.55	9.36	2.73	1.56
		1150	1.55	6.76	4.18	2.38
		1500	1.58	0.888	3.75	2.14
		1500	1.58	0.800	4.04	2.30
		1500	1.58	0.824	4.25	2.42
		1500	1.58	0.763	4.15	2.37

Table III. (Cont.)

T	p_{TOT}	Flash	$[O_2]$ x 10^{-18}	$[Br_2]$ x 10^{-16}	$2k/\sigma$ x 10^{-5}	k^a x 10_3^{12}
K	Torr	Joules	molecule cm^{-3}		cm $molecule^{-1}$	cm^3 $molecule^{-1}$ s^{-1}
	380	1450	1.34	1.20	4.87	2.78
	475	1450	1.30	1.16	4.50	2.57
235	250	1150	1.50	4.27	4.13	3.22
		1150	1.53	2.98	4.55	3.55
		1150	1.56	1.56	4.30	3.35
		1150	1.56	4.66	4.16	3.24
		1150	1.62	1.80	4.20	3.28
		1150	1.61	3.99	4.44	3.46
393	250	1150	1.55	6.12	4.58	2.20
		1150	1.58	3.06	4.13	1.98
		1150	1.61	1.67	5.16	2.48
		1150	1.51	8.54	4.42	2.12
		1150	1.53	6.84	4.49	2.16
		1150	1.57	5.29	4.27	2.05

[a] computed using σvalues from Table I.

molecule cm^{-3}), flash energy (300-1500 J/flash) and total pressure (50-475 Torr helium) within experimental uncertainty. The data at 50 Torr average about 20% less than the data at higher pressures but no significance is attached to this. A small inverse dependence of k_1 on $[Br_2]$ at 298 K was observed with the rate constant decreasing by 20% as $[Br_2]$ was increased from 1 to 10 x 10^{16} molecule cm^{-3}. This effect was not considered to be significant within the scatter of the data and it was not observed at other temperatures. BrO decays were followed over a range of 20 to 100 in concentration with excellent linearity being obtained in the second-order plots ($1/(\sigma[BrO])$ vs. time). One such decay plot is shown in Fig. 2. The ratio $2k_1/\sigma$ was measured at 223, 298 and 388 K and found to be independent of temperature within experimental error (see Table I). Values of k_1/σ obtained using the Br_2-O_3 and Br_2-O_2 systems were in excellent agreement indicating that the measured rate constant is independent of the method of BrO production. The final rate constants in Table I were obtained by averaging the individual measurements of k_1/σ made using both chemical systems.

Determination of Branching Ratio

The quantity k_{1b}/σ was measured using a variation of the Br_2-O_3 system described above. In these experiments, concentrations of Br_2 and O_3 were adjusted to give $[O_3]_o > 100[Br]_o$ after the photolytic flash. Bromine atoms formed in the flash were stoichiometrically converted to BrO by reaction 2,

$$Br + O_3 \rightarrow BrO + O_2 \qquad (2)$$

so that $[BrO]_o = [Br]_o$. Furthermore, atomic bromine subsequently formed by reaction 1a,

$$BrO + BrO \rightarrow 2Br + O_2 \qquad (1a)$$

was also rapidly converted back to BrO by reaction 2. In this manner,

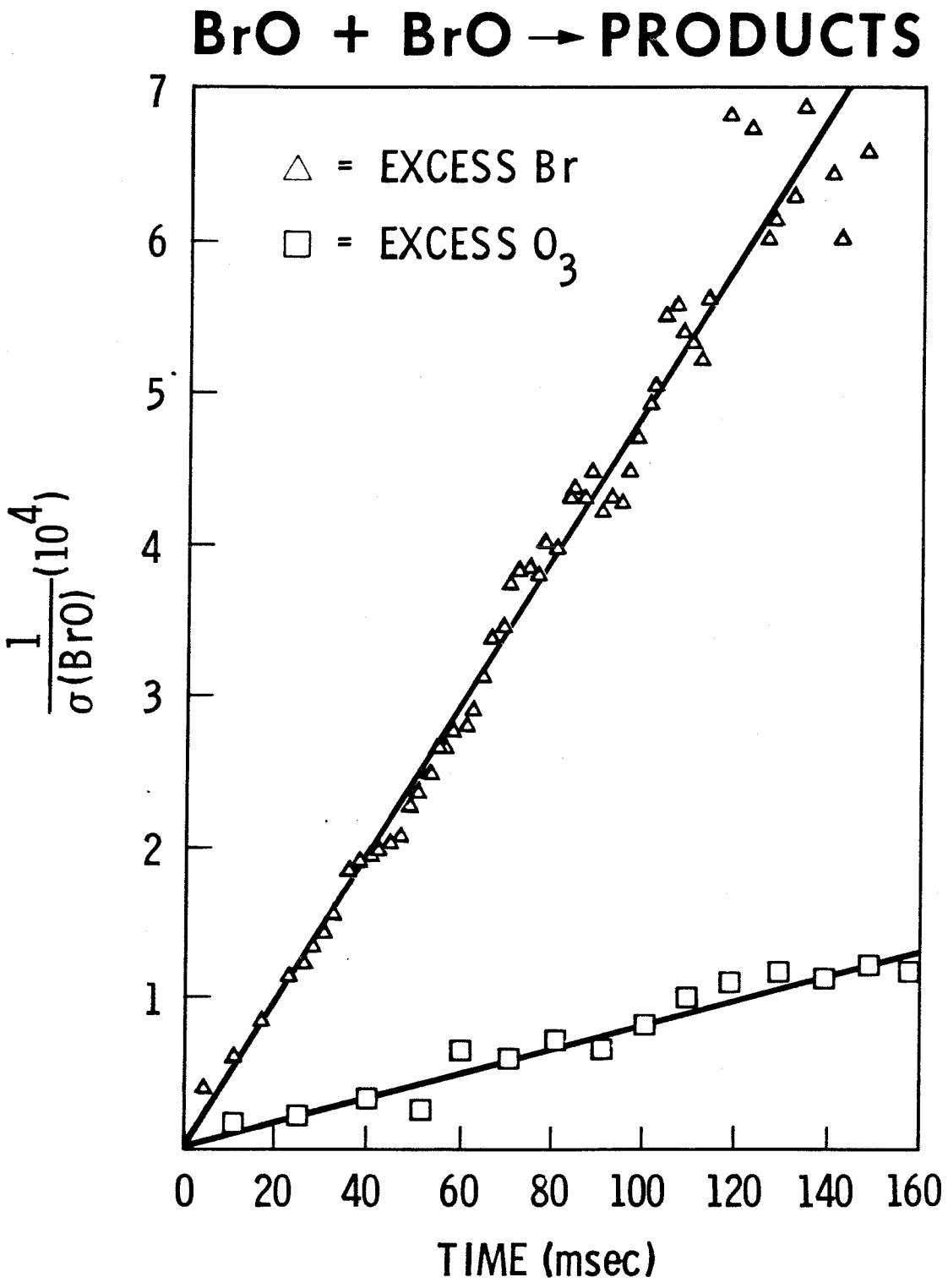

Figure 2. Second-order decay plots of BrO radicals in Br_2-O_3-He mixtures with excess atomic bromine (Δ) and excess O_3 (□).

given a sufficient excess of O_3, the only route by which BrO disappearance could take place was reaction 1b,

$$BrO + BrO \rightarrow Br_2 + O_2 \qquad (1b)$$

and the measurement of the slope of the second-order decay of BrO gave k_{1b}/σ. The branching ratio, f, of reaction 1, is defined by the relation

$$f \equiv \frac{k_{1a}}{k_{1a} + k_{1b}} = \frac{k_{1a}}{k_1} \quad .$$

Measurement of k_{1b}/σ and k_1/σ permits f to be determined from the equation

$$f = 1 - \frac{k_{1b}/\sigma}{(k_{1a} + k_{1b})/\sigma} \quad .$$

In this manner the branching ratio can be determined without explicitly measuring σ. Table IV lists the results of the 23 runs conducted under conditions of excess O_3 over Br. At 298 K, an average value of (6.07 ± 0.45) x 10^4 cm molecule^{-1} s^{-1} was obtained for $2k_{1b}/\sigma$. Combining this with the value of (3.80 ± 0.73) x 10^5 cm molecule^{-1} s^{-1} obtained for $2k_1/\sigma$ (Table I), the branching raio is found to be 0.84 ± 0.03.

A second, indpendent method for the determination of the branching ratio is made possible by the measurement of $\Delta[O_3]$ and $[BrO]_o$ in the excess O_3-BrO system. Since atomic bromine is regenerated in step 1a, O_3 undergoes chain decomposition, the extent of which is determined by the relative rates of the terminating and non-terminating steps. By assuming that Br is in steady-state and utilizing the second-order rate law for BrO disappearance it can be shown that

$$\Delta[O_3] \equiv [O_3]_t - [O_3]_{t=0}$$

$$= 2k_{1a}[BrO]_o^2 \left[\frac{t}{1 + 2k_{1b}[BrO]_o t}\right]$$

Table IV. Experimental Data for the Br_2-O_3 System (excess O_3).

P_{TOT} Torr	T	Flash Energy Joules	$[O_3]$ x 10^{-15} molecule cm^{-3}	$[Br_2]$ x 10^{-14} molecule cm^{-3}	$\Delta[O_3]$ x 10^{-14} molecule cm^{-3}	$2k/\sigma$ x 10^{-4} cm $molecule^{-1}$	y-intercept cm $molecule^{-1}$
250	298	911	4.17	2.31		6.86	1440
			6.91	2.33		6.24	1320
			6.61	2.83		6.31	1070
			4.78	2.35		6.44	1500
			6.03	2.35		5.83	1560
			7.13	2.03		6.34	1430
			5.00	2.27		6.70	1500
			5.75	2.04		6.50	1320
			7.51	2.40		5.26	1470
			8.43	1.58		5.77	1910
			8.46	3.55		5.16	1220
			6.67	3.60	4.42	6.09	1040
			5.84	2.59	3.74	6.42	1270
			6.04	2.50	3.63	6.20	1225
			5.73	2.79	3.62	5.65	1440
			6.23	1.76	2.48	6.16	1660
			6.60	3.53	4.23	6.45	918
			6.81	3.17	3.90	5.57	1230
			6.51	1.03	1.17	6.47	2760
			7.63	1.28	2.79	6.14	2050
			5.39	1.31	1.83	3.73	2340
			6.65	0.839	1.41	5.56	3000
			5.17	0.560	1.20	5.72	5000

In the limit as the reaction goes to completion ($t \rightarrow \infty$),

$$\Delta[O_3] = \frac{k_{1a}}{k_{1b}} [BrO]_o$$

or, in terms of the branching ratio,

$$\Delta[O_3] = \frac{f}{1-f} [BrO]_o \ .$$

In practice, this equation must be modified to account for the additional O_3 loss caused by the initial formation of BrO by reaction 2. Thus,

$$\Delta[O_3] = \frac{f}{1-f} [BrO]_o + [BrO]_o \qquad (1)$$

or,

$$f = \frac{\Delta[O_3] - [BrO]_o}{\Delta O_3} \ .$$

In terms of the quantum yield for O_3 destruction,

$$\phi_{O_3} \equiv \frac{\Delta[O_3]}{I_a}$$

$$= \frac{2}{1-f} \ .$$

Equation 1 predicts that a plot of $\Delta[O_3]$ vs. $[BrO]_o$ should be linear with slope $1/(1-f)$. Twelve experiments were conducted in which $\Delta[O_3]$ and $[BrO]_o$ were both measured, the former by UV absorption before and after the flash, and the latter by back-extrapolation of the second-order BrO decay to $t = 0$. In all cases, the ratio $[O_3]_o/[BrO]_o$ was sufficiently large (≥ 80) that BrO formation was much more rapid than its removal. Values of $\Delta[O_3]$ vs. $[BrO]_o$ are plotted in Fig. 3. The excellent linearity of this plot over a wide range of $[BrO]_o$ confirms that O_3 is being

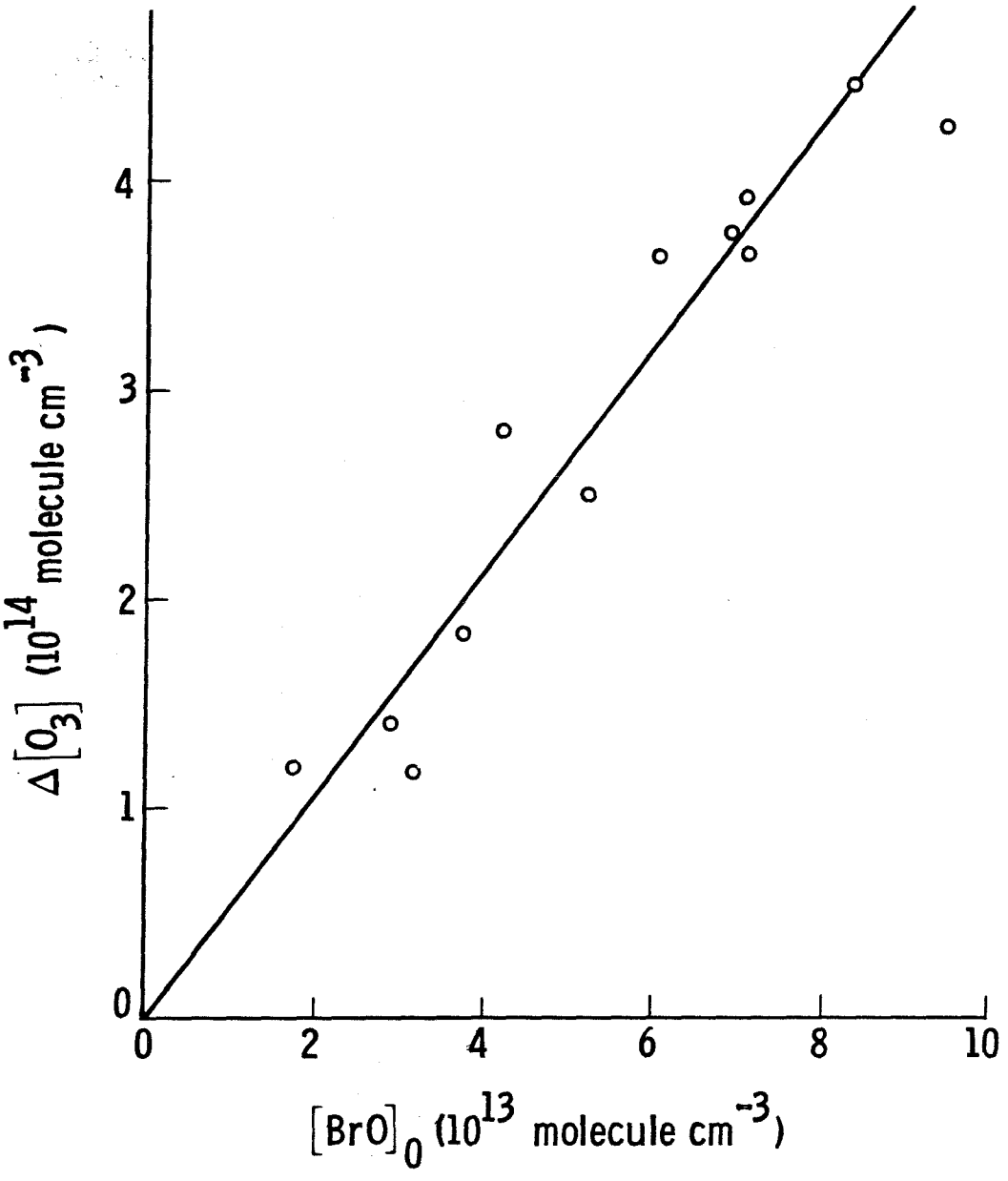

Figure 3. Variation of the ozone loss with the initial BrO concentration in the Br_2-O_3-He system with excess O_3.

destroyed by a catalytic chain. However, if the chain length were limited only by the homogeneous or heterogeneous recombination of atomic bromine, much more ozone removal would be expected. This suggests that Br is being catalytically recombined through a terminating channel in the BrO + BrO reaction (Step 1b). From the slope of the line in Fig. 3, 5.25 ± 0.88, the branching raio is found to be 0.81 ± 0.03. The uncertainty in the branching ratio does not explicitly take into account the uncertainty in σ. The true experimental error is therefore somewhat larger than 0.03. This value of the branching ratio is in excellent agreement with the value 0.84 ± 0.03 determined by measuring the decay rates of BrO directly. The agreement between the two independent methods implies that the measurement of σ is correct and that there are no unknown removal mechanisms for O_3. This allows an upper limit to be placed on the rate constant for the reaction

$$BrO + O_3 \rightarrow Br + 2O_2 \qquad (2)$$

by assuming that if reaction 2 accounted for more than 10% of the total O_3 removal rate, the actual quantum yield for O_3 destruction would exceed the predicted value by an amount equal to the experimental uncertainty. Using typical concentrations of BrO and O_3, one obtains $k_2 \leq 4 \times 10^{-15}$ cm^3 $molecule^{-1}$ s^{-1}.

DISCUSSION

Measurement of k_1/σ and σ

Of the three previous determinations of k_1, two used spectrophotometric detection[9,14] and one utilized mass spectrometry. Since absolute concentrations of BrO are required, use of spectrophotometry requires that the BrO absorption cross section, σ, and the quantity

k_1/σ be determined. The results of these measurements are summarized in Table V.

Clyne and Watson[5,6] have thoroughly examined the methods used by Basco and Dogra,[14] and Clyne and Cruse[10] to obtain σ and k_1/σ and have pointed out the possible sources of error. The method used by Basco and Dogra relies on the assumption that the initial amount of BrO formed in the photolysis of Br_2-OCℓO mixtures is equal to Δ[OCℓO]. Clyne and Watson have shown that because the BrO + CℓO and BrO + BrO reactions regenerate atomic bromine rather than forming BrCℓ and Br_2 exclusively, the mechanistic interpretation of Basco and Dogra is incorrect. This, along with the fact that the rates of formation and removal of BrO were not sufficiently different in their system, cast doubt on their determination of σ.

The method of Clyne and Cruse was based on the spectrophotometric measurement of Br_2, BrO and O_3 in a discharge flow system. The quantity k_1/σ was determined directly from the BrO decay and σ was determined from the equation

$$\Delta\chi + \frac{k_1}{\sigma}\int_{t_1}^{t_2} \chi^2 dt = \sigma\,\Delta[O_3] \qquad (2)$$

where:

$$\chi = \sigma[BrO] = \frac{1}{\ell}\,\ell n(I_o/I_t)$$

ℓ = absorption path length

The need to evaluate σ from an integral expression (Eqn. (2)) arises from an unfavorable choice of reaction conditions. In their experiments, [Br] was not high enough to convert all of the O_3 to BrO on a time scale short compared to the BrO decay. The formation and decay of BrO are fully coupled and, as a result, the determination of σ is dependent on

Table V. Previous Work on the BrO + BrO Reaction at 298 K.

Ref.	Technique[a]	k_1/σ[b] x 10^{-5} cm molec^{-1} s^{-1}	σ[c] x 10^{18} cm^2 molec^{-1}	k_1 x 10^{12} cm^2 molec^{-1}s^{-1}
14	FP/UV	2.2 ± 0.08	4.7 ± 0.4	1.1 ± 0.2
9[d]	DF/UV	6.6 ± 0.7	8.0 ± 0.9	5.2 ± 0.6
5	DF/MS			3.2 ± 0.7
This work	FP/UV	1.9 ± 0.4	11 ± 1.4	2.2 ± 0.7

[a] Flash photolysis (FP), discharge flow (DF), ultraviolet absorption (UV), mass spectroscopy (MS).

[b] Defined such that $-(BrO) = 2k_1(BrO)^2$.

[c] Cross-sections measured near (4-0) band head of BrO at 338.3 nm but not necessarily at the same wavelength or spectral resolution.

[d] Data obtained at 293 K.

the value obtained for k_1/σ. Since the rate constant k_1 is given by the product of k_1/σ and σ, and σ is itself a function of k_1/σ, any error in the measurement of k_1/σ is reflected as a higher-order error in k_1. For instance, using the data given as an example by Clyne and Cruse, increasing k_1/σ by a factor of 3 from 5 to 15 x 10^5 cm s^{-1} results in an increase in k_1 of a factor of $\sim$ 5. Reasons for possible errors in the measurement of k_1/σ have been discussed by Clyne and Watson.

In contrast to the experimental conditions in the Clyne and Cruse study, the methods for determining k_1/σ and σ in this work are totally independent. This is a consequence of the complete decoupling of BrO formation and removal. The back-extrapolation to t = 0 of the $[BrO]^{-1}$ vs. time plots in our excess Br experiments are sufficiently short that errors in the measurement of k_1/σ are not reflected in the determination of σ.

Values for the BrO cross-section obtained in the three absorption studies cannot be meaningfully compared, primarily because σ depends strongly on the experimental spectral parameters. Clyne and Cruse used a spectral bandwidth of about 10Å whereas the bandwidth was only 1Å in this study. As expected, this leads to a higher reported cross-section in this study since the bandwidth encompasses a region of the band with a higher average rotational line density. The spectral bandwidth used in the Basco and Dogra study was not specified.

Determination of k_1 and Branching Ratio

The results of the three previous studies of k_1 are in substantial disagreement, with values of k_1 ranging over a factor of five (see Table V). The final value of k_1 at 298 K from this work, $k_1 = (2.2 \pm 0.7) \times 10^{-12}$ cm^3 $molecule^{-1}$ s^{-1}, is in best agreement with the results of Clyne

and Watson who obtained $k_1 = (3.1 \pm 0.7) \times 10^{-12}$ cm^3 molecule^{-1} s^{-1}. These two values are widely bracketed by the results of Basco and Dogra ($(1.0 \pm 0.1) \times 10^{-12}$ cm^3 molecule^{-1} s^{-1}) and Clyne and Cruse ($(5.2 \pm 0.7) \times 10^{-12}$ cm^3 molecule^{-1} s^{-1} at 293 K). The rate constant temperature dependence found in this study is different in both magnitude and sign from other studies. The Arrhenius activation energy determined here, -510 ± 390 cal mole^{-1}, is based on a somewhat limited data set of three points. Clyne and Cruse obtained a value of 900 ± 600 cal mole^{-1} over the temperature range 293 to 573 K. Brown and Burns,[16] who were unable to determine σ and therefore obtain absolute values of k_1, reported a temperature dependence for k_1/σ which showed distinct non-Arrhenius behavior. The Arrhenius plot in their study had two distinct slopes, giving activation energies of 0.65 and 4.5 kcal mole^{-1} in the 300-500 K and 500-700 K temperature ranges. The negative activation energy reported in this work is consistent with the increasing number of radical-radical reaction studies which have obtained similar results.[19,22,23] The reason for the difference between the activation energies measured in this work and in the other studies is not known, except that the manner in which the temperature-dependence of σ is taken into account may be involved.

Neither the Basco and Dogra nor the Clyne and Cruse studies were capable of determining if reaction 1 had more than one possible channel. Implicit in the analytical scheme of Basco and Dogra is the assumption that the disproportionation of BrO yields only molecular bromine. To assume otherwise would lead to major complications in their determination of σ. Computer simulations of the Clyne and Cruse experiment using both $k_{1b} = 0$ (as assumed by these authors) and $k_{1a}/(k_{1a} + k_{1b}) = 0.84$ as determined in this study, reveal no major differences in the BrO decay profiles between

the two cases except that plots of $[BrO]^{-1}$ vs. time do not become linear in the second case until $t \sim 10$ msec as compared with $t \sim 5$ msec when k_{1b} is assumed to equal zero. As expected, the ozone decay profiles in the two cases are significantly different with more rapid decays being predicted when $k_{1b} = 0$ due to the longer chain length. Despite this prediction, the difference in decay rates would be difficult to observe experimentally since 95% of the O_3 is lost within 4 msec even when the branching ratio is 0.84. Since this time period is comparable to the flow tube mixing time, kinetic measurements on this time scale are extremely inaccurate. Thus, while it is not possible to derive the branching ratio from the Clyne and Cruse experiments directly, our finding that $k_{1a}/(k_{1a} + k_{1b}) = 0.84$ is not inconsistent with their results.

Thermochemistry of Chlorine Oxide and Bromine Oxide Radicals

Comparing the thermodynamic stability of radicals in the chlorine and bromine systems provides some insight into the mechanism of XO + XO reactions. In general, the higher oxides of bromine are less stable than those of chlorine. BrOO, which is a probable intermediate in the BrO + BrO reaction, is estimated[24] to be bound by only 1 kcal $mole^{-1}$ whereas the $Cl-O_2$ bond energy in ClOO is 6-8 kcal $mole^{-1}$.[8,21] This is reflected in the relatively long lifetime of ClOO enabling it to be detected by absorption spectroscopy[7,8] and mass spectroscopy.[25] In contrast, BrOO has never been detected. The same situation applies to OClO and OBrO, the former being extremely stable in the gas phase while the latter is stable only in the condensed phase and in solution.[26]

Heats of reaction for four possible product channels of the XO + XO reaction are listed in Table VI. The most striking difference between the chlorine and bromine systems is that the route to atomic products is

Table VI. Heats of Reaction for Possible Product Channels of the ClO + ClO and BrO + BrO Reactions[a]

Reactant XO	Enthalpy change (kcal mole^{-1}) products				
	$X_2 + O_2$	XOO + X	2X + O_2	OXO + X	X_2O_2
ClO	-48.5	+1.5	+9.4	+3.3	-16.2
BrO	-52.6	-7.3	-6.6	b	b

[a] Data are from Ref. 12 except for the enthalpies of formation of BrOO (Ref. 14) and Cl_2O_2 (Ref. 17).

[b] ΔH_f^o for OBrO and Br_2O_2 not known.

endothermic in the former and exothermic in the latter. This may account for the low absolute rate constant for the ClO + ClO reaction in the low pressure region ($k \sim 1 \times 10^{-14}$ cm^3 molecule^{-1} s^{-1}) compared to the BrO + BrO reaction rate constant (about 100 times larger). The second point is that the routes forming $X_2 + O_2$ in both systems are considerably more exothermic than any of the radical-formation routes and yet the rate constants for the molecular channels are, at most, equal to those of the radical channels. This strongly implies that the reaction forming $X_2 + O_2$ goes through a reasonably tight transition state to form a four-center complex rather than through a free-radical mechanism involving, for example, the reaction

$$X + XOO \rightarrow X_2 + O_2 \quad .$$

Comparison Between ClO + ClO and BrO + BrO Reactions

The ClO + ClO reaction has received considerable attention for many years, and while the complete reaction mechanism remains unknown, a number of interesting points have emerged which are relevant to the analogous BrO + BrO reaction. The first observation is that the reaction appears to go through two distinct mechanisms at high and low pressures. In the low pressure regime (1-25 torr Argon) the rate constant shows little pressure dependence[12,28-30] and the primary mechanism for ClO disappearance appears to consist of the reactions:

$$ClO + ClO \rightarrow Cl_2 + O_2 \qquad (9a)$$

$$\rightarrow Cl + ClOO \qquad (9b)$$

$$\rightarrow Cl + OClO \qquad (9c)$$

Several investigators[15,31-33] have measured the branching ratios for

reactions 9a, 9b and 9c and have found that $k_{9a}/(k_{9a} + k_{9b} + k_{9c}) \sim 0.5$. Above $\sim$ 25 torr Argon the overall rate constant is observed to increase with pressure[7,8,27] suggesting that a termolecular channel is becoming competitive with the bimolecular channels (9a-c) and that the ClO dimer may be the reaction product,

$$ClO + ClO + M \rightarrow Cl_2O_2 + M \qquad (9d)$$

Basco and Hunt[27] have detected a residual UV absorption in the 230-290 nm wavelength region in their flash photolysis studies which they attribute to Cl_2O_2 although this has apparently not been observed in the molecular modulation studies.[7,8] This work suggests that the lifetime of Cl_2O_2 may be as long as 1 second at one atmosphere, which is consistent with the observation of Cox and Derwent[31] that the decay of ClO in their modulated photolysis experiments did not follow second-order kinetics.

While the evidence points strongly toward the existence of both bimolecular and termolecular channels in the ClO + ClO reaction, no such observation is made in the BrO + BrO reaction. The third-order process involving BrO,

$$BrO + BrO + M \rightarrow Br_2O_2 + M$$

which would result in the formation of a collisionally stabilized Br_2O_2 species cannot compete with the spontaneous dissociation of Br_2O_2, presumably into BrOO + Br, or its rearrangement to form a four-center complex which dissociates into Br_2 and O_2. Another point is that in ClOOCl, the O-O bond is weaker than the O-Cl bond by $\sim$ 1.5 kcal mole^{-1} whereas in BrOOBr, the O-O bond is stronger than the O-Br bond by $\sim$ 7.3 kcal mole^{-1}. Decomposition of Br_2O_2 into BrOO + Br is therefore energetically favored

relative to the return to reactants.

Finally, our observation that the photolysis of Br_2-O_2 mixtures in a pyrex cell (in which no atomic oxygen is formed) does not lead to BrO formation implies that the reaction

$$Br + BrOO \rightarrow 2BrO$$

does not occur while the analogous process does occur in the chlorine case.[7] Although the Br + BrOO reaction is expected to be at least as rapid as Cℓ + CℓOO ($k \sim 5 \times 10^{-12}$ cm^3 $molecule^{-1}$ s^{-1}) the steady-state concentration of BrOO is much lower due to its rapid decomposition into Br and O_2.

Mechanism of the BrO + BrO Reaction

In view of the thermodynamic instability of BrOO and Br_2O_2, the formation of Br_2 in the BrO + BrO reaction cannot easily be explained by a free-radical mechanism involving these species. This is confirmed by the fact that Br_2 formation is still observed in O_3-containing systems in which the steady-state Br concentration is expected to be extremely small. Reactions such as Br + BrOO and Br + Br_2O_2 could therefore not occur. A possible formation mechanism for Br_2 is the rearrangement of the Br_2O_2 intermediate to form a trapezoidal four-center complex which subsequently dissociates into Br_2 and O_2. The rate of this process can be estimated using the RRK theory of unimolecular decomposition.[34] Observations of Br and Br_2 formation can be discussed in terms of the following mechanism:

$$BrO + BrO \underset{\leftarrow}{\overset{\rightarrow}{}} BrOOBr^* \qquad (10f,10r)$$

$$BrOOBr^* + M \rightarrow BrOOBr + M \qquad (11)$$

$$BrOOBr^{*} \rightarrow BrOO + Br \qquad (12)$$

$$BrOO \rightarrow Br + O_2 \qquad (13)$$

$$BrOOBr^{*} \rightarrow [Br\overset{O-O}{\cdots\cdots}Br]^{\neq} \rightarrow Br_2 + O_2 \qquad (14)$$

where (*) denotes a vibrationally excited intermediate. In this scheme, BrOOBr can either undergo simple fission to become BrOO and Br (reaction 12) or form the cyclic BrOOBr complex (reaction 14). This mechanism predicts that

$$\frac{d[Br_2]}{dt} = \frac{k_1 k_{14}}{k_{12} + k_{14}} [BrO]^2$$

$$\frac{d[Br]}{dt} = \frac{2 k_1 k_{12}}{k_{12} + k_{14}} [BrO]^2$$

neglecting reactions 10r and 11. The observed branching ratio, f, is then given by:

$$f = \frac{k_{12}}{k_{12} + k_{14}}$$

and has the value 0.84 ± 0.03 or equivalently, $\frac{k_{12}}{k_{14}} = 5.2^{+1.4}_{-1.0}$.

A potential energy diagram for the BrO + BrO reaction is given in Fig. 4. Enthalpies of formation are taken from the recent CODATA review.[21] The location of the BrOOBr potential energy minimum is highly uncertain as is the magnitude of the decomposition barrier. Using estimates based on FOOF and ClOOCl, the heat of formation of BrOOBr is estimated to be 45 ± 10 kcal $mole^{-1}$. The diagram illustrates the large difference between the exothermicities of the two reaction channels.

According to RRK theory, the first-order rate constant for the

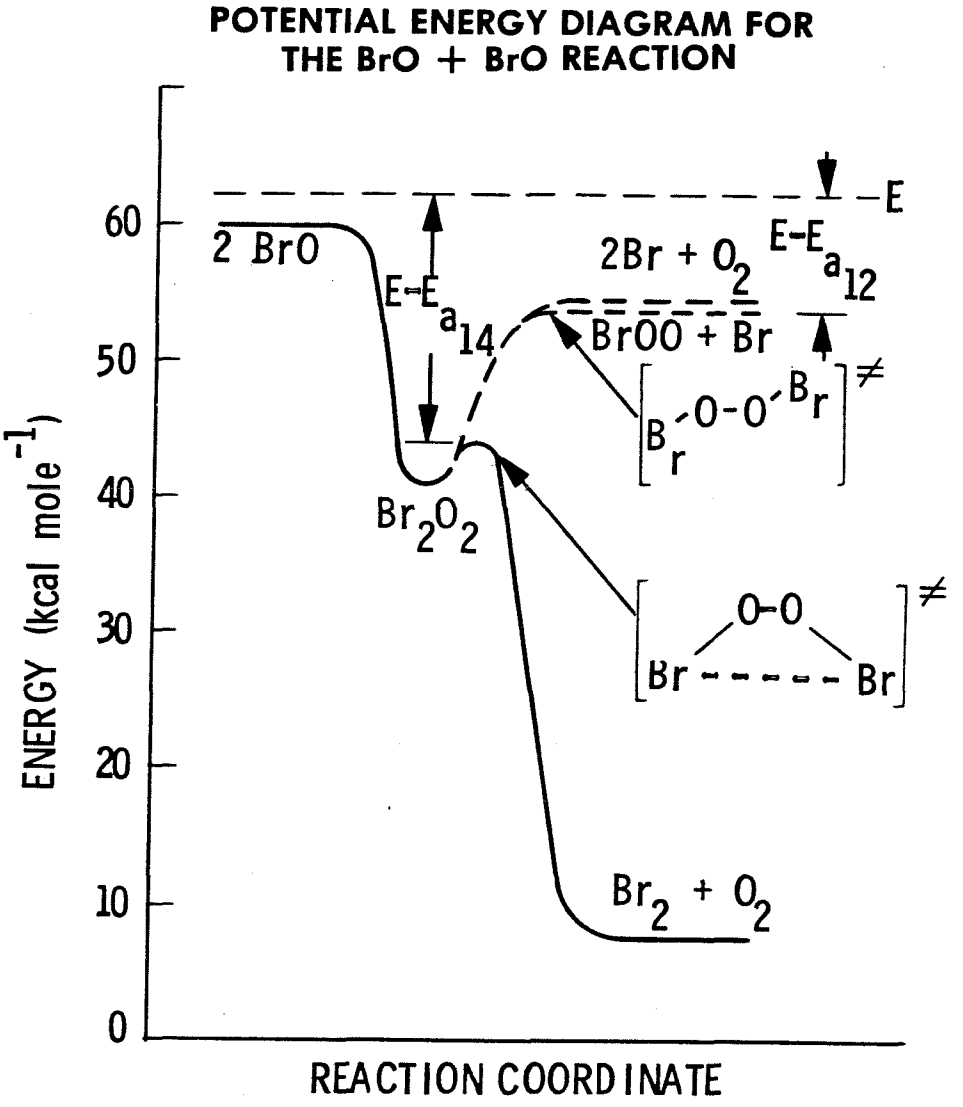

Figure 4. Energetics of the BrO + BrO reaction indicating the transition states that may be involved in the two reaction channels.

decomposition of a vibrationally excited species is given by:

$$k = A\left[\frac{E - E_o}{E}\right]^{s-1}$$

where: A = Arrhenius A-factor

E = total energy

E_o = critical energy for the bond fission

s = effective number of classical oscillators

The A-factor can be expressed in terms of the entropy of activation:[35]

$$A = \frac{ekT}{h}\exp(\Delta S^{\neq}/R)$$

The ratio $\frac{k_{12}}{k_{14}}$ is then given by:

$$\frac{k_{12}}{k_{14}} = \exp[(S_{12}^{\neq} - S_{14}^{\neq})/R]\left[\frac{E - E_{a_{12}}}{E - E_{a_{14}}}\right]^{s-1} \qquad (3)$$

where $S_i^{\neq}$ is the intrinsic entropy of the activated complex of reaction i. Since it is unlikely that there is an appreciable energy barrier for the reverse of reaction 12, $E - E_{a_{12}}$ is equal to the exothermicity of reaction 12 ($\sim$ 7 kcal mole^{-1}) plus the total energy (translational + vibrational) of the reactant BrO molecules ($\sim$ 2 kcal mole^{-1}). From the above estimate of $\Delta H_f^o(Br_2O_2)$, $(E = E_{a_{14}}) = 17 \pm 10$ kcal mole^{-1}. The entropy difference $S_{12}^{\neq} - S_{14}^{\neq}$ can be estimated by comparison with straight-chain and cyclic alkanes that have the same number of carbon atoms. Typical values range from 8-12 e.u. The number of oscillators, s, is approximately equal to $\frac{2}{3}(3N-6)$ where N is the number of atoms in the complex. Reasonable values of s lie in the range of 3 to 4.

Since the estimated energies and entropies are fairly uncertain, and the RRK theory is itself quite approximate, the predicted values of

k_{12}/k_{14} should be interpreted as guidelines rather than precise numerical results. Using the median values for $E - E_{a_{12}}$, $E - E_{a_{14}}$ and $S_{12}^{\neq} - S_{14}^{\neq}$, $s - 1 = 3$, the resulting value of k_{12}/k_{14} is 22. However within the range of uncertainty of the enthalpies and entropies, k_{12}/k_{14} can be as low as 2.0 or as high as 900. Clearly, this simple calculation does not prove or disprove the suggestion that the formation of Br_2 occurs via a four-center complex. However, it shows that the observed rate constant for the molecular channel, $k_{1b} = (3.5 \pm 0.7) \times 10^{-13}$, is not too high to be accounted for by a process of this sort. The calculation indicates that the large, negative entropy of activation involved in forming a trapezoidal complex can be overcome by the energy advantage realized as a result of the large exothermicity of this channel. The most critical and uncertain parameter in the calculation is the enthalpy of formation of Br_2O_2.

ACKNOWLEDGEMENTS

The authors appreciate the many helpful discussions with W. B. DeMore and S. Jaffe. The research described in this paper was carried out at the Jet Propulsion Laboratory, California Institute of Technology, under NASA Contract NAS7-100.

REFERENCES

1. F. J. Lipscomb, R. G. W. Norrish and B. A. Thrush, Proc. Roy. Soc. London A, 223, 455 (1956).

2. G. Porter and F. J. Wright, Discuss. Faraday Soc., 14, 23 (1953).

3. M. A. A. Clyne and R. T. Watson, J.C.S. Faraday I, 70, 1109 (1974).

4. M. A. A. Clyne and R. T. Watson, J.C.S. Faraday I, 70, 2250 (1974).

5. M. A. A. Clyne and R. T. Watson, J.C.S. Faraday I, 71, 336 (1975).

6. M. A. A. Clyne and R. T. Watson, J.C.S. Faraday I, 73, 1169 (1977).

7. H. S. Johnston, E. D. Morris and J. Van den Bogaerde, J. Amer. Chem. Soc., 91, 7712 (1969).

8. R. A. Cox, R. G. Derwent, A. E. J. Eggleton and H. J. Reid, J.C.S. Faraday I, 75, 1648 (1979).

9. M. A. A. Clyne and H. W. Cruse, Trans. Faraday Soc., 66, 2214 (1970).

10. M. A. A. Clyne and H. W. Cruse, Trans. Faraday Soc., 66, 2227 (1970).

11. H. Gg. Wagner, C. Zetsch and J. Warnatz, Ber. Bunsenges. Phys. Chem., 76, 526 (1972).

12. N. Basco and S. K. Dogra, Proc. Roy. Soc. London A, 323, 69 (1971).

13. N. Basco and S. K. Dogra, Proc. Roy. Soc. London A, 323, 401 (1971).

14. N. Basco and S. K. Dogra, Proc. Roy. Soc. London A, 323, 417 (1971).

15. C. L. Lin and W. B. DeMore, to be published.

16. J. Brown and G. Burns, Can. J. Chem., 48, 3487 (1970).

17. Y. L. Yung, J. P. Pinto, R. T. Watson and S. P. Sander, J. Atmos. Sci., in press.

18. W. L. Chameides and D. D. Davis, private communication.

19. R. T. Watson, S. P. Sander and Y. L. Yung, J. Phys. Chem., in press.

20. R. A. Durie and D. A. Ramsay, Can. J. Phys., 36, 35 (1958).

21. D. L. Baulch, R. A. Cox, R. F. Hampson, Jr., J. A. Kerr, J. Troe and R. T. Watson, J. Phys. Chem. Ref. Data, in press.

22. C. J. Howard, J. Chem. Phys., 71, 2352 (1979).

23. M. T. Leu and W. B. DeMore, J. Phys. Chem., 82, 2049 (1978).

24. J. A. Blake, R. J. Browne and G. Burns, J. Chem. Phys., 53, 3320 (1970).

25. C. H. Wu, Ph.D. Thesis, University of California, Berkeley (1970).

26. G. Brauer, ed., Handbook of Preparative Inorganic Chemistry, Second Ed., Academic Press, New York (1963).

27. N. Basco and J. E. Hunt, Int. J. Chem. Kinet., 11, 649 (1979).

28. M. A. A. Clyne and J. A. Coxon, Proc. Roy. Soc. London A, 303, 207 (1968).

29. M. A. A. Clyne and I. F. White, Trans. Faraday Soc., 67, 2068 (1971).

30. R. F. Walker, Ph.D. Thesis, Univ. of London (1972).

31. R. A. Cox and R. G. Derwent, J. Chem. Soc. Faraday I, 75, 1635 (1979).

32. M. A. A. Clyne, D. J. McKenney and R. T. Watson, J. Chem. Soc. Faraday II, 71, 322 (1975).

33. W. Wongdontri-stuper, R. K. M. Jayanty, R. Simonaitis and J. Heicklen, J. Photochem., 10, 163 (1979).

34. P. J. Robinson and K. A. Holbrook, Unimolecular Reactions, Wiley-Interscience, London (1972).

35. S. W. Benson, Thermochemical Kinetics, Second Edition, Wiley-Interscience, New York (1976).

CHAPTER IV

A PRESSURE AND TEMPERATURE DEPENDENCE KINETICS STUDY OF THE NO + BrO → NO_2 + Br REACTION: IMPLICATIONS FOR STRATOSPHERIC BROMINE PHOTOCHEMISTRY

R. T. Watson, S. P. Sander

Molecular Physics and Chemistry Section
Jet Propulsion Laboratory
Pasadena, CA 91103

and

Y. L. Yung

Geological and Planetary Sciences
California Institute of Technology
Pasadena, CA 91125

Abstract

The flash photolysis: ultraviolet absorption technique has been utilized to study the reactivity of nitric oxide with BrO radicals over a wide range of pressure (100-700 torr) and temperature (224-398 K). Pseudo first-order conditions were used in order to minimize complications caused by secondary kinetic processes. The reaction and its corresponding Arrhenius expression in units of $cm^3 molecule^{-1} s^{-1}$ can be written:

$$NO + BrO \rightarrow NO_2 + Br; \qquad \Delta H^\circ_{298} = -17.0 \text{ kcal mol}^{-1} \qquad (1)$$

$$k_1 = (1.28 \pm 0.23) \times 10^{-11} \exp((181 \pm 46)/T); \; 224\text{-}398 \text{ K}.$$

The results are compared with previous measurements and atmospheric implications of the reaction are discussed. It is shown that this reaction is important in controlling the ratios BrO/Br and BrO/HBr in the stratosphere but does not affect the catalytic efficiency of BrO_x in ozone destruction.

Introduction

During the last few years there has been considerable activity in the field of gas phase kinetics involving studies of the behavior of XO (X = HO, F, Cℓ, Br) free radicals. Most of this interest has been stimulated by the need to understand the role of these radicals in atmospheric photochemistry. These radicals play a major role in controlling the ozone concentration in the stratosphere.[1] In addition, during the last few years sensitive experimental techniques have been developed for direct detection of these radicals. High sensitivity is required in order to study kinetic processes where the rate constants approach the gas kinetic collision frequency. Pseudo first-order conditions are used in order to minimize complications which can be caused by secondary processes. The two detection techniques which have been used to study these radicals are laser magnetic resonance (LMR) - HO_2,[2] ClO[3] and collision free sampling mass spectrometry (MS) - ClO,[4] BrO,[5] FO[6]. Unfortunately the LMR technique cannot be used at high pressures due to a loss of sensitivity caused by line broadening, and although the mass spectrometric technique can be interfaced to a high pressure flash photolysis system[7] there is normally a loss of sensitivity and there are problems associated with representative sampling of radicals. Consequently as these radicals cannot be detected using a fluorescence technique (the $A^2\Pi$ states of ClO and BrO exhibit extensive predissociation[8]) all direct studies involving the kinetic behavior of XO radicals (except XO + XO → products) have been studied in low pressure discharge flow systems. The ultraviolet absorption technique has been used in conjunction with the low pressure discharge flow[9] and high pressure flash photolysis,[10] molecular modulation,[11] and pulse radiolysis[12] techniques to study reactions of the type XO + XO → products. However, these techniques have not yet been used to study reactions of the type NO + XO → NO_2 + X, due to a lack of sensitivity.

As stated above, all studies of NO + XO reactions have been performed at low pressure, and each has been shown to be rapid ($k \geq 10^{-11}$ cm^3 $molecule^{-1}s^{-1}$) and to exhibit a negative temperature dependence.[13-17] One hypothesis that has been proposed[13] to explain the negative temperature dependence is that the reaction proceeds through a vibrationally excited intermediate, $XONO^*$, which decomposes to either X + NO_2 or XO + NO. Quenching of this intermediate at pressures up to several atmospheres is expected to be slow, however it was decided to study the pressure and temperature dependence of the NO + BrO reaction using the flash photolysis UV absorption technique to verify that such reactions do exhibit a negative temperature dependence and to test for any pressure dependence up to one atmosphere total pressure. This ensures that the previous results are not artifacts of the discharge flow technique and that the kinetic data can be used in atmospheric photochemical modelling calculations.

In the last few years improvements in the chemical kinetics data base and the use of a more complete reaction scheme have resulted in significant changes in the predictions of stratospheric models, not only for HO_x, NO_x and $C\ell O_x$ but also for BrO_x. Watson[1f] first recognized that the presence of bromine in the stratosphere could lead to the catalytic destruction of ozone in an analogous manner to chlorine. Three basic differences were recognized to exist between the chlorine and bromine systems, (a) hydrogen abstraction reactions by atomic bromine from molecules such as CH_4 and H_2 are strongly endothermic and consequently very slow, (b) XO radical-radical processes are important even at low BrO_x mixing ratios ($\sim$ 100 ppt), and (c) the photolysis rate for BrO is 2-3 orders of magnitude faster than the photolysis rate for $C\ell O$. Watson concluded that these differences resulted in (a) the Br/HBr ratio being significantly greater than the $C\ell/HC\ell$ ratio, (b) BrO being the dominant bromine containing species, and (c) that on a per molecule basis bromine was more efficient than chlorine in destroying ozone. However, Wofsy et al.[1b] while agreeing with the last conclusion, correctly pointed out that the earlier paper had failed to consider the Br + HO_2 and Br + H_2O_2 reactions which

produce HBr, thus reducing the catalytic efficiency of odd oxygen destruction by BrO_x. Whereas Watson[1f] concluded that BrO was the dominant form of BrO_x throughout the stratosphere, Wofsy et al.[1b] concluded that while BrO was the dominant form above 30km, HBr was the dominant form below 30km. Recently Yung et al.[1a] re-examined the role of BrO_x in the stratosphere with a model that included the interaction of the BrO_x and $C\ell O_x$ systems through the $C\ell O + BrO \rightarrow C\ell + Br + O_2$ reaction, and the chemistry of $BrONO_2$ and HOBr. Since the calculations of Wofsy et al.,[1b] the rate coefficients for $NO + HO_2 \rightarrow OH + NO_2$,[15] and $HO_2 + O_3 \rightarrow OH + 2O_2$[15] have been revised, resulting in higher concentrations of OH, and lower concentrations of HO_2 and H_2O_2. These changes when coupled with new rate coefficient data for the OH + HBr reaction (see Table VI) result in a significantly higher Br/HBr ratio than that obtained by Wofsy et al.,[1b] and the prediction that BrO is the dominant bromine containing species at all altitudes. Yung et al.[1a] reviewed atmospheric bromine photochemistry but did not discuss the role of the NO + BrO reaction in detail. This reaction is examined in detail in the discussion section.

Experimental

The flash photolysis system consists of a high pressure xenon arc light source, a reaction cell/gas filter/flash lamp combination and a McPherson model 216.5 half-meter monochromator/polychromator/spectrograph for wavelength selectivity. A schematic diagram of the complete apparatus is shown in Figure 1.

Light from the xenon analytical lamp traverses the reaction cell eight times by reflection from the external White cell optics, and is focussed onto the entrance slit of the monochromator. The pathlength of the optical absorption system was measured using known pressures of gases such as chlorine, bromine, and ozone whose absorption cross-sections are well established and are known to obey Beer's Law. The absorption pathlength determined in this manner was 740 cm, in good agreement (better than 1%) with a simple physical measurement (assuming eight traversals). After the flash, absorption of the analytical light by BrO radicals in the cell at 339.0 nm ($A^2\Pi(v'=4) \leftarrow X^2\Pi(v''=0)$) is detected by an EMI

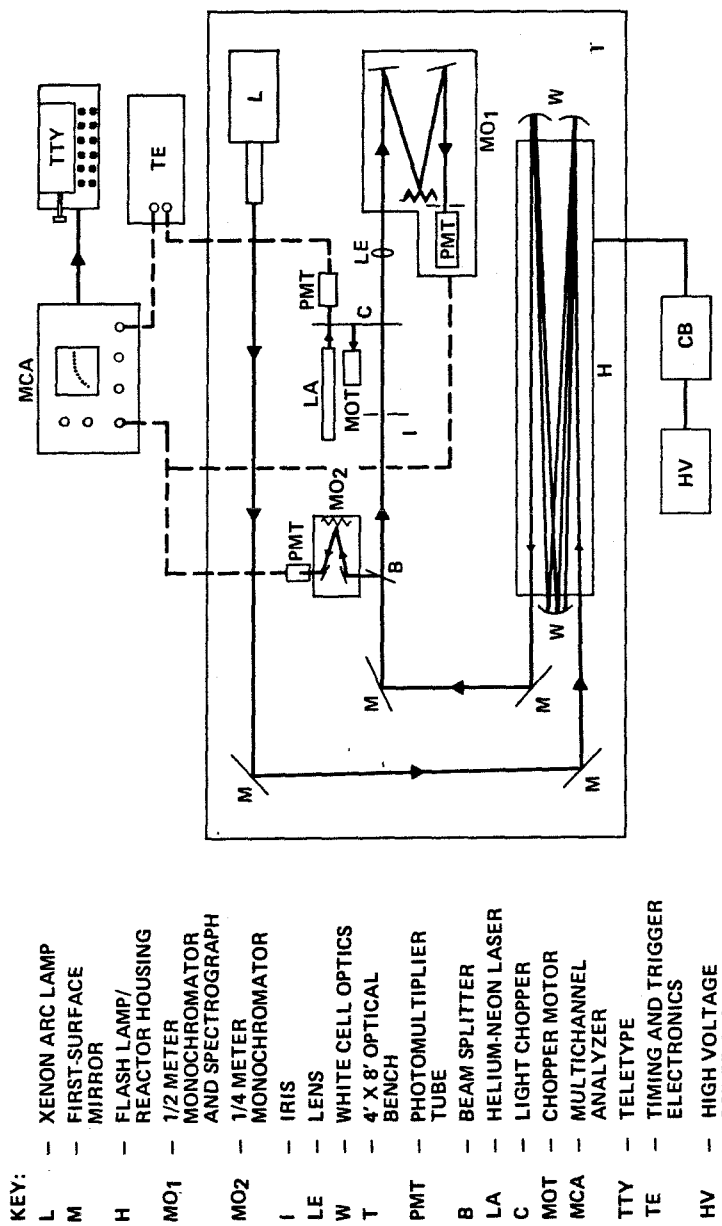

Figure 1. Schematic Diagram of Flash Photolysis/UV Absorption Apparatus

9659 or an EMI 9781B photomultiplier in the monochromator (100 micron slitwidth resulting in a spectral bandwidth of 0.09 nm (FWHM). The photomultiplier signal is initially coupled through a fast electrometer to improve the transient response of the detection system. The photomultiplier signal is recorded on a Tracor-Northern NS-570A multichannel analyzer and punched onto paper tape for subsequent computer analysis. In experiments where light absorption by the BrO radical was weak (initial absorption due to $[BrO]_o$ varied from 8-35% I_o) the signal-to-noise ratio was enhanced by multiple flashes (20-40) in conjunction with signal averaging. The entire apparatus is constructed on a pneumatically isolated optical bench to minimize vibrations which might introduce noise in the analyzing beam.

The annular flash lamp/reaction cell is shown in Figure 2. The cell consists of four concentric quartz tubes. The cell temperature was controlled to within ± 0.5K by flowing methanol (224-298K) or ethylene glycol (298-425K) from a thermostated circulating bath (Haake) through the outer jacket. An iron-constantan thermocouple was used to measure temperature with a precision of better than ± 0.5K. The second jacket is the flash lamp which is filled with 30 torr of pure xenon. The third jacket, which has an annular size of 5mm, can be filled with an absorbing gas or liquid for filtering the photolyzing light. The central tube, 25mm i.d. and 125cm in length, is the reaction cell. As shown in Fig. 2 the region in which the BrO radicals can absorb the analytical light is confined to the central ∿93 cm of the reaction cell which is uniformly irradiated by the flash lamp (important for studying second-order reactions[18]).

At 1000 joules the time for the light pulse to decay to 10% of peak intensity is ∿10 microseconds. The effect of scattered photolytic light entering the analyzing system is minimized by using a trigger pulse in conjunction with a gating circuit to reverse-bias the photomultiplier dynode chain

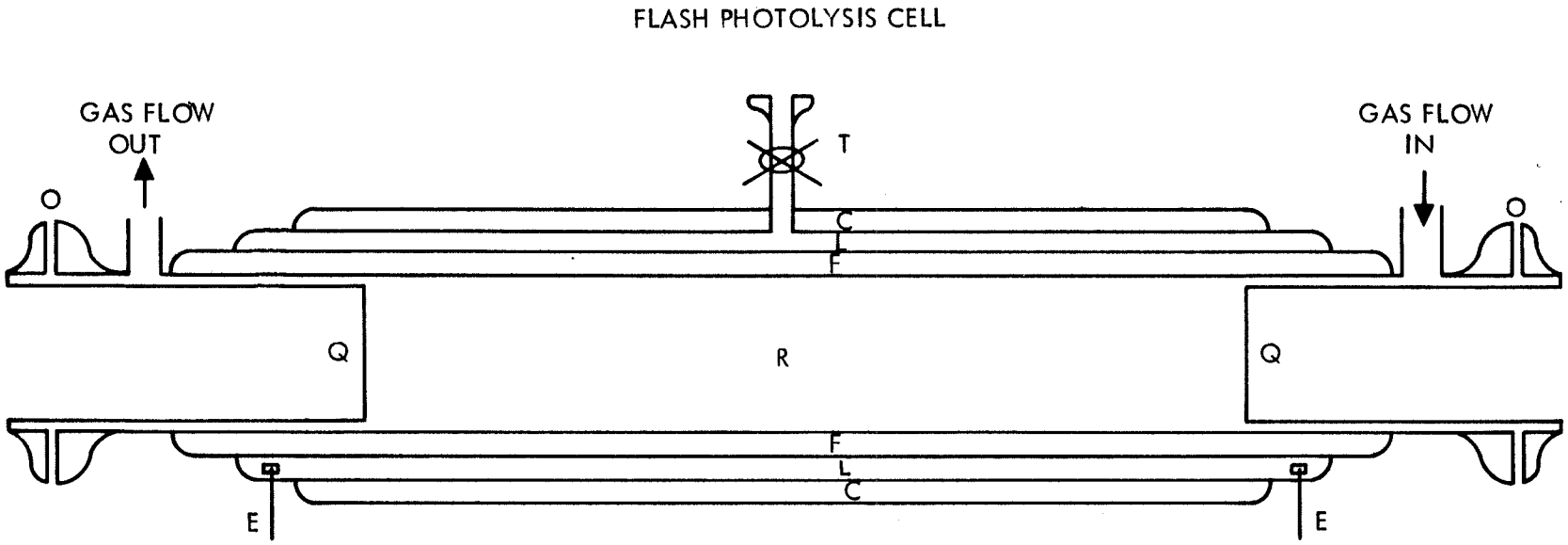

Figure 2. Annular Flash Lamp/Reaction Cell

for a variable time during the flash.[19a] This prevents the dynode chain from being saturated by scattered light. Analysis for BrO was usually started ∿80μs after the start of the photolysis flash, thus allowing for complete removal of atomic oxygen and preventing scattered light from interfering with the analysis beam. Another system which is used for the same purpose consists of a rotating disk mechanical shutter.[19b] A helium-neon laser illuminates a pinhole on the periphery of the disk triggering the flash lamp at a variable preset time before the opening of the shutter.

The BrO radicals are produced as shown below by an intense flash from the photolysis lamp, which is capable of being operated at discharge energies up to 2000 joules per flash. The BrO radicals result from the reaction of photolytically generated atomic oxygen with an excess concentration of molecular bromine in the presence of nitric oxide and a large excess of the diluent gas He or N_2. The reaction system can be simply written:

$$O_2 + h\nu \rightarrow 2\ O \qquad (2)$$

$$O + Br_2 \rightarrow BrO + Br \qquad (3)$$

$$NO + BrO \rightarrow NO_2 + Br \qquad (1)$$

Potential complications from secondary processes will be discussed in detail in the Results section. The reactants (NO, Br_2, O_2 and He or N_2) were premixed prior to entering the reaction cell and were flowed slowly but continuously in order to eliminate problems caused by loss of reagents or buildup of reactive products. The contents of the reaction cell were replaced after each photolysis flash. A flash energy of 1000 J produced ∿3 x 10^{-3}% photodissociation of molecular oxygen. The initial oxygen atom concentration ($[BrO]_o = [O]_o$) was varied from (1-11) x 10^{13} cm^{-3} by changing either $[O_2]$ ((3-40) x 10^{17} cm^{-3}) or flash energy (600-1500 J). Molecular bromine concentrations of ∿(5-20) x 10^{15} cm^{-3} ensured that greater than 99% of the atomic oxygen was converted to BrO radicals within 11-46 microseconds after the photolytic flash (k_{O+Br_2} = 1.4 x 10^{-11} cm^3 $molecule^{-1}$ s^{-1}[20] --assumed to exhibit little temperature dependence). Initial NO concentration ranged from (2-12) x 10^{14} cm^{-3} resulting in initial stoichiometries

($[NO]_o/[BrO]_o$) of 4.8 to 55.5. Temperature and pressure were varied from 224-398K, and 100-700 torr, respectively.

Gas pressures were measured using MKS Baratron pressure gauges (0-10 torr, and 0-1000 torr heads) which were periodically calibrated against dibutyl phthalate and mercury manometers. Flow rates of gases were measured by linear mass flowmeters (Teledyne Hastings-Raydist). Flowmeters were calibrated by a Hastings bubble-type calibrator (Model HBM-1). The calibration for the 0.1% NO/He mixture was identical to that for pure He. A flow controller was used to stabilize the flow of the NO/He mixture.

The helium, nitrogen and oxygen used in this study were Linde UHP grade gases with stated purities of >99.999%, >99.99% and >99.99% respectively. Matheson CP grade NO with stated purity of >99.0% was used without further purification. Baker "Analyzed Reagent Grade" Br_2, with a stated purity of >99.7%, was used after either, (a) freeze-thaw degassing, or (b) fractional distillation.

Results

The results are shown in Tables I and II, and Figures 3-5. The reaction was studied over a range of temperature (224-398K), pressure (100-700 torr), diluent (He and N_2), flash energy (600-1500 J), and initial reactant concentrations. Pseudo first-order kinetic conditions $[NO]_o > [BrO]_o$ ($[NO]_o$ = (2-12) x 10^{14} cm^{-3}, $[BrO]_o$ = (1-11) x 10^{13} cm^{-3}) were employed so that equation (V) could be used to analyze the data:

$$-d[BrO]/dt = k_1[NO][BrO] \qquad (I)$$

$$\ell n([BrO]_o/[BrO]_t) = k_1[NO]t \qquad (II)$$

The BrO concentration was related to the absorption signal using Beer's Law:

$$\ell n(I_o/I_t) = \sigma\, \ell[BrO]_t \qquad (III)$$

By combining equations (II) and (III) it can be seen that knowledge of σ (absorption

Table I. Reaction Rate Data for NO + BrO → NO_2 + Br at 298 K

Diluent (torr)	Flash Energy (joules)	$[Br_2]x10^{-15}$	$[\theta_2]x10^{-17}$	$[BrO]_o x10^{-13}$	$[NO]_o x10^{-14}$	k^1 (s^{-1})	$10^{11}x(k_{bi}$ (corrected) (cm^3 $molecule^{-1}$ s^{-1})
		molecule cm^{-3}					
100(He)	1500	8.2	16.0	7.74	5.05	8723	2.04
	1500	8.2	16.6	7.20	5.04	11776	2.73
	1500	8.9	17.7	6.61	3.19	5889	2.33
	1500	7.8	15.5	6.08	6.69	10860	1.79
	1500	8.2	5.6	4.40	3.17	6469	2.37
	1500	8.5	2.8	2.46	3.15	6433	2.21
	690	8.1	5.5	1.13	3.12	6708	2.23
	1010	7.6	5.2	2.14	5.56	10949	2.05
	600	8.4	5.7	1.27	1.98	4661	2.51
							2.25±.28
250(He)	880	5.0	15.0	3.42	5.09	12206	2.57
	1460	5.0	15.2	4.93	5.06	9368	2.05
	1460	4.9	15.0	4.90	6.98	12210	1.88
	880	4.9	14.9	1.52	6.98	12890	1.89
	1460	4.9	14.9	4.21	6.98	13678	2.09
	1460	4.9	14.9	6.90	4.06	6179	1.83
	1500	5.4	10.5	4.93	5.41	10900	2.22
	1500	4.9	16.0	5.27	5.00	9890	2.21
							2.09±.24
450(He)	1500	8.4	16.8	5.67	5.07	10075	2.24
	880	8.1	19.7	3.47	5.68	9522	1.79
	880	8.0	19.4	3.67	4.03	7140	1.95
	880	7.8	18.9	3.55	7.09	13221	1.96
	880	7.8	19.3	3.34	5.66	9883	1.86
	880	21.7	18.3	3.63	5.35	9446	1.89
							1.95±.16
450(N_2)	1150	5.9	10.8	3.37	5.31	9719	1.95
	650	5.9	22.4	2.33	5.32	10052	1.98
	650	5.9	22.4	2.49	3.53	7544	2.30
	1460	5.9	21.8	5.69	7.96	13869	1.88
	880	5.9	21.8	3.47	7.96	18190	2.39
	880	17.0	21.5	3.06	7.73	16081	2.17
							2.11±.21
700(He)	1500	9.3	15.4	4.10	5.22	8811	1.83
	1460	5.6	15.7	6.34	4.45	8303	2.18
	880	5.6	15.7	2.93	4.45	8626	2.08
	880	5.6	15.7	2.99	6.21	13568	2.30
	880	5.6	15.7	3.34	7.71	16330	2.21
	1460	5.6	15.6	7.00	7.71	17845	2.55
	650	5.7	17.1	2.23	2.79	6410	2.50
	650	5.6	13.9	1.96	3.85	8780	2.40
							2.26±.24

TABLE II. Summary of Reaction Rate Data for NO + BrO → NO_2 + Br

Temp./K	Diluent	Pressure(torr)	#runs	$10^{11} \times k_1$ ($cm^3 molecule^{-1} s^{-1}$)	
224	He	110	8	2.82 ± 0.24	
	He	710	4	2.85 ± 0.09	2.83 ± 0.20
257	He	100	8	2.75 ± 0.14	
	He	700	3	2.56 ± 0.22	2.69 ± 0.18
298	He	100	9	2.25 ± 0.28	
	He	250	8	2.09 ± 0.24	
	He	450	6	1.95 ± 0.16	
	N_2	450	6	2.11 ± 0.21	
	He	700	8	2.26 ± 0.24	2.15 ± 0.25
351	He	100	6	2.22 ± 0.08	
	He	700	6	2.11 ± 0.19	2.16 ± 0.15
398	He	100	7	2.08 ± 0.16	
	He	700	12	1.99 ± 0.19	2.02 ± 0.18

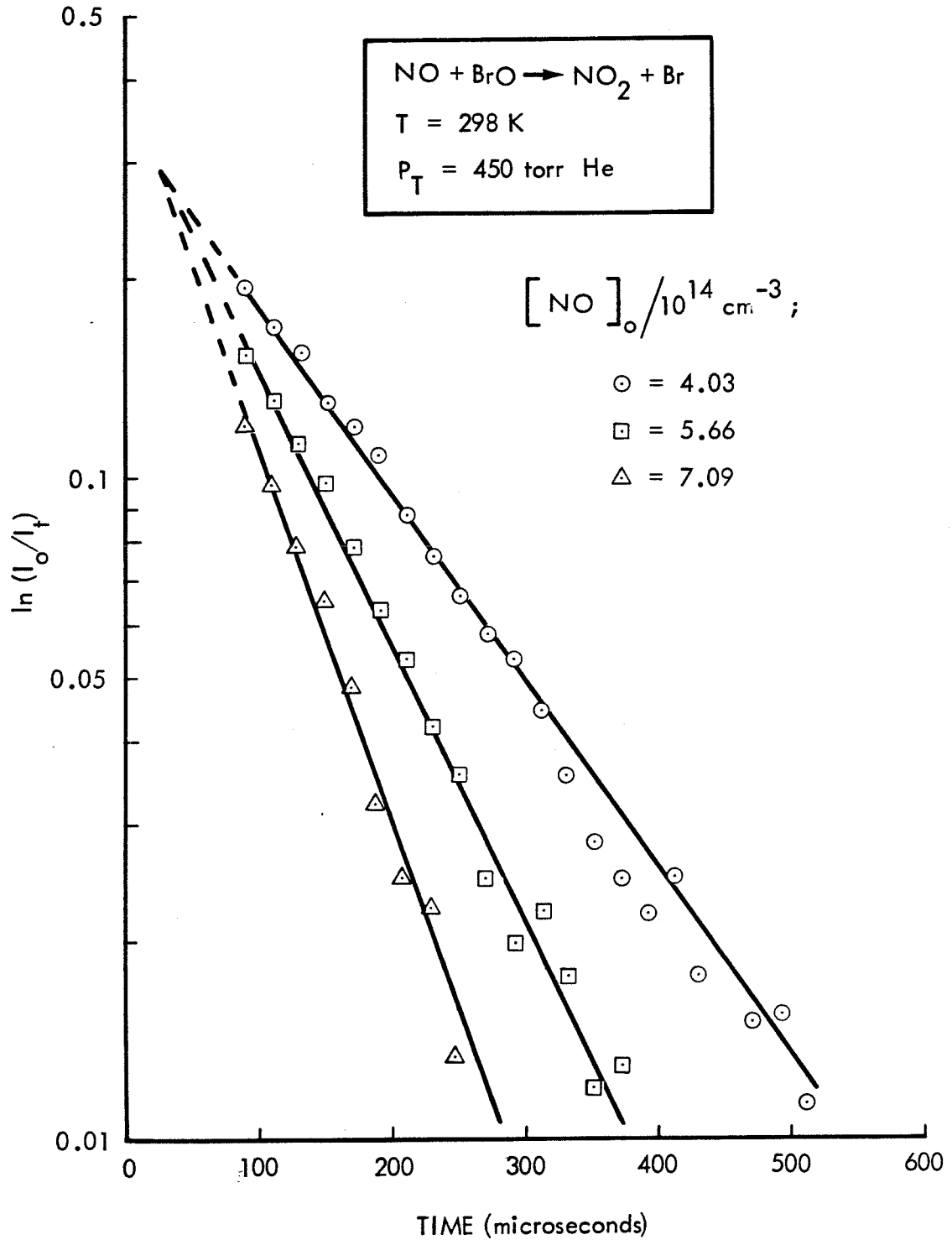

Figure 3. The reaction NO + BrO → NO_2 + Br. Typical first-order plots for [BrO] in the presence of various excess concentrations of NO at 298K, and 450 torr of He.

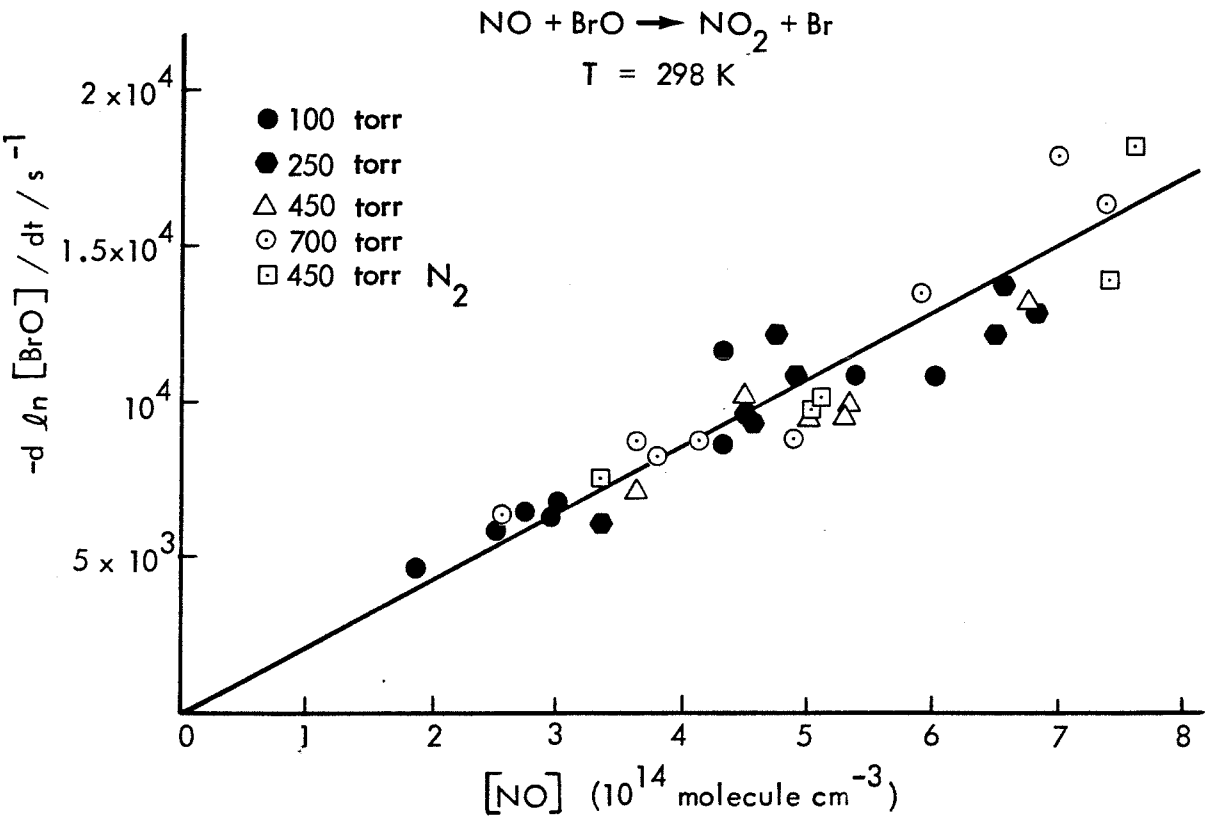

Figure 4. The reaction NO + BrO → NO_2 + Br. Variation of pseudo first-order rate constant, -dln[BrO]/dt (corrected for NO removal) with NO at 298K, and at total pressures from 100-700 torr.

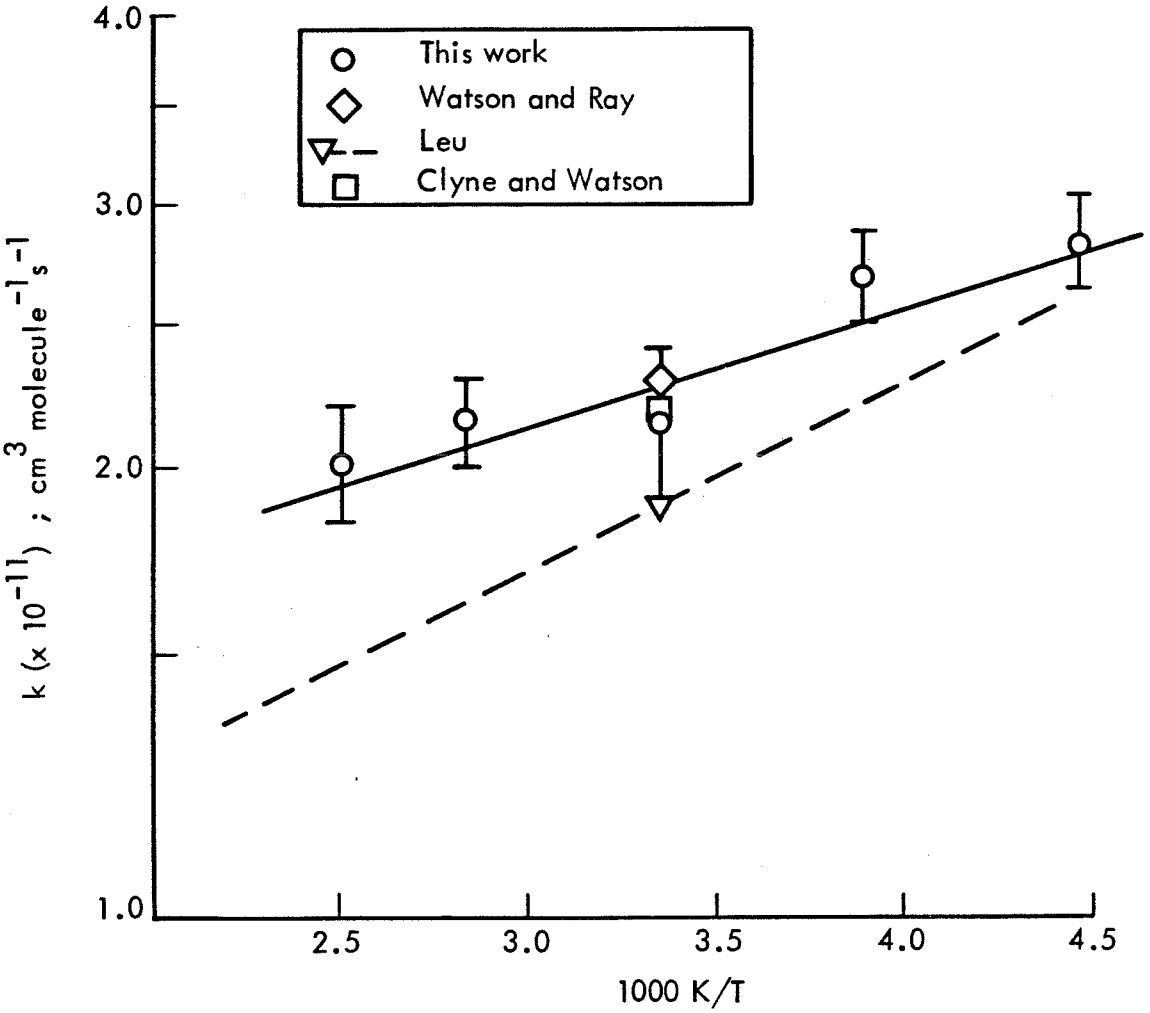

Figure 5. Arrhenius plot for the NO + BrO → NO_2 + Br reaction. o; this work; ∇, - - - -, Ref. 16; ◊, Ref. 24; □ Ref. 5.

cross-section) and ℓ (optical pathlength) is not required in order to determine an absolute value for k_1.

$$\ell n(\ell n(I_o/I_{t_o}) - \ell n(I_o/I_t)) = k_1[NO]t \qquad (IV)$$

A plot of $\ell n(\ell n(I_o/I_t))$ as a function of reaction time (see Fig. 3) should be linear with a slope equal to the first order rate constant, k_1'. The bimolecular rate constant, k_1, is related to k_1' as shown in equation (V),

$$k_1' = k_1[NO] \qquad (V)$$

As the initial stoichiometry, $[NO]_o/[BrO]_o$, only ranged from 4.8 to 55.5, with a mean value of $\sim$18, an allowance was made in the measurement of [NO] for the removal of NO by BrO. The correction factor was typically $\sim$6%. Consequently an accurate determination of $[BrO]_o$ was required in order to correct the data for the finite consumption of NO, thus requiring values for ℓ and σ (as a function of temperature). The temperature dependence of σ was determined by the authors in the same experimental apparatus.[18] The adherence of [BrO] to Beer's Law was demonstrated in the same study. Fig. 3 shows three typical decay plots of BrO with reaction time, where the initial conditions which govern the rate and magnitude of formation of BrO radicals (flash energy, O_2 concentration and Br_2 concentration) were kept constant in the presence of differing NO concentrations. The first data points were taken 90μs after initiation of the photolytic flash. The initial BrO radical concentrations are predicted to be constant for these three runs, and to reach a maximum concentration ($\geq$95% formation) within $\sim$25μs of initiating the photolytic flash (this is based on the pulselength of the flash and the rate of removal of atomic oxygen by molecular bromine). From Fig. 3 it can be seen that back extrapolation of the BrO decay plots to within $\sim$25μs of the start of the photolytic flash indicates that within experimental error the initial BrO concentrations were equal. The back extrapolation procedure is valid given that the rate of formation of BrO radicals via the O + Br_2 reaction is significantly greater than the rate of destruction of BrO radicals by NO:

$$k_3[O][Br_2] >> k_1[NO][BrO]$$

However, even if there were a 20% error in the estimated value of $[BrO]_o$ this would typically only result in a 1% error in k_1. Figure 3 illustrates how BrO had decayed a factor between 1.3 - 1.6 prior to the first analysis point. Consequently the reaction stoichiometries, [NO]/[BrO], after 90μs (the first observation time) were always > 10. The linearity of the BrO decay plots indicates that the system is well behaved, i.e., the reaction is first order with respect to BrO concentration, and there are no rapid complicating secondary processes.

Possible complicating secondary reactions which must be considered are:

$$O + BrO \rightarrow Br + O_2 \qquad (4)$$

$$BrO + BrO \rightarrow 2Br + O_2 \qquad (5a)$$

$$\rightarrow Br_2 + O_2 \qquad (5b)$$

$$BrO + NO_2 + M \rightarrow BrONO_2 + M \qquad (6)$$

and the sequence of reactions

$$Br_2 + h\nu \rightarrow 2Br \qquad (7)$$

$$Br + NO + M \rightarrow BrNO + M \qquad (8)$$

$$Br + BrNO \rightarrow Br_2 + NO \qquad (9)$$

There are no complications due to reaction (4) as the concentration of Br_2 was chosen to ensure that all atomic oxygen formed in process (2) was completely consumed (> 99%) well before the first observation point. A range of Br_2 concentrations (5 - 20 x 10^{15} cm^{-3}) was employed with no observable change in the value of k_1. Interference from the bimolecular disproportionation of BrO radicals (5) was unimportant at all reaction times, for the following reasons. As stated earlier the minimum stoichiometry after 90μs was > 10 which means that rate of removal of BrO by reaction (5) was < 3% of the rate of removal by NO (k_5 taken to be 2.25 x 10^{-12} exp(244/T) from 223-388K and between 50 and 600 torr total pressure[18]). As [BrO] decreases due to removal by NO the contribution of reaction (5) to the rate of removal of BrO rapidly decreases as reaction (5)

is second order in BrO concentration. If reaction (5) had made a significant contribution to the overall rate of removal of BrO the decay plots shown in Fig. 3 should have exhibited a noticeable curvature, and the values of k' would have been dependent not only upon $[NO]_o$ but also $[BrO]_o$. However, as the plots of [BrO] with reaction time did not exhibit any observable curvature, nor was there any dependence of k_1 upon initial stoichiometry, this confirms the calculations which showed that reaction (5) should not have interfered with our determination of k_1. The product of reaction (1), NO_2, can react with BrO radicals as shown in reaction (6) to form $BrONO_2$. However, if this reaction were important in our system the decay plots of BrO would have exhibited a non-linearity, which was not observed. In addition, a value of 3.0×10^{-12} cm^3 $molecule^{-1}s^{-1}$ was determined for k_6 at 700 torr N_2 and 298K.[21] Consequently, with an average initial stoichiometry, $[NO]_o/[BrO]_o$, of 18, this would lead to a prediction that the maximum rate (relative to NO + BrO (1)) at which BrO radicals could be removed by reaction (6) is $\sim$1% at 700 torr N_2 and 298K. At lower total pressures, and with He as the diluent, this contribution is even less due to the third (or intermediate second/third) order nature of reaction (6). Even at lower temperatures (e.g., 224K) where the rate constant, k_6, is expected to be approximately a factor of 3 faster (the process is expected to exhibit a negative temperature dependence of $\sim$1000/T in a manner analogous to the $C\ell O + NO_2 + M$ reaction[22]) there would still be a negligible contribution to the removal of BrO by reaction (6).

Nitrosyl bromide, BrNO, is produced as a result of a rapid equilibrium between reactions 8 and 9. The equilibrium BrNO concentration (approximately .02[NO]) is low enough that depletion of NO is negligible.[23a] Moreover, the equilibrium is reached on a time scale short compared to the loss of BrO by reaction 1 so that the minor absorption of the analytical light by BrNO does not interfere with the detection of BrO or the determination of its true rate of decay.[23b] This being the case, the only effect of reactions 8 and 9 is the NO-catalyzed recombination of Br.

As stated in the experimental section the gases are continuously flowed through the reaction cell so that the contents are completely renewed between successive photolytic flashes. This totally eliminates complications due to removal of reagents, e.g., NO, or the build-up of reactive products, e.g., NO_2.

The stable product of reaction (1), NO_2, has a continuous absorption spectrum which is quite strong throughout the visible and ultraviolet spectral regions. The absorption cross-section of NO_2 at 339.0 nm (where BrO was monitored) has been determined to be $\sim 4.0 \times 10^{-19}$ cm^2 $molecule^{-1}$ [24] compared to the value of 1.17×10^{-17} cm^2 $molecule^{-1}$ for BrO at 298K [18]. Consequently the intensity of the analytical light beam (I_o) does not return to its original value after removal of BrO by NO, due to absorption by the NO_2 product, until the cell contents are replaced by reactants. However, as the absorption by NO_2 is a factor of ~ 29 less than that by an equal concentration of BrO it is easily accounted for in the data analysis and does not lead to any inaccuracy in our determination of k_1.

Table I and Fig. 4 summarize the experimental data obtained at 298K. It can be seen that the value of k_1 is invariant with total pressure from 100-700 torr and with the identity of the diluent, He or N_2. The averaged values of k_1 were obtained at each pressure by taking the mean value of the individual values of $k_1 = k_1'/[NO]$. The uncertainties represent 1σ. The mean value of all the data collected at 298K was $(2.15 \pm 0.25) \times 10^{-11}$ cm^3 $molecule^{-1}$ s^{-1}. Fig. 4 shows a plot of k_1' as a function of [NO] (corrected for the amount removed by BrO). A least squares fit to the data shown in Fig. 4 yields a value of k_1 (slope) of $(1.99 \pm 0.14) \times 10^{-11}$ cm^3 $molecule^{-1}$ s^{-1} with an intercept on the k' axis of 627 s^{-1}. These two values of k_1 are in good agreement ($\sim 7\%$), however, it is felt that the best value of k_1 is obtained by taking a simple mean of the individual values of k_1 rather than from the slope of k_1' versus [NO]. This evaluation is based upon the fact that an intercept (positive or negative) has no physical meaning in

our experiment, and that the extrapolation back to [NO] = 0 is long and as such a small change in the slope can result in a large, yet meaningless, intercept on the k_1' axis. That the two values do agree within 7% is a good indication that the system is well behaved. The linearity of Fig. 4 verifies that the reaction is first order in NO concentration. From Table III, which shows the values of k_1 (slope) and k_1 (mean) at each temperature studied, it can be seen that the agreement is always better than 12%. Table II summarizes all the data, and shows that although the reaction exhibits no pressure dependence at any temperature, it does exhibit a small negative temperature dependence. Fig. 5 is an Arrhenius plot of the data obtained in this and other studies. A weighted linear least squares treatment of all the data shown in Table II results in the following Arrhenius expression: $k_1 = 1.28 \times 10^{-11} \exp((181 \pm 46)/T)$; 224-398K. If the alternate method of data analysis were used then a linear least squares treatment of the data would result in the Arrhenius expression shown in Table III. However, it must be stressed that we feel that the correct procedure is to use k_1 (mean).

Discussion

(i) Comparison and Interpretation of Results

Table IV summarizes the values obtained for k_1 in this and other studies. The results of the three low pressure mass spectrometric studies[5,16,25] and the high pressure ultraviolet absorption study (this work), which all used pseudo first order conditions, are in excellent agreement at 298K, and are more reliable than the earlier low pressure ultraviolet absorption study[9b] where the value of k_1 was somewhat dependent upon the rate constant for BrO + BrO → products owing to low initial stoichiometries of [NO] to [BrO]. The results of the two temperature dependence studies are in good agreement and both show a small negative dependence. An Arrhenius plot (Figure 5) shows how the values of k_1 agree to within 10-40% over the temperature range 220-400K, and at stratospheric temperatures (210-260K) to better than 10%. By combining the data obtained in the study with that in references [5,16,25] it can be

Table III. Comparison of k_1(slope) and k_1(mean)

Temperature (K)	k_1(mean)	k_1(slope)	k_1(m)/k_1(s)
224	2.83 ± 0.20	2.90 ± 0.26	0.98
257	2.69 ± 0.18	2.39 ± 0.27	1.12
298	2.15 ± 0.25	1.99 ± 0.14	1.08
351	2.16 ± 0.15	1.92 ± 0.14	1.12
398	2.02 ± 0.18	1.80 ± 0.12	1.12

$k_1(\text{mean}) = 1.28 \times 10^{-11} \exp((181 \pm 46)/T)$

$k_1(\text{slope}) = 9.52 \times 10^{-12} \exp((240 \pm 40)/T)$

Table IV. Summary of Arrhenius Expressions for $NO + BrO \rightarrow NO_2 + Br$

Reference	Arrhenius Expression $cm^3 molecule^{-1} s^{-1}$	$10^{11} \times k_1(298K)$ $cm^3 molecule^{-1} s^{-1}$	Temp. Range K	Technique[a]
This work	$1.28 \times 10^{-11} \exp((181 \pm 46)/T)$	2.15 ± 0.25	224-398	FP/UV
Leu [16]	$7.11 \times 10^{-12} \exp((296 \pm 10)/T)$	1.89 ± 0.16	230-425	DF/MS
Clyne and Watson [5]	-	2.2 ± 0.4	298	DF/MS
Watson and Ray [24]	-	2.3 ± 0.3	298	DF/MS

(a) FP/UV, flash photolysis-ultraviolet absorption detection system; DF/MS, discharge flow mass spectrometric detection system.

shown that this reaction does not exhibit any observable pressure dependence between 1 and 700 torr total pressure, and is independent of the identity of the foreign gas. The temperature dependences of k for the analogous CℓO[13,14] and HO_2[15,17] are also negative, and are similar in magnitude.

(ii) Negative Temperature Dependence of k

The negative temperature dependence of k observed in this study is characteristic of a growing number of rapid bimolecular reactions involving atoms and radicals[13,14,26-28]. Several different hypotheses have been proposed to account for this behaviour including a temperature dependent A-factor,[26] metastable complex formation,[13,28] and dependence of the collision cross section on reactant energy.[27,29] Alternatively, the observed dependence is small enough to be due to systematic experimental error in several cases.

In this study, the data may be fitted with equal reliability to a negative Arrhenius activation energy of 0.36 kcal or to a function of the form

$$k_{NO + BrO} \propto T^{-0.6\pm0.1}$$

According to Absolute Rate Theory, the A-factor for the bimolecular reaction A + B → products is given by:

$$A = \frac{kT}{h} \frac{q^{\neq}}{q_a q_b}$$

where q is a composite partition function. For two diatomic species (NO + BrO) reacting to form a non-linear activated complex ($NO\cdots BrO^{\neq}$), the product of the translational and rotational partition functions varies as T^{-1}. The temperature dependence of the vibrational partition function ratio was evaluated using trans-HONO and CℓONO as models for the complex.[30] The fundamental vibrational frequencies used in these calculations were derived from infrared spectra.[31-34]

In the model compounds, the frequencies associated with the motions of the N and O atoms are quite similar while those involving the chlorine and hydrogen atoms differ markedly. A similar effect should be seen for BrONO with even lower frequencies expected for the Br-O stretch, the NOBr bend and the out-of-plane torsion. In this analysis, since the O-X (X = H, Cℓ) stretch is the dissociative mode it does not contribute to the entropy of activation.

Over the temperature range 200-400K, the vibrational partition function ratio roughly fits a T^x dependence. For trans-HONO, x is approximately 0.39 while for CℓONO x is 0.78. The T-dependence of the complete A-factor with the T^{-1} term included is therefore $T^{-.61}$ for HONO and $T^{-.22}$ for CℓONO. On this basis, the A-factor for the NO + BrO reaction would be expected to have a zero or small positive temperature dependence, due to the lower frequency vibrations expected for BrONO, in contrast to the $T^{-0.6}$ dependence observed. This model, however, is very sensitive to the presumed structure of the transition state, in particular the values of the low frequency vibrations. A more accurate treatment might include the method of Quack and Troe which locates the transition state at the configuration of maximum free energy on the reaction coordinate.(36)

If the NO + BrO reaction forms a vibrationally excited intermediate as has been suggested by Leu and DeMore(13) for the analogous NO + ClO reaction, then a pressure dependence might be observed for the rate constant if the lifetime of the intermediate is comparable to the inverse collision rate. Since no pressure dependence could be detected up to 700 Torr total pressure of helium the lifetime of the intermediate must be considerably less than 4×10^{-11} s. Because of limited thermochemical data, estimates of the lifetime of the intermediate by RRK theory are unreliable. However, for the NO + ClO reaction, lifetimes in the 10^{-11} - 10^{-12} s range are obtained. This suggests that pressure effects will not be observed until the total pressure exceeds 5 atmospheres. Because BrONO is undoubtedly less stable than CℓONO, and the NO + BrO

reaction is more exothermic than the NO + CℓO reaction, the lifetime of the vibrationally hot BrONO intermediate with respect to dissociation into Br and NO_2 will be quite short, perhaps less than 10^{-12} seconds. Third-body effects for the NO + BrO reaction would therefore not be expected for pressures less than 10-20 atmospheres. As a means of verifying these qualitative predictions, it would be useful to conduct high pressure reaction rate studies of the NO + FO and NO + CℓO reactions. To date, the NO + FO reaction has not been studied and the NO + CℓO rate constant has been measured only at low pressure. Considering the thermodynamic stability of FONO and its isomer FNO_2, both bimolecular and termolecular channels might be expected for this reaction.

(iii) Atmospheric Implications

This section discusses the role of the NO + BrO reaction in stratospheric bromine photochemistry. The discussion will show how the catalytic efficiency of BrO_x in destroying stratospheric ozone is relatively insensitive to the value of k(NO + BrO), but how the concentration ratios of Br/BrO and BrO/HBr are quite sensitive to this rate constant. It is important to determine accurate kinetic data not only for reactions which control the catalytic efficiency of ozone destruction, but also for those reactions which control concentration ratios because it is the comparison between theoretical predictions and field measurement data of ratios such as Br/BrO and BrO/HBr that tests our understanding of atmospheric photochemistry. The roles of the NO + BrO, and NO + CℓO reactions in stratospheric photochemistry will be compared.

Table V summarizes the reactions involving bromine-containing species now thought to be important in the photochemistry of the stratosphere, along with their rate coefficients.[35] Using the reaction scheme and numbering system shown in Table V the following expressions can be derived:

$$\frac{Br}{HBr} = \frac{k_{12}[OH] + k_{13}[O]}{k_{10}[HO_2] + k_{11}[H_2O_2]} \approx \frac{k_{12}[OH]}{k_{10}[HO_2]} \qquad \text{(VI)}$$

$$\frac{BrONO_2}{BrO} = \frac{k_7[NO_2][M]}{J_3} \qquad \text{(VII)}$$

Table V. Key Bromine Reactions and Their Rate Coefficients

	Reaction	A	E/R
1	$Br + O_3 \rightarrow BrO + O_2$	1.4×10^{-11}	755
2	$BrO + O \rightarrow Br + O_2$	3.0×10^{-11}	-
3	$BrO + NO \rightarrow Br + NO_2$	1.2×10^{-11}	-180
4	$BrO + C\ell O \rightarrow Br + OC\ell O$	6.7×10^{-12}	-
5	$\rightarrow Br + C\ell + O_2$	6.7×10^{-12}	-
6	$BrO + HO_2 \rightarrow HOBr + O_2$	5.0×10^{-12}	-
7	$BrO + NO_2 + M \rightarrow BrONO_2 + M$ (a)	See below	-
8	$BrO + BrO \rightarrow 2Br + O_2$	1.9×10^{-12}	-244
9	$\rightarrow Br_2 + O_2$	3.5×10^{-13}	-244
10	$Br + HO_2 \rightarrow HBr + O_2$	2.0×10^{-11}	-
11	$Br + H_2O_2 \rightarrow HBr + HO_2$	2.0×10^{-12}	>1400
12	$OH + HBr \rightarrow H_2O + Br$	8.5×10^{-12}	-
13	$O + HBr \rightarrow OH + Br$	7.6×10^{-12}	1571
J_1	$BrO + h\nu \rightarrow Br + O$ (b)	10^{-2}; 10^{-2}; 10^{-2}	
J_2	$HOBr + h\nu \rightarrow OH + Br$ (b)	1.7×10^{-3}; 1.3×10^{-3}; 1.1×10^{-3}	
J_3	$BrONO_2 + h\nu \rightarrow Br + NO_3$ (b)	1.6×10^{-3}; 1.1×10^{-3}; 9.8×10^{-4}	
J_4	$Br_2 + h\nu \rightarrow 2Br$ (b)	1.5×10^{-2}; 1.5×10^{-2}; 1.5×10^{-2}	

(a) $k = 2k(C\ell O + NO_2 + M) = \dfrac{1.3 \times 10^{-22}\ T^{-3.34}}{1 + 8.7 \times 10^{-9}\ T^{-0.6}\ M^{0.5}}$

(b) 40km; 30km; 20km.

$$\frac{BrO}{Br} = \frac{k_1[O_3]}{k_2[O] + k_3[NO] + (k_4+k_5)[C\ell O] + k_7[NO_2][M] + k_{10}[HO_2] + J_1} \quad \text{(VIII)}$$

$$\frac{BrO}{HOBr} = \frac{J_2}{k_6[HO_2]} \quad \text{(IX)}$$

Equation (VIII) was derived neglecting the BrO + BrO reactions (8,9). However, at low concentrations of BrO_x (< 100 ppt) this does not lead to any significant error. By combining equations (VI - IX) it can be shown that:

$$\frac{BrO}{BrO_x} = \left\{1 + \frac{D(k_{12}[OH] + k_{10}[HO_2])}{k_1 k_{12}[OH][O_3]} + \frac{k_7[NO_2][M]}{J_3} + \frac{k_6[HO_2]}{J_2}\right\}^{-1} \quad \text{(X)}$$

where D is the denominator in equation (VIII).

Using the rate coefficients and J values shown in Table V and the altitude profiles of stratospheric trace constituents calculated by the diurnally-averaged one dimensional photochemical model of Yung et al.[1a] the photochemical partitioning of BrO_x shown in Figure 6 is obtained. The photochemical model attempts to simulate the present day atmosphere which is assumed to contain 2.3 ppbv $C\ell O_x$, 19 ppbv NO_x, 6 ppmv H_2O and 20 pptv BrO_x at 40 km. In order to test the sensitivity of the BrO/Br, BrO/HBr and BrO/BrO_x ratios to the NO + BrO rate constant, k_3, equations VI, VIII and X were evaluated using concentrations derived from the model. Table VI presents these ratios as a function of altitude for three cases; (a) k_3 as determined in this study, (b) k_3 multiplied by 2 and, (c) k_3 divided by 2. It is apparent that variations of ± a factor of 2 in k_3 have a significant effect on BrO/Br and BrO/HBr (average deviations of ± 50%) but only a small effect on BrO/BrO_x (average deviation of ± 8%). The sensitivity of the BrO/Br and BrO/HBr ratios to changes in k_3 is attributable to the relatively large contribution of the NO + BrO reaction to the overall BrO to Br conversion rate. This point is illustrated in Table VII which compares the magnitudes of the terms in the denominator (D) of equation

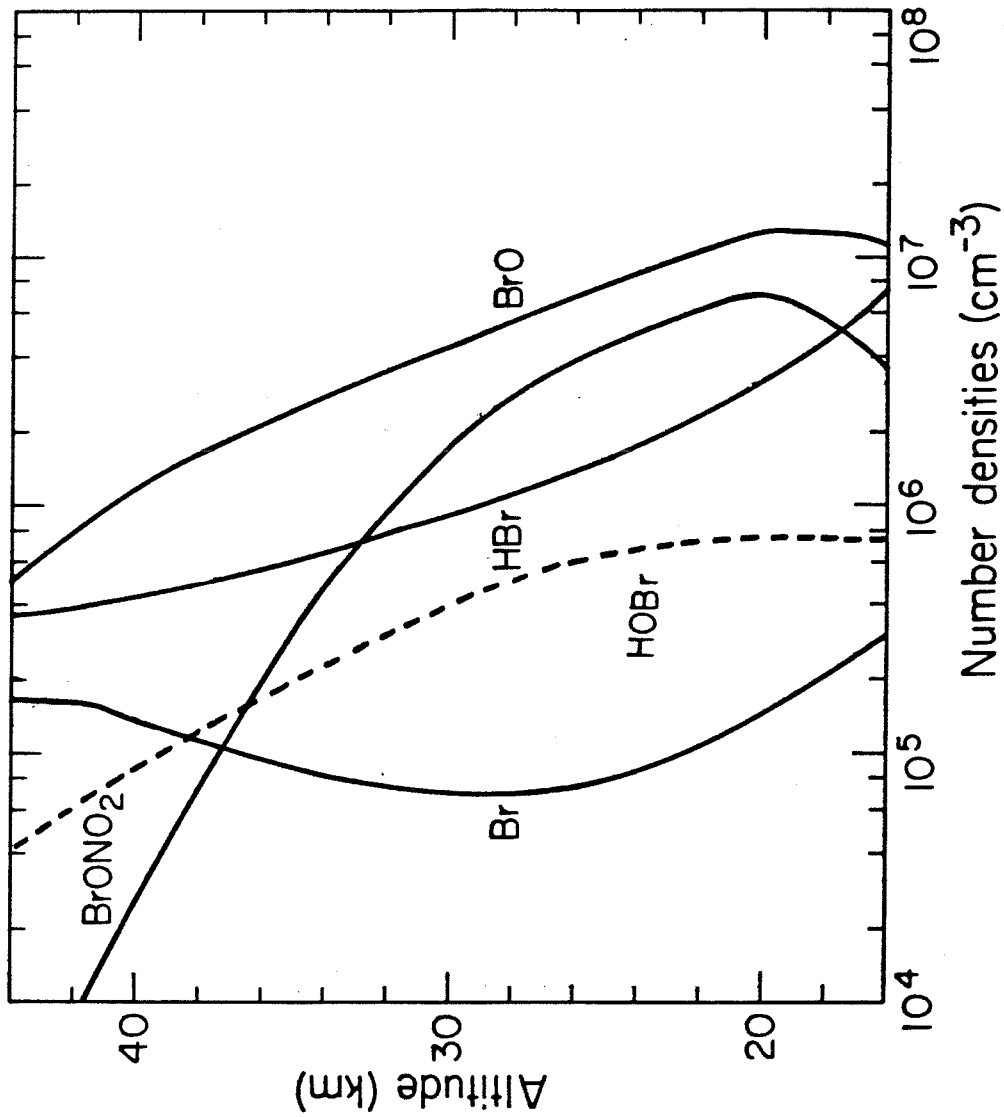

Figure 6. Altitude profiles for major bromine species in the stratosphere (taken from photochemical model of Yung et al.(1a)). Total BrO_x at 40km equals 20 pptv.

Table VI. Photochemical Partitioning of BrO_x

Altitude (km)	A			B			C		
	%BrO	BrO/Br	BrO/HBr	%BrO	BrO/Br	BrO/HBr	%BrO	BrO/Br	BrO/HBr
16	49	39	1.7	45	30	1.3	52	47	2.0
20	52	86	4.0	49	62	2.9	53	107	5.0
24	53	100	4.9	50	70	3.4	54	127	6.2
28	53	78	4.7	50	50	3.0	55	107	6.5
32	61	47	4.3	56	30	2.7	64	68	6.2
36	67	20	3.9	60	12	2.4	72	29	5.6
40	65	8.0	2.9	56	5.2	1.9	70	110	4.0
44	46	2.8	1.3	39	2.1	0.99	51	3.4	1.6
24*	54	146	7.1	52	90	4.4	56	212	10.4
24**	48	53	2.6	46	43	2.1	49	60	2.9
24+	43	100	1.7	39	70	1.1	46	127	2.1

Column (A): BrO_x partitioning in standard model.

Column (B): BrO_x partitioning in a model where k_3 was multiplied by a factor of 2.

Column (C): BrO_x partitioning in a model where k_3 was divided by a factor of 2.

* : $J_1(BrO) = 3 \times 10^{-3} s^{-1}$

** : $J_1(BrO) = 3 \times 10^{-2} s^{-1}$

\+ : $k_{10}(Br + HO_2) = 6 \times 10^{-11} cm^3 s^{-1}$

Table VII. Magnitude of the Terms That Control the Br:BrO Ratio

Altitude (km)	$k_3[NO]$	J_1	$2k_5[ClO]$	$k_2[O]$	$k_7[NO_2][M]$	$k_{10}[HO_2]$	$k_3[NO]/D$		
				(s^{-1})			A	B	C
16	5.2(-3)	1.0(-2)	3.8(-4)	2.3(-6)	3.2(-4)	7.4(-5)	.33	.50	.20
20	7.3(-3)	1.0(-2)	1.1(-3)	2.5(-5)	6.0(-4)	6.8(-5)	.38	.55	.24
24	9.6(-3)	1.0(-2)	1.6(-3)	1.3(-4)	6.2(-4)	1.0(-4)	.43	.60	.27
28	1.6(-2)	1.0(-2)	1.5(-3)	5.3(-4)	5.8(-4)	1.4(-4)	.55	.71	.38
32	2.1(-2)	1.0(-2)	1.6(-3)	1.7(-3)	3.2(-4)	1.7(-4)	.60	.75	.43
36	2.7(-2)	1.0(-2)	1.3(-3)	4.3(-3)	1.2(-4)	1.4(-4)	.63	.77	.46
40	2.6(-2)	1.0(-2)	7.6(-4)	1.1(-2)	2.6(-5)	1.1(-4)	.54	.70	.37
44	1.9(-2)	1.0(-2)	2.5(-4)	2.6(-2)	3.8(-6)	9.4(-5)	.34	.51	.20

Column (A) = $k_3[NO]/D$

Column (B) = $k_3[NO]/D$ where k_3 was multiplied by a factor of 2.

Column (C) = $k_3[NO]/D$ where k_3 was divided by a factor of 2.

VIII and the fractional contribution of $k_3(NO)$ to this sum as a function of altitude and k_3. Columns A, B and C, which tabulate the ratio $k_3(NO)/D$ for different values of k_3, show the strong dependence on k_3. This accounts for the sensitivity of BrO/Br and BrO/HBr to k_3 since the ratios are inversely proportional to D. In contrast, equation X shows that the ratio BrO/BrO_x depends upon D in a much less direct fashion. The BrO/BrO_x ratio is relatively insensitive to variations in D, and thus k_3, owing to the relative magnitudes of the terms in equation X , e.g. at 24 km:

standard model:	1	0.21	0.60	.087
$k_3 \times 2$	1	0.31	0.60	.087
$k_3 \div 2$	1	0.17	0.60	.087

From these values it can be seen that large variations in D are not reflected in the BrO/BrO_x ratio due to damping by the other terms in equation X . This is a result of the fact that BrO, rather than HBr, is the dominant form of bromine throughout most of the stratosphere.

To a first approximation (BrO_x < 100 ppt) the catalytic efficiency with which O_3 is destroyed by BrO_x is linearly proportional to [BrO] since each of the catalytic cycles which results in the removal of odd oxygen involves the BrO radical in the rate determining step.[1a] Since, as shown above, variations in k_3 have only a small effect on the BrO/BrO_x ratio, the catalytic efficiency of BrO_x in destroying ozone is not particularly sensitive to this rate constant. However, the concentration ratios BrO/Br and BrO/HBr are strongly dependent on k_3.

Two major uncertainties in the photochemical data base are the values of J_1 and k_{10}. The values of J_1 and k_{10} are uncertain by approximately a factor of ±3 each. Table VI shows the sensitivity of the photochemical partitioning of BrO_x to the value of k_3 for values of J_1 equal to 3×10^{-3} and $3 \times 10^{-2} s^{-1}$, and k_{10} equal to $6 \times 10^{-11} cm^3 s^{-1}$ (results are shown for 24km which is taken to be a representative altitude). It can be seen that when the value of J_1 was taken to be $3 \times 10^{-2} s^{-1}$ each of the ratios, BrO/Br, BrO/HBr and BrO/BrO_x was less sensitive to the value of k_3 than when the value of J_1 was taken to be

$3 \times 10^{-3} s^{-1}$ due to the increased buffering effect of J_1. When k_{10} was assumed to be $6 \times 10^{-11} cm^3 s^{-1}$ the BrO/BrO_x ratio was twice as sensitive to the value of k_3 than in the standard model, but a variation in k_3 of a factor of 4 still led to only an 18% change in BrO/BrO_x.

The insensitivity of the BrO/BrO_x ratio to the value of k_3 is in sharp contrast to the sensitivity of the $C\ell O/C\ell O_x$ ratio to the value of k(NO + CℓO). As stated earlier a major difference between the BrO_x and $C\ell O_x$ system is that the photolysis rate of BrO is several orders of magnitude greater than the photolysis rate of CℓO. This results in the NO + CℓO reaction being the only important process for converting CℓO into Cℓ below 32km. Above 32km the O + CℓO reaction becomes increasingly important. Consequently throughout most of the stratosphere the CℓO/Cℓ and CℓO/HCℓ ratios are linearly proportional to k(NO + CℓO). An equation can be derived for $C\ell O/C\ell O_x$ which is analogous to that derived for BrO/BrO_x (eqn. X). Using this equation it can be shown that variations in k(NO + CℓO) of ± factor of 2 result in ±50% variations in $C\ell O/C\ell O_x$ at altitudes ≤36km. The sensitivity of $C\ell O/C\ell O_x$ to k(NO + CℓO) is in contrast to the insensitivity of BrO/BrO_x to k(NO + BrO), and is due to the importance of the term containing D. This arises because HCℓ and $C\ell ONO_2$ are the dominant forms of $C\ell O_x$, whereas BrO is the dominant form of BrO_x.

Acknowledgements

We thank J. Linke for his indispensable glass blowing services, G. Tennant and M. Patapoff for their expert assistance in constructing the experimental apparatus, and J. Pinto for use of the output of our 1-D photochemical model prior to publication. We benefited greatly from discussions with W. B. DeMore.

This paper presents the results of one phase of research carried out at the Jet Propulsion Laboratory, California Institute of Technology, under Contract No. NAS7-100, sponsored by the National Aeronautics and Space Administration. Part of this work was supported by NASA Grant NSG 2229 to the California Institute of Technology.

References and Notes

(1) (a) Y. L. Yung, J. Pinto, R. T. Watson, and S. P. Sander, accepted, J. Atmos. Sci., (1979); (b) S. C. Wofsy, M. B. McElroy, and Y. L. Yung, Geophys. Res. Lett. 2, 215 (1975); (c) J. A. Logan, M. J. Prather, S. C. Wofsy and M. B. McElroy, Philosophical Transactions of the Royal Society of London. A Mathematical and Physical Sciences, 290, 187, (1978); (d) NASA Ref. Pub. No. 1010, "Chlorofluoromethanes and the Stratosphere", R. D. Hudson, editor, (1977); (e) National Academy of Sciences, Halocarbons: Effects on Stratospheric Ozone. Washington, D.C. (1976), and (f) R. T. Watson, "Chlorine, Chlorine Oxides and Other Halogen Species", Sec. 5.7.5, CIAP Monograph 1, "The Natural Stratosphere of 1974", DOT-TST-75-51, September, 1975.

(2) C. J. Howard and K. M. Evenson, Geophys. Res. Lett. 4, 437 (1977).

(3) C. J. Howard, private communication, 1979.

(4) M. A. A. Clyne and R. T. Watson, JCS, Far. Trans. I, 70, 2250 (1974).

(5) M. A. A. Clyne and R. T. Watson, JCS, Far. Trans. I, 71, 336 (1975).

(6) M. A. A. Clyne and R. T. Watson, Chem. Phys. Letters, 12, 344 (1971).

(7) C. E. McDade, T. M. Lenhardt, and K. D. Bayes, "Flash Photolysis Using a Photoionization Mass Spectrometer", 13th Informal Conference on Photochemistry. Florida, January (1978).

(8) R. A. Durie and D. A. Ramsay, Can. J. Phys., 36, 35 (1958).

(9) (a) M. A. A. Clyne and J. A. Coxon, Proc. Roy. Soc. A., 303, 207 (1968); (b) M. A. A. Clyne and H. W. Cruse, Trans. Far. Soc., 66, 2227 (1970).

(10) N. Basco and S. K. Dogra, Proc. Roy. Soc. A., 323, 29 (1971).

(11) (a) H. S. Johnston, E. D. Morris, Jr. and J. Van den Bogaerde, J. Amer. Chem. Soc., 91, 7712 (1969);
(b) R. A. Cox, R. G. Derwent, A. E. J. Eggleton and H. J. Reid, "Kinetics of ClOO and ClO Radicals Using Molecular Modulation Spectrometry-The Cl Atom Catalyzed Disproportionation of ClO". In press, JCS Faraday Trans I.

(12) E. J. Hamilton, Jr. and R. R. Lii, Int. J. Chem. Kinet., 9, 875 (1977).

(13) M. T. Leu and W. B. DeMore, J. Phys. Chem., 82, 2049 (1978).

(14) M. S. Zahniser and F. Kaufman, J. Chem. Phys., 66, 3673 (1977).

(15) C. J. Howard, results presented at the WMO Symposium, Toronto, June 1978.

(16) M. T. Leu, Chem. Phys. Lett., 61, 275 (1979).

(17) M. T. Leu, Chem. Phys. Lett., 61, 275 (1979).

(18) S. P. Sander and R. T. Watson, "Rates and Mechanism of the Bimolecular Disproportionation of BrO Radicals", manuscript in preparation.

(19) (a) S. Singer, L. K. Neher and R. Ruehle, Rev. Sci. Instrum., 27, 40 (1956).
(b) S. Yatsiv and J. J. Ewing, Rev. Sci. Instrum., 45, 705 (1974).

(20) M. A. A. Clyne, P. B. Monkhouse, and L. W. Townsend, Int. J. Chem. Kinet. 8, 425 (1976).

(21) G. W. Ray, S. P. Sander and R. T. Watson, "A Pressure-Dependence Kinetics Study of the Reaction NO_2 + BrO + M → $BrONO_2$ + M", manuscript in preparation.

(22) (a) M. T. Leu, C. L. Lin and W. B. DeMore, J. Phys. Chem., 81, 190 (1977);
(b) M. Zahniser, J. S. Chang and F. Kaufman, J. Chem. Phys., 67, 997 (1977);
(c) J. W. Birks, B. Shoemaker, T. J. Leck, R. A. Borders and L. J. Hart, J. Chem. Phys., 66, 4591 (1977).

(23) (a) the ratio $[BrNO]_{ss}/[NO]$ is given by $\frac{[BrNO]_{ss}}{[NO]} = \frac{k_8}{k_9}$. Substituting $k_8 = 4.3 \times 10^{-13}$ cm^3 s^{-1} (Van den Bergh and Troe, J. Chem. Phys., 64, 736 (1976)) and $k_9 \simeq 2 \times 10^{-11}$ cm^3 s^{-1}, an average of the rate constants for the Cℓ + CℓNO and Br + CℓNO reactions, (M. A. A. Clyne and H. Cruse, JCS, Far. Trans. II, 68, 1281 (1972)) one obtains $[BrNO]_{ss} \simeq .02[NO]$.
(b) The time required for BrNO to reach equilibrium is related to [Br], [NO], k_8 and k_9. For typical values of [Br] and [NO] (.16 x 10^{13} cm^{-3} and 5 x 10^{14} cm^{-3} respectively), BrNO reaches 95% of its equilibrium concentration in 94μsec, which is short compared to the decay time for BrO.

(24) A. M. Bass, A. E. Ledford, Jr. and Allen H. Laufer, J. Research, 80A, 143 (1976).

(25) G. W. Ray and R. T. Watson, "Kinetic Studies of XO + NO Reactions Using Mass Spectrometry: X = Cℓ, Br, F and CH_3O", manuscript in preparation.

(26) P. P. Bemand, M. A. A. Clyne and R. T. Watson, JCS, Far. Trans. II, 70, 564 (1974).

(27) D. D. Davis, R. E. Huie and J. T. Herron, J. Chem. Phys., 59, 628 (1973).

(28) D. L. Singleton and R. J. Cvetanovic, J. Am. Chem. Soc., 98, 6812 (1976).

(29) R. L. Jaffe, "Can A Bimolecular Gas Phase Reaction Have A Negative Activation Energy?", 175th National Meeting of the American Chemical Society, Anaheim, California, (1978).

(30) T. L. Hill, An Introduction to Statistical Thermodynamics, Addison-Wesley, Reading, Mass., 1960.

(31) G. E. McGraw, D. L. Bernitt and I. C. Hisatsune, J. Chem. Phys., 45, 2447 (1966).

(32) A. Carrington and P. N. Dyer, J. Chem. Phys., 52, 309 (1970).

(33) G. Herzberg, Spectra of Diatomic Molecules, D. Van Nostrand, Princeton.

(34) B. Janowski, H. D. Knauth and H. Martin, Ber. Bunsenges Phys. Chem., 81, 1262 (1977).

(35) Rate coefficient data base consistent with, "Chemical Kinetic and Photochemical Data for Use in Stratospheric Modelling", W. B. DeMore, L. J. Stief, F. Kaufman, D. M. Golden, R. F. Hampson, M. J. Kurylo, J. J. Margitan, M. J. Molina, and R. T. Watson, JPL Report 79-27 (1979).

(36) M. Quack and J. Troe, Ber. Bunsenges Phys. Chem., 81, 329 (1977).

CHAPTER V

A PRESSURE - DEPENDENCE KINETICS STUDY OF THE FORMATION OF BROMINE NITRATE AT 298 K

S. P. Sander and R. T. Watson*

Molecular Physics and Chemistry Section

Jet Propulsion Laboratory
Pasadena, CA 91103

ABSTRACT

The kinetics of the reaction $BrO + NO_2 + N_2 \rightarrow BrONO_2 + N_2$ were studied from 50-700 Torr at 298 K. The flash photolysis-ultraviolet absorption technique was used to monitor the pseudo first-order decay of BrO ($^2\Pi$) radicals in the presence of excess NO_2. The reaction was found to be in the fall-off region between second- and third-order kinetics in this pressure range. Estimates of the limiting third- and second-order rate constants, k_o and k_∞, were determined by fitting the observed fall-off curve to a theoretical expression developed by Troe and co-workers. The value of k_o so derived was in good agreement with a preliminary determination of this rate constant made in our laboratory using the technique of discharge flow-mass spectrometry. The stratospheric implications of these measurements are discussed.

INTRODUCTION

Within the last few years, there has been considerable interest in the catalytic destruction of stratospheric ozone by trace (ppt-ppb) concentrations of NO_x,[1] ClX[2] and most recently, BrX.[3] Each chemical family, e.g. ClX, can be partitioned into precursors (e.g. $CFCl_3$), radicals (Cl, ClO) and reservoirs (HCl, $ClONO_2$ and HOCl). Molecules such as $ClONO_2$ and HOCl are normally thought of as reservoir species, implying that they act to reduce the concentrations of radicals which participate in ozone destroying catalytic cycles, thus decreasing the efficiency of odd oxygen destruction by ClX. However, depending on the rates and mechanisms of their photodissociation, these species may also participate in ozone destruction cycles. The net effect of these temporary reservoir species with respect to ozone depletion can be determined only by solving the coupled equations of atmospheric chemistry and transport. Doing so requires accurate kinetic data applicable to atmospheric conditions of pressure and temperature.

The rate constant for the formation of chlorine nitrate has been measured both in its third-order kinetic region[4] (1 to 7 Torr total pressure) and in the fall-off region between second- and third-order kinetics[5-7] (25 to 600 Torr). Discrepancies exist between rate measurements obtained by observing the overall rate of decay of ClO as in the flash photolysis, discharge flow and molecular modulation studies, and a technique based on the thermal decomposition of chlorine nitrate, leading to the speculation that several different $ClNO_3$ isomers may be formed. In contrast no rate data presently exist for the formation of bromine nitrate,

$$BrO + NO_2 + M \rightarrow BrONO_2 + M \qquad (1)$$

In this study, we report the rate constant for reaction 1 over the pressure range 50 to 700 Torr total pressure of N_2 at 298K using the flash photolysis-ultraviolet absorption technique. Like chlorine nitrate, the reaction is found to be in the intermediate second-third-order kinetic region over this pressure range. Using theoretical methods developed recently by Troe and co-workers[8,9] it was possible to use this fall-off data to estimate the low- and high-pressure limiting rate constants, k_o and k_∞. The value determined for k_o was consistent with a preliminary experimental determination performed in our laboratory using the discharge flow-mass spectrometric technique. Because only BrO was observed in this study, the issue of isomer formation in reaction 1 could not be addressed.

EXPERIMENTAL SECTION

The flash photolysis-ultraviolet absorption apparatus has been described in detail previously.[10] The quartz reaction cell was operated in the continuously flowing mode with a flashing frequency equal to the cell residence time (15-30s). As in our previous studies of BrO kinetics,[10,11] BrO radicals were monitored by their absorption at 339.0 nm, near the band head of the $A^2\Pi(v' = 4) \leftarrow X^2\Pi(v'' = 0)$ transition. Using a monochromator slit width of 100 μm and an absorption path length of 720 cm, the effective BrO cross-section was previously determined to be $(1.14 \pm 0.14) \times 10^{-17}$ cm^2.[11] However, this parameter is not required for the data analysis because pseudo-first-order kinetics were employed. An analog multichannel analyzer was employed to average from 10-50 separate BrO decay profiles. The temperature of the reaction cell was main-

tained at 298 ± 1K by circulating methanol through the outer cell jacket from a constant temperature circulator.

Since pseudo-first-order conditions were employed ($[NO_2]_o >> [BrO]_o$), [BrO] obeyed the rate equation

$$\ell n([BrO]_o/[BrO]) = k_1[NO_2]t.$$

Beer's Law was used to relate the absorption signal to [BrO];

$$\ell n(\ell n(I_o/I_{t_o}) - \ell n(I_o/I_t)) = k_1[NO_2]t$$

where I_{t_o}, I_t and I_o are the transmitted light intensities immediately after the flash, at time t and after many BrO half-lives, respectively.

BrO radicals were produced by the reaction of oxygen atoms with molecular bromine;

$$O_2 + h\nu \rightarrow 2O \qquad (2)$$

$$O + Br_2 \rightarrow BrO + Br \qquad (3) \quad k_3 = 1.4\times10^{-11} cm^3 molecule^{-1} s^{-1}$$

(Rate constants quoted in the text are from ref. 12 unless otherwise indicated.) Oxygen atoms were produced from the photolysis of molecular oxygen in the wavelength region $\lambda > 180nm$. A flash energy of 500J dissociated only 0.0015% of the molecular oxygen, necessitating large O_2 concentrations, typically around 1×10^{18} molecule cm^{-3} to produce BrO concentrations of $(1\text{-}2) \times 10^{13}$ molecule cm^{-3}. At the lowest total pressures employed in this study (50-100 Torr) where such high O_2 concentrations would have contributed a non-negligible third-body effect, O_2 was not added. Photolysis of the NO_2 present as a reactant provided a sufficient number of oxygen atoms via reaction 4 to produce BrO in concentrations less than $\sim 2 \times 10^{13}$ molecule cm^{-3}.

$$NO_2 + h\nu \rightarrow NO + O(^3P) \qquad (4)$$

N_2O was used as an additional oxygen atom source in a few runs at 50 and 100 Torr.

$$N_2O + h\nu \rightarrow N_2 + O(^1D) \qquad (5)$$

However, because N_2O photolyzes relatively inefficiently it was not a good source of atomic oxygen. The disadvantage of both these oxygen atom precursors is that NO, which reacts rapidly with BrO via reaction 6, is formed as a by-product.

$$NO + BrO \rightarrow NO_2 + Br \qquad (6) \quad k_6 = 2.1\times10^{-11} cm^3 molecule^{-1} s^{-1}$$

NO is formed directly from the photolysis of NO_2, and in reaction 7a when N_2O is added.

$$O(^1D) + N_2O \rightarrow 2NO \qquad (7a) \quad k_{7a} = 8.6\times10^{-11} cm^3 molecule^{-1} s^{-1}$$

$$\rightarrow N_2 + O_2 \qquad (7b) \quad k_{7b} = 7.4\times10^{-11} cm^3 molecule^{-1} s^{-1}$$

NO production from NO_2 photolysis, both by the photolysis flash lamp and the analyzing lamp, was minimized by a series of measures. First, the lowest possible flash lamp energy was used that was consistent with a given signal-to-noise ratio. This was typically less than 700J per flash. Second, the flash lamp filter cell was filled with a Cl_2-Br_2 mixture which, at equilibrium, contained 60 Torr BrCl and 200 Torr Cl_2. BrCl has an absorption band centered at 370nm. The BrCl and Cl_2 absorbed a portion of the light which would otherwise have resulted in NO_2 photolysis. Photolysis also occurred in the spectroscopic analysis beam. This was suppressed by placing a 10cm cell containing 200 Torr Br_2 in the analysis beam to filter out its near-UV spectral component. A manually operated shutter was also placed in the analytical beam path which was opened a few seconds before the photolysis flash and closed

immediately thereafter. These measures reduced the NO_2 photolysis due to the flash lamp to 0.18% per flash at 389J flash energy without reducing the efficiency of O_2 photolysis, and practically eliminated NO_2 photolysis from the analysis lamp. The effect of photolytically produced NO is treated in the Results section.

The range of reagent concentrations were (in molecule cm^{-3}):

$[Br_2] \times 10^{-15}$: 1.0 - 18.9; $[O_2] \times 10^{-18}$: 1.5 - 3.4; $[N_2O] \times 10^{-17}$: 1.0 - 5.3; $[NO_2] \times 10^{-15}$: 0.34 - 8.6. $[BrO]_o$ ranged from 0.5 to 4 $\times 10^{13}$ molecule cm^{-3} by changing $[O_2]$ or flash energy (300-700J). This resulted in initial analytical beam absorptions of 4 - 28%. Molecular bromine concentrations were high enough to ensure that 99% of the atomic oxygen was converted to BrO radicals within 50μs after the photolytic flash. Characteristic times for BrO formation were always at least ten times shorter than those for BrO loss by reaction 1. Diluent gases (He, N_2, O_2) all had a stated purity >99.99%. Br_2 was purified by extensive freeze-thaw degassing followed by fractional distillation. NO_2-O_2 mixtures were made by reacting small amounts of NO (Matheson C.P. Grade, 99.0% purity) with a large excess of O_2 and allowing sufficient time for complete conversion. NO_2 mixtures were stored and transferred in darkened bulbs and lines.

RESULTS

Pseudo-first-order rate constants (k_1') for bromine nitrate formation were measured at total pressures of 50, 100, 200, 300, 400, 500, 600 and 700 Torr using N_2 as the diluent gas. Values of $[NO_2]_o/[BrO]_o$, the initial reactant stoichiometry, ranged from 10-200 thus maintaining good pseudo-first-order conditions at all times. A total of 129 kinetic

runs were conducted. The most important parameters for each kinetic run are given in Table I. Values of $[BrO]_o$ are obtained by extrapolating the BrO concentration back from the first measurable point ($t \sim 90$ μs) to the estimated point of maximum [BrO] at $t \sim 25$ μs.[10]

BrO decays were typically observed over 2 to 5 half-lives, depending on initial radical concentrations. Plots of k_1' vs. $[NO_2]$ at each pressure were linear with small y-intercepts. These plots show no evidence of a BrO removal process other than reaction with NO_2. An obvious trend of k_1 with pressure is observed with the rate constant increasing by a factor of about five as the pressure is increased from 50 to 700 Torr of N_2. A graph containing several k_1' vs. $[NO_2]$ plots at different pressures is shown in Figure 1 illustrating that the reaction is first order in NO_2 and that the rate constant has a pressure dependence. The variation of k_1 with pressure is shown in Figure 2.

Table II contains the measured bimolecular rate constants derived both by averaging the values of $k_1'/[NO_2]$ for each run, and by computing the least-squares slopes of the k_1' vs. $[NO_2]$ plots. While differences of up to 22% are observed between the rate constants calculated by the two methods, the average difference over the entire pressure range is only about 2% indicating that the differences are due only to experimental scatter. The preferred rate constants are obtained from the averages of the individual runs rather than the slopes. In the 50 and 100 Torr experiments, the runs which contain N_2O have higher average rate constants than the ones which do not. This effect may be due to a higher N_2O third-body efficiency or a small amount of NO formation from reaction 7a. For these pressures, the final rate constant has been obtained by averaging the two sets of data.

Table I. Reaction Rate Data for[137] $BrO + NO_2 + M$

Flash Energy J	$[O_2]$ x 10^{-18} molecule cm^{-3}	$[Br_2]$ x 10^{-15} molecule cm^{-3}	$[BrO]_o$ x 10^{-13} molecule cm^{-3}	$[NO_2]$ x 10^{-15} molecule cm^{-3}	k' measured s^{-1}	k' corrected s^{-1}	k x 10^{12} cm^3 $molec^{-1}s^{-1}$
P_{TOT} = 50 Torr N_2							
529	0.0	18.9	0.65	1.12	521	450	0.402
389	0.36	13.9	0.62	1.28	929	870	0.680
529	0.0	18.9	0.58	1.49	711	620	0.416
529	0.0	18.9	0.79	1.56	669	580	0.372
389	0.39	12.4	1.1	1.91	1340	1250	0.654
529	0.0	18.9	0.95	1.95	928	810	0.415
389	0.36	13.9	1.1	2.47	1630	1520	0.615
529	0.0	18.9	1.1	3.00	1560	1370	0.457
389	0.36	13.9	1.1	3.01	1890	1750	0.581
389	0.36	13.9	1.1	3.01	2100	1960	0.651
389	0.38	12.4	1.2	3.48	2610	2440	0.701
529	0.0	18.9	1.2	4.36	2592	2310	0.530
389	0.18	12.4	1.2	4.45	2580	2360	0.530
389	0.098	12.4	1.1	4.75	2510	2270	0.478
389	0.0	12.4	1.0	5.05	2800	2550	0.505
389	0.36	13.9	1.5	5.15	3330	3070	0.596
389	0.0	13.9	1.3	5.15	3360	3100	0.601
389	0.0	13.9	1.3	5.65	3380	3100	0.549
389	0.35	12.4	1.2	6.01	3100	2790	0.464
529	0.0	18.9	1.5	6.50	3930	3500	0.538
389	0.36	13.9	2.7	6.60	4230	3890	0.589
389	0.36	13.9	1.5	7.49	3950	3560	0.475
529	0.0	18.9	1.8	8.11	5059	4500	0.555
389	0.36	13.9	3.1	8.63	6250	5790	0.671
389	0.36	13.9	3.1	8.63	6360	5900	0.684
							$\bar{k}$ = (5.49 ± 0.97) x 10^{-13}
P_{TOT} = 100 Torr N_2							
389	1.73*	9.94	0.80	0.511	667	645	1.26
389	1.82*	10.0	0.79	0.590	447	420	0.712

Table I. (Cont.)

Flash Energy J	$[O_2]$ x 10^{-18} molecule cm^{-3}	$[Br_2]$ x 10^{-15} molecule cm^{-3}	$[BrO]_o$ x 10^{-13} molecule cm^{-3}	$[NO_2]$ x 10^{-15} molecule cm^{-3}	k' measured s^{-1}	k' corrected s^{-1}	k x 10^{12} cm^3 $molec^{-1}$ s^{-1}
389	1.82*	10.0	0.91	0.950	771	729	0.767
389	0.37	10.9	1.3	1.13	1140	1090	0.965
529	0.0	18.9	0.67	1.30	1140	1060	0.815
389	0.37	10.9	0.90	1.31	1370	1310	1.00
389	0.53	10.0	1.0	1.40	1760	1700	1.21
389	1.73*	9.94	1.0	1.51	1169	1100	0.728
389	1.82*	10.0	1.0	1.58	1330	1260	0.797
389	0.17	11.4	1.0	1.65	1820	1750	1.06
389	0.37	10.9	1.3	1.70	1610	1530	0.900
691	0.37	10.9	3.0	1.70	1930	1680	0.988
941	0.37	10.9	5.3	1.75	2170	b	
200	0.48	10.9	0.48	1.77	2030	1990	1.12
527	0.0	18.9	0.95	1.93	2110	1990	1.03
389	1.82*	10.0	1.1	2.23	1732	1630	0.731
389	0.37	10.9	1.4	2.27	2170	2060	0.907
389	1.73*	9.94	1.1	2.54	1719	1600	0.630
529	0.0	18.9	0.97	2.55	2750	2590	1.02
691	0.37	10.9	4.4	2.84	3280	3040	1.07
389	0.37	10.9	1.5	2.84	3000	2860	1.01
389	0.37	10.9	1.6	2.89	3280	3140	1.09
941	0.37	10.9	6.9	2.95	3780	b	
200	0.37	10.9	0.51	2.98	3050	2980	1.00
389	1.82*	10.0	1.3	3.05	2197	2050	0.672
529	0.0	18.9	1.2	3.33	3920	3710	1.11
389	0.37	10.9	1.5	3.40	3070	2900	0.853
389	1.73*	9.94	1.2	3.56	2248	2070	0.581
389	0.53	10.0	1.3	3.85	3720	3530	0.917
691	0.37	10.9	1.4	3.97	3880	3530	0.889
389	0.37	10.9	3.5	3.97	3640	3440	0.866
389	1.82*	10.0	1.5	3.98	3731	3530	0.887
941	0.37	10.9	6.7	4.11	5420	b	

Table I. (Cont.)

Flash Energy J	$[O_2]$ x 10^{-18} molecule cm^{-3}	$[Br_2]$ x 10^{-15} molecule cm^{-3}	$[BrO]_o$ x 10^{-13} molecule cm^{-3}	$[NO_2]$ x 10^{-15} molecule cm^{-3}	k' measured s^{-1}	k' corrected s^{-1}	k x 10^{12} cm^3 $molec^{-1}$ s^{-1}
529	0.0	18.9	1.0	4.32	4350	4070	0.942
389	0.17	11.4	1.1	4.34	3480	3260	0.751
389	0.37	10.9	2.4	4.54	5360	5130	1.13
389	1.82*	10.0	2.1	4.58	4888	4510	0.985
389	1.73*	9.94	2.0	4.60	4941	4710	1.02
529	0.0	18.9	0.97	4.89	3950	3630	0.742
389	0.37	10.9	2.5	5.10	4520	4260	0.835
							$\bar{k}$ = (9.18 ± 1.64) x 10^{-13}
p_{TOT} = 200 Torr, N_2							
389	3.40	11.1	1.2	0.522	656	634	1.21
			1.2	0.994	1390	1350	1.36
			1.2	1.48	1916	1850	1.25
			1.3	1.99	3007	2920	1.47
			1.3	2.96	3506	3360	1.14
			1.2	3.49	6264	6090	1.74
			2.3	4.02	5190	4990	1.24
			3.0	4.52	6906	6680	1.48
							$\bar{k}$ = (1.36 ± 0.20) x 10^{-12}
p_{TOT} = 300 Torr, N_2							
389	1.5	9.9	0.82	0.6883	1289	1260	1.84
			0.77	1.31	2276	2220	1.69
			0.75	1.62	2417	2340	1.44
			0.93	1.92	3157	3070	1.60
			0.72	2.24	3374	3270	1.46
			0.94	2.55	4107	3990	1.56
							$\bar{k}$ = (1.60 ± 0.15) x 10^{-12}

Table I. (Cont.)

Flash Energy J	$[O_2]$ x 10^{-18} molecule cm^{-3}	$[Br_2]$ x 10^{-15} molecule cm^{-3}	$[BrO]_o$ x 10^{-13} molecule cm^{-3}	$[NO_2]$ x 10^{-15} molecule cm^{-3}	k' measured s^{-1}	k' corrected s^{-1}	k x 10^{12} cm^3 $molec^{-1}$ s^{-1}
P_{TOT} = 400 Torr, N_2							
389	3.0	10.0	1.0	0.341	720	705	2.07
			0.95	0.501	1085	1060	2.12
			0.98	0.661	1176	1130	1.71
			1.0	0.814	1870	1830	2.25
			1.3	0.983	2232	2190	2.23
			1.2	1.14	2748	2700	2.37
			1.2	1.34	2849	2790	2.08
			1.3	2.75	5570	5440	1.98
			2.7	4.04	6346	6140	1.52
			2.8	4.09	10394	10200	2.49
			1.3	4.73	7609	7370	1.56
			1.9	5.41	9181	8900	1.65
			2.4	5.50	8539	8250	1.50
			3.7	6.12	10664	10300	1.68
						$\bar{k}$ = (1.94 ± 0.33) x 10^{-12}	
P_{TOT} = 500 Torr, N_2							
389	0.36	10.0	1.3	0.544	1300	1280	2.35
	2.3		0.85	0.586	1410	1380	2.35
	2.3		1.1	1.17	3010	2960	2.53
	0.36		1.5	1.62	3950	3880	2.40
	2.3		0.75	1.76	3490	3410	1.94
	2.3		1.3	2.34	5190	5080	2.17
	0.36		2.0	2.67	6310	6180	2.31
	0.36		1.2	2.93	5470	5330	1.82
	2.3		1.4	3.51	7750	7580	2.16
	0.36		3.0	3.70	9490	9310	2.52
	2.3		1.4	4.10	7956	7750	1.89

Table I. (Cont.)

Flash Energy J	$[O_2]$ x 10^{-18} molecule cm^{-3}	$[Br_2]$ x 10^{-15} molecule cm^{-3}	$[BrO]_o$ x 10^{-13} molecule cm^{-3}	$[NO_2]$ x 10^{-15} molecule cm^{-3}	k' measured s^{-1}	k' corrected s^{-1}	k x 10^{12} cm^3 $molec^{-1}$ s^{-1}
	2.3		1.5	4.69	8200	7960	1.70
	0.36		1.8	4.72	15100	14900	3.16
						$\bar{k}$ = (2.25 ± 0.38) x 10^{-12}	
p_{TOT} = 600 Torr, N_2							
389	3.1	13	1.0	0.427	1248	1230	2.88
			1.2	0.872	2464	2430	2.79
			1.5	1.74	4219	4140	2.38
			1.1	2.18	5320	5220	2.39
			1.6	2.62	7142	7020	2.68
	2.5	12	1.3	2.74	7572	7440	2.72
	3.1	13	1.9	3.49	7716	7550	2.16
	2.5	12	2.0	5.47	13868	13600	2.49
						$\bar{k}$ = (2.56 ± 0.24) x 10^{-12}	
p_{TOT} = 700 Torr, N_2							
389	3.2	11	1.0	0.408	1220	1200	2.94
			1.1	0.621	2111	2080	3.35
			1.0	0.842	2441	2400	2.85
			0.97	1.05	2650	2600	2.48
			0.95	1.33	3508	3450	2.59
			1.0	1.59	4409	4340	2.73
			1.4	1.93	5169	5080	2.63
			1.6	2.63	7462	7340	2.79
			2.5	2.78	9420	9290	3.34
			2.1	3.75	12154	12000	3.20

Table I. (Cont.)

Flash Energy J	$[O_2]$ x 10^{-18} molecule cm^{-3}	$[Br_2]$ x 10^{-15} molecule cm^{-3}	$[BrO]_o$ x 10^{-13} molecule cm^{-3}	$[NO_2]$ x 10^{-15} molecule cm^{-3}	k' measured s^{-1}	k' corrected s^{-1}	k x 10^{12} cm^3 $molec^{-1}$ s^{-1}
			2.5	3.92	11869	11700	2.98
			2.0	4.75	15598	15400	3.24
			3.0	5.82	18732	18400	3.16
			3.6	5.85	20354	20000	3.42
						$\bar{k}$ = (2.98 ± 0.31) x 10^{-12}	

[a] For p_{TOT} = 50 and 100 Torr runs, N_2O is used instead of O_2 unless indicated by an (*).

[b] Experiments at high flash energy (941J) were not averaged into the final results.

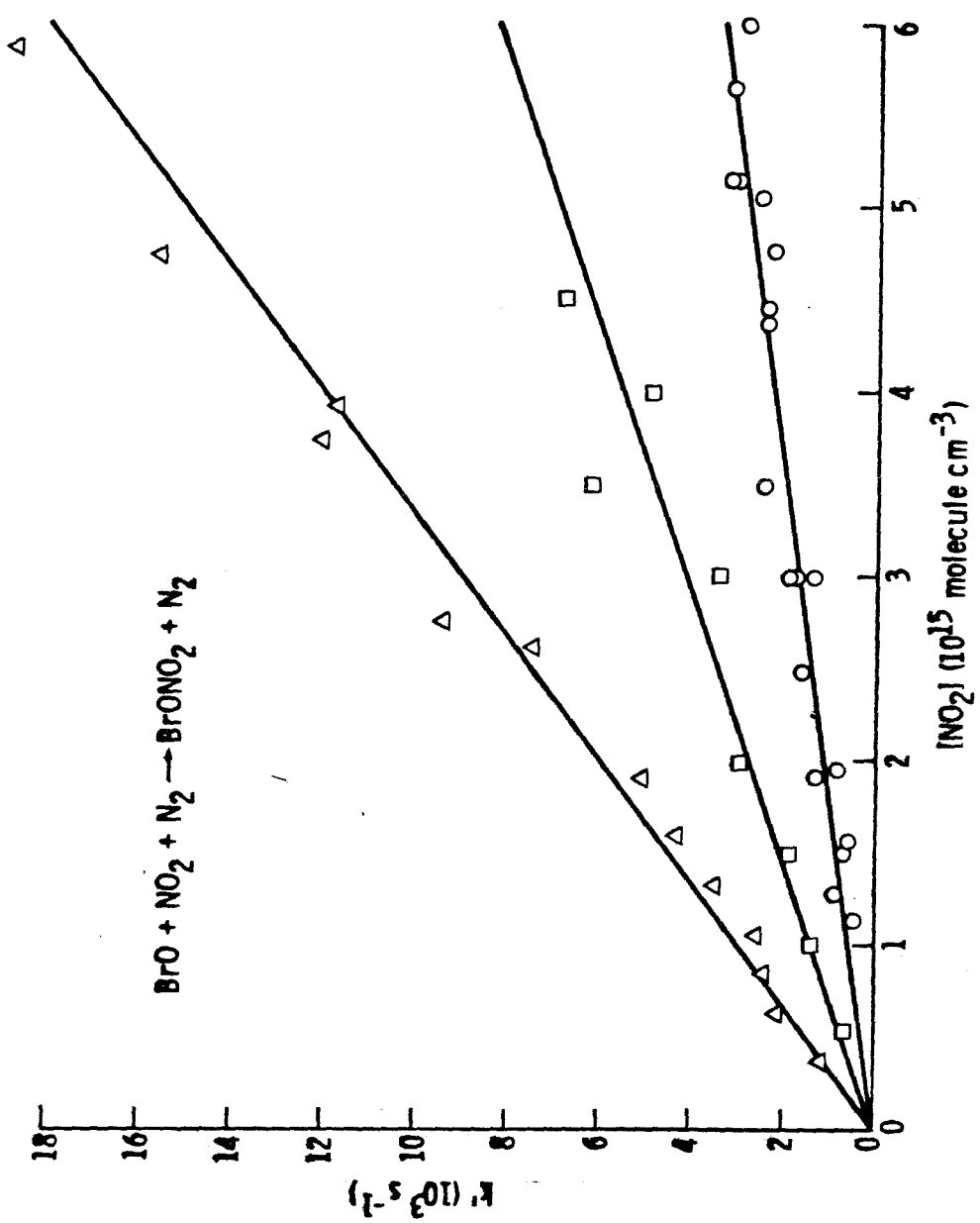

Figure 1. Variation of the pseudo first-order rate constant for the decay of BrO with $[NO_2]$ at pressures of 100 Torr (○), 400 Torr (□) and 700 Torr (Δ) of nitrogen.

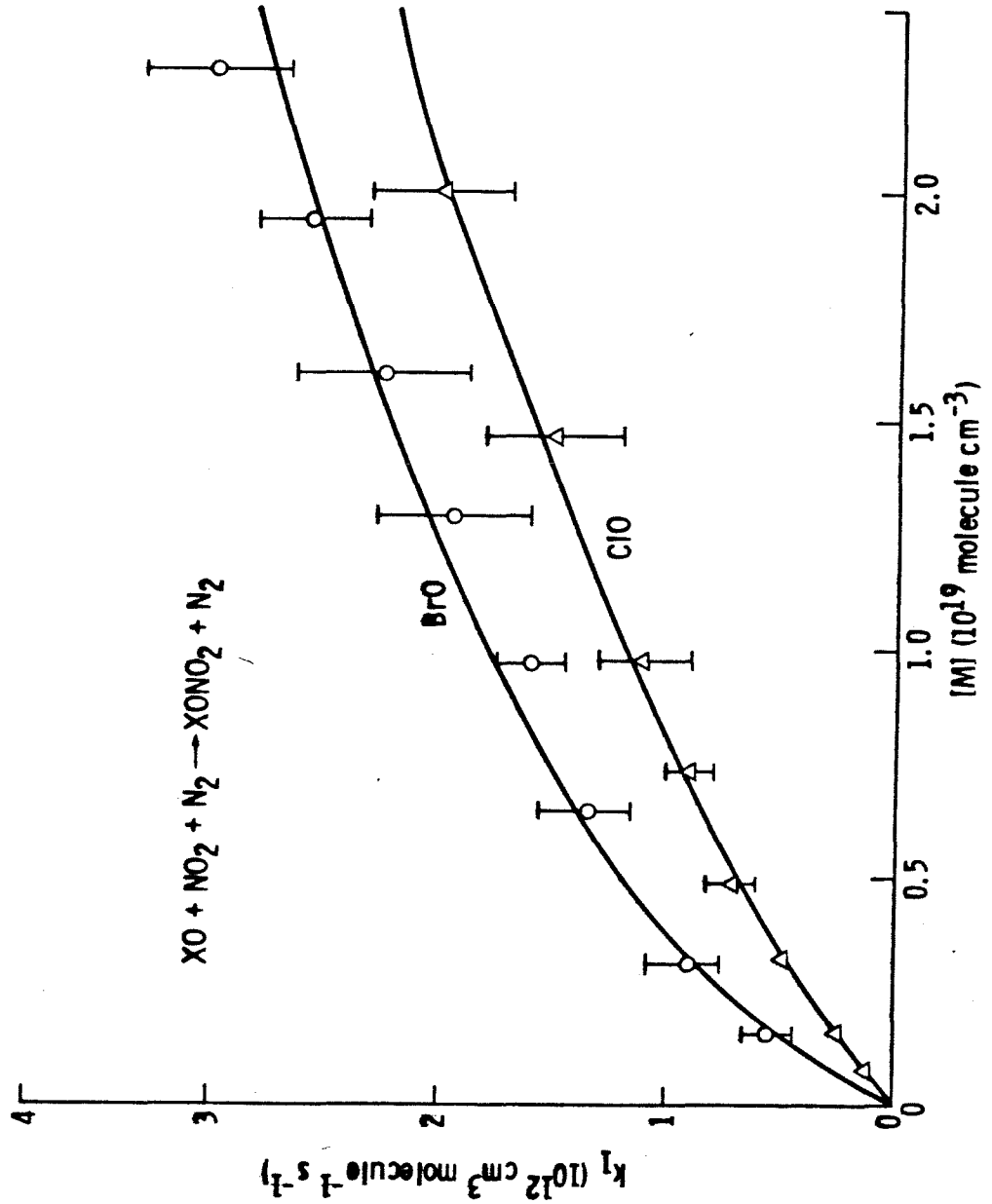

Figure 2. Variation of the effective bimolecular rate constant for the reaction XO + NO_2 + M → $XONO_2$ + M for X = Br (this work) and Cl (data of Cox and Lewis, ref. 6).

Table II. Effective Bimolecular Rate Constants for the Reaction $BrO + NO_2 + M \rightarrow BrONO_2 + M$ at 298K

Total pressure Torr	k_1 x 10^{12} cm^3 $molecule^{-1}s^{-1}$ mean[a]	slope[b]	y-intercept[b] (s^{-1})
50	0.549 ± 0.10	0.615	-248
100	0.918 ± 0.16	0.874	83
200	1.36 ± 0.20	1.46	-174
300	1.60 ± 0.15	1.41	273
400	1.94 ± 0.33	1.59	564
500	2.25 ± 0.38	2.31	-168
600	2.56 ± 0.24	2.40	212
700	2.98 ± 0.31	3.36	-708
50 (without N_2O)	0.485 ± 0.076	0.595	-298
50 (with N_2O)	0.598 ± 0.082	0.603	-63
100 (without N_2O)	0.943 ± 0.14	0.772	482
100 (with N_2O, O_2)	0.977 ± 0.12	0.828	354

[a] Average of $k_1'/[NO_2]$ values for each run at the stated pressure.

[b] Least-squares slope and y-intercept of k_1' vs. $[NO_2]$ plot.

Experimental fall-off parameters (see text):

$k_o = (4.5 \pm 1.5) \times 10^{-31}$ cm^6 $molecule^{-2}$ s^{-1}

$k_\infty = (1.05 \pm 0.15) \times 10^{-11}$ cm^3 $molecule^{-1}$ s^{-1}

$F_c = 0.53 \pm 0.10$

A number of potentially complicating reactions may take place which must be considered. These include the reactions of BrO with BrO and NO;

$$BrO + BrO \rightarrow 2Br + O_2 \qquad (8a)$$
$$\rightarrow Br_2 + O_2 \qquad (8b)$$

$$BrO + NO \rightarrow Br + NO_2 \qquad (6)$$

Previous work in this laboratory has shown[11] that $k_{8a} + k_{8b} = (2.2 \pm 0.7) \times 10^{-12}$ cm^3 $molecule^{-1}$ s^{-1}. The effect of reaction 8 on the BrO decay rate can be estimated by evaluating the ratio $k_8[BrO]/k_1[NO_2]$ for each kinetic run. The average value of this ratio for all runs is 0.015 using $[BrO] = [BrO]_o$ and 0.004 using $[BrO] = [BrO]_o/4$, the "average value" of [BrO] for each run. The effect of reaction 8 is therefore negligible.

Reaction 6 can occur as a result of NO being formed from three processes: photolysis of NO_2 (reaction 4), the reaction of O with NO_2,

$$O + NO_2 \rightarrow NO + O_2 \qquad (9) \quad k_9 = 9.2\times10^{-12} cm^3 molecule^{-1} s^{-1}$$

and reaction 7a,

$$O(^1D) + N_2O \rightarrow 2NO \qquad (7a)$$

when N_2O is present. Of these reactions, NO_2 photolysis is most significant, followed in importance by reaction 9. Because of the low N_2O photodissociation rate in our system, reaction 7a can be ignored. The value of k_1' obtained in each kinetic run was corrected for the amount of BrO which reacted with the NO formed in reactions 4 and 9. The NO formed by photodissociation was calculated by two methods. In the first, NO_2-O_2 mixtures were repeatedly photolyzed and the NO_2 dis-

appearance measured. The percentage NO_2 dissociation per flash was calculated assuming a quantum yield of 2.0. In the second method, the NO_2 dissociation was calculated from measured values of $[BrO]_o$ in runs where NO_2 photolysis was the only source of oxygen atoms. Agreement between the two methods was good, however the first method was assumed to be more accurate and was therefore used to compute the amount of NO formed. The value of 0.18% NO_2 photolyzed per flash at 389J was linearly scaled with flash energy. The average correction decreased monotonically from 8.8% at 50 Torr to 1.6% at 700 Torr reflecting the increase in the ratio of k_1/k_6 with pressure.

At a flash energy of 700J, about 5% of the molecular bromine is dissociated leading to initial atomic bromine concentrations of 0.5-2 x 10^{15} molecule cm^{-3}. In the presence of NO_2, Br undergoes rapid catalytic recombination by the sequence of reactions

$$Br + NO_2 + M \rightarrow BrNO_2 + M \qquad (10)$$

$$Br + BrNO_2 \rightarrow Br_2 + NO_2 \qquad (11)$$

Reactions 10 and 11 pose a complication if a significant fraction of the NO_2 becomes tied up in the form of $BrNO_2$. Rate constants for these reactions have not been measured; however, there are rate data for the X + NO_2 + M reaction (X = F, Cℓ, I and M = He, N_2) and for the X + XNO_2 reaction (X = F, I).[13,14] On this basis, we estimate k_{10} = 2.2 x 10^{-31} cm^6 $molecule^{-2}$ s^{-1}, M = He and 4.4 x 10^{-31} cm^6 $molecule^{-2}$ s^{-1}, M = N_2, and k_{11} = 8.0 x 10^{-11} cm^3 $molecule^{-1}$ s^{-1} with uncertainty factors of two for k_{10} and four for k_{11}. Numerical simulations of reactions 10 and 11 were performed using a range of conditions representative of the actual experiments and rate constant uncertainties: $[NO_2]_o$ = 1-10 x 10^{15} molecule cm^{-3} s^{-1}, k_{10} = 1.2-12 x 10^{-12} cm^3 $molecule^{-1}$ s^{-1} and k_{11} = 2-8 x

10^{-11} cm^3 molecule^{-1} s^{-1}. The variation in k_{10} also incorporates the effect of changing the total pressure over an order of magnitude from 76 to 760 Torr N_2, assuming that reaction 10 is third-order up to one atmosphere. The results indicate that at low pressure, the maximum depletion of NO_2 expected under worst-case conditions (low $[NO_2]_o$, $k_{11} = 2 \times 10^{-11}$ cm^3 $molecule^{-1}$ s^{-1}) is 5.5%. This increases to 34% at high pressure. Under more realistic conditions ($k_{11} = 8 \times 10^{-11}$ cm^3 $molecule^{-1}$ s^{-1}) the NO_2 depletion drops to 1.5% and 10%, respectively. These results indicate that the formation of $BrNO_2$ should have had no discernible effect except at pressures exceeding 300-400 Torr where the effect would be dependent on $[NO_2]_o$. Because of this $[NO_2]$ dependence, the formation of $BrNO_2$, if it was significant, should have manifested itself as curvature and a negative y-intercept in the plots of k_1' vs. $[NO_2]$. Since neither feature was observed, and the rate constants required to make an accurate correction are unavailable, the effect of $BrNO_2$ was ignored. Since reactions 10 and 11 occur on a rapid time scale (less than 100 μs to reach 95% of equilibrium conditions), bromine atoms are removed much more rapidly than if bimolecular recombination,

$$Br + Br + M \rightarrow Br_2 + M \quad (12) \quad k_{12} = 9.1 \times 10^{-33} cm^6 molecule^{-2} s^{-1}$$

was the only reaction. The rapid approach to equilibrium also ensures that any changes in the baseline analytical light absorption due to Br_2 and $BrNO_2$ will not interfere with the detection of BrO.

Thermal decomposition of $BrONO_2$,

$$BrONO_2 + M \rightarrow BrO + NO_2 + M \qquad (-1)$$

can also affect the determination of k_1 is it occurs on the same time scale as the formation step. Although direct measurements of the gas-

phase unimolecular decomposition rate have not been conducted for $BrONO_2$, data do exist for $ClONO_2$.[5] Assuming the same decomposition rate constants for $ClONO_2$ and $BrONO_2$, an upper limit for k_{-1} at 700 Torr is obtained by assuming that the decomposition is still in the second-order region at this pressure. At 298K and 700 Torr the equivalent first-order rate constant is $\sim 0.0013\ s^{-1}$. This compares with a value of $1200\ s^{-1}$, the smallest first-order rate constant observed at 700 Torr for the association reaction. The effects of the thermal decomposition of $BrONO_2$ can therefore be ignored.

Absorption of the analytical light by the product $BrONO_2$ does not pose a problem in the determination of k_1. $BrONO_2$ absorbs very weakly at 339.0 nm; the ratio of the absorption cross-sections for BrO[11] and $BrONO_2$[15] is 126. Even if the $BrONO_2$ absorption were appreciable, it can be shown[16] that an absorber ($BrONO_2$) formed as a primary product of the reaction of the species being monitored (BrO) does not interfere with the measurement of k' as long as I_o is evaluated at a time long compared with the BrO reaction time but short compared with the cell residence time.

As indicated above, the system was operated in the continuously flowing mode with the cell contents being entirely replaced between flashes. Problems due to depletion of NO_2 and build-up of reaction products such as $BrONO_2$ and $BrNO_2$ were therefore not encountered.

DISCUSSION

There are no published measurements of k_1 although Ray and Watson,[17] using discharge flow-mass spectroscopy, have obtained the following preliminary third-order values of k_1: $(2.33 \pm 0.42) \times 10^{-31}$ cm^6 molecule^{-2} s^{-1} (M = He, 1-7 Torr total pressure) and $(5.3 \pm 0.7) \times 10^{-31}$ cm^6

molecule^{-2} s^{-1} (M = N_2, 1-4 Torr total pressure). Quoted uncertainties are 2σ. There are a number of studies of the analogous ClO + NO_2 reaction.

$$ClO + NO_2 + M \rightarrow ClONO_2 + M \qquad (13)$$

both in the third-order region (1-7 Torr)[4] and the fall-off region between second- and third-order kinetics.[5-7] Knauth and co-workers[5] found little fall-off (<5%) at pressures up to 210 Torr of N_2, with the fall-off increasing to 20% at 350 Torr. Cox and Lewis,[6] who measured k_{13} in the pressure range 25 to 612 Torr of N_2 observed somewhat more fall-off. Their value obtained at 25 Torr is in excellent agreement with the extrapolated third-order rate constant obtained by averaging the results of the five discharge-flow studies ((1.7 ± 0.2) x 10^{-31} cm^6 molecule^{-2} s^{-1}). Moreover, the rate constant found by Cox and Lewis at 612 Torr of N_2 is only about 1.7 less than the average third-order rate constant extrapolated to this pressure. In contrast, the value of k_1 at 600 Torr obtained in this study is a factor of 4.0 less than the extrapolated third-order rate constant of Ray and Watson. These results indicate that not only is the third-order rate constant for the BrO + NO_2 + M reaction two to three times faster than the ClO + NO_2 + M reaction third-order rate constant, but the rate constant fall-off is more pronounced in the BrO case.

The rate constant data obtained for M = N_2 show significant deviations from Lindemann-type behavior. Recent work by Troe and co-workers[8,9] has shown that the three-parameter equation,

$$k([M],T) = \frac{k_o(T)[M]}{1 + \frac{k_o(T)[M]}{k_\infty(T)}} F_c\{1 + [\log_{10}(k_o(T)[M]/k_\infty(T))]^2\}^{-1} \qquad (1)$$

which contains a correction to the usual Lindemann expression, can be

used to fit rate constant fall-off curves. The details of this procedure as applied to the reaction

$$CH_3O_2 + NO_2 + M \rightarrow CH_3O_2NO_2 + M \qquad (14)$$

have been described previously.[16] The parameters derived from non-linear least squares curve fitting of the data for M = N_2 to eqn. 1 were: $k_o = (4.5 \pm 1.5) \times 10^{-31}$ cm^6 molecule^{-2} s^{-1}, $k_\infty = (1.05 \pm 0.15) \times 10^{-11}$ cm^3 molecule^{-1} s^{-1} and $F_c = 0.53 \pm 0.10$. The uncertainties represent the variation in the fitted parameters obtained when the mean-squared error is allowed to increase by $\sim$ 10-20% from its minimum value (see Table III).

Because the Troe fall-off expression contains three parameters, satisfactory fits to the data are obtainable with a wide range of parameter choices, particularly when the extent of fall-off is relatively small. Table III presents the results of curve fitting calculations on the $BrONO_2$ system (this work) and the $ClONO_2$ system (Cox and Lewis[6]) in which k_o was specified and k_∞ and F_c were determined. In the chlorine nitrate case, both k_∞ and F_c are extremely sensitive to small changes in k_o, particularly in the neighborhood of the minimum in the χ^2 hypersurface. Bromine nitrate is somewhat less sensitive in this region because of its greater fall-off. However, as the results in Table III indicate, there is a second set of parameters ($k_o \simeq 2.0 \times 10^{-30}$ cm^6 molecule^{-2} s^{-1}, $k_\infty \simeq 1.0 \times 10^{-11}$ cm^3 molecule^{-1} s^{-1}, $F_c = 0.22$) which gives a good fit to the data. Since this k_o value is unreasonably high in view of the low-pressure discharge-flow results[4] and the F_c value is extremely low, the second set of parameters can be ruled out as an artifact of the curve-fitting procedure. However, this

Table III. Fall-Off Parameters for the Reactions $BrO + NO_2 + M$ and $ClO + NO_2 + M$[a]

k_o[b] $\times 10^{-31}$ cm^6 $molec^{-2}$ s^{-1}	k_∞ $\times 10^{-12}$ cm^3 $molec^{-1}$ s^{-1}	F_c	χ^2 $\times 10^5$ Arb units
$BrO + NO_2 + M \rightarrow BrONO_2 + M$			
2.0	14.1	0.84	6.00
3.0	11.3	0.65	2.57
4.0	12.2	0.53	2.34
5.0	9.31	0.53	2.58
6.0	9.16	0.49	2.87
8.0	8.85	0.42	3.04
10.0	8.58	0.38	2.84
20.0	10.2	0.22	1.28
30.0	9.18	0.16	1.70
40.0	7.63	0.14	2.61
$ClO + NO_2 + M \rightarrow ClONO_2 + M$			
1.0	2.32	1.82	0.862
1.6	0.76	0.78	0.382
1.7	15.6	0.60	0.368
1.8	24.1	0.45	0.367
1.9	10.6	0.63	0.515
2.0	12.4	0.56	0.602
3.0	7.87	0.52	2.65

[a] BrO data from this study, ClO data from Ref. 6.

[b] k_o was fixed while k_∞ and F_c were optimized.

is illustrative of the problem of fitting data to an equation that has several adjustable parameters. To determine the fall-off parameters for a termolecular reaction as accurately as possible, two experimental procedures are recommended. First, fall-off curves should be measured using several diluent gases that have a wide range of collision efficiencies, e.g. He, N_2 and SF_6. Since k_∞ is independent, and F_c is almost independent of the collider, additional constraints are placed on the parameters if more than one data set is used. Second, to enhance the observed fall-off, experiments should be conducted up to the highest possible pressure. Unfortunately, for complexes with a relatively large number of effective vibrational modes ($C\ell ONO_2$, $BrONO_2$, $CH_3O_2NO_2$, etc.) which have fall-off curves with low F_c values (0.4 - 0.6) the asymptotic approach to the high-pressure limit is extremely slow. For example using the experimentally determined fall-off parameters for the BrO + NO_2 and $C\ell O$ + NO_2 reactions, the N_2 pressures at which $k = 0.95\ k_\infty$ are calculated to be 2970 and 1300 atm., respectively.

The low-pressure limit, k_o, for reaction 1 obtained by curve-fitting is in excellent agreement with the preliminary experimental value of k_o, $(5.3 \pm 0.7) \times 10^{-31}$ cm^6 $molecule^{-2}$ s^{-1}, obtained by Ray and Watson.[17] The agreement between the two techniques is gratifying in view of the differences in the methods of BrO formation (O + Br_2 vs. Br + O_3), BrO detection (UV absorption vs. mass spectrometry) and reactor type (flash photolysis vs. discharge flow).

Luther and Troe have shown how to estimate the broadening factor (F_c) at the point where $k_o[M] = k_\infty$, from structural information about the product of an addition reaction.[8] The broadening factor is the product of a strong collision factor, F_c^{sc}, and a correction factor

for weak-collision effects, F_c^{wc}. F_c^{sc} is a function of the parameters S_k and B_k, given by:

$$S_k \simeq S_{eff} + 1 \text{ or } S_{eff} + 2$$

$$B_k = \frac{(S_k - 1)}{S - 1} \frac{(E_o + a(E_o)E_z)}{kT}$$

where: S_{eff} = effective number of transition-state oscillators

$$= -\frac{1}{T} \frac{\partial \ell n\, Q_V}{\partial (1/T)}$$

E_o = critical energy for the decomposition of the adduct

E_z = adduct vibrational zero-point energy

$a(E_o)$ = Whitten-Rabinovitch factor

Q_V = vibrational partition function

S = number of internal degrees of freedom

Values of F_c^{sc} as a function of S_k and B_k are tabulated in Ref. 8. The fundamental vibrational frequencies of $BrONO_2$ are required to evaluate Q_V. These were obtained from the infrared special measurements of Spencer and Rowland,[15] and, for the low-frequency bands which could not be observed, estimated using the frequencies of $C\ell ONO_2$ and $FONO_2$ as models.[18] The vibrational frequencies used in this calculation are listed in Table IV. At 300K, $S_k = 3.7 \pm 0.5$, $E_z = 9.3$ kcal mole^{-1} and $a(E_o) = 0.94$. The resulting value of B_k is 18.5 ± 3.5 and from the tables in ref. 8, $F_c^{sc} = 0.49 \pm 0.11$. The weak collision broadening factor at the center ($[M] = \frac{k_\infty}{k_o}$) is approximated by,

$$F_c^{wc} \simeq \beta_c^{0.14}$$

where β_c is the collision efficiency at the low-pressure limit. β_c has

Table IV. Fundamental Vibrational Frequencies of $XONO_2$

Frequency cm^{-1}		Type	Ref	
X = Cℓ	X = Br		X = Cℓ	X = Br
1735	1711	NO_2 asym-stretch	18	15
1292	1285	NO_2 sym-stretch	18	15
780	802	NO_2 scis.	18	15
711	720	NO_2 wag	18	15
809	690	O-X stretch	18	15
560	560	NO_2 stretch	18	15
434	390	NO_2 rock	18	15
270	240	OX bend	18	est.
121	90	OX torsion	18	est.

been estimated[13] to be in the range 0.2 - 0.4 for similar reactions for M = N_2 giving F_c^{wc} = 0.84 ± 0.03. The predicted value for F_c is therefore 0.41 ± 0.11. This result is in good agreement with the observed value. The primary source of uncertainty in the calculation comes from the estimation of the parameter S_k as F_c^{sc} is much more sensitive to S_k than to B_k.

Applying the same procedure to the $C\ell O + NO_2$ reaction, F_c is predicted to be 0.45 ± 0.11 in good agreement with the value $(0.52^{+0.2}_{-0.1})$ determined by fitting the data of Cox and Lewis to equation (1) (see Table III). The high-pressure limit derived from the data, k_∞ = $(2.0^{+0.5}_{-1.0}) \times 10^{-11}$ cm^3 molecule^{-1} s^{-1}, agrees with the estimates of Smith and Golden[19] (1.45×10^{-11} cm^3 molecule^{-1} s^{-1}) and Zellner[20] ($(1.2 \pm 0.4) \times 10^{-11}$ cm^3 molecule^{-1} s^{-1}).

Knauth[5] and Chang et al.[21] have suggested the existence of alternative channels for the $C\ell O + NO_2$ reaction beside the direct formation of $C\ell ONO_2$. These include the formation of the isomers $OC\ell NO_2$ and CℓOONO. Evidence for these reactions comes from the discrepancy between measurements of k_{13} by techniques which monitor the overall disappearance of CℓO (including all of the discharge flow, flash photolysis and molecular modulation work) and the static method of Knauth based on the thermal decomposition of chlorine nitrate. While the analogous reactions may take place in the $BrO + NO_2$ system, this experiment is not capable of distinguishing the different isomeric forms of $BrNO_3$. Experiments of the sort performed by Knauth but using bromine nitrate would therefore be quite useful.

Stratospheric Implications

Calculations have recently been carried out by Yung et al.[3] on

the concentration profiles of trace stratospheric constituents, including bromine-containing species, using a one-dimensional diurnally-averaged model. The results of the model indicated that the chemical cycle involving bromine which causes the greatest net loss of odd-oxygen is the following:

$$Br + O_3 \rightarrow BrO + O_2 \qquad (15)$$

$$Cl + O_3 \rightarrow ClO + O_2 \qquad (16)$$

$$BrO + ClO \rightarrow Br + Cl + O_2 \qquad (17)$$

$$2O_3 \rightarrow 3O_2$$

Since reaction 17 is the rate-determining step in this cycle, the catalytic efficiency for ozone destruction is proportional to $k_{17}[BrO][ClO]$. The effect of bromine nitrate as a temporary reservoir for bromine is to lower the steady-state BrO concentration thus reducing the efficiency of this catalytic cycle. However, since photolysis of $BrONO_2$ probably results in the formation of NO_3 as well as other products, bromine nitrate may take part in an odd-oxygen destruction cycle of its own:

$$Br + O_3 \rightarrow BrO + O_2 \qquad (15)$$

$$BrO + NO_2 + M \rightarrow BrONO_2 + M \qquad (1)$$

$$BrONO_2 + h\nu \rightarrow Br + NO_3 \qquad (18)$$

$$NO_3 + h\nu \rightarrow NO + O_2 \qquad (19)$$

$$NO + O_3 \rightarrow NO_2 + O_2 \qquad (20)$$

$$2O_3 \rightarrow 3O_2$$

Since NO_3 photodissociates to NO and O_2 about one-third of the time, the over-all rate of ozone destruction by this cycle is $2/3\ J_{18}[BrONO_2]$. Whether the net effect of bromine nitrate is to increase or decrease

the column odd-oxygen loss rate can be estimated using concentrations of species in the HO_x, ClX and NO_x families calculated in the fully coupled model (ref. 3). In the absence of bromine nitrate, the concentrations of species in the BrX family (Br, HBr, BrO) can be re-partitioned using steady-state considerations and by assuming that the effect on other radical concentrations can be neglected. This is a valid assumption since the mixing ratio of BrX is small (20-100 pptv). The result of this simple calculation is that in the vicinity of the ozone maximum (20-24km) the sum of the odd-oxygen destruction rates for the various bromine cycles in the absence of bromine nitrate exceeds by about 26% the value when bromine nitrate is included. Determining the exact magnitude of the effect would involve computing the change in the catalytic efficiency over the total ozone column, but the primary contribution to the sum occurs between 20 and 24km.

The analogous process involving chlorine nitrate is more difficult to analyze for several reasons. Since the mixing ratio of ClX is 100-1000 times greater than that for bromine, chlorine nitrate significantly perturbs the NO_x cycle as well as the ClX cycle. The effect of chlorine nitrate must therefore be determined by solving the equations for the fully coupled chemical model rather than by the simple steady-state treatment. Also, the maximum mixing ratio of chlorine nitrate is reached at about 24km which is well below the region of the stratosphere where the most important ClX catalytic cycle, which involves the O + ClO reaction, is most efficient. Chlorine nitrate therefore does not affect the ClX partitioning significantly in this region. It does affect [ClO] in the 20-30km region which, in turn, has an impact on the catalytic efficiency of the ClO + BrO cycle.

ACKNOWLEDGEMENTS

The authors thank R. A. Cox and R. Lewis (Harwell), and G. W. Ray, (Jet Propulsion Laboratory) for their experimental results prior to publication. The research described in this paper was carried out at the Jet Propulsion Laboratory, California Institute of Technology, under NASA Contract NAS7-100.

REFERENCES AND NOTES

1. (a) P. J. Crutzen, Quart. J. Roy. Met. Soc., 96, 320 (1970);
   (b) H. S. Johnston, Science, 173, 517 (1971).

2. (a) R. S. Stolarski and R. J. Cicerone, Can. J. Chem. 52, 1610 (1974);
   (b) S. C. Wofsy and M. B. McElroy, Can. J. Chem., 52, 1582 (1974);
   (c) M. J. Molina and F. S. Rowland, Nature, 249, 810 (1974).

3. Y. L. Yung, J. P. Pinto, R. T. Watson and S. P. Sander, J. Atmos. Sci., in press.

4. (a) M. S. Zahniser, J. S. Chang and F. Kaufman, J. Chem. Phys., 67, 997 (1976);
   (b) J. W. Birks, B. Shoemakers, T. J. Leck, R. A. Borders and L. J. Hart, J. Chem. Phys., 66, 4591 (1977);
   (c) M. T. Leu, C. L. Lin and W. B. DeMore, J. Phys. Chem., 81, 190 (1977);
   (d) R. Stimpfle, R. A. Perry and C. J. Howard, manuscript in preparation.

5. (a) H.-D. Knauth, Ber. Bunsenges, Phys. Chem., 82, 212 (1978);
   (b) G. Schönle, H.-D. Knauth and R. N. Schindler, submitted to J. Phys. Chem.

6. R. A. Cox and R. Lewis, J. Chem. Soc. Faraday Trans., in press.

7. V. Handwerk and R. Zellner, manuscipt in preparation.

8. K. Luther and J. Troe, presented at the XVIIth International Symposium on Combustion, Leeds, August, 1978.

9. J. Troe, J. Phys. Chem., 83, 114 (1979).

10. R. T. Watson, S. P. Sander and Y. L. Yung, J. Phys. Chem., in press.

11. S. P. Sander and R. T. Watson, manuscript in preparation.

12. D. L. Baulch, R. A. Cox, R. F. Hampson, Jr., J. A. Kerr and J. Troe, J. Phys. Chem. Ref. Data, in press.

13. NASA Panel for Data Evaluation, Jet Propulsion Laboratory Report No. 79-27, (1979).

14. H. Van den Bergh and J. Troe, J. Phys. Chem., 64, 736 (1976).

15. J. E. Spencer and F. S. Rowland, J. Phys. Chem., 82, 7 (1978).

16. S. P. Sander and R. T. Watson, submitted to J. Phys. Chem.

17. G. W. Ray and R. T. Watson, manuscript in preparation.

18. T. Shimanouchi, J. Phys. Chem. Ref. Data, 6, 993 (1977).

19. G. P. Smith and D. M. Golden, Int. J. Chem. Kinet., 10, 489 (1978).

20. R. Zellner, Z. Naturforsch. Teil. A., 329, 648 (1977).

21. J. S. Chang, A. C. Baldwin and D. M. Golden, J. Chem. Phys., 71, 2021 (1979).

APPENDIX I

CHEMICAL KINETICS OF HOMOGENEOUS ATMOSPHERIC OXIDATION OF SULFUR DIOXIDE

S. P. Sander and J. H. Seinfeld

Department of Chemical Engineering

California Institute of Technology
Pasadena, CA 91125

Reprinted from ENVIRONMENTAL SCIENCE & TECHNOLOGY, Vol. 10, Page 1114, November, 1976

Chemical Kinetics of Homogeneous Atmospheric Oxidation of Sulfur Dioxide

Stanley P. Sander and John H. Seinfeld*

Department of Chemical Engineering, California Institute of Technology, Pasadena, Calif. 91125

■ A systematic evaluation of known homogeneous SO_2 reactions which might be important in air pollution chemistry is carried out. A mechanism is developed to represent the chemistry of NO_x/hydrocarbon/SO_2 systems, and the mechanism is used to analyze available experimental data appropriate for quantitative analysis of SO_2 oxidation kinetics. Detailed comparisons of observed and predicted concentration behavior are presented. In all cases, observed SO_2 oxidation rates cannot be explained solely on the basis of those SO_2 reactions for which rate constants have been measured. The role of ozone–olefin reactions in SO_2 oxidation is elucidated.

The oxidation of sulfur dioxide in the atmosphere occurs by both heterogeneous and homogeneous paths. Heterogeneous routes, involving the catalytic oxidation of SO_2 in water droplets, are reasonably well understood (*1–6*). Homogeneous gas-phase reactions of SO_2 in the atmosphere have been reviewed (*7–12*), although the detailed mechanism by which SO_2 is oxidized in the presence of other air pollutants has not been established. The object of this work is to study the rates and mechanisms of the homogeneous atmospheric oxidation of SO_2 through detailed analysis of available laboratory data on SO_2-containing systems.

For a number of years there has been considerable interest in elucidating the mechanism of photochemical smog reactions (*13–17*). Although it has long been recognized that SO_2 is generally present with hydrocarbons and oxides of nitrogen in the atmosphere, comparatively little experimental work has been conducted on systems containing SO_2. The sulfate aerosol formation which often takes place in such systems has been viewed as an undesirable feature in laboratory smog chambers, particularly when the primary objective of the experiment is the study of hydrocarbon/NO_x chemistry. It has been suggested that heterogeneous paths may account for most of the photochemical sulfate aerosol observed in the atmosphere (*18*). However, since the hydration of SO_3 leads readily to aerosol, the homogeneous oxidation of SO_2 to SO_3 is a potential key step in sulfate aerosol formation.

This work consists of a systematic evaluation of all known atmospheric SO_2 reactions which might be important in air pollution chemistry. We begin by considering the photochemistry of SO_2 in air, in mixtures of air and oxides of nitrogen, and in mixtures of air, oxides of nitrogen, and hydrocarbons. We then summarize available experimental data appropriate for quantitative analysis of SO_2 oxidation kinetics, and present comparisons of predicted and measured concentrations of the species involved. Finally, we draw conclusions pertaining to additional information needed to understand more completely the atmospheric chemistry of SO_2.

Atmospheric Chemistry of Sulfur Dioxide

In this section we summarize atmospheric reactions involving SO_2, hydrocarbons, and oxides of nitrogen.

Photochemistry of SO_2. The photooxidation of SO_2 alone or in mixtures of SO_2 and O_2 has been studied by several investigators (*9*). Rao et al. (*19*) and Okuda et al. (*20*) have suggested that the most active species involved in the photochemistry of SO_2 is the excited triplet state, $^3SO_2$. The principal reactions in the photochemistry are believed to be those given in Table I. Where rate constant determinations are available, they are indicated in the table. Reactions 1–7 are apparently the major reactions which occur subsequent to light absorption by an SO_2 molecule. Reaction 8a has a relatively low activation energy but because it is spin-forbidden also has a low preexponential factor (*21*). Reaction 8b is spin-allowed but endothermic. The oxygen atoms produced in Reactions 8a and 8b will combine readily with O_2 to form O_3. Because there is no direct evidence to date for the existence of O_3 or SO_4 in irradiated SO_2/air mixtures, Reactions 8a–8c are probably unimportant in this system. Although reported overall quantum yields for SO_2 photooxidation vary over several orders of magnitude, even the most optimistic estimates place these reactions in a position of minor importance (*56*).

Photochemistry of SO_2 and NO_x. The primary effect of adding NO_2 to an SO_2/air mixture is the oxidation of SO_2 by Reaction 9 by the oxygen atoms formed from NO_2 photolysis. A large number of studies of this reaction have resulted in a

wide range of reported rate constants (*22, 26, 28, 57–60*). Mulcahy et al. (*22*) found that Reaction 10 has a relatively large rate constant but proceeds slowly because of the low concentrations of both oxygen atoms and excited SO_2 molecules. Cadle and Magill (*23*), Cox and Penkett (*24*), and Daubendiek and Calvert (*25*) all report a slow rate for Reaction 11 in the gas phase. Based on the rate constant determined by Davis et al. (*54*), Reaction 11 is probably unimportant in this system. Reactions 12–14 reconvert SO and SO_3 to SO_2. Smith and Urone (*27*) observed a decrease in SO_2 oxidation rate at high SO_2 levels in a system of SO_2/NO_x/air, an effect possibly attributable to Reactions 12–14. However, based on the available rate constants, it appears that these reactions are too slow to account for such an observation.

It has been suggested that a series of possible SO_2 removal paths in the SO_2/NO_x/air system is:

$$SO_2 + NO_2 \xrightarrow{15} SO_3 + NO$$

$$SO_2 + NO_3 \xrightarrow{16} SO_3 + NO_2$$

$$SO_2 + N_2O_5 \xrightarrow{17} SO_3 + N_2O_4$$

Several experimental determinations of the rate constant for Reaction 15 establish an upper limit of 9.1×10^{-9} ppm^{-1} min^{-1} at 25 °C (*28, 29, 54*). Daubendiek and Calvert (*25*) set an upper limit on the rate constant of Reaction 16 of 2.5×10^{-5} ppm^{-1} min^{-1}. A similar determination places the rate constant of Reaction 17 at 1.7×10^{-8} ppm^{-1} min^{-1} (*25*). Thus, Reactions 15–17 apparently play an unimportant role in the SO_2/NO_x/air system.

In summary, despite the low rates of Reaction 9 at atmospheric concentration levels, this reaction is apparently the most important SO_2 consumption reaction in irradiated SO_2/NO_x/air systems that have been studied experimentally.

SO_2/NO_x/Hydrocarbon Photochemistry. When hydrocarbons are added to a system of SO_2 and NO_x and the mixture is irradiated, observed SO_2 oxidation rates become much greater than in the SO_2/NO_x system. The direct reaction of SO_2 and hydrocarbons has been studied since 1950 (*35*). Recently, Badcock et al. (*32*) studied SO_2–hydrocarbon reactions, in which laser excitation was used to populate the triplet state of SO_2 (see also *21*). The SO_2–hydrocarbon reaction was suggested as being either an insertion of the form

$$^3SO_2 + RH \xrightarrow{18a} RSO_2H$$

or a hydrogen atom abstraction

$$^3SO_2 + RH \xrightarrow{18b} SO_2H + R\cdot$$

with the former being the more likely path for olefins.

Recent mass spectrometric studies by Penzhorn et al. (*36, 37*) have provided additional insight into the mechanism of SO_2–alkane reactions. In addition to the sulfinic and sulfonic acids identified by others (*35*), a number of adducts, including RSO_2R, RSR, RSO_3R, and RSO_2SR, were found. The authors suggest that the occurrence of these products can be explained by an initiation step of the form 18b followed by propagation steps of the form

$$R\cdot + SO_2 \xrightarrow{19} RSO_2$$

In spite of the existence of direct SO_2–hydrocarbon reactions, these reactions are too slow to account for the increased rate of SO_2 disappearance when hydrocarbons are added to an SO_2/NO_x system.

It is now felt that of the known SO_2 reactions the most important are those involving oxygenated free radicals, such as hydroxyl and hydroperoxyl. Table II summarizes the SO_2-free

Table I. Photochemistry of SO_2

	Reaction	Rate constant, 25 °C ppm, min units	Ref
	Primary photophysical processes		
1	$SO_2 + h\nu \rightarrow {}^1SO_2$	1.19×10^{-2} [a]	*21*
2a	$^1SO_2 + SO_2 \rightarrow SO_3 + SO$	5400	*30*
2b	$\rightarrow {}^3SO_2 + SO_2$	4400	*19*
3a	$^1SO_2 \rightarrow SO_2 + h\nu_f$	1.3×10^4	*19*
3b	$\rightarrow {}^3SO_2$	9×10^4	*19*
4	$SO_2 + h\nu \rightarrow {}^3SO_2$	4.8×10^{-5} [b]	*21*
5	$^3SO_2 + SO_2 \rightarrow SO_3 + SO$	100	*30*
6a	$^3SO_2 \rightarrow SO_2 + h\nu_p$	8400	*19*
6b	$\rightarrow SO_2$	7800	*19*
7	$^3SO_2 + M \rightarrow SO_2 + M$	200 (M = N_2, CO)	*21, 31*
		512 (M = C_2H_6)	*21, 32*
		2.08×10^5 (M = C_3H_6)	*21, 32*
	Secondary reactions		
8a	$^3SO_2 + O_2(^3\Sigma_g^-) \rightarrow SO_3 + O(^3P)$		*21*
8b	$^3SO_2 + O_2(^3\Sigma_g^-) \rightarrow SO_3 + O(^1D)$		*21*
8c	$\rightarrow SO_4^*$		*21*
9	$O(^3P) + SO_2 + M \rightarrow SO_3 + M$	2.8×10^{-5}	*26*
10	$O + SO_2 + {}^3SO_2 \rightarrow SO_3 + SO_2$	0.001	*22*
11	$O_3 + SO_2 \rightarrow SO_3 + O_2$	3×10^{-7}	*54*
12a	$SO + O_3 \rightarrow {}^3SO_2 + O_2$	0.1 (27 °C)	*33*
12b	$\rightarrow SO_2 + O_2$	110 (27 °C)	*33*
13	$SO_3 + O \rightarrow SO_2 + O_2$	0.088	*34, 49*
14	$SO + SO_3 \rightarrow 2SO_2$	2.9	*30*

[a] Estimated rate of absorption of solar radiation in first allowed band, $z = 40°$. [b] Estimated rate of absorption of solar radiation in "forbidden" band, $z = 40°$.

radical reactions believed to be most important in the homogeneous atmospheric oxidation of SO_2. Because of the importance of the OH radical in hydrocarbon/NO_x chemistry, Reaction 20 may be expected to play a significant role in SO_2 chemistry. Reactions 21a and 22a between peroxyalkyl radicals and SO_2 are also potentially important removal paths for SO_2. However, only the rate constants for Reactions 20 and 21a have been measured. The rate constants given for Reactions 21b, 22a, and 22b are estimates explained in the footnotes to Table II.

In addition to the free radicals listed in Table II, a product of ozone–olefin reactions has been suggested to be an important oxidizer of SO_2 (*24, 38, 39*). This possibility is discussed in detail in a later section.

Summary. In this section we have summarized most known atmospheric reactions involving SO_2. Tentative estimates of importance in their contribution to the overall oxidation of SO_2 indicate the free radical reactions of Table II to be potentially dominant. The remainder of this work is devoted to a detailed, quantitative evaluation of the adequacy of known SO_2 reactions to account for observed laboratory SO_2 oxidation rates. We begin with a brief summary of available experimental data on SO_2 photooxidation in systems containing oxides of nitrogen and hydrocarbons.

Table II. SO_2-Free Radical Reactions

	Reaction	Rate constant, 25 °C ppm, min units	Ref
20	$SO_2 + OH + M \rightarrow HOSO_2 + M$	780[a]	*40*
21a	$SO_2 + HO_2 \rightarrow SO_3 + OH$	1.3	*41*
21b	$\rightarrow SO_2HO_2$	0.16[b]	...
22a	$SO_2 + RO_2 \rightarrow SO_3 + RO$	1.5[c]	...
22b	$\rightarrow SO_2RO_2$	0.19[b]	...
23	$SO_2 + RO \rightarrow ROSO_2$	5[d]	
24	$SO_2 + RCO(O_2) \rightarrow RCO_2 + SO_3$	1.5[d]	...

[a] Pseudo-second order rate constant at 760 torr. [b] An estimate based on Calvert's suggestion that Reactions 21b and 27b should be about one-eighth as fast as Reactions 21a and 22a (*11*). [c] An estimate based on the assumption that Reactions 22a and 24 should proceed about 30% faster than Reaction 21a at comparable concentrations. [d] Estimate.

SO_2 Photooxidation Data

Ideally, one would like a base of experimental data spanning a wide range of initial reactant concentrations to deduce the chemical kinetics of the system. Unfortunately, only a few studies are available which report enough adequate concentration-time data to afford a mechanistic analysis.

The data used in this study came from five sources. Results of SO_2/NO_x photooxidation experiments have been reported by Bradstreet (*42, 43*) and Smith and Urone (*27*). Ozone/hydrocarbon/SO_2 systems have been studied by Cox and Penkett (*24, 38, 39*) and McNelis (*44*), although, of these, only McNelis reports full concentration-time data. Finally, smog chamber experiments with SO_2/NO_x/hydrocarbon mixtures have been reported by Wilson and Levy (*45, 46*) and Smith and Urone (*27*). A summary of experimental conditions for each data set appears in Table III.

In the remainder of this study we simulate to the extent possible the experimental data summarized in Table III. The primary objective of the simulations is to determine if the reported data can be explained in terms of the reactions discussed earlier. In view of the shortage of measured rate constants for certain SO_2 reactions, we have carried out these simulations using only those reactions for which reliable rate constants are available. This approach will indicate whether the present set of SO_2 reactions is sufficient to explain observed data.

One important parameter which is frequently not measured or reported in sufficient detail in experimental studies is the light intensity in the system. The light intensity is reflected most strongly in the rate constant for NO_2 photolysis, k_1. When k_1 was not directly measured (*47*) or could not be inferred from other information, estimates of the light intensity were made through the NO_2 concentration-time behavior.

Table III. Experimental Conditions Associated with Available Smog Chamber Data

Investigator(s)	Initial species concn	Reactor	Radiation conditions
	Systems without hydrocarbons		
Smith and Urone (*27*)	$[SO_2]_o$ = 2 ppm $[NO_2]_o$ = 0,.0.9, 1.7, 3.4, 5.1, 10.2 ppm $[NO]_o$ = 0 RH = 0, 50%	2-l. pyrex flasks; static conditions; 38 °C	16–24-W UV lamps, 90% of intensity centered at 3500 ± 50 Å; photon flux = 4.3 × 10^{15}; photons cm^{-3} s^{-1}; k_1 = 0.5 min^{-1} (estd)
Bradstreet (*42, 43*)	$[SO_2]_o$ = 0–3.2 ppm $[NO_2]_o$ = 0–1 ppm $[NO]_o$ = 0–2.23 ppm RH = 0–75%	22.4-l. borosilicate vessel; static conditions	94% of intensity in range 3200–4000 Å, photon flux not reported
	Systems containing hydrocarbons		
McNelis (*44*)	$[O_3]_o$ = 0.2–2.0 ppm $[C_3H_6]_o$ = 1–10 ppm $[SO_2]_o$ = 0–1 ppm RH = 25%	437-l. Tedlar bag; static conditions; 27 °C	No illumination
Smith and Urone (*27*)	$[SO_2]_o$ = 2 ppm $[NO_2]_o$ = 0–10.2 ppm $[NO]_o$ = 0 $[C_3H_6]_o$ = 3–12 ppm	Same as (*27*) above	Same as (*27*) above
Wilson and Levy (*45, 46*)	$[SO_2]_o$ = 0.75 ppm $[NO_2]_o$ = 0 $[NO]_o$ = 1 ppm $[C_4H_8]_o$ = 4 ppm RH = 0–65%	2 100-l. pyrex bell jars; dynamic conditions; flow rate = 800 cm^3 min^{-1}; 27 °C	34 UV lamps; k_d = 0.5 min^{-1}; k_1 = 0.35 min^{-1} (estd)

Mechanism for NO_x/Hydrocarbon/SO_2 Systems

In this section we present a general kinetic mechanism capable of representing the experimental systems considered. The basic hydrocarbon/NO_x mechanism is that developed by Hecht et al. (*17*). In this mechanism, certain free radicals are lumped into general classes. The stoichiometric coefficients in the mechanism are determined by the particular hydrocarbon(s). The use of such coefficients is necessary only when describing reactions which are not represented as elementary processes, such as the ozone–olefin reaction.

The general mechanism employed in the current study is given in Table IV. Two sets of stoichiometric coefficients are required: one for the propylene systems of Smith and Urone (*27*) and McNelis (*44*) and one for the 1-butene system of Wilson and Levy (*45, 46, 55*). Since the McNelis system contained no NO_x, an explicit propylene mechanism, not presented here, was used in analyzing these experiments. The detailed propylene mechanism with NO_x reactions gave computed concentrations very close to those predicted by the lumped mechanism of Table IV. The mechanism of O'Neal and Blumstein (*48*) was used for the ozone–olefin reaction. The manner in which the rate constants were determined for the ozone–olefin reaction is outlined in the Appendix. The values of the stoichiometric coefficients used are given in Table IV, and the primary photolysis rate constants are given in Table V. The values of k_1 for the experimental systems were: Bradstreet, 0.5 min^{-1}; Smith and Urone, 0.5; and Wilson and Levy, 0.35.

Considerable confusion currently exists as to the exact mechanism of the reaction

$$NO + NO_2 + H_2O \underset{k_r}{\overset{k_f}{\rightleftharpoons}} 2HONO$$

which may take place heterogeneously (*52, 61*). In simulating results from smog chambers, several groups have chosen to account for nitrous acid formation by including an initial wall desorption rate (*62*). We have lumped the possible heterogeneous behavior of the nitrous acid system into the rate constant k_f. A value for k_f was selected which provides the requisite initial HONO charge and lies near the wide range of experimentally determined values.

Analysis of Experimental Systems

SO_2/NO_x Systems. *Smith and Urone* (*27*). The observed and predicted rates of initial SO_2 oxidation for the experi-

Table IV. General Mechanism for Homogeneous Oxidation of SO_2

Reaction	Rate constant, 25 °C ppm, min units	Propylene	1-Butene
$NO_2 + h\nu \rightarrow NO + O$	ϕI_a (1)[a]		
$O + O_2 + M \rightarrow O_3 + M$	2×10^{-5}		
$NO + O_3 \rightarrow NO_2 + O_2$	29.5		
$O + NO + M \rightarrow NO_2 + M$	2.3×10^{-3}		
$O + NO_2 \rightarrow NO + O_2$	1.38×10^{4}		
$O + NO_2 + M \rightarrow NO_3 + M$	4.5×10^{-3}		
$NO_2 + NO_3 \rightarrow N_2O_5$	4.4×10^{3}		
$N_2O_5 \rightarrow NO_2 + NO_3$	13.8		
$NO + NO_3 \rightarrow 2NO_2$	1.48×10^{4}		
$O_3 + NO_2 \rightarrow NO_3 + O_2$	0.047		
$2NO + O_2 \rightarrow 2NO_2$	7.6×10^{-16}		
$O_3 + h\nu \rightarrow O + O_2$	ϕI_a (0.035)[a]		
$O_3 + h\nu \rightarrow O(^1D) + O_2(^1\Delta)$	ϕI_a (0.026)[a]		
$O(^1D) + M \rightarrow O + M$	1.1×10^{5}		
$O_2(^1\Delta_g) + O_3 \rightarrow 2O_2 + O$	5.6		
Terminal addition[b]			
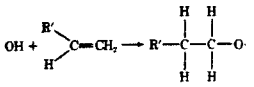		390	1000
Internal addition			
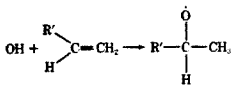		9400	2.3×10^{4}
H-abstraction			
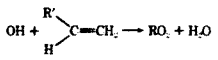		1.5×10^{4}	3.6×10^{4}
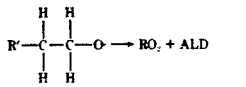		8500	8500
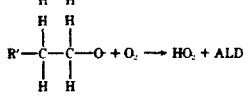		0.04	0.04

(*Continued on page 1118*)

Table IV. *(Continued)*

Reaction	Rate constant, 25 °C ppm, min units	Propylene	1-Butene
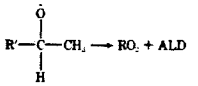		8500	8500
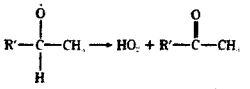		0.04	0.04
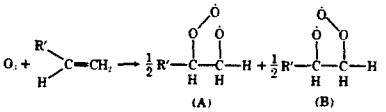 (A) (B)		0.015	0.015
α-*H* abstraction			
(A) → OH + CO + HO_2 + ALD		1.7×10^4	4.5×10^5
(B) → OH + ALD + RCO_3		1.7×10^4	4.5×10^5
β-*H* abstraction			
(A) → ALD + Stable Products		1200	1.0×10^5
Criegee decomposition			
(A) → ALD + $\frac{1}{2}$RO + $\frac{1}{2}$OH + $\frac{1}{2}RCO_3 + \frac{1}{2}HO_2 + \frac{1}{2}CO$		1000	1000
(B) → ALD + CO + H_2O		1000	1000
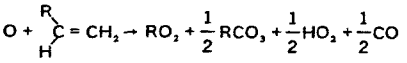		5320	5900
NO + RO_2 → NO_2 + RO	1000		
RO + O_2 → HO_2 + ALD	0.024		
RO + NO_2 → RNO_3	490		
RCO_3 + NO_2 → PAN	490		
OH + NO → HNO_2	3000		
RO + NO → RNO_2	2000		
NO + HO_2 → NO_2 + OH	300		
NO_2 + OH → HNO_3	1.2×10^4		
NO + RCO_3 → NO_2 + RO_2 + CO_2	910		
$2RCO_3$ → $2RO_2$ + $2CO_2$ + O_2	3.8		
$2HO_2$ → H_2O_2 + O_2	8200		
RO_2 + HO_2 → RO + OH + O_2	100		
ALD + $h\nu$ → CO + HO_2 + 1/2 RO_2	ϕI_a (0.01)[a]		
OH + ALD → H_2O + 1/3 CO + 1/3 HO_2 + 2/3 RCO_3	2.2×10^4		
O_3 + OH → HO_2 + O_2	87		
O_3 + HO_2 → OH + $2O_2$	2		
H_2O_2 + $h\nu$ → 2OH	ϕI_a (0.0036)[a]		
HNO_2 + $h\nu$ → OH + NO	ϕI_a (0.07)[a]		
$2HNO_2$ → NO + NO_2 + H_2O	5.1×10^{-5}		
$O(^1D)$ + H_2O → 2OH	5.2×10^5		
NO + NO_2 + H_2O → $2HNO_2$	2×10^{-6}		
OH + CO → HO_2 + CO_2	219		
O + SO_2 + M → SO_3 + M	2.8×10^{-5}		
OH + SO_2 → HSO_3	780		
HO_2 + SO_2 → SO_3 + OH	1.3		
NO_3 + SO_2 → SO_3 + NO_2	10^{-5}		
SO_3 + H_2O → H_2SO_4	1300		
O + SO_3 → SO_2 + O_2	0.082		
N_2O_5 + SO_2 → SO_3 + $2NO_2$	6.2×10^{-7}		
O_3 + SO_2 → SO_3 + O_2	1.2×10^{-8}		
SO_2 + $h\nu$ → $^1SO_2$	ϕI_a (0.02)[a]		
$^1SO_2$ + SO_2 → SO_3 + SO	5400		
$^1SO_2$ + SO_2 → $^3SO_2$ + SO_2	4400		
$^1SO^2$ → SO_2 + $h\nu_f$	1.3×10^4		
$^1SO_2$ → $^3SO_2$	9×10^4		
$^3SO_2$ + SO_2 → SO_3 + SO	100		
$^3SO_2$ → SO_2 + $h\nu_p$	8400		
$^3SO_2$ → SO_2	7800		
$^3SO_2$ + M → SO_2 + M	200		

[a] The quantity in parentheses is the value of the absolute photolysis rate constant relative to that for NO_2, k_1, for a solar spectral distribution and zenith angle of 40°. [b] R' = CH_3 (propylene). R' = C_2H_5 (1-butene).

Table V. Observed and Predicted Rates of Initial SO_2 Oxidation Rate for Smith-Urone Experiments[a]

$[NO_2]_o$, ppm	Obs rate, ppm min^{-1} × 10^{4}[b]	Pred rate, ppm min^{-1} × 10^{4}[b]
0	1.7 ± 0.3	1.70
0.85	3.3 ± 0.3	1.77
1.7	2.9 ± 0.3	1.77
3.4	1.6 ± 0.3	1.79
5.1	1.7 ± 0.3	1.82
10.2	1.8 ± 0.3	1.89

[a] $[SO_2]_o$ = 2 ppm. [b] Over initial 1500 min.

ments of Smith and Urone are given in Table V. The observed rate reached a maximum at an initial NO_x concentration of 0.85 ppm. At $[NO_2]_o$ = 10.2 ppm, the initial SO_2 oxidation rate returned to the value of 1.7×10^{-4} ppm min^{-1}, observed for $[NO_2]_o = 0$. The predicted initial SO_2 oxidation rate increases monotonically from the base value, 1.7×10^{-4} ppm min^{-1} accounted for by the photooxidation process, to 1.89×10^{-4} ppm min^{-1} at $[NO_2]_o$ = 10.2 ppm and does not show the inhibition observed experimentally. Smith and Urone proposed an explanation based on oxygen atom competition between NO_2 and SO_2. Such a competition cannot, however, explain the NO_2 inhibition. If we ignore the effects of O_3 photolysis, which are minor in dry systems, and the N_2O_5 equilibrium, the simplified mechanism consists of the following reactions:

$$NO_2 + h\nu \xrightarrow{1} NO + O$$

$$O + O_2 + M \xrightarrow{2} O_3 + M$$

$$O_3 + NO \xrightarrow{3} NO_2 + O_2$$

$$O + NO + M \xrightarrow{4} NO_2 + M$$

$$O + NO_2 + M \xrightarrow{5} NO_3 + M$$

$$O_3 + NO_2 \xrightarrow{6} NO_3 + O_2$$

$$O + SO_2 + M \xrightarrow{7} SO_3 + M$$

$$SO_2 + h\nu \xrightarrow{8} SO_2^*$$

$$SO_2 + SO_2^* \xrightarrow{9} SO_3 + SO$$

The reactions between SO_2 and O_3, NO_3 and N_2O_5 are too slow to affect the system. Based on the above reactions, the rate equation for SO_2 is

$$-\frac{d[SO_2]}{dt} = \phi I_a^{SO_2} + \frac{k_1 k_7 [SO_2][NO_2]}{k_2[O_2] + k_4[NO] + k_5[NO_2] + k_7[SO_2]}$$

Evaluating the initial SO_2 removal rate, we find the rate to be a monotonically increasing function of $[NO_2]_o$. Since, following Urone and Smith, we have evaluated the initial SO_2 oxidation rate at the 1500-min point in the runs rather than at $t = 0$, the results in Table VI do not follow this law exactly.

Addition of the reaction

$$O + SO_3 \rightarrow SO_2 + O_2$$

Table VI. Predicted Percentage Contributions to SO_2 Removal in Water-Contaminated NO_x/SO_2/Air System

Time, min	Reaction no.[a] 7	8–9	17–19
150	4.3	94.4	1.3
800	1.6	97.9	0.5
1600	0.9	98.8	0.3
3600	0.4	99.4	0.2

[a] See text for reactions.

provides a path for the reformation of SO_2 at high NO_2 levels. Based on the latest value of its rate constant (*49*), the rate of this reaction is too slow to account for the observed NO_2 inhibition.

Contamination of the experimental system is a possible explanation for the observed inhibition. Considering the photolysis of O_3 in the presence of water, the following reactions will occur:

$$O_3 + h\nu \xrightarrow{10} O(^1D) + O_2$$

$$O_3 + h\nu \xrightarrow{11} O + O_2$$

$$O(^1D) + M \xrightarrow{12} O + M$$

$$H_2O + O(^1D) \xrightarrow{13} 2OH$$

$$O_3 + O(^1D) \xrightarrow{14} 2O_2$$

$$O_3 + OH \xrightarrow{15} HO_2 + O_2$$

$$O_3 + HO_2 \xrightarrow{16} OH + 2O_2$$

$$SO_2 + OH \xrightarrow{17} HSO_3$$

$$SO_2 + HO_2 \xrightarrow{18} HSO_4$$

$$\xrightarrow{19} SO_3 + OH$$

Table VI shows the relative rates of SO_2 removal by paths 7, 9, 17, 18, and 19 in a system containing 0.85 ppm NO_2, 2 ppm SO_2, and 5000 ppm H_2O. We note that the observed increase in SO_2 oxidation rate when 0.85 ppm of NO_2 is added to the system cannot be accounted for either by the O–SO_2 reaction path or by the effect of water contamination. Neither the acceleration of the SO_2 oxidation rate at low NO_2 levels nor its inhibition at high NO_2 levels can be explained on the basis of known chemistry at this point.

Bradstreet (*42, 43*). Data from the experiments of Bradstreet cover a somewhat wider range of initial conditions than those of Smith and Urone. Comparisons of the observed and predicted rates of SO_2 disappearance for these experiments are given in Table VII. As in the Smith and Urone experiments, an inhibition of the SO_2 oxidation rate is observed as $[NO]_o$ is increased. Again, this inhibition, as well as the strong effect of $[NO]_o$ on the SO_2 oxidation rate, cannot be predicted.

O_3/Hydrocarbon/SO_2 System. Cox and Penkett (*24*) found that SO_2 added to olefin/O_3 systems was converted to sulfuric acid aerosol. They inferred that a short-lived inter-

mediate of the ozone–olefin reaction, which they speculated might be a biradical, was responsible for SO_2 oxidation.

McNelis (44). In this system, O_3, SO_2, and propylene were mixed in a large batch reactor in the dark. The purpose of the experiments was to provide data on the role of the ozone–olefin reaction in SO_2 oxidation. The primary paths for removal of propylene are by reaction with OH and O_3. In the ozone–olefin reaction the current understanding is that the initial step is the formation of a molozonide. Ring opening then results in a rapid equilibrium between the forms of the oxy-peroxy biradical. The biradical may then decompose by the Criegee mechanism or abstract a hydrogen atom from the α- or β-carbon atom (*48*). The reaction rate constants for each of these paths were calculated thermochemically, and the calculations are summarized in the Appendix.

Predicted and observed concentration-time profiles for O_3, propylene, and SO_2 are shown in Figure 1. Whereas the predicted ozone and propylene decay rates are close to those observed, the predicted SO_2 removal rate is far too low. Possible reasons for this discrepancy will be discussed in the next section. Excellent agreement is obtained between observed and predicted final acetaldehyde concentrations. These values, together with initial SO_2, O_3, and C_3H_6 concentrations appear in Table VIII. The agreement between predicted and observed acetaldehyde concentrations is important in that it implies that the hydrocarbon–NO_x chemistry is accurately represented by the mechanism.

Although the SO_2 mechanism fails to predict the observed SO_2 oxidation rate, the proposed biradical–SO_2 reaction is incapable of accounting for the difference. Steady-state biradical concentrations predicted by the O'Neal-Blumstein mechanism are on the order of 10^{-11} ppm. Thus, rate constants for an SO_2–biradical reaction would have to be several orders of magnitude above those expected for an SO_2 oxygen abstraction from a peroxy biradical for this path to be competitive with spontaneous decomposition.

NO_x/Hydrocarbon/SO_2 Systems. *Smith and Urone (27).* The authors reported the initial rates of SO_2 oxidation in systems containing NO_2, SO_2, and propylene. The results of these experiments and their simulations are presented in Table IX. Both the data and the simulation exhibit an inhibition in the SO_2 oxidation rate with increasing $[NO_2]_o$. Analysis of the reactions which contribute to SO_2 consumption indicates that the reaction

$$HO_2 + SO_2 \rightarrow SO_3 + OH$$

is primarily responsible for the inhibition. As $[NO_2]_o$ is increased, NO becomes increasingly more effective in competing with SO_2 for hydroperoxyl radicals. The HO_2 radical, not present in pure SO_2/NO_x systems, is then the key to the observed inhibitory effect of $[NO_2]_o$.

It should be noted that predicted initial SO_2 oxidation rates are considerably smaller than observed values. Predicted propylene oxidation rates, however, are comparable to experimental values. The SO_2 results point to the existence of SO_2 oxidation mechanisms unaccounted for here.

Wilson and Levy (45, 46). These experiments are currently the only available for SO_2/NO_x/hydrocarbon mixtures for which concentration-time data for all important species are reported. Nevertheless, the high degree of scatter in the experimental data makes quantitative comparisons with predicted data difficult. The experimental data indicate that increasing $[SO_2]_o$ increases the time to the NO_2 maximum in dry systems but has little effect on NO_2 behavior in moist systems. Large amounts of SO_2 caused an increase in the time to the O_3 maximum and led to a slight increase in the peak O_3 concentration in dry systems while reducing it in moist systems. In addition, increasing $[SO_2]_o$ decreased the overall 1-butene reaction rate and increased the final 1-butene concentration. SO_2 was observed to react more quickly in moist (65% RH) runs than in dry runs.

The sudden rapid disappearance of SO_2 in certain high humidity runs and the dramatic effect of relative humidity on the overall reaction rate are suggestive of heterogeneous steps. Aerosol was observed in many of the experiments, suggesting that SO_2 may have dissolved in droplets.

The accuracy of the data can be judged by examining the degree of satisfaction of the photostationary state for ozone (*50, 51*). If the photostationary state is obeyed, the group $\theta = k_1[NO_2]/k_3[NO][O_3]$ should be nearly unity at all times. For the experimental data of run 46, $\bar{\theta} = 0.172$ with a standard deviation σ of 0.051. A similar evaluation for the simulation of run 46 gives $\bar{\theta} = 1.16$ with $\sigma = 0.039$. The unexpectedly low measured value of $\bar{\theta}$ suggests that the light intensity and/or concentration measurements may be in error.

A summary of the results of the simulations is given in Table X. Concentration-time profiles for an experiment characteristic of high humidity conditions (run no. 53) are given in Figure 2. The hydrocarbon/NO_x mechanism simulates the observed concentration profiles well, except in the following respects. First, in dry systems the observed O_3 peak is considerably higher than predicted. This is consistent with the fact that observed final C_4H_8 concentrations in dry systems

Table VII. Observed and Predicted Rates of SO_2 Oxidation for Bradstreet Experiments[a]

ppm			Obs rate,	Pred rate,
$[NO]_o$	$[NO_x]_o$	$[H_2O]_o$	% h^{-1}	% h^{-1}
0	0	0	0.54	0.59
0.45	0	0	0.72	0.60
1.21	0	0	0.80	0.60
1.52	0	0	0.62	0.60
2.23	0	0	0.34	0.60
1.21	0	1.5×10^3	0.74	0.60
1.21	0	3	0.90	0.62
1.52	0	1.5	0.82	0.60
1.52	0	3.0	1.23	0.64
2.23	0	1.5	0.90	0.60
2.23	0	3.0	1.76	0.63
0.45	0.71	0	0.82	0.62
0.89	0.71	0	0.74	0.62
1.52	0.71	0	0.67	0.62
0.89	0.71	1.5	0.15	0.71

[a] $[SO_2]_o$ = 3.2 ppm.

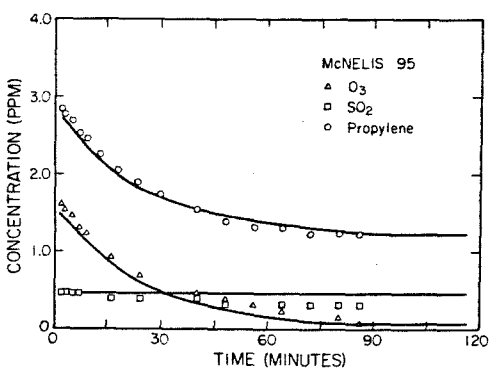

Figure 1. Comparison of observed and predicted concentrations for McNelis run 95

are lower than predicted. Second, observed SO_2 oxidation rates are much higher than predicted, an effect perhaps attributable in part to heterogeneous effects. In spite of these deficiencies, the principal qualitative features of the data are reproduced by the mechanism. For example, both experiment and mechanism show an increase in overall system reactivity with increasing relative humidity. A major influence of relative humidity is through the formation of nitrous acid by

$$NO + NO_2 + H_2O \rightarrow 2HNO_2$$

The subsequent photolysis of HNO_2 then leads to the initiation of 1-butene oxidation.

Discussion. The simulations reported in this section indicate that the NO_x/hydrocarbon mechanism of Table IV is capable of simulating observed concentration-time behavior in smog chamber systems. However, in every case, observed SO_2 oxidation rates could not be explained solely on the basis of those SO_2 reactions for which rate constants have been measured. Certainly other reactions involving SO_2 are possible, for example, Reactions 22a, 22b, and 23 in Table II. Using the rate constants estimated in Table II, the contributions of Reactions 22–24 (with $R = CH_3$) to observed SO_2 removal rates can be estimated in a system containing 1-butene. Figure 3 shows the relative importance of these reactions in removing SO_2 from a system containing initially 0.10 ppm SO_2, 0.15 ppm NO, 0.05 ppm NO_2, 0.10 ppm C_4H_8, 10 ppm CO, and 50% relative humidity. The results are similar to those obtained by Calvert and McQuigg (*12*) who used trans-2-butene and a more detailed mechanism but with identical initial conditions. A maximum SO_2 oxidation rate of 4.5% h^{-1} is predicted with the OH and HO_2 reactions accounting for at least 90% of the predicted rate. The balance is due to reaction of SO_2 with RO_2, RCO_3, and $O(^3P)$.

Although reactions of the type $RO_2 + SO_2$ may be important, rate constants for them are essentially unknown. Before an accurate assessment of their role in SO_2 chemistry can be made, rate constants must be obtained.

Davis et al. (*53*) have suggested that the product HSO_3 formed in Reaction 20 of Table II could participate in reactions of the form:

$$HSO_3 + O_2 \rightarrow HSO_5$$

$$HSO_5 + NO \rightarrow HSO_4 + NO_2$$

$$HSO_4 + O_2 \rightarrow HSO_6$$

$$HSO_6 + NO \rightarrow HSO_5 + NO_2$$

[Other possible reactions of HSO_4 and HSO_5 have been suggested (*12*), including hydrogen abstractions from alkanes and HO_2 and addition to olefinic double bonds.] The reactions were proposed to explain ozone buildup in the Potomac Electric Power Co.'s Morgantown plume. However, laboratory data have shown that addition of SO_2 to a hydrocarbon/NO_x system does not lead to ozone enhancement (*45*). For this reason, the above reactions were not incorporated in our mechanism.

Several important questions concerning the mechanism of SO_2 oxidation in SO_2/NO_x/hydrocarbon systems can be examined by performing a series of simulations in which key parameters, such as initial concentrations and relative humidity, are systematically varied. In the initial stage of the reaction, the SO_2–OH reaction is the most important oxidation path, since OH radicals are being produced rapidly by HNO_2 photolysis and by the reaction of NO and HO_2. In the middle and latter stages of the reaction, the HO_2–SO_2 reaction may become comparable to that with OH, although the OH radical is being produced continually by the ozone–olefin reaction. At all times the purely photolytic oxidation of SO_2 to SO_3 is negligible compared to other reaction paths. Of the initial concentrations, the largest effect on the SO_2 oxidation rate results from variation of the hydrocarbon level in the system. Nitric oxide tends to inhibit SO_2 oxidation, largely because of its ability to scavenge free radicals. Increasing

Table VIII. Observed and Predicted Acetaldehyde Concentrations for McNelis Experiments

Run no.	ppm $[C_3H_6]_0$	ppm $[O_3]_0$	ppm $[SO_2]_0$	Final values of $[CH_3CHO]$, ppm Obs	Pred
25	1.88	2.38	0.58	0.73	0.77
26	3.55	1.08	0.62	0.45	0.49
27	3.46	0.98	0.19	0.58	0.46
31	8.55	2.71	0.52	1.80	1.36
87	1.11	2.06	0.65	0.48	0.45
90	2.74	1.97	0.58	0.82	0.86
95	3.02	1.81	0.56	0.79	0.80
98	2.82	2.02	0.20	0.84	0.90

Table IX. Results of Smith-Urone NO_x/SO_2/Propylene Simulations

ppm $[NO_2]_0$	ppm $[C_3H_6]_0$	$(-d[SO_2]/dt)$, ppm $min^{-1} \times 10^3$ Obs	Pred	$(-d[C_3H_6]/dt)_0$, ppm $min^{-1} \times 10^2$ Obs	Pred
0	6	0.13	0.13	0	0
0.85	6	15 ± 3	6	9	2.2
1.7	6	12 ± 3	3.7	13 ± 1	6.3
5.1	6	5.6 ± 0.1	3.8	12 ± 1	11.8
10.2	6	3.7 ± 0.1	2.2	8.3 ± 0.5	15.0

Table X. Results of Simulation of Wilson-Levy Experiments

Run no.	ppm $[NO_2]_0$	ppm $[NO]_0$	ppm $[C_4H_8]_0$	ppm $[SO_2]_0$	RH	$[C_4H_8]$ final, ppm Obs	Pred	$[NO_2]^a$ t-max, min Obs	Pred	$[NO_2]$ max, ppm Obs	Pred	$[O_3]^a$ t-max, min Obs	Pred	$[O_3]$ max, ppm Obs	Pred	$\Delta[SO_2]$, %[b] Obs	Pred
33	0.04	0.96	3.80	0.75	0	0.75	1.30	80	65	0.78	0.78	129	108	0.93	0.38	47	13
36	0.03	1.00	4.00	0.25	0	0.80	1.53	87	70	0.82	0.81	130	113	0.92	0.40	60	13
45	0.06	1.02	3.90	0.75	22	1.15	1.36	51	40	0.75	0.76	88	84	0.72	0.41	53	15
46	0.20	1.17	3.95	0.75	55	1.55	1.35	27	30	0.85	0.82	50	70	0.54	0.44	35	17
49	0.05	1.00	3.98	0.53	0	0.94	1.46	92	65	0.78	0.82	137	105	0.85	0.41	68	13
53	0.02	1.02	3.98	0.25	65	1.68	1.51	34	40	0.63	0.67	69	80	0.39	0.38	100	15
55	0.02	1.00	3.96	0.52	65	1.64	1.46	34	40	0.68	0.65	68	75	0.36	0.38	100	15
56	0	1.00	3.91	0.75	65	1.57	1.40	42	46	0.71	0.65	77	84	0.29	0.39	69	15

[a] Times and concentrations of species maxima. [b] Percent disappearance over duration of experimental run.

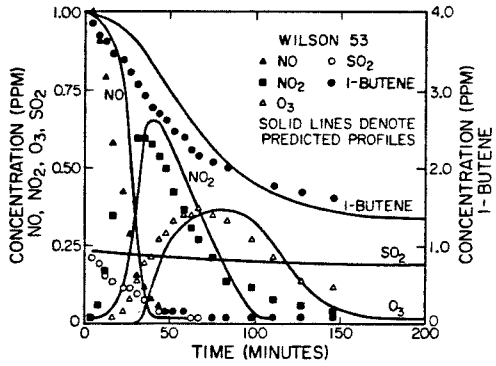

Figure 2. Comparison of observed and predicted concentrations for Wilson-Levy run 53

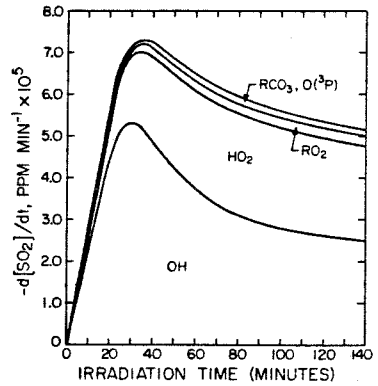

Figure 3. Relative contributions of free-radical reactions to overall homogeneous SO_2 removal rate in simulated polluted atmosphere containing initially 0.10 ppm SO_2, 0.15 ppm NO, 0.05 ppm NO_2, 0.10 ppm 1-butene, 10 ppm CO, and relative humidity = 50%; solar zenith angle = 40°

relative humidity increases the SO_2 oxidation rate through homogeneous and heterogeneous paths involving OH-production. (Not all heterogeneous paths involving water have been considered here.)

Based on the frequent literature reports of films and coatings that cover reactor surfaces in smog chamber experiments involving SO_2 as well as the positive identification of sulfur-containing aerosol in such systems, it seems likely that heterogeneous effects play an important if not predominant role in laboratory SO_2 studies. The importance of such effects in polluted atmospheres must be determined if rates of sulfate formation are to be predicted with accuracy.

Conclusions

The chemical kinetics of the homogeneous atmospheric oxidation of SO_2 were studied. Known reactions involving SO_2 for which rate constants have been measured are insufficient in themselves to account for observed SO_2 oxidation rates in NO_x/hydrocarbon/SO_2 systems. Reactions involving peroxy-radicals and SO_2 may play an important role in these systems, and rate constant determinations for them are needed. The extent to which heterogeneous reactions may be responsible for observed SO_2 oxidation rates in smog chambers could not be assessed.

Appendix. Estimation of Rate Constants for O_3–Olefin Pathways

In this Appendix, we show how the relative rate constants were derived for the various decomposition pathways available to the O_3–olefin molozonide intermediate. 1-Butene will be used as the example olefin. Details of the procedure used for calculating thermochemical quantities may be found in O'Neal and Blumstein (*48*).

For the molozonides of propylene and 1-butene, collisional deactivation and spontaneous decomposition may proceed at comparable rates. Both processes must be considered in the overall kinetic scheme shown below:

$$O_3 + C_4H_8 \xrightarrow{k_1} MOL^*$$

$$MOL^* + M \xrightarrow{k_2} MOL + M$$

$$\left.\begin{array}{l} MOL^* \xrightarrow{k_C} \\ MOL \xrightarrow{k_{CT}} \end{array}\right\} \text{Criegee decomposition products}$$

$$\left.\begin{array}{l} MOL^* \xrightarrow{k_\alpha} \\ MOL \xrightarrow{k_{\alpha T}} \end{array}\right\} \alpha\text{-}H \text{ abstraction products}$$

$$\left.\begin{array}{l} MOL^* \xrightarrow{k_\beta} \\ MOL \xrightarrow{k_{\beta T}} \end{array}\right\} \beta\text{-}H \text{ abstraction products}$$

$$\left.\begin{array}{l} MOL^* \xrightarrow{k_\gamma} \\ MOL \xrightarrow{k_{\gamma T}} \end{array}\right\} \gamma\text{-}H \text{ abstraction products}$$

We are interested in the constants ϕ_{CR}, ϕ_α, ϕ_β, and ϕ_γ which represent the ratio of the rate of product formation by the subscripted path to the rate of product formation by all pathways.

Thus,

$$\phi_i = \frac{k_i[MOL^*] + k_{iT}[MOL]}{[MOL^*]\sum_{i=1}^{4} k_i + [MOL]\sum_{i=1}^{4} k_{iT}} = \frac{\text{Rate of Product Formation by Path } i}{\text{Rate of Product Formation by All Pathways}}$$

[MOL] and [MOL*] may be calculated from steady-state considerations. This formulation assumes that no intermediate complexes are formed which may affect the distribution of decomposition products.

The rate constants k_i and k_{iT} may be calculated by estimating activation energies and A-factors for the reactions of the molozonide. RRK theory is used to calculate k_{iT}. O'Neal and Blumstein obtain:

$$k_{CT} = 1.8 \times 10^{-5}\ \text{min}^{-1} \quad k_C = 4.1 \times 10^8\ \text{min}^{-1}$$

$$k_{\alpha T} = 1.2 \quad k_\alpha = 2.9 \times 10^{10}$$

$$k_{\beta T} = 0.03 \quad k_\beta = 3.8 \times 10^{10}$$

$$k_{\gamma T} = 3.6 \quad k_\gamma = 1.3 \times 10^{10}$$

From kinetic theory, the rate constant for the collisional deactivation of a vibrationally excited molecule is given by:

$$k_2 = \pi\sigma_{12}^2\left(\frac{8\,kT}{\pi\mu}\right)^{1/2}$$

where

σ_{12} = average molecular diameter of collision complex
μ = reduced mass of complex (molozonide + N_2)

For a 1-butene molozonide we estimate $\sigma_{12} \approx 5$ Å and $\mu = 3.5 \times 10^{-23}$ g/molecule, giving $k_2 = 4.25 \times 10^{-10}$ cm^3 molec^{-1} s^{-1} at 25 °C. This assumes that deactivation occurs at the collision rate (strong collision assumption). Using the expression derived above, we obtain the following ratios:

$$\phi_{CR}:\phi_\alpha:\phi_\beta:\phi_\gamma = 1:450:100:1200$$

For propylene, where no γ-abstraction path is possible, we obtain

$$\phi_{CR}:\phi_\alpha:\phi_\beta = 1:17:1.2$$

The rate constants in Table IV are obtained by assuming that the rate constant for the overall molozonide decomposition by Criegee pathways = 1000 min^{-1}. The exact value is relatively unimportant, and as long as steady-state conditions prevail, only the ratios are important.

Literature Cited

(1) Junge, C. E., Ryan, T. G., *Q. J. R. Meteorol. Soc.*, **84**, 46 (1958).
(2) Scott, W. D., Hobbs, P. V., *J. Atmos. Sci.*, **24**, 54 (1967).
(3) Matteson, M. J., Stöber, W., Luther, H., *Ind. Eng. Chem. Fundam.*, **8**, 677 (1969).
(4) Foster, P. M., *Atmos. Environ.*, **3**, 157 (1969).
(5) Cheng, R. T., Corn, M., Frohliger, J. O., *ibid.*, **5**, 987 (1971).
(6) Brimblecomb, P., Spedding, D. J., *Chemosphere*, **1**, 29 (1974).
(7) Urone, P., Schroeder, W. H., *Environ. Sci. Technol.*, **3**, 436 (1969).
(8) Katz, M., *Can. J. Chem. Eng.*, **48**, 3 (1970).
(9) Bufalini, M., *Environ. Sci. Technol.*, **5**, 685 (1971).
(10) Urone, P., Lutsep, H., Noyes, C. M., Parcher, J. F., *ibid.*, **2**, 611 (1968).
(11) Calvert, J. G., "Modes of Formation of the Salts of Sulfur and Nitrogen in an NO_x–SO_2–Hydrocarbon-Polluted Atmosphere", presented at the Conference on Atmospheric Salts and Gases of Sulfur and Nitrogen in Association with Photochemical Oxidant, University of California, Irvine, Calif., Jan. 7–9, 1974.
(12) Calvert, J. G., McQuigg, R. D., *Int. J. Chem. Kinet.*, Symp. No. 1, **7**, 113 (1975).
(13) Leighton, P. A., "Photochemistry of Air Pollution", Academic Press, New York, N.Y., 1961.
(14) Niki, H., Daby, E. E., Weinstock, B., *Adv. Chem. Ser.*, **113**, 16 (1972).
(15) Hecht, T. A., Seinfeld, J. H., *Environ. Sci. Technol.*, **6**, 47 (1972).
(16) Demerjian, K. L., Kerr, J. A., Calvert, J. G., *Adv. Environ. Sci. Technol.*, **4**, 1 (1974).
(17) Hecht, T. A., Seinfeld, J. H., Dodge, M. C., *Environ. Sci. Technol.*, **8**, 327 (1974).
(18) Goetz, A., Pueschel, R., *Atmos. Environ.*, **1**, 287 (1967).
(19) Rao, T. N., Collier, S. S., Calvert, J. G., *J. Am. Chem. Soc.*, **91**, 1609 (1969).
(20) Okuda, S., Rao, T. N., Slater, D. H., Calvert, J. G., *J. Phys. Chem.*, **73**, 4412 (1969).
(21) Sidebottom, H. W., Badcock, C. C., Jackson, G. E., Calvert, J. G., Reinhardt, G. W., Damon, E. K., *Environ. Sci. Technol.*, **6**, 72 (1972).
(22) Mulcahy, M.F.R., Stevens, J. R., Ward, J. C., *J. Phys. Chem.*, 71, 2124 (1967).
(23) Cadle, R. D., Magill, P. L., "Chemistry of Contaminated Atmospheres", in "Air Pollution Handbook", P. L. Magill, F. R. Holden, and C. Ackley, Eds., McGraw-Hill, New York, N.Y., 1956.
(24) Cox, R. A., Penkett, S. A., *J. Chem. Soc., Faraday Trans. I.*, **68**, 1735 (1972).
(25) Daubendiek, R. L., Calvert, J. G., *Environ. Lett.*, **8**, 103 (1975).
(26) Davis, D. D., *Can. J. Chem.*, **52**, 1405 (1974).
(27) Smith, J. P., Urone, P., *Environ. Sci. Technol.*, **8**, 743 (1974).
(28) Jaffe, S., Klein, F. S., *Trans. Faraday Soc.*, **62**, 2150 (1966).
(29) Boreskov, G. K., Illarionov, V. V., *J. Phys. Chem. Moscow*, **14**, 1428 (1940).
(30) Chung, K., Calvert, J. G., Bottenheim, J. W., *Int. J. Chem. Kinet.*, **7**, 161 (1975).
(31) Jackson, G. E., Calvert, J. G., *J. Am. Chem. Soc.*, **93**, 2593 (1971).
(32) Badcock, C. C., Sidebottom, H. W., Calvert, J. G., Reinhardt, G. W. Damon, E. K., *ibid.*, p 3115.
(33) Levy, A., Merryman, E. L., Reid, W. T., *Environ. Sci. Technol.*, **4**, 653 (1970).
(34) Jacob, A., Winkler, C. A., *J. Chem. Soc. Faraday Trans. I.*, **68**, 2077 (1972).
(35) Dainton, F. S., Ivin, K. J., *Trans. Faraday Soc.*, **46**, 374, 382 (1950).
(36) Penzhorn, R.-D., Stieglitz, L., Filby, W. G., Günther, K., *Chemosphere*, **3**, 111 (1973).
(37) Penzhorn, R.-D., Filby, W. G., Günther, K., Stieglitz, L., *Int. J. Chem. Kinet.*, Symp. No. 1, **7**, 611 (1975).
(38) Cox, R. A., Penkett, S. A., *Nature*, **230**, 1321 (1971).
(39) Cox, R. A., Penkett, S. A., *ibid.*, **229**, 486 (1971).
(40) Castleman, A. W., Jr., Davis, R. E., Munkelwitz, H. R., Tang, I. N., Wood, W. P., *Int. J. Chem. Kinet.*, Symp. No. 1, **7**, 629 (1975).
(41) Payne, W. A., Stief, L. J., Davis, D. D., *J. Am. Chem. Soc.*, **95**, 7615 (1973).
(42) Bradstreet, J. W., PhD dissertation, Syracuse University, Syracuse, N.Y., 1972.
(43) Bradstreet, J. W., Paper 73-113, 66th Annual Meeting of the Air Pollution Control Assoc., Chicago, Ill., June 24–28, 1973.
(44) McNelis, D. N., "Aerosol Formation from Gas-Phase Reactions of Ozone and Olefin in the Presence of Sulfur Dioxide", Office of Research and Development Report, EPA-650/4-74-034, August 1974.
(45) Wilson, W. E., Jr., Levy, A., "A Study of Sulfur Dioxide in Photochemical Smog", Battelle Memorial Institute Report to the American Petroleum Institute, August 1968.
(46) Wilson, W. E., Jr., Levy, A., *J. Air Pollut. Control Assoc.*, **20**, 385 (1970).
(47) Holmes, J. R., O'Brien, R. J., Crabtree, J. H., Hecht, T. A., Seinfeld, J. H., *Environ. Sci. Technol.*, **7**, 519 (1973).
(48) O'Neal, H. E., Blumstein, C., *Int. J. Chem. Kinet.*, **5**, 397 (1973).
(49) Westenberg, A. A., deHaas, N., *J. Chem. Phys.*, **7**, 2496 (1974).
(50) O'Brien, R. J., *Environ. Sci. Technol.*, **8**, 579 (1974).
(51) Jackson, J. O., Stedman, D. H., Smith, R. G., to be published.
(52) Graham, R. F., Tyler, B. J., *J. Chem. Soc. Faraday Trans. I.*, **68**, 683 (1972).
(53) Davis, D. D., Smith, G., Klauber, G., *Science*, **186**, 733 (1974).
(54) Davis, D. D., Prusazcyk, J., Dwyer, M., Kim, P., *J. Phys. Chem.*, **78**, 1775 (1974).
(55) Levy, A., personal communication, Nov. 1975.
(56) Richards, J. R., Fox, D. L., Reist, P. C., *Atmos. Environ.*, **10**, 211 (1976).
(57) Westenberg, A. A., de Haas, N., *J. Chem. Phys.*, **63**, 5411 (1975).
(58) Halstead, C. J., Thrush, B. A., *Proc. R. Soc. London, Ser. A.*, **295**, 363 (1966).
(59) Timmons, R. B., LeFevre, H. F., Hollinden, G. A., "Chemical Reactions in Urban Atmospheres", Elsevier, Amsterdam, The Netherlands, 1971.
(60) Atkinson, R., Pitts, J. N., Jr., *Chem. Phys. Lett.*, **29**, 28 (1974).
(61) Zafonte, L., Rieger, P. L., Holmes, J. R., paper presented at the 1975 Pacific Conference on Chemistry and Spectroscopy, Los Angeles, Calif., Oct. 28–30, 1975.
(62) Whitten, G. Z., private communication, Dec. 1975.

Received for review January 5, 1976. Accepted April 26, 1976. Work supported in part by the Jet Propulsion Laboratory and in part by National Science Foundation Grant 71ENG-02486.

APPENDIX II

ATMOSPHERIC BROMINE AND OZONE PERTURBATIONS IN THE LOWER STRATOSPHERE

Y. L. Yung

California Institue of Technology
Pasadena, California

J. P. Pinto

Goddard Institute for Space Studies
New York, New York

R. T. Watson
S. P. Sander
Jet Propulsion Laboratory
Pasadena, California

ABSTRACT

The role of bromine compounds in the photochemistry of the natural and perturbed stratosphere has been re-examined using an expanded reaction scheme and the results of recent laboratory studies of several key reactions. The most important finding is that through the reaction $BrO + ClO \rightarrow Br + Cl + O_2$ there is a synergistic effect between bromine and chlorine which results in an efficient catalytic destruction of ozone in the lower stratosphere. One-dimensional photochemical model results indicate that BrO is the major bromine species throughout the stratosphere, followed by $BrONO_2$, HBr, HOBr, and Br. We show from the foregoing that bromine is more efficient than chlorine as a catalyst for destroying ozone, and discuss the implications for stratospheric ozone of possible future growth in the industrial and agricultural use of bromine. Bromine concentrations of 20 pptv (2×10^{-11}), as suggested by recent observations, can decrease the present-day integrated ozone column density by 2.4%, and can enhance ozone depletion from steady-state chlorofluoromethane release at 1973 rates by a factor of 1.1-1.2.

INTRODUCTION

In recent years, photochemical models have been used to understand the factors that control the distribution and column abundance of ozone in the present stratosphere, and to assess the impact of perturbations by stratospheric aviation (Crutzen 1970; Johnston 1971) and the release of chlorofluoromethanes (McElroy et al. 1974; Molina and Rowland 1974; Cicerone et al. 1974; Wofsy et al. 1974; NAS 1976; NASA 1010 1977; Crutzen et al. 1978). Although the importance of HO_x, NO_x, and Cl_x in controlling stratospheric ozone is now well recognized, the close coupling that exists between members of different families has only recently become fully apparent. Indeed, the net effect of these interactions can be subtle, e.g., $ClONO_2$ is a reservoir species for Cl_x, but the formation of $ClONO_2$ via the reaction $ClO + NO_2 + M \rightarrow ClONO_2 + M$ can result either in a decrease or in an increase in the catalytic destruction of odd oxygen depending upon the photolytic fragmentation products of $ClONO_2$ (Smith et al., 1977, Barker et al., 1979). Although both Watson (1975) and Wofsy, McElroy and Yung (1975) recognized the importance of bromine for catalytic destruction of ozone, neither paper considered the coupling of the chlorine and bromine systems. Derwent and Eggleton (1978) included the coupling of the chlorine and bromine systems in a calculation of ozone depletion in the natural atmosphere due to 10 pptv Br_x and 1.3 ppbv Cl_x, but did not discuss the catalytic cycles or the effect on ozone in any detail.

Wofsy et al. (1975) calculated the magnitude of the ozone perturbation by bromine through two catalytic cycles:

$$\left.\begin{array}{ll} Br + O_3 \rightarrow BrO + O_2 & (1) \\ BrO + O \rightarrow Br + O_2 & (8) \end{array}\right\} \quad (I)$$

$$\text{net} \qquad O + O_3 \rightarrow 2O_2$$

$$\left.\begin{array}{ll} 2(Br + O_3 \rightarrow BrO + O_2) & (1) \\ BrO + BrO \rightarrow 2Br + O_2 & (9) \end{array}\right\} \quad (II)$$

net $\quad 2O_3 \rightarrow 3O_2$

However, Wofsy et al. (1975) did not consider the following catalytic cycles:

$$\left.\begin{array}{ll} Br + O_3 \rightarrow BrO + O_2 & (1) \\ Cl + O_3 \rightarrow ClO + O_2 & (15) \\ BrO + ClO \rightarrow Br + Cl + O_2 & (10a) \end{array}\right\} \quad (III)$$

net $\quad 2O_3 \rightarrow 3O_2$

$$\left.\begin{array}{ll} Br + O_3 \rightarrow BrO + O_2 & (1) \\ BrO + NO_2 + M \rightarrow BrONO_2 + M & (11) \\ BrONO_2 + h\nu \rightarrow Br + NO_3 & (J_1) \\ NO_3 + h\nu \rightarrow NO + O_2 & (J_8) \\ NO + O_3 \rightarrow NO_2 + O_2 & (20) \end{array}\right\} \quad (IV)$$

net $\quad 2O_3 \rightarrow 3O_2$

$$\begin{array}{ll} Br + O_3 \rightarrow BrO + O_2 & (1) \\ BrO + HO_2 \rightarrow HOBr + O_2 & (12) \\ HOBr + h\nu \rightarrow OH + Br & (J_3) \\ OH + O_3 \rightarrow HO_2 + O_2 & (24) \end{array} \quad (V)$$

net $\quad 2O_3 \rightarrow 3O_2$

$$\left.\begin{array}{ll} Br + O_3 \rightarrow BrO + O_2 & (1) \\ BrO + O_3 \rightarrow Br + 2O_2 & (13) \\ \hline \text{net} \quad 2O_3 \rightarrow 3O_2 & \end{array}\right\} \quad \text{(VI)}$$

We shall argue that cycle (III) is an example of an interaction between radical species from different families which may provide an important additional photochemical sink for ozone, especially in the lower stratosphere, where competing rate determining reactions such as

$$ClO + O \rightarrow Cl + O_2 \qquad (16)$$

and $$NO_2 + O \rightarrow NO + O_2 \qquad (17)$$

are rapidly falling off with decreasing altitude. Cycle (IV) requires that the photolysis products of $BrONO_2$ and NO_3 are $Br + NO_3$ and $NO + O_2$ respectively. For alternative dissociation paths $BrONO_2 \rightarrow BrO + NO_2$, $BrONO_2 \rightarrow O + BrONO$, and $NO_3 \rightarrow NO_2 + O$, the cycle would not result in a net destruction of ozone. This paper will discuss the close coupling of the Br_x system with the HO_x, NO_x, and Cl_x systems with emphasis on the reactions

$$BrO + h\nu \rightarrow Br + O \qquad (J_2)$$

$$BrO + ClO \rightarrow Br + Cl + O_2 \qquad (10a)$$

$$BrO + NO_2 + M \rightarrow BrONO_2 + M \qquad (11)$$

and $$BrO + HO_2 \rightarrow HOBr + O_2 \qquad (12)$$

which have not been previously examined. Our discussion also includes other catalytic cycles involving Cl_x - NO_x and Cl_x - HO_x systems which might also lead to an efficient destruction of ozone in the lower stratosphere:

$$\left.\begin{array}{rl} Cl + O_3 \rightarrow ClO + O_2 & (15) \\ ClO + NO_2 + M \rightarrow ClONO_2 + M & (19) \\ ClONO_2 + h\nu \rightarrow Cl + NO_3 & J_{10} \\ NO_3 + h\nu \rightarrow NO + O_2 & J_8 \\ NO + O_3 \rightarrow NO_2 + O_2 & (20) \end{array}\right\} \text{(VII)}$$

$$\text{net} \quad 2O_3 \rightarrow 3O_2$$

$$\left.\begin{array}{rl} Cl + O_3 \rightarrow ClO + O_2 & (15) \\ ClO + HO_2 \rightarrow HOCl + O_2 & (21) \\ HOCl + h\nu \rightarrow OH + Cl & J_9 \\ OH + O_3 \rightarrow HO_2 + O_2 & (24) \end{array}\right\} \text{(VIII)}$$

$$\text{net} \quad 2O_3 \rightarrow 3O_2$$

We may note that in all one-dimensional modeling studies of the effect of halogenated compounds on ozone (see for example Chang 1976; Logan et al. 1978), perturbations above 25 km are significantly larger than those between 16 and 25 km. The present work raises the possibility of additional ozone reductions in the lower stratosphere not considered in the previous works. In another paper (Wang et al. 1979), we calculate the effects of ozone depletion in the lower stratosphere on the earth's surface temperature. A net cooling of the surface ($\Delta T_s \sim -0.3$ K) could result, a value which is sufficient to nearly cancel the chlorofluoromethane induced greenhouse effect.

PHOTOCHEMISTRY OF BROMINE COMPOUNDS

Table 1a summarizes the reactions involving bromine-containing species, thought to be important in the photochemistry of the stratosphere, along with the preferred values of their rate coefficients. As will be shown later, the partitioning of inorganic bromine into its constituent species ($Br_x \equiv HBr + BrONO_2 + BrO + HOBr + Br$), and the magnitude of its effect on ozone, is sensitive to only a few of these rate coefficients. The reaction scheme is similar to that suggested by Watson (1975) and Wofsy et al. (1975), but has been expanded somewhat to include the formation and destruction of $BrONO_2$, and HOBr and the interaction between the Br_x and Cl_x systems. The basic set of key reactions in the Br_x system is similar to that in the Cl_x system, with a few important exceptions: (1) hydrogen atom abstraction by atomic bromine from H_2 and CH_4 are highly endothermic; consequently, these reactions are too slow to be important in the stratosphere; and (2) radical-radical processes such as the bimolecular disproportionation of BrO radicals may play an important role in Br_x chemistry (the magnitude of the effect is critically dependent upon the mixing ratio of total inorganic bromine), whereas their chlorine analogs are thought to be of little importance; and (3) the photolysis rate for BrO is 2-3 orders of magnitudes faster than that for ClO.

Atomic bromine can be converted into the inactive form of HBr by three processes:

TABLE 1a

Partial list of essential reactions discussed in this paper with their preferred rate coefficients. We use the rate coefficients recommended by NASA 1010 (1977), except as otherwise given in this table. The units for diurnally-averaged photolysis rates (J), two-body and three-body reactions (k) are s^{-1}, cm^3s^{-1}, and cm^6s^{-1}, respectively. The numerical values or J refer to 40, 30, and 20 km for 30°N, spring-fall season.

$BrONO_2 + h\nu \rightarrow Br + NO_3$	$J_1 = 1.6 \times 10^{-3}, 1.1 \times 10^{-3}, 9.8 \times 10^{-4}$	(d)
$BrO + h\nu \rightarrow Br + O$	$J_2 = 1 \times 10^{-2}$	(e)
$HOBr + h\nu \rightarrow OH + Br$	$J_3 = 1.7 \times 10^{-3}, 1.3 \times 10^{-3}, 1.1 \times 10^{-3}$	(f)
$Br_2 + h\nu \rightarrow Br + Br$	$J_4 = 1.5 \times 10^{-2}$	(g)
$HBr + h\nu \rightarrow H + Br$	$J_5 = 5.8 \times 10^{-6}, 4.9 \times 10^{-6}, 2.8 \times 10^{-9}$	(c)
$CH_3Br + h\nu \rightarrow CH_3 + Br$	$J_6 = 7.3 \times 10^{-6}, 4.1 \times 10^{-8}, 2.2 \times 10^{-9}$	(c)
$NO_3 + h\nu \rightarrow NO_2 + O$	$J_7 = 1 \times 10^{-2}$	(a)
$NO_3 + h\nu \rightarrow NO + O_2$	$J_8 = 5 \times 10^{-3}$	(a)
$HOCl + h\nu \rightarrow OH + Cl$	$J_9 = 2 \times 10^{-4}$	(h)
$ClONO_2 + h\nu \rightarrow Cl + NO_3$	$J_{10} = 3.5 \times 10^{-4}, 8.8 \times 10^{-5}, 5.7 \times 10^{-5}$	(a)
$NO_2 + h\nu \rightarrow NO + O$	$J_{11} = 7.5 \times 10^{-3}$	(a)
$HNO_3 + h\nu \rightarrow OH + NO_2$	$J_{12} = 2.8 \times 10^{-5}, 5.7 \times 10^{-6}, 3.9 \times 10^{-7}$	(a)
$Br + O_3 \rightarrow BrO + O_2$	$k_1 = 1.4 \times 10^{-11} e^{-755/T}$	(i)
$Br + HO_2 \rightarrow HBr + O_2$	$k_2 = 2 \times 10^{-11}$	(j)
$Br + H_2O_2 \rightarrow HBr + HO_2$	$k_3 < 2 \times 10^{-12} e^{-1400/T}$	(k)
$Br + H_2CO \rightarrow HBr + HCO$	$k_4 \leq 1 \times 10^{-13}$	(l)

$OH + HBr \rightarrow H_2O + Br$	$k_5 = 8.5 \times 10^{-12}$	(m)
$O + HBr \rightarrow OH + Br$	$k_6 = 7.6 \times 10^{-12} e^{-1571/T}$	(n)
$BrO + NO \rightarrow Br + NO_2$	$k_7 = 8.7 \times 10^{-12} e^{265/T}$	(o)
$BrO + O \rightarrow Br + O_2$	$k_8 = 3 \times 10^{-11}$	(p)
$BrO + BrO \rightarrow 2Br + O_2$	$k_{9a} = 2.1 \times 10^{-12} e^{244/T}$	(q)
$\rightarrow Br_2 + O_2$	$k_{9b} = 3.5 \times 10^{-13} e^{244/T}$	
$BrO + ClO \rightarrow Br + Cl + O_2$	$k_{10a} = 6.7 \times 10^{-12}$	(r)
$\rightarrow Br + OClO$	$k_{10b} = 6.7 \times 10^{-12}$	
$BrO + NO_2 + M \rightarrow BrONO_2 + M$	$k_{11} = 2k_{19}$	(s)
$BrO + HO_2 \rightarrow HOBr + O_2$	$k_{12} = 4 \times 10^{-12}$	(t)
$BrO + O_3 \rightarrow Br + 2O_2$	$k_{13} < 1 \times 10^{-12} e^{-1600/T}$	(u)
$BrO + OH \rightarrow HO_2 + Br$	k_{14a}	(v)
$\rightarrow HBr + O_2$	k_{14b}	
$Cl + O_3 \rightarrow ClO + O_2$	k_{15}	(a)
$ClO + O \rightarrow Cl + O_2$	k_{16}	(a)
$NO_2 + O \rightarrow NO + O_2$	k_{17}	(a)
$HO_2 + O_3 \rightarrow OH + 2O_2$	$k_{18} = 1.1 \times 10^{-14} e^{-580/T}$	(b)
$ClO + NO_2 + M \rightarrow ClONO_2 + M$	k_{19}	(a)
$NO + O_3 \rightarrow NO_2 + O_2$	k_{20}	(a)
$ClO + HO_2 \rightarrow HOCl + O_2$	$k_{21} = 3.8 \times 10^{-12}$	(b)
$HO_2 + NO \rightarrow NO_2 + OH$	$k_{22} = 3.4 \times 10^{-12} e^{250/T}$	(b)
$ClO + ClO \rightarrow$ Products	k_{23}	(a)
$OH + O_3 \rightarrow HO_2 + O_2$	k_{24}	(a)
$Cl + CH_4 \rightarrow HCl + CH_3$	$k_{25} = 9.9 \times 10^{-12} e^{-1359/T}$	(b)
$OH + C_2H_4Br_2 \rightarrow$ Products	$k_{26} = 2.5 \times 10^{-13}$	(w)
$OH + CF_3Br \rightarrow$ Products	$k_{27} < 1 \times 10^{-15}$	(x)

$OH + CHBr_3 \rightarrow$ Products	$k_{28} = 4.7 \times 10^{-12} e^{-1134/T}$	(y)
$OH + CH_3CBr_3 \rightarrow$ Products	$k_{29} = 2.5 \times 10^{-12} e^{-1450/T}$	(y)
$OH + CH_3Br \rightarrow CH_2Br + H_2O$	$k_{30} = 7.9 \times 10^{-13} e^{-889/T}$	(y)
$ClO + NO \rightarrow Cl + NO_2$	k_{31}	(a)
$HCl + OH \rightarrow H_2O + Cl$	k_{32}	(a)
$Cl + H_2CO \rightarrow HCl + HCO$	$k_{33} = 7.5 \times 10^{-11}$	(z)

Footnote to Table 1

a NASA 1010 (1977)

b NASA 2 (1979)

c Wofsy et al., (1975)

d Spencer and Rowland (1978), recommended by b.

e based on Durie and Ramsay (1958), Clyne and Cruse (1970)

f based on Molina and Molina (private communication, 1979) cross-section for HOCl, red-shifted by 300 nm

g Calvert and Pitts (1966)

h Molina and Molina (private communication, 1979).

i evaluated from the data of Clyne and Watson (1975), Leu and DeMore (1977), Michael et al., (1979) and Michael and Payne (1979), recommended by b

j estimated

k based upon the unpublished upper limit reported for k(298K) by Leu and DeMore, recommended by b

l estimated

m mean of values reported by Takacs and Glass (1973a) and Ravishankara et al., (private communication, 1979), recommended by b.

n NASA 1010, based upon Tackacs and Glass (1973b), Brown and Smith (1975) and Singleton and Cvetanovic (1976, based on paper presented at the 12th Informal Conference on Photochemistry, NBS, Wash. D.C.).

o Watson, Sander, and Yung, to be published, 1979.

p NASA 1010, based upon Clyne et al., (1976)

q Sander and Watson, to be published, 1979.

r NASA 1010, Clyne and Watson (1977)

s based on provisional data obtained between 50 and 700 torr N_2 at 298 K, by Watson and Sander, to be published, 1979.

t estimate based upon k(ClO + HO_2)

u estimated Arrhenius expression based upon upper limit of 5 x 10^{-15} cm^3 s^{-1} at 298 K reported by Sander and Watson (1979), not included in normal model, see text

v see text

w Howard and Evenson (1975)

x LeBras and Combourieu (1978)

y based on chlorine analogs, Davis et al., (1976), Watson et al. (1977)

z Stief et al. (1978)

TABLE 1b

List of reactions used in our model in addition to those given in Table 1a. Values for the mean dissociation rate J are given for 40 km.

Reaction	J
$O_2 + h\nu \rightarrow 2O$	1.8 (-10)
$O_3 + h\nu \rightarrow O_2 + O$	9.0 (-4)
$O_3 + h\nu \rightarrow O_2 + O(^1D)$	6.8 (-4)
$H_2O + h\nu \rightarrow H + OH$	6.6 (-10)
$H_2O_2 + h\nu \rightarrow 2OH$	1.9 (-5)
$N_2O + h\nu \rightarrow N_2 + O(^1D)$	1.4 (-7)
$NO + h\nu \rightarrow N + O$	9.1 (-8)
$N_2O_5 + h\nu \rightarrow NO_2 + NO_3$	9.8 (-5)
$Cl_2 + h\nu \rightarrow 2Cl$	1.2 (-3)
$HCl + h\nu \rightarrow H + Cl$	8.6 (-8)
$ClO + h\nu \rightarrow Cl + O$	6.2 (-5)
$CFCl_3 + h\nu \rightarrow$ products	3.4 (-6)
$CF_2Cl_2 + h\nu \rightarrow$ "	3.8 (-7)
$CH_3Cl + h\nu \rightarrow$ "	7.7 (-8)
$CCl_4 + h\nu \rightarrow$ "	1.6 (-5)
$COF_2 + h\nu \rightarrow$ "	9.5 (-8)
$COFCl + h\nu \rightarrow$ "	1.3 (-6)
$CO_2 + h\nu \rightarrow CO + O$	1.8 (-11)
$CH_4 + h\nu \rightarrow CH_3 + H$	6.4 (-36)
$CH_2O + h\nu \rightarrow CHO + H$	1.5 (-5)
$CH_2O + h\nu \rightarrow H_2 + CO$	2.4 (-5)
$CH_3OOH + h\nu \rightarrow CH_3O + OH$	1.9 (-5)

TABLE 1b (continued)

Reaction	k
$O^1D + O_2 \rightarrow O + O_2$	a
$O^1D + N_2 \rightarrow O + N_2$	a
$O^1D + H_2O \rightarrow OH + OH$	a
$O^1D + H_2 \rightarrow H + OH$	a
$O^1D + CH_4 \rightarrow CH_3 + OH$	a
$O^1D + N_2O \rightarrow NO + NO$	a
$O^1D + N_2O \rightarrow N_2 + O_2$	a
$O + O_2 + M \rightarrow O_3 + M$	b
$O_3 + O \rightarrow 2O_2$	b
$O + O + M \rightarrow O_2 + M$	b
$N + O_3 \rightarrow NO + O_2$	b
$O + OH \rightarrow O_2 + H$	a
$O + HO_2 \rightarrow OH + O_2$	a
$H + O_3 \rightarrow OH + O_2$	a
$H + O_2 + M \rightarrow HO_2 + M$	a
$N + O_2 \rightarrow NO + O$	a
$N + NO \rightarrow N_2 + O$	a
$OH + NO_2 + M \rightarrow HNO_3 + M$	a
$OH + HNO_3 \rightarrow H_2O + NO_3$	a
$OH + HO_2 \rightarrow H_2O + O_2$	a
$H + HO_2 \rightarrow H_2 + O_2$	b
$H + HO_2 \rightarrow OH + OH$	b
$H + HO_2 \rightarrow H_2O + O$	b
$HO_2 + HO_2 \rightarrow H_2O_2 + O_2$	a
$H_2O_2 + OH \rightarrow H_2O + HO_2$	a
$H_2O_2 + O \rightarrow OH + HO_2$	a
$OH + CH_4 \rightarrow CH_3 + H_2O$	a
$NO_3 + NO \rightarrow NO_2 + NO_2$	b
$NO_2 + O_3 \rightarrow NO_3 + O_2$	a
$NO_3 + NO_2 + M \rightarrow N_2O_5 + M$	b
$NO_2 + NO_3 \rightarrow NO_2 + O_2 + NO$	b

TABLE 1b (continued)

Reaction	k	
$Cl + HO_2 \rightarrow HCl + O_2$	d	4.1×10^{-11}
$CO + OH \rightarrow CO_2 + H$	a	
$H_2 + OH \rightarrow H_2O + H$	b	
$HNO_3 + O \rightarrow OH + NO_3$	b	
$N_2O_5 + M \rightarrow NO_2 + NO_3 + M$	b	
$Cl + Cl + M \rightarrow Cl_2 + M$	b	
$ClNO_3 + O \rightarrow ClO + NO_3$	a	
$Cl + H_2 \rightarrow HCl + H$	a	
$Cl + O_2 + M \rightarrow ClOO + M$	a	
$CH_3Cl + OH \rightarrow$ products	a	
$ClOO + M \rightarrow Cl + O_2 + M$	b	
$CH_3O_2 + NO \rightarrow CH_3O + NO_2$	b	
$CH_3O + O_2 \rightarrow CH_2O + HO_2$	a	
$CH_3O_2 + CH_3O_2 \rightarrow 2\ CH_3O + O_2$	b	
$CH_2O + OH \rightarrow CHO + H_2O$	b	
$CHO + O_2 \rightarrow O + HO_2$	a	
$CH_3O_2 + HO_2 \rightarrow CH_3OOH + O_2$	b	
$CH_3OOH + OH \rightarrow CH_3O_2 + H_2O$	c	
$CH_3 + O_2 + M \rightarrow CH_3O_2 + M$	c	
$CH_3 + O_2 \rightarrow CH_2O + OH$	c	

a NASA 1010 (1977).

b Logan et al. (1978).

c Wofsy (1976).

d DeMore (1978) private communication. This value is close to 4.5×10^{-11} recommended by NASA 2 (1979)

$$Br + HO_2 \rightarrow HBr + O_2 \qquad (2)$$

$$Br + H_2O_2 \rightarrow HBr + HO_2 \qquad (3)$$

$$Br + H_2CO \rightarrow HBr + HCO \qquad (4)$$

An estimated value of 2×10^{-11} cm^3s^{-1} has been used for k_2 in most of our calculations as there has not been a direct study of this reaction using a modern kinetic technique. The sensitivity of our model to the absolute value of k_2 has been tested by using values of 0.5 and 4×10^{-11} cm^3s^{-1}. Using the upper limit tabulated for k_3, it can be shown that reaction (3) is not an important loss mechanism for Br. It can also be shown that reaction (4) is unlikely to be comparable in magnitude to reaction (2) as a loss process for Br, as k_4 would have to be greater than 1×10^{-12} cm^3s^{-1} at stratospheric temperatures (this assumes that the mixing ratio for H_2CO is $\sim$ 0.1 ppbv), whereas an estimated value of $\leqslant 10^{-13}$ cm^3s^{-1} is more realistic. Consequently, the only important formation process for HBr is reaction (2). (the formation of HBr via the reaction of BrO with OH is discussed later). The major process by which atomic bromine is regenerated from HBr is:

$$OH + HBr \rightarrow H_2O + Br \qquad (5)$$

Other minor loss mechanisms for HBr are

$$HBr + h\nu \rightarrow J + Br \qquad (J_5)$$

$$HBr + O \rightarrow OH + Br \qquad (6)$$

Since the calculations of Wofsy et al. (1975), the rate coefficients for

$$HO_2 + NO \rightarrow OH + NO_2 \qquad (22)$$

and

$$HO_2 + O_3 \rightarrow OH + 2O_2 \qquad (18)$$

have been revised (Howard and Evenson 1977; Howard 1978), resulting in higher concentrations of OH, and lower concentrations of HO_2 and H_2O_2.

The net result is that the Br:HBr ratio is significantly higher in the present model than in previous models. We may note that the Br:HBr ratio is significantly higher than the Cl:HCl ratio in the stratosphere due to slower rates of formation of HBr compared to HCl, combined with the much greater reactivity of HBr, over HCl, toward OH radicals.

The other major pathway for atomic bromine is its reaction with O_3 to form BrO:

$$Br + O_3 \rightarrow BrO + O_2 \qquad (1)$$

Once formed, BrO participates in a series of reactions similar to those of the ClO radical in the Cl_x system:

$$BrO + h\nu \rightarrow Br + O \qquad (J_2)$$

$$BrO + NO \rightarrow Br + NO_2 \qquad (7)$$

$$BrO + O \rightarrow Br + O_2 \qquad (8)$$

$$BrO + BrO \rightarrow 2Br + O_2 \qquad (9a)$$

$$\rightarrow Br_2 + O_2 \qquad (9b)$$

$$BrO + ClO \rightarrow Br + Cl + O_2 \qquad (10a)$$

$$\rightarrow Br + OClO \qquad (10b)$$

$$BrO + NO_2 + M \rightarrow BrONO_2 + M \qquad (11)$$

$$BrO + HO_2 \rightarrow HOBr + O_2 \qquad (12)$$

$$BrO + O_3 \rightarrow Br + 2O_2 \qquad (13)$$

$$BrO + OH \rightarrow HO_2 + Br \qquad (14a)$$

$$\rightarrow HBr + O_2 \qquad (14b)$$

Reactions (J_2, 7, 8, and 11 - 14) play the same roles as their chlorine analogs. Using the absorption data obtained by Durie and Ramsay (1958) and Clyne and Cruse (1970), we repeat Watson's (1975) analysis and estimate a diurnally-averaged photolysis rate $J_2 = 1 \times 10^{-2} s^{-1}$ (including corrections for Rayleigh scattering and ground albedo). Since the possibility of continuum absorption underlying the series of bands in the region 289-355 nm is not ruled out from either Durie and Ramsay's (1958) or Clyne and Cruse's (1970) data, J_2 could be as high as $3 \times 10^{-2} s^{-1}$. In the stratosphere, reactions (J_2) and (7) are both important, but not as effective in limiting the catalytic efficiency of Br_x as the NO + ClO reaction is in the Cl_x system. The primary reason is that while BrO is the major form of Br_x, ClO is not the major form of Cl_x in the stratosphere. Although the rate coefficient for reaction (8) is uncertain by a factor of 3 this does not introduce a significant uncertainty in the magnitude of the ozone perturbation, for reasons which will be discussed in the section on atmospheric modeling. The formation and destruction of $BrONO_2$ through

$$BrO + NO_2 + M \rightarrow BrONO_2 + M \qquad (11)$$

$$BrONO_2 + h\nu \rightarrow Br + NO_3 \qquad (J_1)$$

results in cycle (IV). The rate coefficient for reaction (11) is taken to be twice that for the formation of $ClONO_2$ via reaction (19), based on data collected between 50 and 700 Torr at 298 K by Watson and Sander (1979, manuscript in preparation).

Reactions (9a) and (9b) (BrO + BrO) are several orders of magnitude faster than reactions (23a), (23b), and (23c) (ClO + ClO). Therefore, reactions (9a) and (9b) can become important at high BrO concentrations ($Br_x \geq 100$ pptv). Even though the branching ratio of reaction 9 has been

incorporated into the model, it is unimportant as Br_2 undergoes rapid photolysis in the stratosphere. Cl_x and Br_x reactions are unimportant at night as both ClO and BrO are tied up as $ClONO_2$ and $BrONO_2$, respectively. The Cl_x and Br_x systems are coupled through reactions (10a) and (10b). It is unimportant whether process (10a) actually proceeds through either Br + ClOO or Cl + BrOO as both peroxy radicals undergo rapid thermal decomposition. Even if the products were BrCl + O_2, it is equivalent to writing Br + Cl + O_2 as BrCl rapidly photolyzes in the stratosphere. Unfortunately reaction (10a), which is the key reaction, has only been studied at 298 K and the two published studies report values which differ by a factor of 3. k_{10a} could exhibit either a small positive or negative temperature dependence. Reaction (10b) only participates in a net-nothing cycle, as the photolysis products of OClO are $O(^3P)$ and ClO:

$$\begin{aligned} Br + O_3 &\rightarrow BrO + O_2 && (1)\\ BrO + ClO &\rightarrow Br + OClO && (10b)\\ OClO + h\nu &\rightarrow O + ClO\\ O + O_2 + M &\rightarrow O_3 + M\\ \hline \text{net} &\quad \text{nothing} \end{aligned}$$

For cycles (V) and (VI) to be important, the rate limiting steps (12) and (13) must be comparable to the rate limiting steps in cycles (I-IV). The important formation and destruction processes for HOBr are:

$$HO_2 + BrO \rightarrow HOBr + O_2 \qquad (12)$$

$$HOBr + h\nu \rightarrow OH + Br \qquad (J_3)$$

The steady state concentration of HOBr is

$$[HOBr] = k_{12}[HO_2][BrO]/J_3$$

Substituting our best estimates for k_{12} and J_3 (see table 1) results in a ratio of ~ 0.1 for [HOBr]/[BrO]. Therefore, HOBr is not a significant reservoir of Br_x. In the current atmosphere (assuming 20 pptv Br_x and 2.3 ppbv Cl_x) cycle (V) is not important unless $k_{12} \gg 4 \times 10^{-12}$ $cm^3 s^{-1}$, an unlikely possibility. Cycle (VI) does not become important unless $k_{13} \geq 3 \times 10^{-16}$ $cm^3 s^{-1}$ at stratospheric temperatures. An upper limit of $\leq 5 \times 10^{-15}$ $cm^3 s^{-1}$ has recently been reported for k_{13} at 298 K by Sander and Watson (1979). However, it must be stressed that no reaction was observed, and that the chlorine analog of reaction (13) is very slow with an upper limit of $\sim 10^{-18}$ $cm^3 s^{-1}$ (DeMore et al. 1975). In our calculations we do not include reaction (13).

The OH + BrO reaction (14) has not been included in the model as neither the overall rate coefficient nor the product distribution is known. Although reaction (14a) can participate in the following catalytic cycle:

$$\begin{aligned} Br + O_3 &\rightarrow BrO + O_2 && (1) \\ OH + BrO &\rightarrow Br + HO_2 && (14a) \\ \underline{HO_2 + O_3 &\rightarrow OH + 2O_2} && (18) \\ \text{net } 2O_3 &\rightarrow 3O_2 \end{aligned}$$

it is unimportant as the magnitude of the rate determining step is not comparable to those in cycles (I-IV) unless $k_{14a} \geq 10^{-10} cm^3 s^{-1}$ which is quite unlikely (the magnitude of k_{14} is expected to be quite similar to k(OH + ClO) which has recently been reported to be $9.1 \times 10^{-12} cm^3 s^{-1}$ at

298 K by Leu and Lin (1979). Reaction (14b) can be important in reducing the catalytic efficiency of Br_x by decreasing the BrO/Br_x ratio. For reaction (14b) to be important the magnitude of $k_{14b}[OH][BrO]$ must be comparable to $k_2[Br][HO_2]$ in order to influence the rate of formation of HBr and the partitioning of Br_x. This occurs when $k_{14b}/k_2 \simeq 0.1$, i.e., $k_{14b} \simeq 2 \times 10^{-12} cm^2 s^{-1}$.

ATMOSPHERIC MODELING

Singh et al.'s (1977) measurements of halogenated organic species indicate that methyl bromide (CH_3Br) is probably the major bromine species in the troposphere with concentrations ranging from 1 to 300 pptv. The average concentration is about 5-10 pptv in clean air and 20 pptv in marine air (Singh, 1979, private communication). The main source of CH_3Br is marine biological activity (Lovelock, 1975). There is a smaller contribution from anthropogenic sources, associated with its use as a soil fumigant. Other bromine compounds such as dibromomethane (CH_2Br_2), bromoform ($CHBr_3$), and dibromochloromethane ($CHClBr_2$) could also be produced in the marine environment and subsequently released to the atmosphere (Burreson et al., 1975; Theiler et al., 1978; Helz and Hsu 1978), but they have not yet been detected in the atmosphere. Leinster et al. (1978) and Singh (1979, private communication) have detected ethylene dibromide in urban air. Its concentration lies in the range from 0.1 to 20 pptv, and is clearly related to the use of ethylene dibromide as a gasoline additive. Spencer and Rowland (1978) have suggested that additional anthropogenic sources of bromine could come from some bromofluorocarbon compounds (e.g., CF_3Br, CF_2BrCF_2Br) which are used extensively as flame retardants, and will be ultimately released to the atmosphere. The lifetimes and source strengths of important organic bromine species are summarized in Table 2. Compounds with long lifetimes in the troposphere are eventually transported into the stratosphere, where they can be readily decomposed to provide a source of inorganic stratospheric bromine.

Table 2

Lifetimes and Sources of Important Organic Bromine Compounds

	CH_3Br	$C_2H_4Br_2$	CF_3Br	$CHBr_3$	CH_3CBr_3
Globally averaged mixing ratio (pptv)	5 - 10 (a)	0.1 - 1 (b)	< 1 (c)	(d)	(d)
Major sink	CH_3Br + OH(e)	$C_2H_4Br_2$ + OH(e)	CF_3Br + hν(f)	$CHBr_3$ + OH(e)	CH_3CBr_3 + OH(c)
Mean lifetime	2.1 years	3 months	70 years	1 year	5.7 years
Globally averaged source strength (10^9gm Br yr^{-1})	35 - 70	12 - 120	< 0.21	(d)	(d)
Global industrial production (10^9gm Br yr^{-1})(g)	14 (h)	182 (h)	1.1 (h, i)	(d)	(d)

a based on Singh et al. (1977), and Singh (1979, private communication).

b estimated from Leinster et al. (1979). These numbers must be considered as illustrative rather than representative of true mean values.

c Singh (1979, private communication).

d information not available.

e we assume a mean tropospheric OH concentration of $5 \times 10^5 cm^{-3}$ (Singh, 1977; Chang and Penner, 1978). The rate coefficients are given in Table 1.

f based on dissociation cross-sections measured by Molina and Molina (1979).

g a much more difficult quantity to estimate is the release rate to the atmosphere, which probably ranges from 10 to 50% of the production rate for most of the compounds considered here.

h based on 1975 and 1976 data published in Bureau of Mines Yearbook, U.S. Department of Interior. Since the U.S. accounts for 67% of all bromine produced, we estimate the global production rate by multiplying the U.S. production rate by a factor of 1.5.

i based on U.S. 1976 production of 0.75×10^9 gmBr, see text.

In the stratosphere the presence of small concentrations of bromine was first reported by Lazrus et al. (1976), using an air filter technique for capturing stratospheric halogens from a balloon platform. Recently, Lazrus, Gandrud and Sedlacek† performed a comprehensive set of measurements of stratospheric bromine and chlorine, using analytical techniques that include neutron activation analysis. Neither the neutral nor base impregnated filters collect organic compounds (e.g., CH_3Br, CF_3Br). The collection efficiencies for the alkaline-based filters have been calibrated for HCl, ClO, $ClONO_2$, HBr, and BrO, but not for $BrONO_2$ or HOBr. However, we do not expect large deviations in collection efficiencies among the major inorganic halogen species. Figure 1 shows the mixing ratio ratio for total inorganic bromine Br_x(= Br + $2Br_2$ + BrO + HBr + $BrONO_2$ + HOBr), at 19 km from the equator to 70° N. The dots and crosses represent data obtained in April 1976 and July 1977, respectively. The noticeable increase in Br_x both as a function of altitude and latitude suggests that stratospheric bromine is derived from a tropospheric precursor, such as CH_3Br or CF_3Br. In subsequent computations, we shall assume that all Br_x is derived from a CH_3Br source. A vertical profile for Br_x, obtained by averaging all of the 1976 and 1977 data, is given in Figure 2. We have decided to ignore the anomalously high data point at 37 km. Indeed, for the last two altitudes, 32 and 37 km, a different air injection technique, used to collect the samples, might have led to spurious results. Alternatively,

---

†Private communication based on work to be published, 1979.

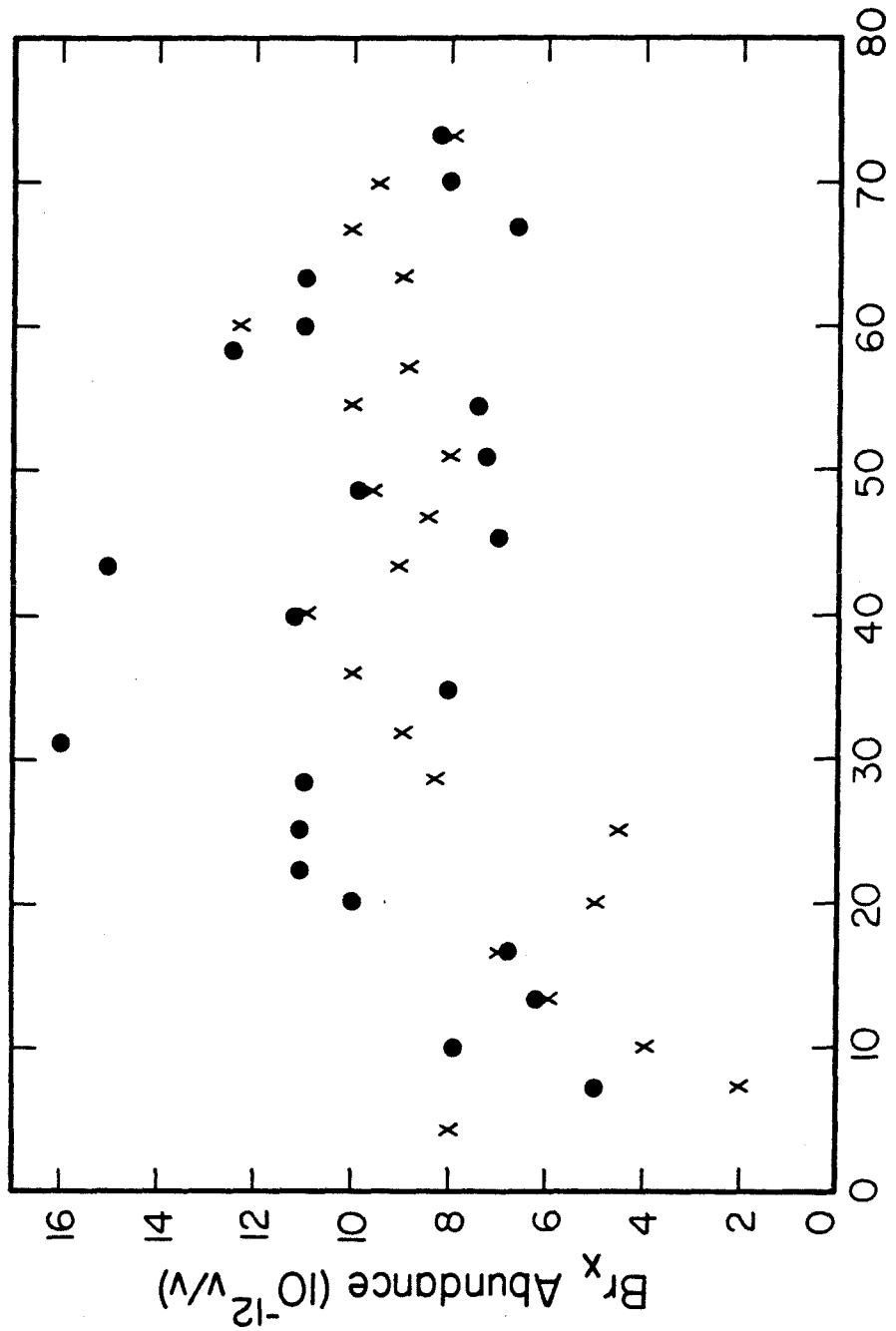

Figure 1 - Mixing ratio for total inorganic bromine Br_x (=Br + $2Br_2$ + BrO + HBr + $BrONO_2$ + HOBr) at 19 km from the equator to 70° N. The dots and crosses represent data taken in April 1976 and July 1977 by Lazrus et al. (1979).

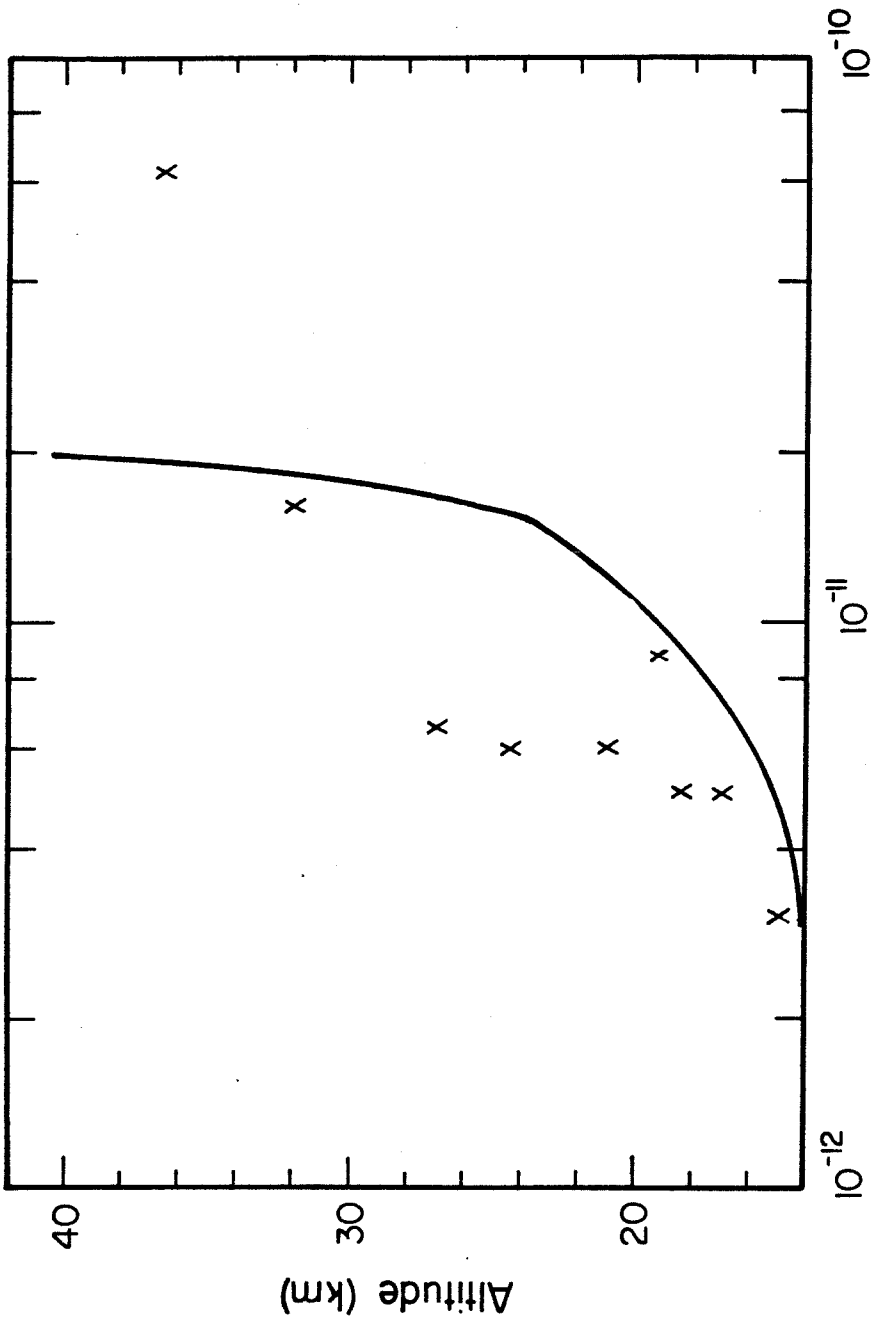

Figure 2 - Vertical distribution for Br_x obtained by averaging all available data taken by Lazrus et al. (1979) in 1976 and 1977. The curve is obtained from model calculation by assuming that all Br_x is derived from CH_3Br.

the collection efficiencies of the filters may have been influenced by the exceedingly reactive chemical environment in the middle and upper stratosphere. However, the anomalously high bromine values are reminiscent of Anderson et al.'s (1977) high chlorine values. These measurements may reflect our imperfect understanding of the sources of stratospheric halogens and the species partitioning amongst them.

The major bromine species in the stratosphere and important paths for cycling between species are schematically summarized in Figure 3. Figure 4 presents height profiles computed for BrO, $BrONO_2$, HBr, HOBr, and Br in the present stratosphere with 20 pptv total bromine (Br_x), as prescribed by the profile shown in Figure 2. The computations were carried out with a diurnally-averaged one-dimensional photochemical model. Our model is based on a set of about 100 essential reactions recommended by NASA 1010 (1977), whose rate coefficients we adopt, except as otherwise stated in Table 1a and 1b. We adopt the U.S. Standard Atmosphere model for 30° N, spring-fall season. Diurnally averaged photodissociation rates were obtained by integration over a 24 hour cycle. Corrections to mean dissociation rates due to Rayleigh scattering and ground albedo for species that dissociate at wavelengths longward of 200 nm are approximately made by modifying these quantities by factors taken from NASA 1010 (1977) and Wofsy (1978). The equations of continuity are solved from 0 to 80 km for all major O_x, HO_x, NO_x, Cl_x, and Br_x species, and their precursors, allowing transport by eddy diffusion for long-lived species. We use Hunten's (1975) eddy diffusivity profile, with modifications recommended by NASA 1010 (1977). Altitude profiles of the major stratospheric free radicals computed by the

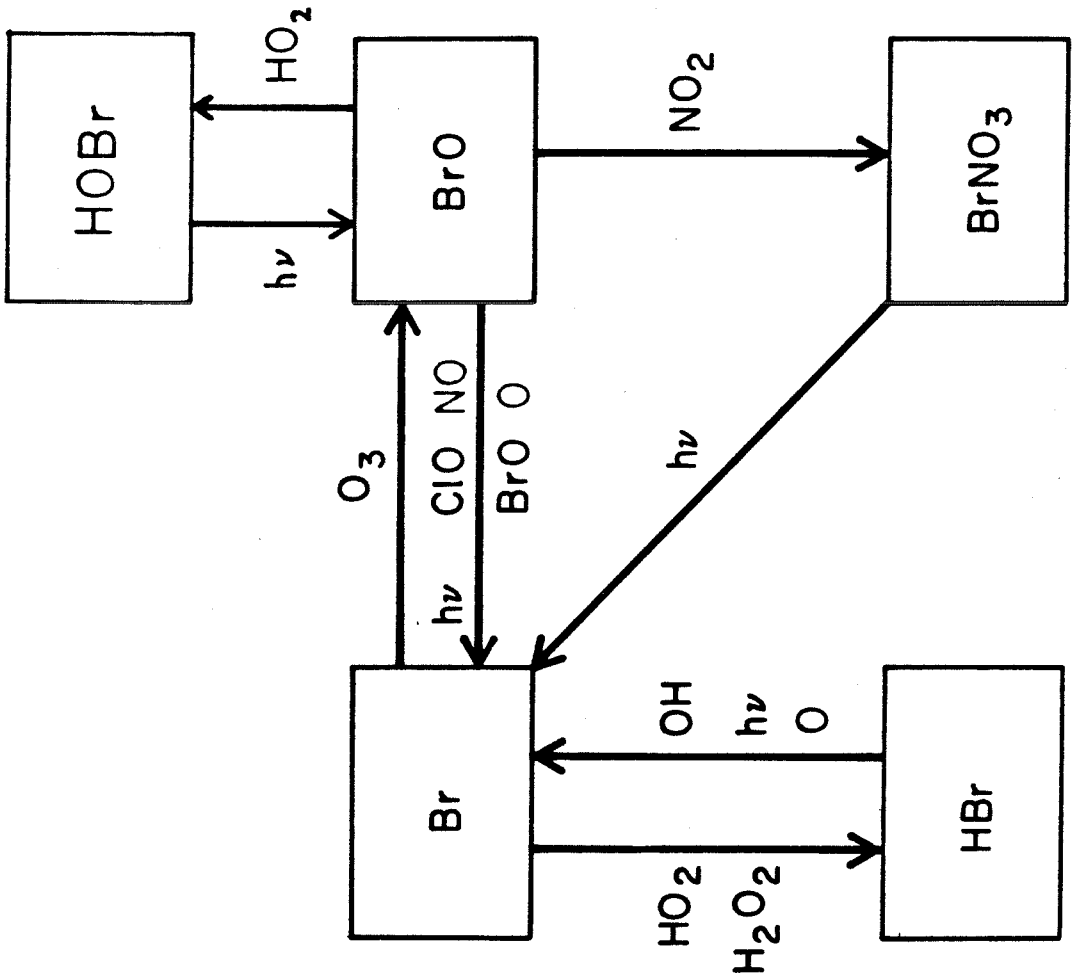

Figure 3 - Schematic diagram summarizing the major bromine species and their interactions.

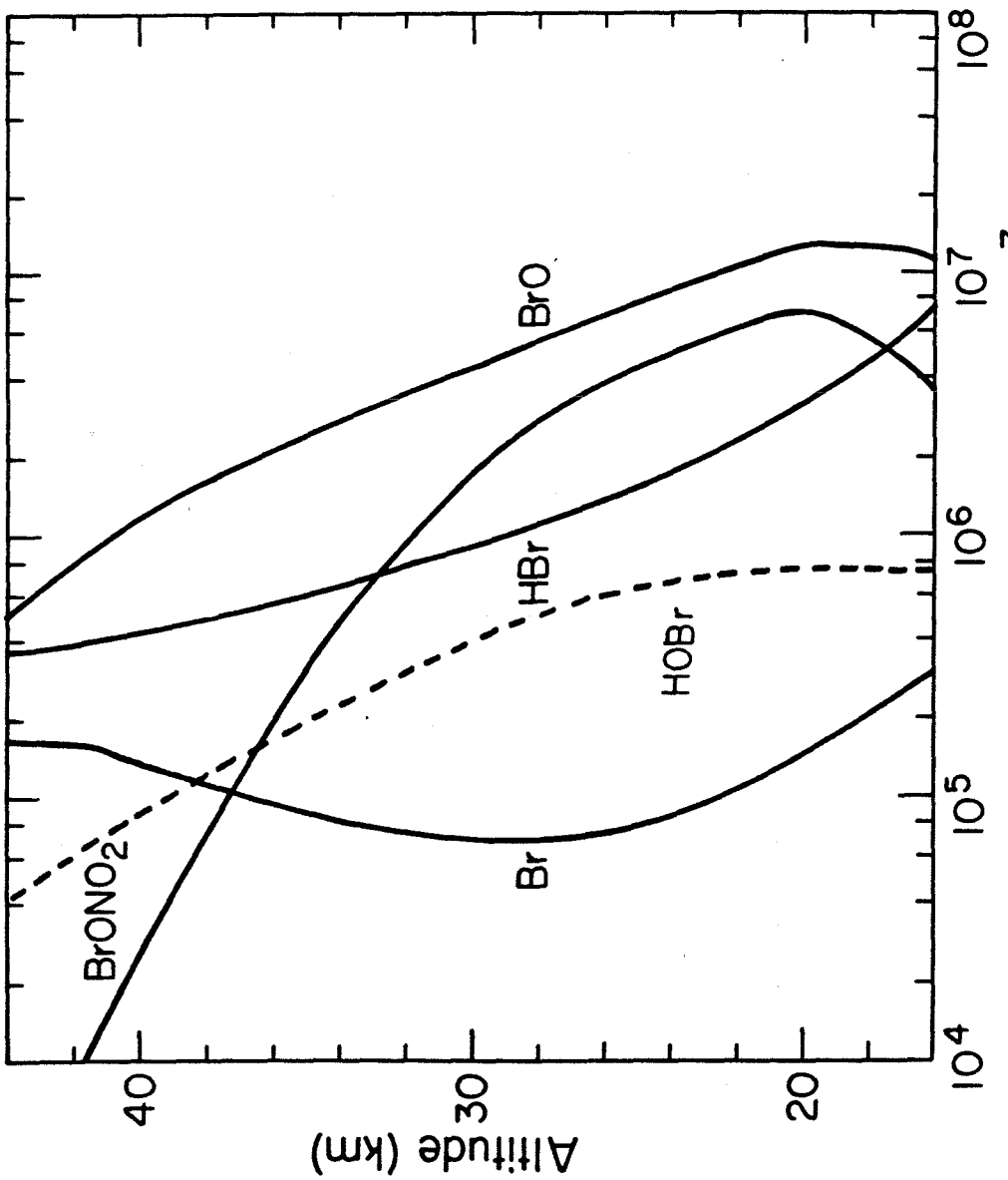

Figure 4 - Altitude profiles for major bromine species in the stratosphere, calculated using the reactions and rate coefficients of Table 1.

Total Br_x at 40 km equals 20 pptv.

photochemical model are given in Figure 5. Unless otherwise stated, the number densities in Figure 4 and 5 will be taken to be representative of the present atmosphere, containing 2.3 ppbv Cl_x 19 ppbv NO_x, 6 ppmv H_2O, and 20 pptv Br_x at 40 km. For these calculations, we have assumed a surface mixing ratio of 20 pptv for CH_3Br (or total organic bromine), as suggested by the measurements. The mixing ratio of total inorganic bromine was 10 pptv at the ground (Wofsy et al., 1975). Heterogeneous removal of inorganic bromine, and other soluble trace constituents in the troposphere was modeled in the same way as Wofsy et al. (1975). Our results, summarized in Figure 4, show that BrO, an active form of bromine, is the major bromine species in the stratosphere, followed by $BrONO_2$, HBr, HOBr, and Br. Here lies an important difference between the chemistry of bromine and chlorine. According to current models (see for example Logan et al. 1978), the relatively inert forms of chlorine, HCl or $ClONO_2$, dominate over ClO throughout most of the stratosphere.

The presence of bromine at today's level is important in controlling the abundance of ozone in the present atmosphere (with 2.3 ppbv of Cl). Figure 6 shows a comparison of ozone profiles computed with 0 and 20 pptv bromine. The difference in ozone concentrations reaches 6% in the lower stratosphere, but effectively vanishes above 30 km. The column integrated ozone (from 0 to 80 km) for the two profiles in Figure 6 differs by 2.4%. The result is somewhat surprising,

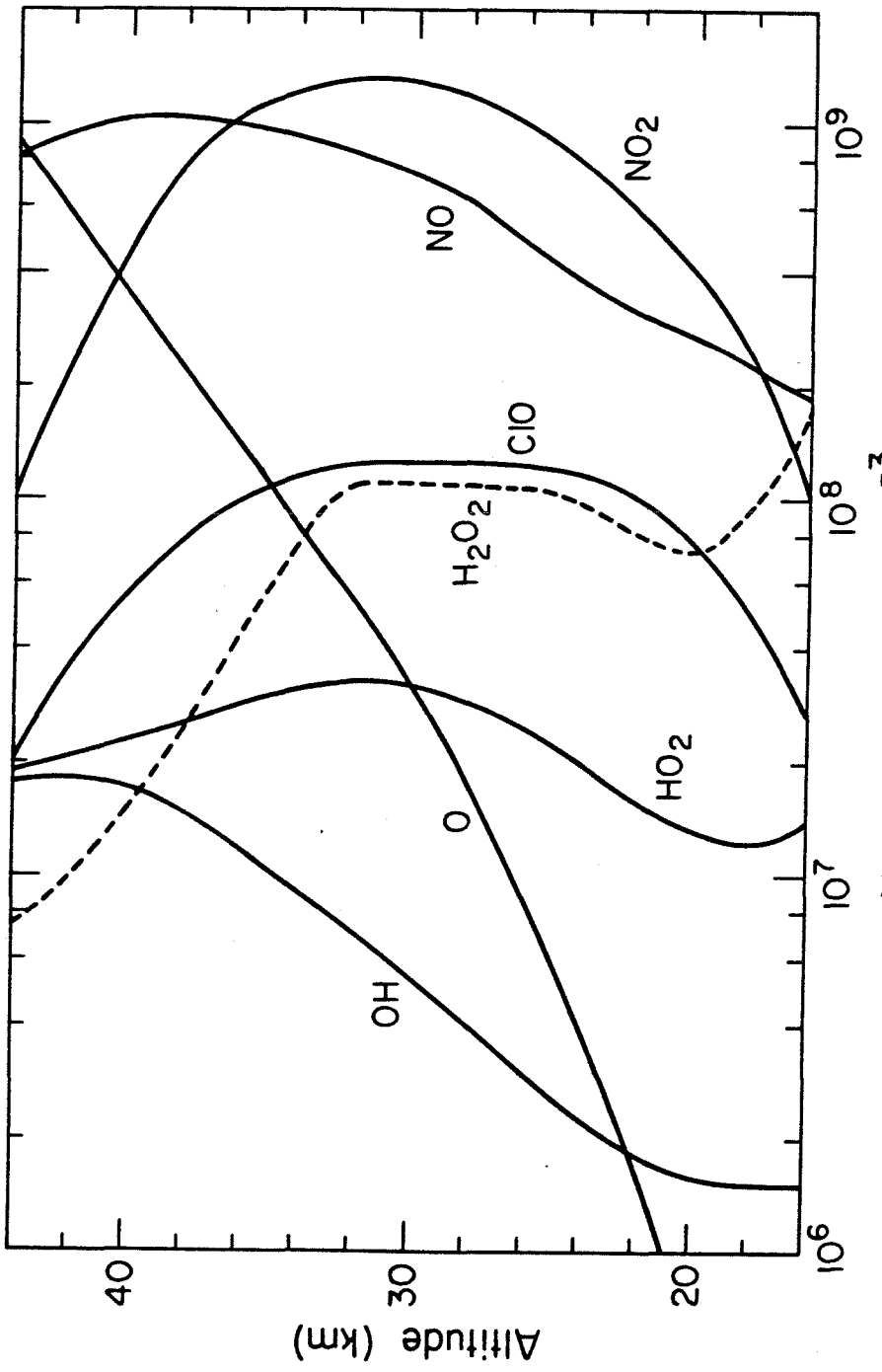

Figure 5 - Altitude profiles for important species in the stratosphere. The standard model contains 2.3 ppbv Cl_x, 19 ppbv NO_x, 6 ppmv H_2O, and 20 pptv Br_x at 40 km.

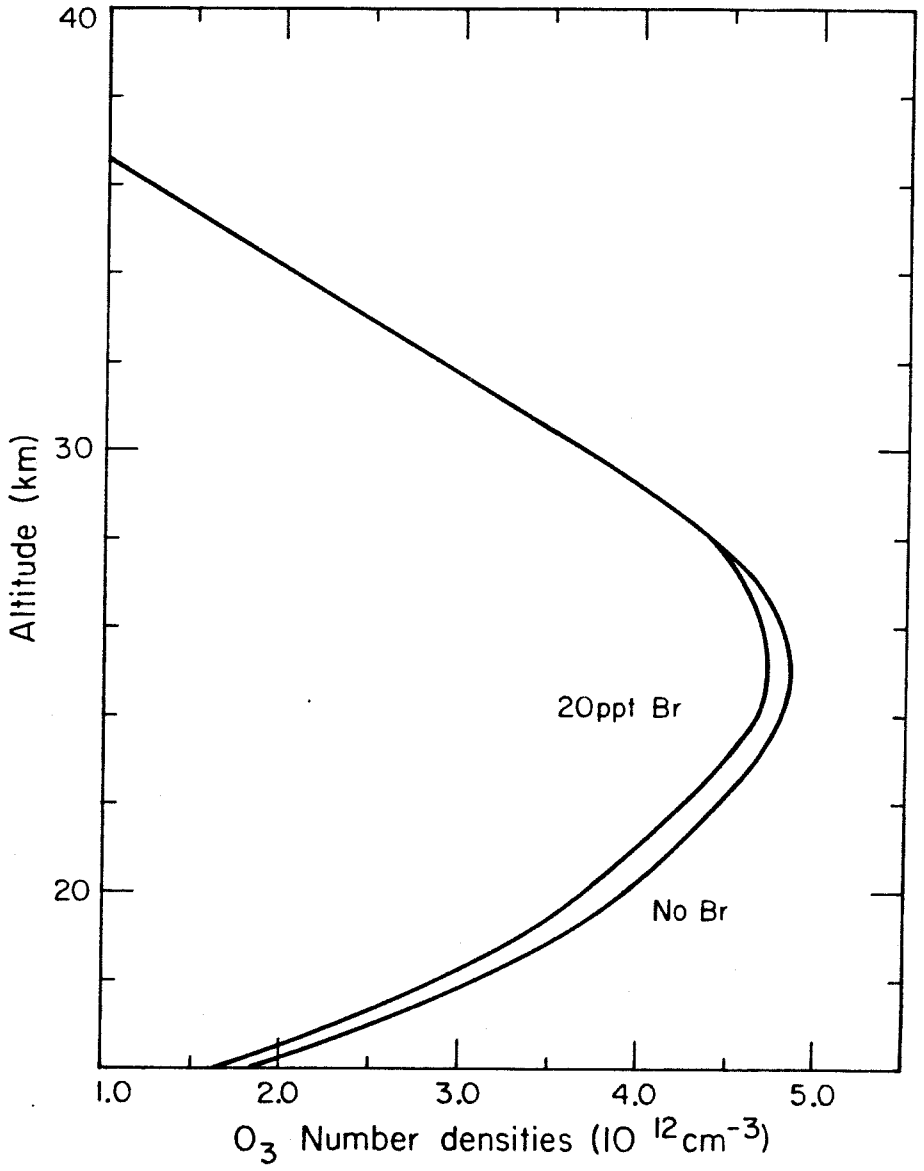

Figure 6 - Altitude profile for ozone computed with and without 20 pptv bromine.

that such a small amount of bromine can be so effective. Figure 7 compares the rates of the bromine-related destruction of odd oxygen with other reactions, where "all others" is taken to be equal to $2k(O_3 + O) + 2k_{18}(HO_2 + O_3) + 2k_{17}(NO_2 + O) + 2k_{16}(ClO + O) + \frac{2}{3} J_{10}(ClONO_2) + k_{21}(HO_2 + ClO)$. The rate-determining reactions for cycles (I-V) are the reactions BrO + O (8), respectively. It is clear from Figure 7 that the impact of bromine on ozone is mostly through cycle (III). Cycle (I) becomes active only in the upper stratosphere, where it competes rather unfavorably with "all others". On the other hand, cycle (III) peaks in the lower stratosphere, where it can act as a major additional sink for odd oxygen. Cycles (II) (IV) and (V) are insignificant compared with cycle (III) at current Br_x and NO_x levels. We now understand why the action of bromine on ozone is almost totally controlled by reaction (10a), and that factors of 3 uncertainty in reaction (8) are of no consequence. In all our computations, the production and loss of odd oxygen are calculated rigorously from the continuity equations. However, this procedure is equivalent to the use of catalytic cycles discussed here.

As discussed in the previous sections, bromine, when coupled with chlorine can be an efficient catalyst for destroying ozone. This poses an obvious cause for concern over possible increases in atmospheric bromine as a result of future growth in the bromine industry. The importance of reaction (10a) in the lower stratosphere suggests that previous ozone depletion assessments (NAS, 1976; NASA 1010, 1977) due to steady-state chlorofluoromethane release have been underestimated by not including the effects of bromine. We shall explicitly investigate two problems:

(a) The depletion of ozone by bromine as the bromine concentration increases, while keeping the chlorine concentration fixed at its present level (2.3 ppbv).

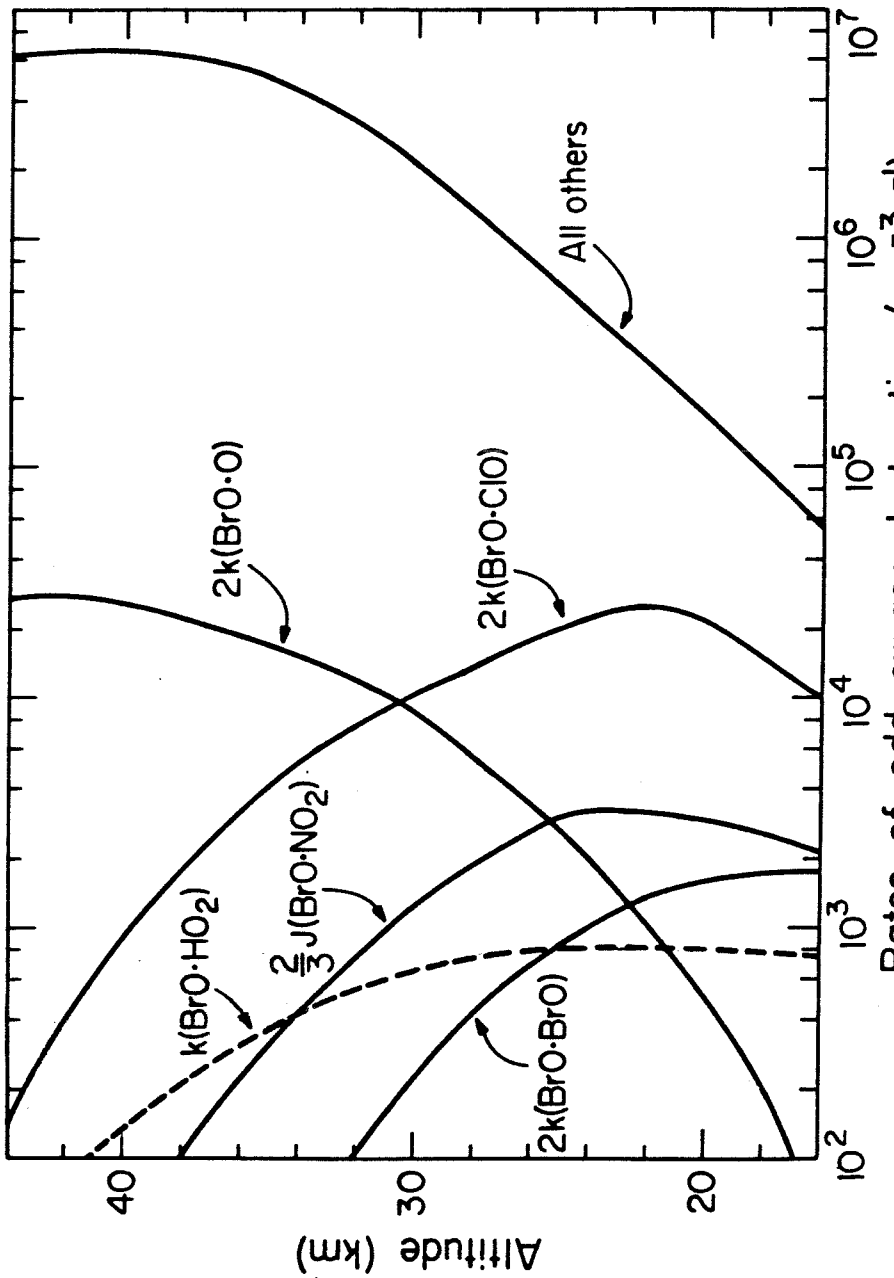

Figure 7 - Rates of the bromine-related destruction of odd oxygen. "All others" is the total odd oxygen destruction rate excluding that due to bromine (see text).

(b) The depletion of ozone by chlorine due to steady-state chlorofluoromethane release at 1973 rates, while keeping the bromine concentration fixed at its present level (20 pptv).

In attacking the first problem, we must first estimate the source strength of bromine compounds in the present atmosphere. Table 2 lists a number of stable bromine compounds that can be derived from natural or anthropogenic sources, the global production rates required to maintain the steady state abundances of the observed species, and the current world production rates for compounds that are widely used in industry. According to our estimates, the natural source of CH_3Br should be around 35-70 x 10^9 gm-Br yr^{-1}. The global industrial production rate of CH_3Br in recent years has been about 14 x 10^9 gm-Br yr^{-1}, which could account for 20-40% of the total atmospheric budget of CH_3Br, if all of it has been released to the atmosphere. However, there are increasingly larger demands for the agricultural use of methyl bromide, and its production has been rising since 1962 at the rate of 7% a year (Klingman 1972-1975; Foster 1975-1978). If this trend were to continue to the end of the century, the industrial source could exceed the natural source, and the bromine concentration in the atmosphere would greatly increase. Atmospheric bromine can also increase for another reason. The major sink for CH_3Br and $C_2H_4Br_2$ in the troposphere is by reaction with OH. Wofsy (1976), Sze (1977) and Penner et al. (1977) have suggested that mean OH concentrations in the troposphere could decrease due to an increase in atmospheric CO. This could result in a longer lifetime for CH_3Br and $C_2H_4Br_2$, and hence a higher concentration of these compounds,

even if the sources remain constant. For similar reasons, the concentrations of chlorine containing compounds (e.g., CH_3Cl, $CHCl_3$, CH_3CCl_3) could also increase. There is at least one more potential future source of stratospheric bromine as pointed out by Spencer and Rowland (1978). The 1976 U.S. production of CF_3Br was 0.75×10^9 gm-Br†. The upper limit for the rate coefficient for reaction with OH reported by LeBras and Combourieu (1978), implies a minimum tropospheric lifetime of 60 years. However, because the reaction is highly endothermic, it is more likely that CF_3Br behaves like $CFCl_3$ and CF_2Cl_2 towards reaction with OH, and photolysis in the stratosphere is the major sink. We estimate a photolytic lifetime of 70 years for CF_3Br based on the absorption cross-section data of Molina and Molina*. In this case, a constant industrial production rate as small as 1×10^9 gm-Br yr^{-1} would result in a steady-state concentration of 5 pptv CF_3Br in the lower atmosphere (assuming complete release to the atmosphere).

Figure 8 summarizes the results of the model calculations of ozone depletion as a function of bromine concentration in the atmosphere. In these calculations we take as "standard" a model atmosphere with 2.3 ppbv Cl_x but no bromine. In the perturbation calculations, we assume that the vertical profile of Br_x is the same as that due to a CH_3Br source (see Figure 2). The procedure should yield an exact answer if all stratospheric inorganic bromine is derived from CH_3Br, but must be considered as an approx-

---

†Based on data released to the EPA in 1977 by F.A. Bower of DuPont de Nemours & Co., Wilmington, Delaware.

*Private communication, paper to be published, 1979.

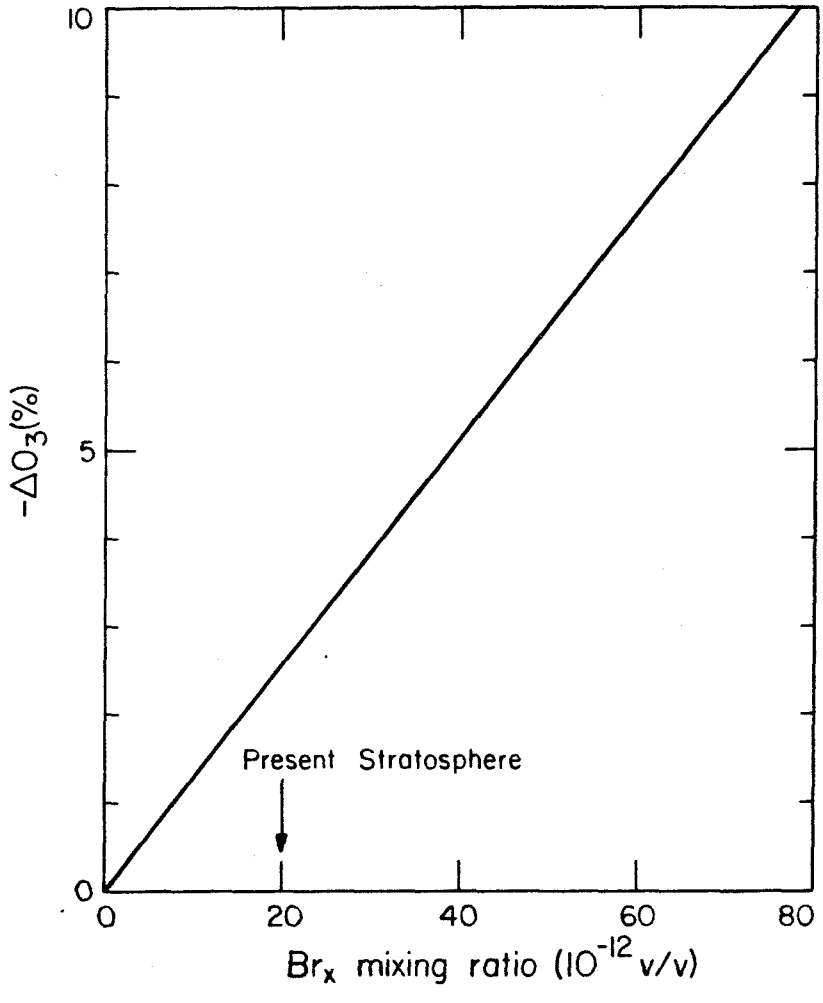

Figure 8 - Ozone depletion as a function of bromine concentration in the stratosphere. ΔO_3 refers to the difference in column integrated ozone density (from 0 to 80 km). Calculations are summarized in Table 3.

imation if other sources such as CF_3Br and $CH\ Br_3$ become important. ΔO_3 in the figure refers to the difference in column integrated ozone abundance (from the ground to 80 km), and is nearly proportional to Br_x, at least to concentrations about 80 pptv.

Figure 9 shows the results of model calculations of ozone depletion due to steady-state chlorofluoromethane release at 1973 rates with and without including an amount of bromine equal to that in the present atmosphere. Curve B_1 is obtained by assuming that the present stratosphere contains 2.3 ppbv Cl_x, and that the perturbed atmosphere contains 8.2 ppbv Cl_x, reflecting a rise in chlorine concentration due to the release of chlorofluoromethanes. The concentrations of $CFCl_3$ and CF_2Cl_2 used to model the present and perturbed atmosphere are 0.1, 0.2, and 0.8, 2.3 ppbv, respectively. Following NAS (1976), we assume that yield of Cl atoms from $CFCl_3$ and CF_2Cl_2 photolysis are 2.5 and 2.0, respectively. Curve B_3 is obtained in the same way as curve B_1 with the additional assumption of the presence of 20 pptv bromine (as given by the profile in Figure 2) in both the present and the perturbed atmosphere. To isolate the effect of cycles (V) and (VII), we also show curves B_1^* and B_3^*, which are obtained in the same manner as that for B_1 and B_3, but with the additional assumption that photolysis of $XONO_2$ (X = Br, Cl) proceeds by the path $XONO_2 \rightarrow XO + NO_2$ (or $O + XONO$) rather than the path $XONO_2 \rightarrow X + NO_3$. The effect on the vertically integrated ozone column abundance is summarized in Table 3. The difference between the present and previous assessments of the chlorofluoromethane impact on stratospheric ozone is about 11%. The difference would be greater ($\sim$ 17%) if cycles (IV) and (VII) were suppressed as in B_1^* and B_3^*. Our model predicts

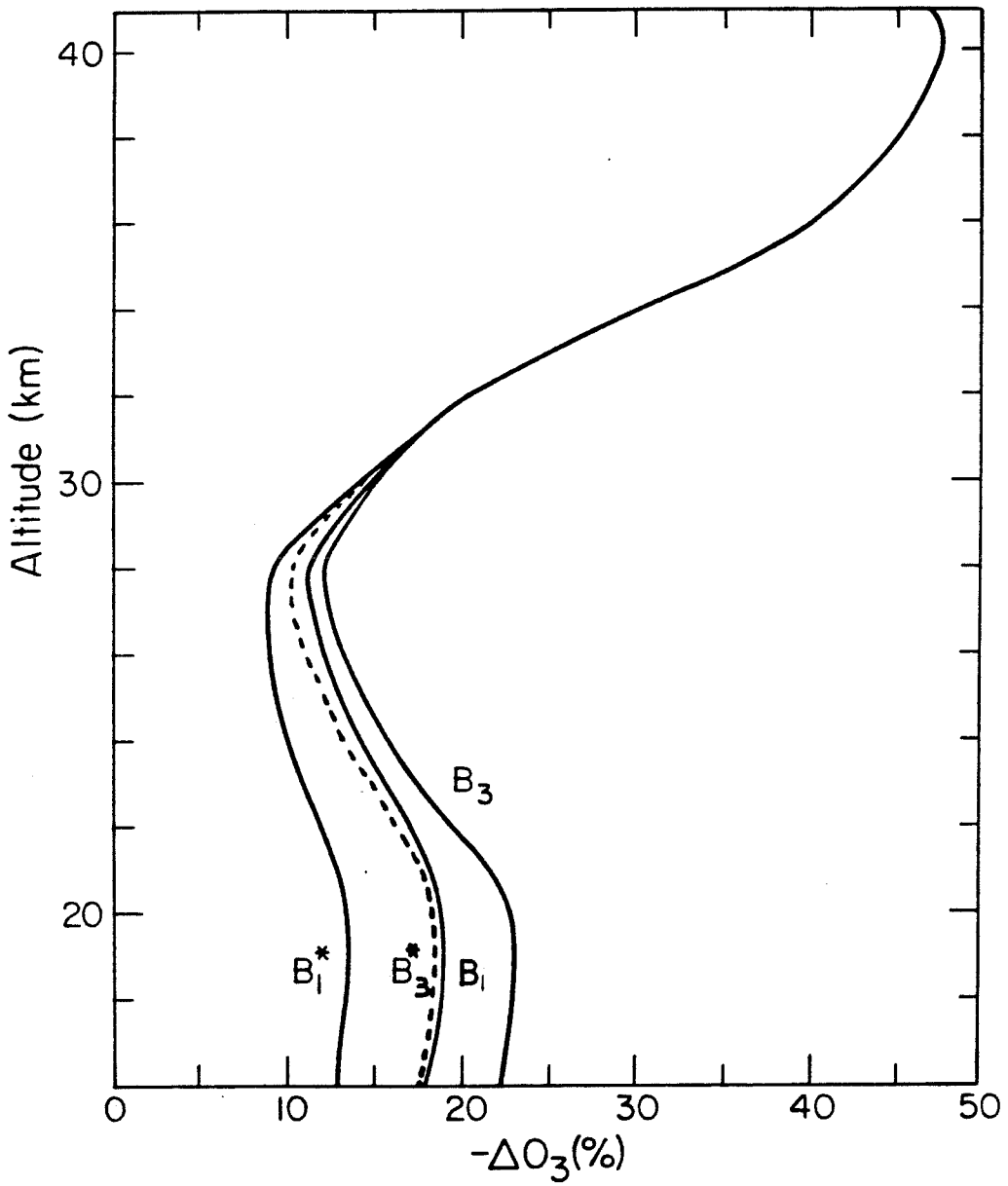

Figure 9 - Altitude profiles of ozone resuction due to steady-state chlorofluromethane release at 1973 rates. B_1 is based on our standard model with no bromine. B_3 includes 20 pptv Br_x. B_1* and B_3* are the same as B_1 and B_3 except that photolysis for $XONO_2$ proceeds by the path $XONO_2 \rightarrow XO + NO_2$ or $O + XONO$(X = Br, Cl). Details are referred to in Table 3.

TABLE 3

Column integrated (from 0 to 80 km) ozone abundance calculated by our photochemical model for various concentrations of Cl_x and Br_x in steady-state. The units for ozone, Cl_x, and Br_x abundances are cm-atm (1 cm-atm = 2.6×10^{19} molecules cm^{-2}), ppbv and pptv, respectively. For the cases marked by (*) we assume that photolysis of $XONO_2$ proceeds by the path $XONO_2 \rightarrow XO + NO_2$ (or O + XONO), where X = Br or Cl. For all other cases, photolysis of $XONO_2$ proceeds by the path given in Table 1. Runs C_1, C_2, D_1, and D_2 show the sensitivity of the results for A_3 to the uncertainties in the rate coefficients for reactions $2(Br + HO_2)$ and $J_2(BrO + h\nu)$. For runs C_1 and C_2, k_2 was set equal to 4×10^{-11} and 5×10^{-12} cm^3s^{-1}, respectively, in runs D_1 and D_2, J_2 was set equal to 3×10^{-2} and $3 \times 10^{-3}s^{-1}$.

Br_x (pptv) \ Cl_x (ppbv)	2.3		8.2		$\Delta O_3/O_3 = \frac{B}{A} - 1$
0	A_1	0.327	B_1	0.268	-18.0%
10	A_2	0.323	B_2	0.262	-18.9%
20	A_3	0.319	B_3	0.256	-19.7%
30	A_4	0.315	B_4	0.251	-20.6%
80	A_5	0.294	B_5	-----	---
0	A_1*	0.333	B_1*	0.283	-15.0%
20	A_3*	0.326	B_3*	0.269	-17.5%
20	C_1	0.321			
20	C_2	0.318			
20	D_1	0.321			
20	D_2	0.319			

0.2 ppbv $ClONO_2$ at 20 km, a value that should be compared with Murcray et al.'s (1978) upper limit of 0.3 ppbv (at 5% absorption level) at 20 km. As discussed earlier, the additional ozone depletion by bromine is primarily through the effect of cycle (III). The result for column-integration ozone depletion can be approximately expressed as

$$\frac{\Delta O_3 \text{ (cycle III)}}{O_3} \approx -\frac{1}{40}\left(\frac{Br_x}{(Br_x)_o}\right)\left(\frac{Cl_x}{(Cl_x)_o}\right)^{1/3}$$

where $(Br_x)_o$ = 20 pptv, $(Cl_x)_o$ = 2.3 ppbv, $Br_x \leq$ 100 pptv and 2 ppbv $\leq Cl_x \leq$ 10 ppbv. The exponent, (1/3), in Cl_x acts as a damping factor and is due to a "self-healing" effect caused by the destruction of O_3 at high altitudes. More photons are then allowed to penetrate deeper into the atmosphere where they can photolyze O_2. With bromine, however, most of the ozone perturbation takes place in the lower stratosphere below the level of maximum concentration for O_3, and the corresponding radiative feedback is absent. Our results for ΔO_3 fall between curves A and B, in Figure 2 of Wofsy et al. (1975). It is not meaningful to seek a more detailed comparison between Wofsy et al.'s calculations and ours since the major catalytic cycles and the number densities of important chemical species in the two models are different. Some photochemical models (see for example Derwent and Eggleton, 1978) predict lower concentrations of ClO in the lower stratosphere, for reasons to be discussed in the next paragraph, and the bromine effect is accordingly smaller. Our calculations are based on diurnally averaged values for all stratospheric species. A fully time-dependent calculation will (a) increase the daytime ClO concentration due to J_{10}, (b) increase the daytime BrO concentration due to J_1, and (c) decrease the daytime BrO concentration due to J_2 and NO. At low values for $J_2 (\leq 3 \times 10^{-3} s^{-1})$ (b)

is much larger than (c), and our calculations have underestimated the effect of bromine. A comparison between time-dependent and diurnally-averaged calculations has been performed by Sze (1979, private communication) using a similar photochemical model with $J_2 = 1 \times 10^{-2} s^{-1}$. Sze's results are close to ours. However, his time-dependent calculations predict a 30% larger ΔO_3 than is obtained with the diurnally averaged model.

A number of uncertainties in the current modeling effort of stratospheric bromine can be readily identified. The major bromine-related catalytic cycle is cycle (III), whose effect on O_3 is, to first order, given by

$$-\delta O_3 \propto 2k_{10a}\,[ClO]\,[BrO] \quad .$$

In the lower stratosphere, we can derive approximate expressions for ClO and BrO

$$\frac{[Cl]}{[Cl_x]} \approx \left\{ 1 + \frac{k_{25}\,k_{31}[CH_4]\,[NO]}{k_{32}\,k_{15}[OH]\,[O_3]} + \frac{k_{19}M[NO_2]}{J_{10}} \right\}^{-1}$$

$$\frac{[Br]}{[Br_x]} \approx \left\{ 1 + \frac{k_2[HO_2]\,(J_2 + k_7[NO])}{k_1 k_5[OH]\,[O_3]} + \frac{k_{11}M[NO_2]}{J_1} \right\}^{-1} \quad .$$

The quantities most critical for a better understanding of stratospheric bromine are summarized and critiqued in Table 4. For simplicity, we choose to evaluate all the relevant quantities at 20 km. We may note that ClO in the lower stratosphere is a minor chlorine species, whose concentration is controlled by NO, NO_2, k_{25}

and CH_4. A comparison between predicted and measured ClO concentrations below 25 km shows considerable disagreement (Anderson et a., 1977), with the measurements suggesting lower ClO concentrations, especially in winter. If the missing ClO has been converted into HCl, this would result in a net decrease in the catalytic destruction of O_3 in the lower stratosphere. However, if the missing ClO has been converted into $ClONO_2$ and if the photolysis products are Cl + NO_3, (Murcray et al.'s, (1978) upper limit measurement of $ClONO_2$ is for March), then cycle (VII) would operate in favor of cycle (III), and lead to a net destruction of ozone. The major uncertainty in the bromine chemistry is the absolute concentration of Br_x. The way in which the uncertainties in Table 4 affect δO_3 is, in most cases, explicitly given by the approximate expressions we derived earlier. We do, however, include in Table 3, the results of four runs (C_1, C_2, D_1, D_2) on the sensitivity of δO_3 to a range of values for k_2 and J_2. The results suggest that δO_3 does not vary by more than 50% over the considerable uncertainty range for k_2 and J_2, except in the unlikely event that drastically k_2, J_2, and k_5 all happen to take on extreme values which would lower the $[BrO]$ to $[Br_x]$ ratio. We have also examined the sensitivity of the results to the choice of eddy diffusivity profile. A factor of 1.5 increase or decrease in values of eddy diffusivities leads to a 20% decrease and a 20% increase in δO_3, respectively. In addition to the uncertainties associated with the photochemistry in our model, there is the question of whether the one-dimensional model approach is really valid for modeling the lower stratosphere.

Table 4

The major uncertainties in the modeling of the coupled photochemistry of bromine in the lower atmosphere.

Quantity	Magnitude at 20 km	Uncertainty
Cl_x	0.99 ppbv	factor of 1.5
Br_x	11 pptv	factor of 2
k_{10a}	$6.7 \times 10^{-12} cm^3 s^{-1}$	$2.5 \times 10^{-12} - 1.3 \times 10^{-11} cm^3 s^{-1}$
k_{25}	$1.6 \times 10^{-14} cm^3 s^{-1}$	$1.3 - 2.1 \times 10^{-14} cm^3 s^{-1}$
NO	$2.7 \times 10^{8} cm^{-3}$	factor of 2
ClO	$7.8 \times 10^{7} cm^{-3}$	factor of 2 (see text)
J_2	$1 \times 10^{-2} s^{-1}$	$3 \times 10^{-2} - 3 \times 10^{-3} s^{-1}$
k_2	$2.0 \times 10^{-11} cm^3 s^{-1}$	$4 \times 10^{-11} - 5 \times 10^{-12} cm^3 s^{-1}$
k_5	$8.5 \times 10^{-12} cm^3 s^{-1}$	factor of 1.5
BrO	$1.2 \times 10^{7} cm^{-3}$	factor of 2

It is well known that dynamical processes play a major role in determining the distributions of ozone and other trace gases in the lower stratosphere. The one dimensional model considers vertical transport only, whereas the motion field is more nearly horizontal. Quasi-horizontal motions transport trace gases poleward, where they will meet different conditions of temperature and the availability of solar ultra-violet radiation. These variations will play an important role in determining the species partitioning between the total inorganic chlorine and bromine reservoirs. The relative importance of either HCl or $ClNO_3$, (as chlorine reservoirs) on the destruction of ozone at high latitudes has already been mentioned. A detailed treatment of stratospheric-tropospheric exchange processes is also required, in order to accurately determine the lifetime, in the lower stratosphere, of substances which may deplete ozone. Indeed, the study of compositional changes in the lower stratosphere on ozone may require the use of a multi-dimensional dynamical model.

CONCLUSIONS

In the lower stratosphere (16 - 26 km) ozone can be efficiently removed by a mixed bromine-chlorine catalytic cycle [cycle (III)], with additional contributions from cycle (IV) and cycle (VII). All three cycles involve a synergistic coupling between radical species from different families. We have investigated the effect of bromine in the present atmosphere, and in an atmosphere perturbed by large concentrations of halogens derived from anthropogenic sources. In both cases, the results (summarized in Table 3) suggest that bromine is important for controlling stratospheric ozone at a few percent level, and should be included in photochemical models. The major uncertainties in the modeling of bromine chemistry are in the concentrations of ClO and Br_x in the lower stratosphere and the rate coefficients for the key reactions k_{10a}, k_2, and J_{2r}(see Table 4). These uncertainties can be removed by suitable experimental work in the future. This work raises the possibility of large ozone depletions (20 - 30%) in the lower stratosphere, associated with the release of chlorofluoromethanes.

ACKNOWLEDGMENTS

We thank A.L. Lazrus and W.A. Sedlacek for permission to use their data prior to publication. We benefited from discussions with W.B. DeMore, H.B. Singh, J.S. Chang, S.C. Liu, N.D. Sze, J.A. Logan, S.C. Wofsy, M.T. Molina, and F.S. Rowland. We appreciate the constructive criticisms given by the referees P.J. Crutzen and R.J. Cicerone in their reviews of this paper.

This research was supported by NASA grant NSG 2229 to the California Institute of Technology, NASA grant NSG 5163 Scope M to Columbia University, and also represents one phase of NASA sponsored research carried out at the Jet Propulsion Laboratory under contract No. NAS 7-100

REFERENCES

Anderson, J.G., J.J. Margitan, D.H. Stedman, 1977: Atomic chlorine and the chlorine monoxide radical in the stratosphere: Three in situ observations. Science 198, 501-503.

Barker, J., J.S. Chang, J.E. Davenport, and D.M. Golden, 1979: Chlorine nitrate photolysis at low pressure. Submitted to Chem. Phys. Lett. (also based on paper presented at Am. Chem. Soc. Meeting, Miami, FL., Sept. 1978).

Brown, R.D., and I.W.M. Smith, 1975: Absolute rate constants for the reactions $O(^3P)$ with HCl and HBr. Int. J. Chem. Kinet., 7, 301-315.

Burreson, B.J., R.E. Moore, and P. Roller, 1975: Haloforms in the essential oil of the alga Asparagopis Taxiformis (Rhodophyta). Tetrahedron Lett., 7, 473-476.

Calvert, J.G. and J.N. Pitts, 1966: Photochemistry, J. Wiley & Sons, N.Y.

Chang, J.S., 1976: Calculations presented in NAS report, see reference NAS, 1976.

Chang, J.S. and J.E. Penner, 1978: Analysis of global budgets of halocarbons. Atm. Environ., 12, 1867-1873.

Cicerone, R.J., R.S. Stolarski, and S. Walters, 1974: Stratospheric ozone destruction by man-made chlorofluoromethanes. Science, 185, 1165-1167.

Clyne, M.A.A. and H.W. Cruse, 1970: Rates of elementary reactions involving the $BrO(X^2\Pi)$ radicals, Part 1, Formation and decay of the BrO radical, Part 2, Reactions of the BrO and IO radicals. Trans. Faraday Soc. 66, 2214-2243.

Clyne, M.A.A. and R.T. Watson, 1973: Kinetic studies for diatomic free radicals using mass spectrometry, Part 3-Elementary reactions involving BrO $X^2\Pi$ radicals. J.C.S. Far. Trans. I, 71, 336-350.

Crutzen, P.J., 1970: The influence of nitrogen oxides on the atmospheric ozone content. Quart. J. Roy. Meterol. Soc., 96, 320-325.

Crutzen, P.J., I.S.A. Isaksen, and J.S. McAfee, 1978: The impact of the chlorocarbon industry on the ozone layer. J. Geophy. Res., 83, 345-363.

Davis, D.D., G. Machado, B. Conaway, Y. Oh, and R.T. Watson, 1976: A temperature dependent kinetic study of the reaction OH with CH_3Cl, CH_2Cl_2, $CHCl_3$, and CH_3Br. J. Chem. Phy., 65, 1268-1274.

Derwent, R.G. and A.E.J. Eggleton, 1978: Ozone depletion estimates for global halocarbon and fertilizer usage employing one-dimensional modelling techniques. Environmental and Medical Sciences Division, Aere, Harwell, U.K. Internal Report, AERE-R-9112.

Durie, R.A. and D.A. Ramsay, 1958: Absorption spectra of the halogen monoxides. Can. J. Phys. 36, 35-53.

Foster, R.J., 1975-1978: Bromine, Bureau of Mines Minerals Yearbook 1975-1978, Information on years 1977, 1978 are in preprint form.

Helz, G.R. and R.Y. Hsu, 1978: Volatile chloro- and bromocarbons in coastal waters. Limnol. Oceanogr. 23, 858-869.

Howard, C.J. and K.M. Evenson, 1975: Rate constants for reactions of OH with ethane and some halogen substituted ethanes at 296 K. J. Chem. Phys., 64, 4303-4306.

Howard, C.J. and K.M. Evenson, 1977: Kinetics of the reactions of HO_2 with NO. Geophys. Res. Lett., 4, 437-440.

Howard, C.J., 1978: Recent developments in atmospheric HO_2 chemistry. WMO Symposium, Toronto, p. 11.

Hunten, D.M., 1975: Vertical transport in atmospheres. In Atmospheres of Earth and the Planets, Dordrecht, Holland, B.M. McCormac, ed., p. 59-72.

Johnston, H.S., 1971: Reduction of stratospheric ozone by nitrogen oxide catalysts from SST exhaust. Science, 173, 517-522.

Klingman, C.L., 1972-1975: Bromine, Bureau of Mines Minerals Yearbook.

Lazrus, A.L., Gandrud, B.W., and Woodard, R.N., and W.A. Sedlacek, 1976: Direct measurements of stratospheric chlorine and bromine. J. Geophys. Res., 81, 1067-1070.

LeBras, G. and J. Combourieu, 1978: EPR Kinetic study of the reactions of CF_3Br with H atoms and OH radicals. Int. J. Chem. Kinet. X, 1205-1213.

Leinster, P., R. Perry, and R.J. Young, 1978: Ethylene dibromide in urban air. Atm. Environ., 12, 2383-2387.

Leu, M.T. and W.B. DeMore, 1977: Rate constant for the reaction of atomic bromine with ozone. Chem. Phys. Lett., 48, 317-320.

Leu, M.T. and C.L. Lin, 1979: Rate constants for the reaction OH with ClO, Cl_2, and Cl_2O, at 298 K. Geophys. Res. Lett., 6, 425-428.

Logan, J.A., M.J. Prather, S.C. Wofsy, and M.B. McElroy, 1978: Atmospheric chemistry: response to human influence. Philosophical Transactions of the Royal Society of London 290, 187-234.

Lovelock, J.E., 1975: Natural halocarbons in the air and in the sea. Nature, 256, 193-194.

McElroy, M.B., S.C. Wofsy, J.E. Penner, and J.C. McConnell, 1974: Atmospheric ozone: possible impact of stratospheric aviation. J. Atm. Sci., 31, 287-303.

Michael, J.V., J.H. Lee, W.A. Payne, and L.J. Stief, 1978: Absolute rate of the reaction of bromine atoms with ozone from 200 to 360 K. J. Chem. Phys., 68, 4093-4097.

Michael, J.V., J.H. Lee, W.A. Payne, and L.J. Stief, 1979: to be published in J. Chem. Phys.

Michael, J.V. and W.A. Payne, 1979: submitted to Int. J. Chem. Kinetics.

Molina, M.J. and F.S. Rowland, 1974: Stratospheric sink for Chlorofluoromethanes: chlorine-atom catalyzed destruction of ozone. Nature, 249, 810-815.

Murcray, D.G., J.W. Williams, D.B. Barker, A. Goldman, C. Bradford, and G. Cook, 1978: Measurements of constituents of interest in the photochemistry of the ozone layer using infrared techniques. WMO Symposium, Toronto, 1978, p. 61-68. World Meteorological Secretariat of the World Meteorological Organization, publication ISBN 92-63-10511-1, published by Secretariat of the World Meteorological Organization, Geneva, Switzerland.

NAS, 1976: Halocarbons: Effects on stratospheric ozone. National Academy of Sciences, 2101 Constitution Ave., Washington, D.C., 20418.

NASA 1010, 1977: NASA Reference Publication 1010, Chlorofluromethanes and the stratosphere. R.D. Hudson, ed., Scientific and Technical Information Service, Springfield, VA, 22151.

NASA 2, 1979: Chemical kinetic and photochemical data for use in stratospheric modeling. Evaluation No. 2, NASA Panel for Data Evaluation, JP. 70-27, Jet Propulsion Laboratory, California Institute of Technology, 4800 Oak Grove Dr., Pasadena, CA 91103.

Penner, J.E., M.B. McElroy, and S.C. Wofsy, 1977: Sources and sinks for atmospheric H_2: A current analysis with projections for the influence of anthropogenic activity. Planet. Sp. Sci., 25, 521-540.

Selwyn, G., J. Podolske , and H.S. Johnston, 1977: Nitrous oxide ultraviolet absorption spectrum at stratospheric temperatures. Geophys. Res. Lett., 4, 427-430.

Singh, H.B., L. Salas, H. Shiegeshi, and A. Crawford, 1977: Urban non-urban relationships of halocarbons, SF_6, N_2O, and other atmospheric trace constituents. Atmos. Envir., 11, 819-828.

Smith, W.S., C.C. Chou, and F.S. Rowland, 1977: The mechanism for ultraviolet photolysis of gaseous chlorine nitrate at 302.5 nm. Geophys. Res. Lett. 4, 517-519.

Spencer, J.E. and F.S. Rowland, 1978: Bromine nitrate and its stratospheric significance. J. Phys. Chem., 82, 7-10.

Stief, L.J., J.V. Michael, W.A. Payne, D.F. Nava, D.M. Butler, and R.S. Stolarski, 1978: The reaction Cl + $H_2CO \rightarrow$ HCl + HCO: decreased sensitivity of stratospheric ozone to chlorine perturbations, Geophys. Res. Lett. 5, 829-831.

Sze, N.D., 1977: Anthropogenic CO emissions: Implications for atmospheric CO-OH-CH_4 cycle. Science, 195, 673-675.

Takacs, G.A. and G.P. Glass, 1973a: Reactions of hydroxyl radicals with some hydrogen halides. J. Phys. Chem. 77, 1948-1951.

Takacs, G.A. and G.P. Glass, 1973b: Reaction of atomic oxygen with hydrogen bromide. J. Phys. Chem. 77, 1182-1186.

Theiler, R., J.C. Cook, L.P. Hager, and J.F. Siuda, 1978: Halohydrocarbon synthesis by bromoperoxidase. Science, 202, 1094-1096.

Wang, W.C., J.P. Pinto, and Y.L. Yung, 1979: The effect of halogenated compounds on earth's surface temperature. Submitted to J. Atmos. Sci.

Watson, R.T., 1975: Chlorine, the Chlorine Oxides, and other Halogen Species, CIAP Monograph I. Publication DOT-TST-75-51 by Dept. of Transportation, Climatic Impact Assessment Program, Office of the Secretary of Transportation, Wash. D.C. 20590. See section 5.7.5.

Watson, R.T., G. Machado, B. Conaway, S. Wagner, and D.D. Davis, 1977: A temperature dependent kinetic study of the reaction of OH with CH_2ClF, $CHCl_2F$, $CHClF_2$, CH_3CCl_3, CH_3CF_2Cl, and $CF_2ClCFCl_2$. J. Phys. Chem., 81, 256-262.

Wofsy. S.C., M.B. McElroy, and Y.L. Yung, 1975: The chemistry of atmospheric bromine. Geophys. Res. Lett., 2, 215-218.

Wofsy, S.C., 1976: Interactions of CH_4 and CO in the earth's atmosphere. Ann. Rev. Earth Planet. Sci., 4, 441-469.

Wofsy, S.C., M.B. McElroy, and N.D. Sze, 1975: Freon consumption: Implications for atmospheric ozone. Science, 187, 535.

APPENDIX III

TEMPERATURE DEPENDENT RATE CONSTANTS FOR THE REACTION OF GROUND STATE ATOMIC CHLORINE WITH SIMPLE ALKANES

R. S. Lewis, S. P. Sander, S. G. Wagner and R. T. Watson

Molecular Physics and Chemistry Section

Jet Propulsion Laboratory
Pasadena, CA 91103

ABSTRACT

The low pressure discharge flow resonance fluorescence technique has been utilized to study the rates and temperature dependences of three chlorine atom-alkane reactions. The reactions have been studied using a wide range of experimental conditions to insure the absence of complicating secondary processes. The Arrhenius expressions for each bimolecular reaction are expressed in units of cm^3 $molecule^{-1}$ s^{-1}: $C\ell + C_2H_6 \rightarrow C_2H_5 + HC\ell$ (1), $k_1 = 9.01 \times 10^{-11} \exp(-(133 \pm 15)/T)$ 220 - 604 K; $C\ell + C_3H_8 \rightarrow C_3H_7 + HC\ell$ (2), $k_2 = 1.36 \times 10^{-10} \exp(+(44 \pm 25)/T)$ 220 - 607 K; $C\ell + nC_4H_{10} \rightarrow C_4H_9 + HC\ell$ (3), $k_3 = 2.15 \times 10^{-10} \exp(+(12 \pm 26)/T)$ 298 - 598 K. In addition the following reaction was studied at 298 K: $C\ell + isoC_4H_{10} \rightarrow C_3H_9 + HC\ell$ (4), $k_4 = (1.46 \pm 0.06) \times 10^{-10}$.

The present results are compared with earlier absolute and relative rate constant measurements.

INTRODUCTION

Reactions involving abstraction of a hydrogen atom from an RH molecule by atomic chlorine have been of interest to kineticists for many years. In addition to the need for accurate experimental rate data in order to test current kinetic theories, recent interest in these reactions stems from the now well known stratospheric chlorine-ozone problem.[1] This renewed interest in reactions between atomic chlorine and hydrogen containing molecules ($Cl + RH \rightarrow HCl + R$) is due to the role of HCl as a reservoir for active chlorine in the stratosphere. This has led to numerous studies of the kinetic behavior of atomic chlorine with molecular hydrogen[2-9] and methane[4,5,10-20] over a wide range of temperature and pressure using direct kinetic techniques. However, except for a single temperature dependence study with ethane,[14] the reactions of higher alkanes with atomic chlorine have received relatively little recent attention.

The introduction of gas chromatography allowed competitive chlorination experiments between molecular hydrogen, alkanes, and chlorinated alkanes to be studied by product analysis,[21,22] thus providing more accurate results than those available using the consumption method.[23,24] The early work is reviewed by Fettis and Knox.[25] In addition to activation energy differences and Arrhenius A-factor ratios determined in the competitive chlorination studies, Fettis and Knox derived absolute Arrhenius parameters for the competitors by employing the absolute Arrhenius expression of 1.38×10^{-10} $\exp(-2750/T)$ cm^3 $molecule^{-1}$ s^{-1} for the $Cl + H_2$ reaction as the primary standard. However, as this Arrhenius expression is now thought to be incorrect,[26-28] the competitive chlorination results should be combined with the best available

Arrhenius expression for the Cℓ + H_2 reaction to yield re-evaluated absolute Arrhenius parameters for the competitors.

The present study utilizes the discharge flow-resonance fluorescence technique to investigate the kinetic behavior of ground state atomic chlorine with ethane, propane, and n-butane over a range of temperature, and with isobutane at room temperature. The results obtained from the present study will be compared to the re-evaluated competitive chlorination results, and the recent absolute determination of the Arrhenius expression for Cℓ + C_2H_6.

EXPERIMENTAL

A schematic of the low pressure discharge flow-resonance fluorescence system is shown in figure 1a. The 25mm id flow tube, shown in figure 1b, was mounted vertically and continuously evacuated by a ~ 50 ℓs^{-1} rotary pump (Welch 1396) through two traps cooled to 77 K. Two pressure measurement ports are provided with a calibrated MKS Baratron BHS-10 pressure head. Measurements at each port allow a correction for viscous pressure drop to be made. Flow velocities of ~ 35 m s^{-1} at room temperature are obtainable, but velocities under 25 m s^{-1} were normally used in order to minimize the pressure drop correction. However, high flow velocities reduce the magnitude of the axial diffusion correction factor. Three flow tubes were used in this study; the first was constructed in pyrex and only operated at room temperature; the second was constructed in quartz and wrapped with Nichrome wire and insulation for operation from 300 - 700 K; the third was a doubled walled quartz tube whose temperature could be controlled from 220 - 400 K by circulating either methanol or ethylene glycol through the outer jacket from a Haake constant temperature bath and heat exchanger. A temperature range of ~ 220 - 600 K was used in this study. Chromel-Constantan thermocouples were used to monitor temperature. The low temperature

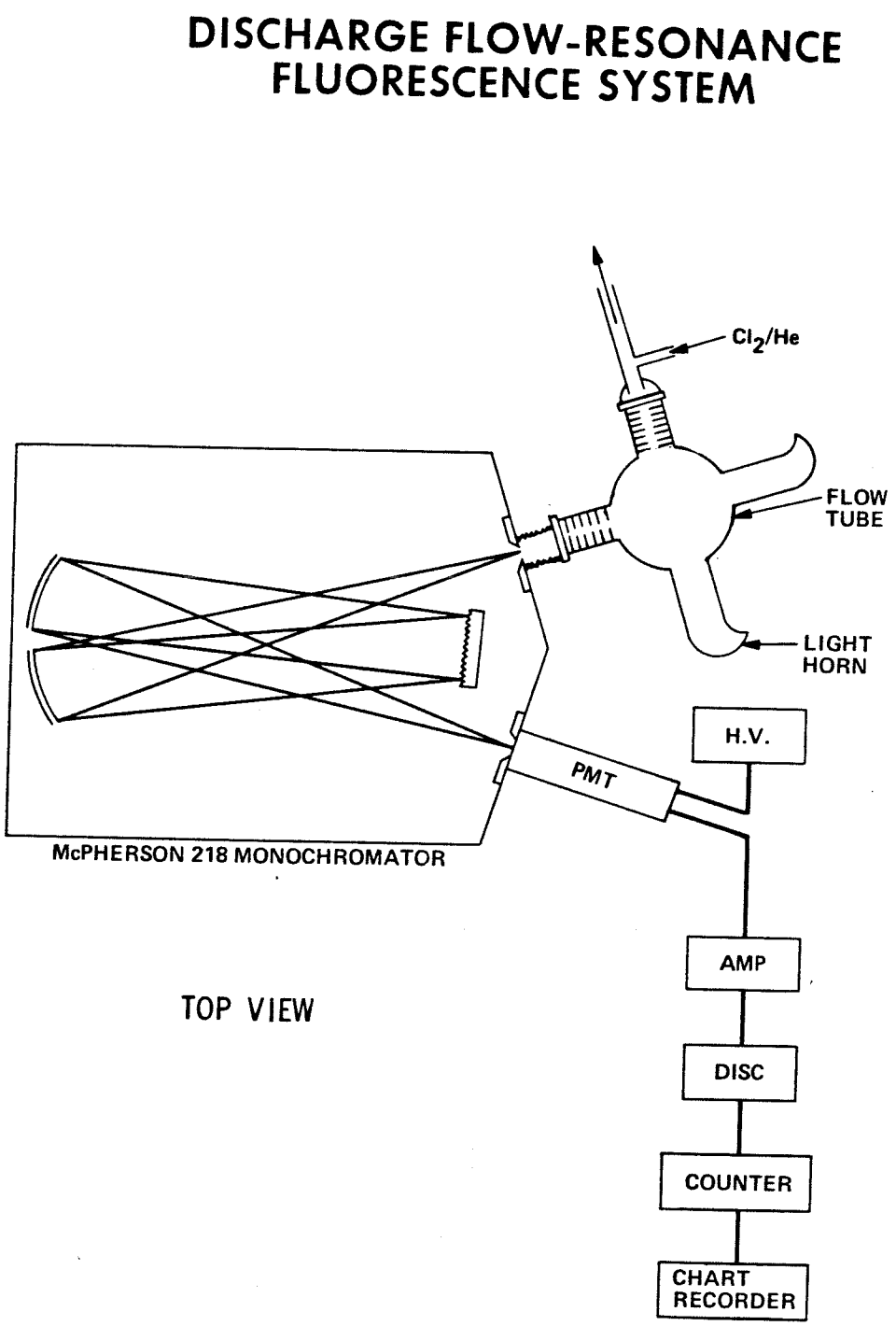

Figure 1a Schematic Diagram of Discharge Flow: Resonance Fluorescence Apparatus

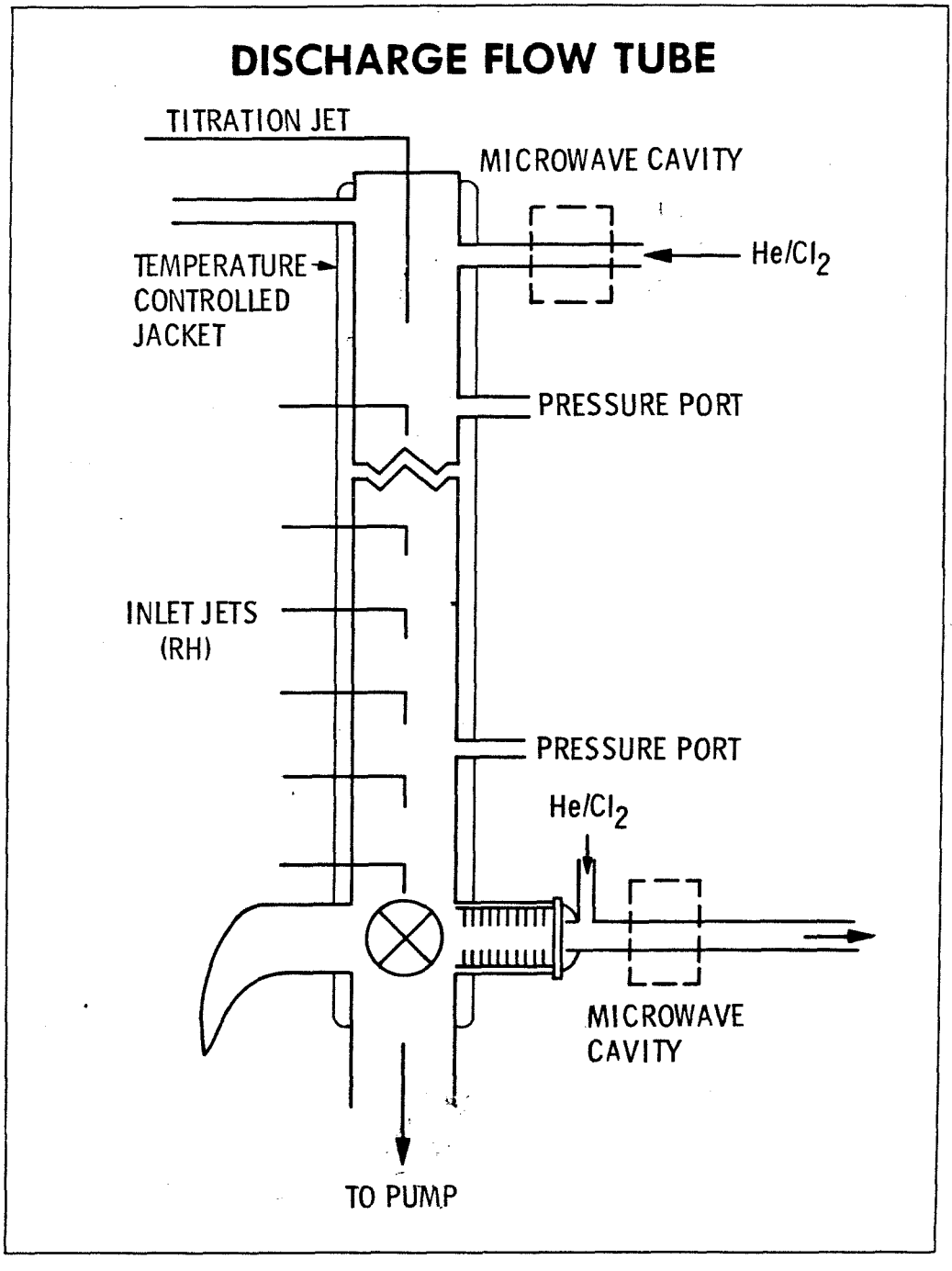

Figure 1b Discharge flow tube showing the resonance fluorescence scattering chamber

liquid-cooled tube showed < ½ K variation throughout the length of the tube, whereas the high temperature tube showed variations of ± 10 K (at 700 K) probably due to non-uniform heating and insulation of the tube. The flow tubes are 80 cm in length and equipped with 14 fixed position inlet jets for adding reactant gases to the flow of atomic chlorine. Chlorine atoms (~ 10^{11} cm^{-3}) were produced in a microwave discharge. To minimize heterogeneous removal of atomic chlorine both the reactor tube and discharge region were coated with a dilute phosphoric acid solution and baked to remove the water content. The walls were further treated by atomic oxygen formed in a He/O_2 microwave discharge prior to each kinetic run. An unusual wall effect (to be discussed later) was observed if this careful conditioning procedure was not followed. Some $Cl + C_2H_6$ experiments were performed with an untreated reactor.

At the end of the reaction cell, the atomic species are detected by means of a resonance fluorescence scattering cell. A flowing microwave plasma lamp (~ 0.1% Cl_2 in helium) operated at ~ 30 watts, and 1-2 torr total pressure, was used as the excitation source. The fluorescent signal was detected at right angles to both the direction of gas flow and the collimated excitation beam. The wavelength resolved fluorescent flux of the $Cl(3p^4 4s)^2P_{3/2}$ - $(3p^5)^2P_{3/2}$ transition at 134.7 nm was monitored using a McPherson 0.3 m vacuum monochromator (Model 218), EMR 542G solar blind photomultiplier, and Brookdeal 5C1 photon counting system. The background signal (scattered light plus photomultiplier dark noise) was minimized using collimators in front, and Wood's horns opposite the resonance lamp and monochromator. The atomic chlorine fluorescence signal was calibrated by generating known concentrations of chlorine atoms from the reaction of Cl_2O with excess oxygen atoms. The intensity of fluorescence was found to be linearly proportional to the atomic chlorine

concentration up to ~ 3 x 10^{11} cm^{-3}. The fluorescent signal was typically ~ 5000 cps for a chlorine atom concentration of 10^{11} cm^{-3}, in contrast to a background signal of 20-30 cps. Consequently, a detection limit of ~ 10^{8} cm^{-3} (S/N = 1) was obtainable when the normal experimental procedure of averaging six ten-second counting periods was used. In some of the earlier experiments the sensitivity of the system was up to a factor of 5 greater, i.e., $I_F \simeq$ 2.5 x 10^{4} cps when $[C\ell] \simeq 10^{11}$ cm^{-3}.

Reagent flow rates were determined using calibrated mass flow-meters (Hasting-Raydist). The helium used in this study was Matheson "Ultra High Purity" with a stated purity of 99.999%, and was used after passing through a trap at 77 K. The alkanes used in this study were all Phillips Research grade with stated purities of: C_2H_6 (99.99%); C_3H_8 (99.97%); n-C_4H_{10} (99.95%) and iso-C_4H_{10} (99.99%). Matheson Research Grade chlorine was used with a stated purity of 99.96%.

RESULTS

Since the kinetic behavior of atomic chlorine with C_2H_6 (1), C_3H_8 (2), n-C_4H_{10} (3) and iso-C_4H_{10} (4) was studied using pseudo first order conditions, $[RH]_o > [C\ell]_o$ {$[RH]_o \simeq$ (2-87) x 10^{11} cm^{-3}; $[C\ell]_o$ = (0.8-13) x 10^{10} cm^{-3}; giving a range of initial stoichiometry of 8-426}, the chlorine atom decay rates could be simply analyzed using equation (I):

$$C\ell + RH \xrightarrow{k_{bi}} HC\ell + R; \quad [RH]_o >> [C\ell]_o$$

$$\ell n([C\ell]_o/[C\ell]_t) = k_{bi}[RH]_o t \qquad (I)$$

The wide variation in experimental conditions which was used (flow velocity,

$[C\ell]_o$, $[RH]_o$, P_T), verified that kinetic complications due to secondary homogeneous processes were unimportant in our study. Table I summarizes the experimental conditions used in this study. The attenuation of the chlorine atom signal with time was normally followed for at least one order of magnitude decrease. Figure 2 shows several typical decay plots of atomic chlorine with time from the $C\ell + C_2H_6$ system. It should be noted that the plots are indeed linear over the reaction time of the experiment thus indicating that the reaction is first order in [Cℓ] (this observation is discussed in more detail later). The values of the first order rate constants, k', ($k' = -d[C\ell]/dt$) which were obtained from plots of $\ell n([C\ell]_o/[C\ell])$ versus time as shown in figure 2 were corrected for the pressure gradient along the length of the reaction zone, and for axial diffusion (the magnitude of the corrections were typically less than 5 and 10%, respectively). The correction factor for axial diffusion was obtained using the following equation[29,30],

$$k = k'(1 + \frac{k'D}{v^2}) \qquad \text{(II)}$$

where k = corrected first order rate constant, k' = observed first order rate constant, D = diffusion coefficient for Cℓ atoms in helium, and v = flow tube velocity. Equation (II) is valid in this study, and assumes that $k' >> k_w$, where k_w = first order rate constant for heterogeneous removal of atomic chlorine. The diffusion coefficient for Cℓ in He was taken to be 1.06 x D(He - Ar), where the factor of 1.06 equals the ratio of the square roots of the molecular weights of Ar and Cℓ. D(He - Ar) was taken to be $1.521 \times 10^{-2}\ T^{1.552}/(\ell n(T/4.1 \times 10^7))^2\ \exp(1.71/T)$ atm. $cm^2\ s^{-1}$[31]. Studies performed at the higher temperatures, i.e., 500 - 600 K, normally employed higher flow velocities, i.e., ~ 25ms, than were employed for studies at ≤ 300 K in order to minimize the magnitude of the correction factor. The average corrections were: 3% (~ 220K); 4% (~ 298K) and 8% (~ 600 K). No corrections were necessary for radial diffusion, i.e., $\alpha(=D/kr^2)$ was normally much greater than unity, resulting in minimal radial concentration gradients of Cℓ atoms across the flow tube.[29,30,32] Figure 3 shows a typical plot of the pseudo first order rate constant, k', versus alkane concentration from the $C\ell + C_2H_6$ system. The slopes

Table I. Summary of Experimental Conditions

Reagent	Temp./K	Surface	# runs	[Cℓ] x 10^{-10} cm^3	[RH] x 10^{-12} cm^3	$[RH]_o/[Cℓ]_o$	$k'.s^{-1}$
C_2H_6	220	coated	10	1.6 - 4.5	1.2 - 4.3	32 - 253	78 - 210
	223	uncoated	14	1.4 - 6.7	1.0 - 6.5	26 - 330	52 - 306
	250	coated	8	1.1 - 2.4	2.3 - 5.5	57 - 323	53 - 266
	298	both	26	2.0 - 13.0	0.7 - 8.7	13 - 426	43 - 472
	402	uncoated	6	3.4 - 6.9	1.4 - 4.3	35 - 104	92 - 245
	410	coated	6	3.3 - 7.0	1.0 - 3.5	24 - 86	54 - 220
	515	uncoated	14	1.5 - 6.8	0.6 - 4.0	19 - 164	45 - 245
	604	coated	11	2.6 - 12.8	0.7 - 3.8	24 - 149	68 - 266
C_3H_8	220	coated	13	2.3 - 4.8	0.3 - 1.6	9.2 - 48	47 - 256
	298	coated	12	1.9 - 5.9	0.6 - 2.3	12 - 59	82 - 327
	607	coated	10	0.8 - 2.0	0.4 - 1.8	14 - 201	63 - 262
n - C_4H_{10}	298	coated	13	1.2 - 4.8	0.2 - 1.5	8.1 - 76	50 - 299
	422	coated	8	1.5 - 3.3	0.3 - 1.7	13 - 64	73 - 320
	598	coated	14	1.1 - 3.3	0.3 - 1.9	12 - 97	50 - 350
iso - C_4H_{10}	298	coated	9	1.6 - 4.2	0.2 - 1.3	9.0 - 82	31 - 175

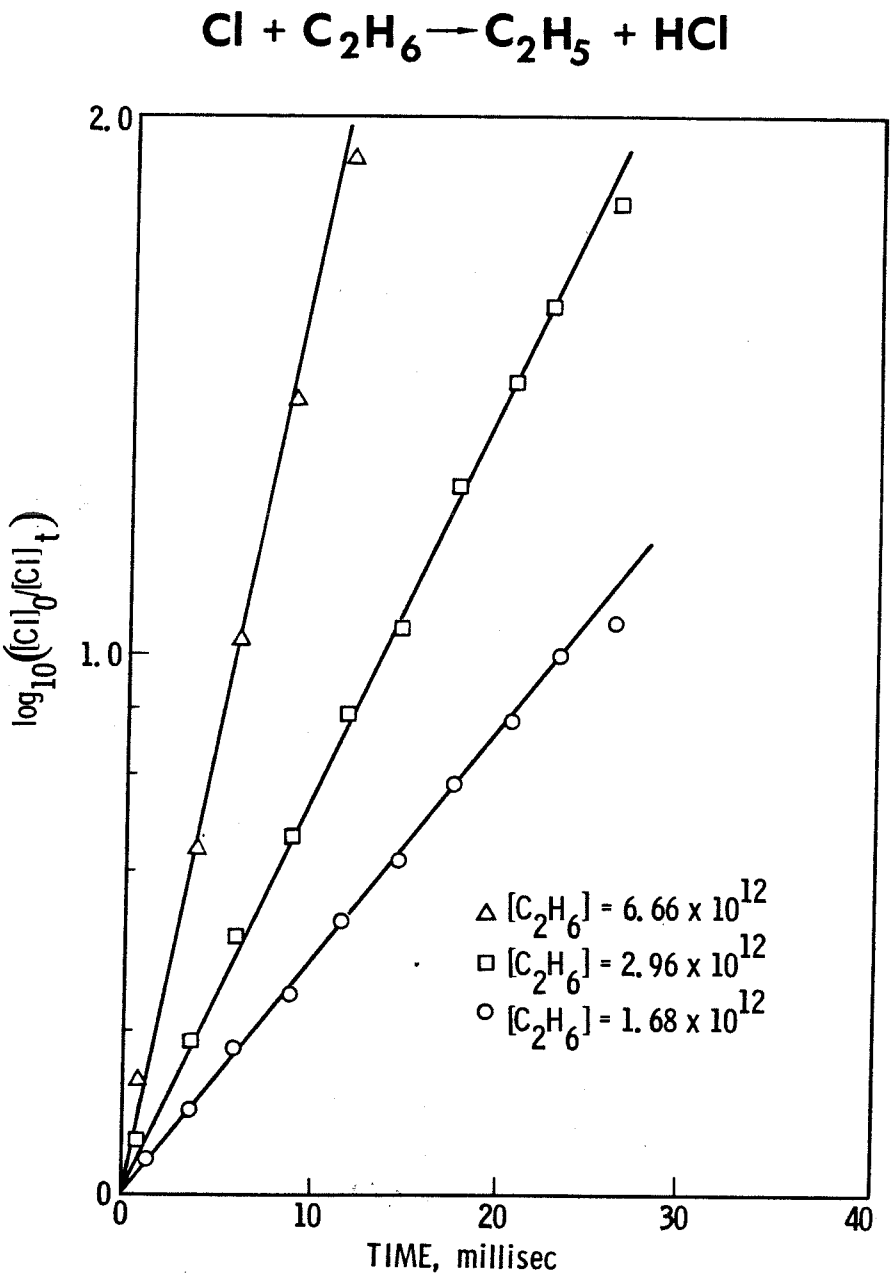

Figure 2 The reaction Cℓ + C_2H_6 → C_2H_5 + HCℓ. Typical first-order plots for [Cℓ] in the presence of various excess concentrations of C_2H_6 at 298K.

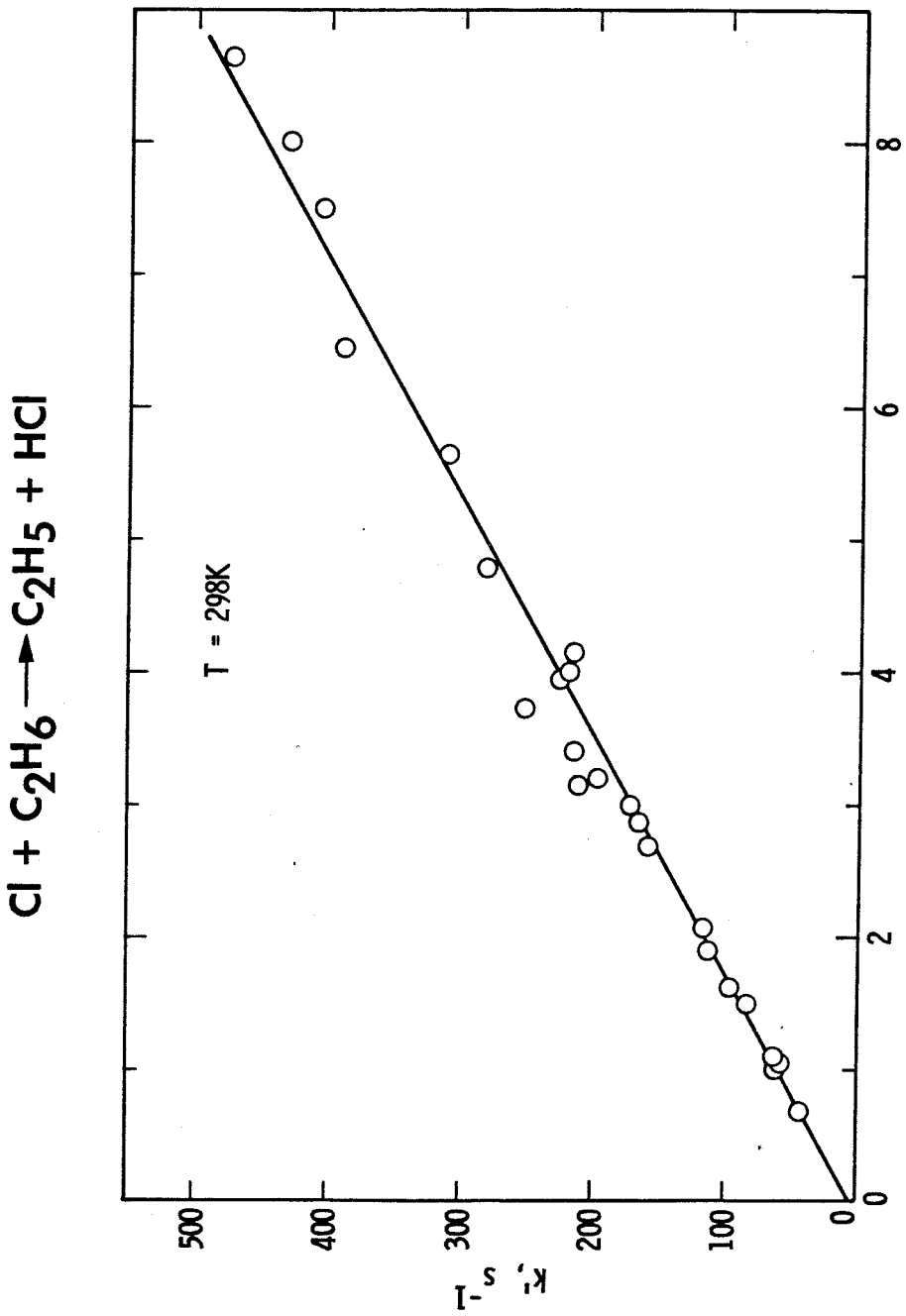

Figure 3 The reaction Cℓ + C_2H_6 → C_2H_5 + HCℓ. Variation of pseudo first-order rate constant, $-d\,ln[C\ell]/dt$, with $[C_2H_6]$ at 298K.

(bimolecular rate constants) and intercepts of such plots are obtained from a least-squares treatment of the data. The bimolecular rate constants and "wall loss coefficients" generated in this manner are shown in Table II. From Table II it can be seen that the rate constants expressed in units of cm^3 $molecule^{-1}$ s^{-1} for reaction of Cℓ with C_2H_6 (1), C_3H_8 (2), n-C_4H_{10} (3) and iso-C_4H_{10} (4) at 298 K are:

$$C\ell + C_2H_6 \rightarrow C_2H_5 + HC\ell;\ k_1 = (5.48 \pm 0.3) \times 10^{-11} \quad (1)$$

$$C\ell + C_3H_8 \rightarrow C_3H_7 + HC\ell;\ k_2 = (1.51 \pm 0.06) \times 10^{-10} \quad (2)$$

$$C\ell + n\text{-}C_4H_{10} \rightarrow C_4H_9 + HC\ell;\ k_3 = (2.25 \pm 0.1) \times 10^{-10} \quad (3)$$

$$C\ell + iso\text{-}C_4H_{10} \rightarrow C_4H_9 + HC\ell;\ k_4 = (1.46 \pm 0.06) \times 10^{-10} \quad (4)$$

It can be seen from Table II that the values of k_1-k_4 derived using the alternate analysis procedure, i.e., the mean of the values of k'/[reagent], are in excellent agreement with those derived from the slopes of k' versus [reagent]. The linearity of plots of k' versus excess reagent concentration, e.g. figure 3, are normally used to argue that the reaction was first order in excess reagent (RH in this study), and that the system was well behaved and free from complicating secondary processes.

During experiments performed at higher temperatures with C_2H_6, and at most temperatures with the other alkanes, a wall effect was observed which appeared to exhibit a first order dependence on the concentrations of both atomic chlorine and alkane.

$$C\ell + RH \xrightarrow{wall} \text{products} \quad (5)$$

as opposed to the more commonly observed mechanism.

$$C\ell \xrightarrow{wall} \tfrac{1}{2}C\ell_2$$

The latter process is unimportant, and not observed, if the experiments are performed using pseudo first order conditions and the fixed observation point technique, i.e., the only significant loss processes for atomic chlorine are first order in [Cℓ], and the magnitude of k_{wall} is unchanged upon addition of alkane to the reactor. However, the wall effect observed in these experiments resulted in an increase in both k' and k_{bi}. Figure 4 shows some typical chlorine atom decay plots obtained in the Cℓ + n-C_4H_{10} study at 298 K using both a

Table II. Bimolecular Rate Constants

Reagent	Temp./K	10^{11} x k(slope) cm^3 $molecule^{-1}$ s^{-1}	Intercept s^{-1}	10^{11} x k(mean) cm^3 $molecule^{-1}$ s^{-1}
C_2H_6	220	5.33 ± 0.22	-3.7	5.17 ± 0.25
	223	4.70 ± 0.21	8.3	4.99 ± 0.33
	250	5.03 ± 0.25	-2.3	4.92 ± 0.32
	298	5.48 ± 0.30	7.5	5.74 ± 0.68
	402	6.83 ± 0.33	6.3	7.10 ± 0.20
	410	6.61 ± 0.33	-7.1	6.20 ± 0.32
	515	7.04 ± 0.53	5.6	7.34 ± 0.57
	604	7.09 ± 0.32	-0.1	7.07 ± 0.39
C_3H_8	220	1.68 ± 0.05	1.5	1.69 ± 0.10
	298	1.51 ± 0.06	9.3	1.59 ± 0.10
	607	1.55 ± 0.12	-2.0	1.53 ± 0.12
n-C_4H_{10}	298	2.25 ± 0.10	-2.2	2.20 ± 0.13
	422	2.17 ± 0.09	-7.8	2.09 ± 0.13
	598	2.19 ± 0.03	-3.5	2.11 ± 0.12
iso-C_4H_{10}	298	1.46 ± 0.06	1.3	1.49 ± 0.08

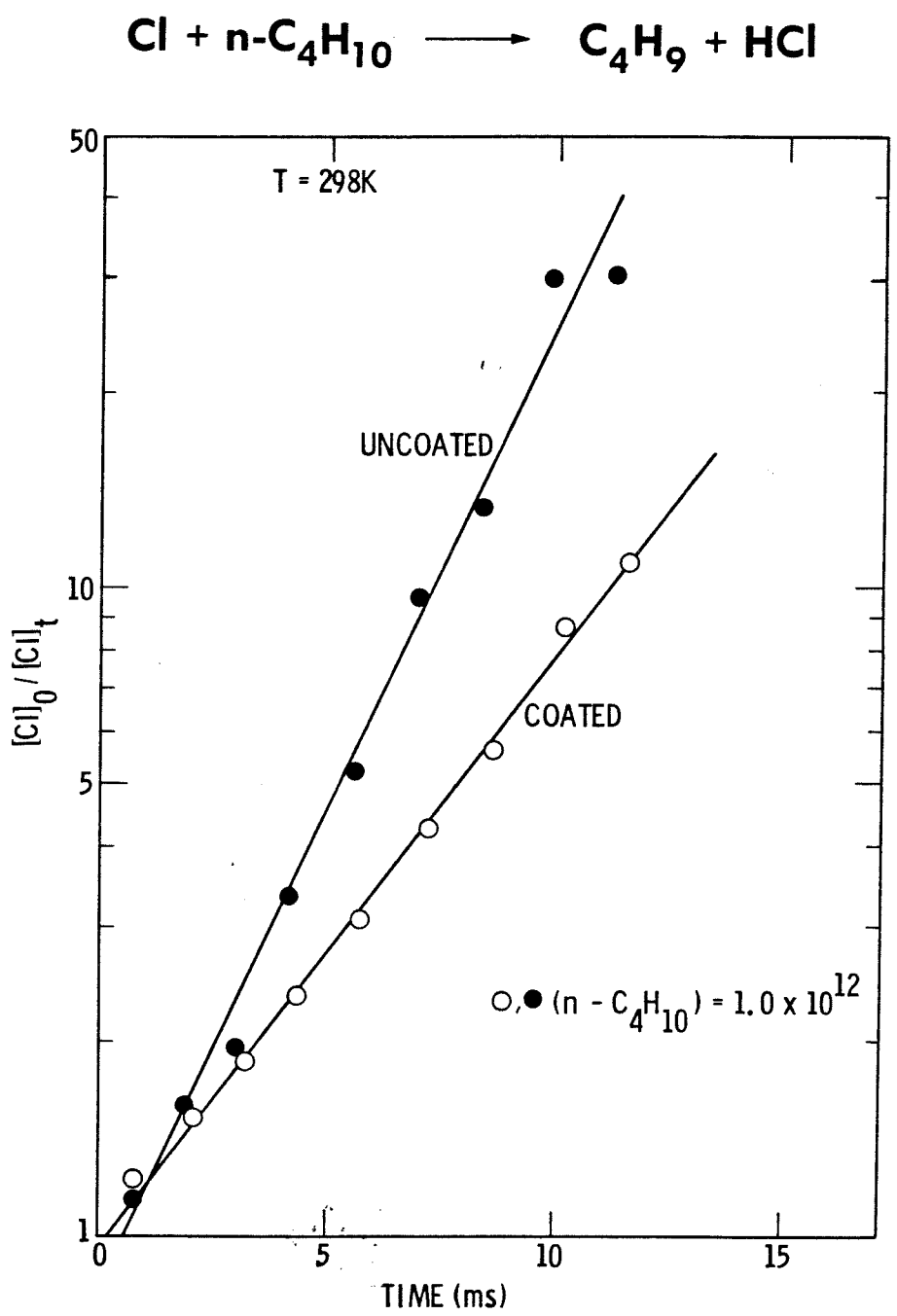

Figure 4 The reaction Cℓ + n-C_4H_{10} → C_4H_9 + HCℓ. First-order plots for [Cℓ] in the presence of 1 x 10^{12} cm^{-3} n-C_4H_{10} in a coated and uncoated flow reactor.

"treated," and "untreated" flow system. Figure 5 shows a plot of the pseudo first order rate constant, k', versus n-C_4H_{10} concentration taken at 598 K in both a treated and untreated flow reactor. It can be observed that plots of $\ell n([C\ell]_o/[C\ell])$ versus time (figure 4) and k' versus $[n\text{-}C_4H_{10}]$ (figure 5) are linear in both treated and untreated flow reactors, but the values of k' and k_{bi} are significantly greater in the untreated flow reactors. Consequently it can be stated that the linearity of plots such as those shown in figures 4 and 5 is not a good indication that the system is free from complicating processes, e.g. heterogeneous removal of Cℓ. In our experiments it was found that unless the conditioning procedure described in the experimental section was carefully adhered to, irreproducible data resulted, i.e., the results were consistent and reproducible if the reactor walls were either untreated or carefully treated, but if the conditioning procedure was not carefully followed values of k_{bi} intermediate between the "treated" and "untreated" values were observed. Therefore, a significant effort was made to eliminate interference by heterogeneous processes by careful conditioning of the reactor surfaces.

The Cℓ + C_2H_6 (1) and Cℓ + C_3H_8 (2) reactions were studied over the temperature range ~ 220 - 600 K, while the Cℓ + n-C_4H_{10} (3) reaction was studied from 298 - 600 K due to excessive absorption of the n-C_4H_{10} on the reactor surfaces at low temperatures. The Cℓ + iso-C_4H_{10} (4) reaction was only studied at 298 K due to experimental difficulties associated with heterogeneous effects.

The Arrhenius plots of these data are shown in figures 6 (C_2H_6) and 7 (C_3H_8, n-C_4H_{10}) and the data can be summarized as follows:

$$k_1 = 9.01 \times 10^{-11} \exp(-(133 \pm 15)/T) \qquad 220 - 604 \text{ K};$$

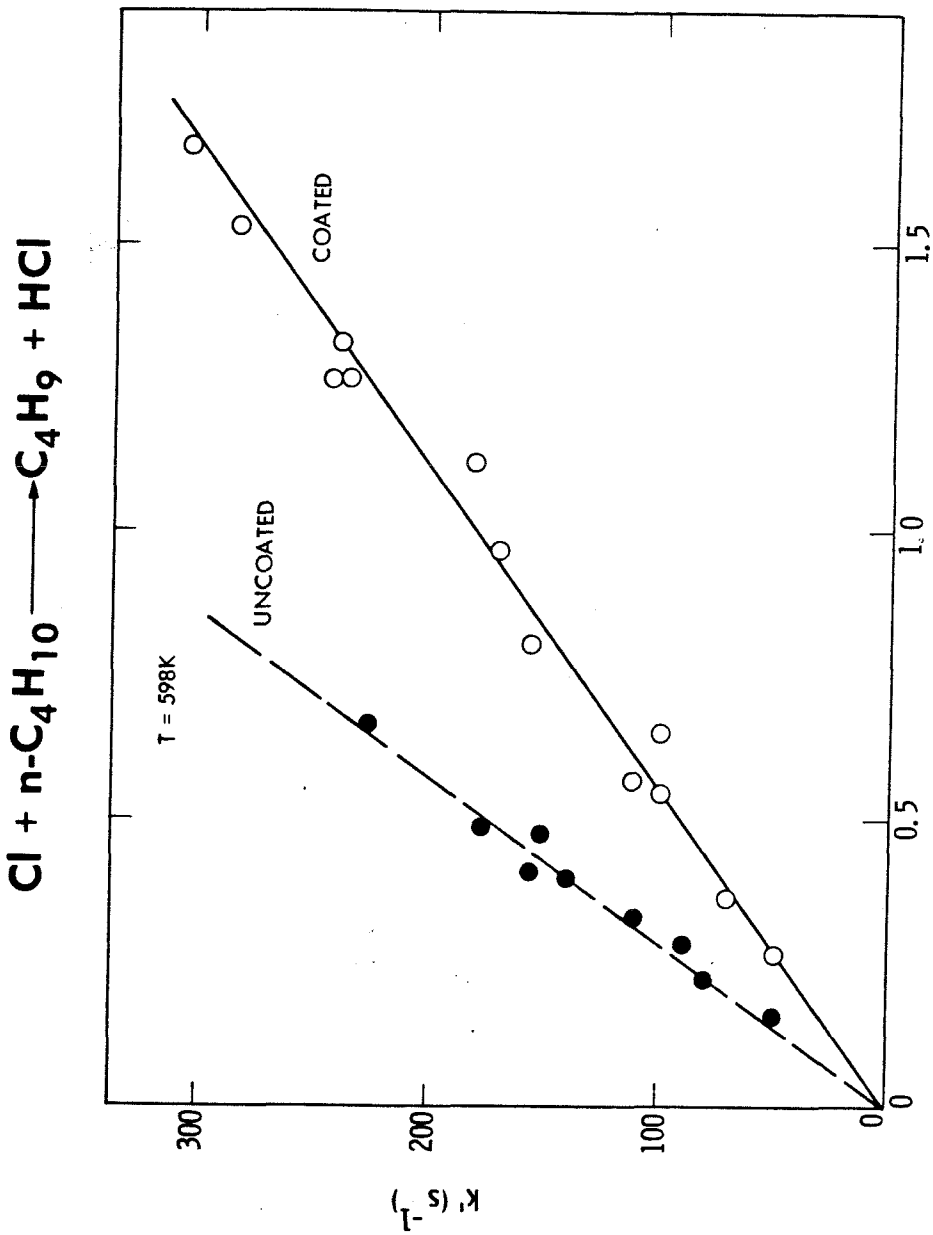

Figure 5 The reaction Cℓ + n-C_4H_{10} + C_4H_9 + HCℓ. Variation of pseudo first-order rate constant, -d ℓn[C]/dt, with [n-C_4H_{10}] in both a coated and uncoated flow reactor at 598K.

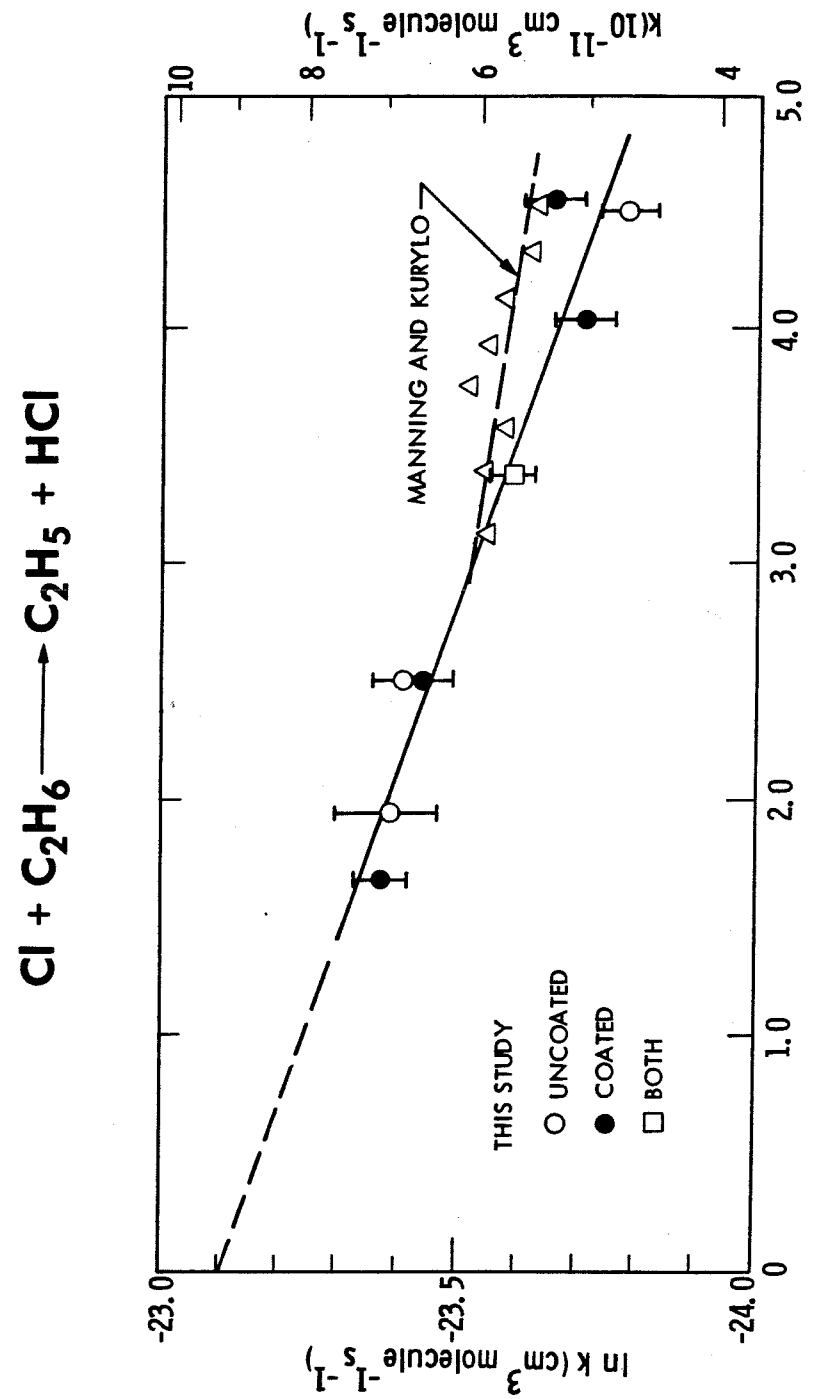

Figure 6 Arrhenius plot for the Cℓ + C_2H_6 → C_2H_5 + HCℓ reaction. ○, ●, □, this work; Δ, Ref. 14.

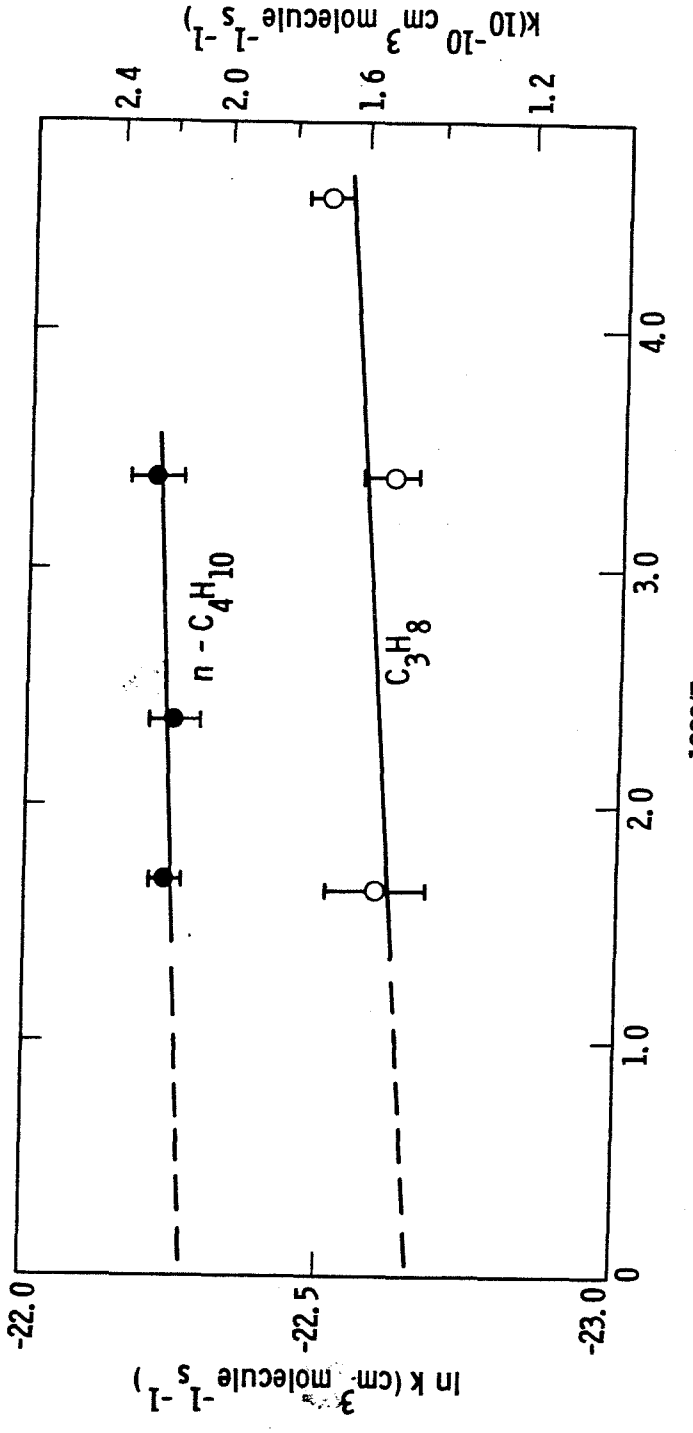

Figure 7 Arrhenius plot for the Cℓ + C_3H_8 → C_3H_7 + HCℓ, and Cℓ + n-C_4H_{10} → C_4H_9 + HCℓ reactions. O, C_3H_8; ●, n-C_4H_{10}.

$$k_2 = 1.36 \times 10^{-10} \exp(+(44 \pm 25)/T) \qquad 220 - 607 \text{ K};$$

$$k_3 = 2.15 \times 10^{-10} \exp(+(12 \pm 26)/T) \qquad 298 - 598 \text{ K}.$$

The units used here are cm^3 $molecule^{-1}$ s^{-1}, and the activation energies are expressed in terms of K^{-1}. The uncertainty factors listed here represent 1σ standard deviation obtained from a weighted, according to 1σ uncertainties of $k_{bimolecular}$ at each temperature, least squares treatment of the data tabulated for k_{bi} (slope) shown in Table II. Alternate Arrhenius parameters can be obtained by using the values of k_{bi} (mean) shown in Table II, and are listed in Table III. It can be seen that within the experimental uncertainties the magnitude of the Arrhenius parameters are similar for both sets of k_{bi}. Owing to the difficulties associated with the heterogeneous removal of Cℓ in the presence of RH in an untreated, or poorly treated, flow reactor it is clear that a realistic assessment of the accuracy of the data is somewhat less than that indicated by the precision of the data. Realistic uncertainties in the values of k_{bi} at any particular temperature should be ~ ± 15%.

DISCUSSION

Cℓ + C_2H_6

A comparison of the results obtained in this study with data from other studies[4,14,33,34] is shown in Table IV. It can be seen that the experimentally-determined room temperature values of all of the recent direct studies are in excellent agreement. The value of Davis, et al.[4] has been revised downward from the original value by ~ 10%.[26] The E/R value reported by Manning and Kurylo[14] is in good agreement with that determined in this work, especially when the difficulty of measuring small temperature dependences is considered.

Table III. Summary of Arrhenius Expressions for $C\ell + C_nH_{2n+2}$

Alkane		$10^{11} \times A$ $cm^3 molecule^{-1} s^{-1}$	E/R K	k(298K) $\times 10^{11}$ cm^3 $molecule^{-1}$ s^{-1}
C_2H_6	(slope)	9.01 ± 0.48	133 ± 15	5.48 ± 0.30
	(mean)	9.57 ± 0.52	142 ± 18	5.74 ± 0.68
C_3H_8	(slope)	13.6 ± 1.3	-(44 ± 25)	15.1 ± 0.6
	(mean)	14.3 ± 1.7	-(35 ± 33)	15.9 ± 1.0
n-C_4H_{10}	(slope)	21.5 ± 1.0	-(12 ± 26)	22.5 ± 1.0
	(mean)	20.1 ± 1.0	-(27 ± 19)	22.0 ± 1.3
iso-C_4H_{10}	(slope)	-	-	14.6 ± 0.6
	(mean)	-	-	14.9 ± 0.8

Table IV (A) Absolute Rate Coefficients for $C\ell + C_2H_6 \rightarrow C_2H_5 + HC\ell$

Reference	10^{11} x A (cm^3 $molecule^{-1}s^{-1}$)	E/R K	10^{11} x k(298) (cm^3 $molecule^{-1}s^{-1}$)	Temperature Range/K
Davis et al. 1970 [4]	-	-	6.0 ± 0.15	298
Manning and Kurylo, 1977 [14]	7.29 ± 1.23	61 ± 44	5.93 ± 0.44	222-322
Watson et al. 1979 [29]	-	-	5.5 ± 0.50	298
Watson and Ray, 1979 [30]	-	-	5.65 ± 0.40	298
This study	9.01 ± 0.48	133 ± 15	5.48 ± 0.30	220-604

Table IV (B) Absolute Coefficients for $C\ell + C_2H_6 \rightarrow C_2H_5 + HC\ell$ Derived from Competitive Chlorination Studies

Source of the $C\ell + H_2$ Arrhenius Expression	10^{11} x A (cm^3 $molecule^{-1}s^{-1}$)	E/R K	10^{11} x k(298) (cm^3 $molecule^{-1}s^{-1}$)
Watson, 1977 [26]*; CODATA, 1979 [28]*	6.35	81	4.84
NASA, 1977 [27]*	4.73	31	4.26
Watson et al. 1975 [13]	7.43	132	4.77
Whytock et al. 1977 [12]	3.59	-29	3.96

*Reviews

References [26,28]: $k(C\ell + H_2) = 4.7 \times 10^{-11} \exp(-2340/T)$ cm^3 $molecule^{-1}$ s^{-1}

Reference [27]: $k(C\ell + H_2) = 3.5 \times 10^{-11} \exp(-2290/T)$ cm^3 $molecule^{-1}$ s^{-1}

Reference [13]: $k(C\ell + H_2) = 5.5 \times 10^{-11} \exp(-2391/T)$ cm^3 $molecule^{-1}$ s^{-1}

Reference [12]: $k(C\ell + H_2) = 2.66 \times 10^{-11} \exp(-2230/T)$ cm^3 $molecule^{-1}$ s^{-1}

An absolute value for $k(Cl + C_2H_6)$ can be obtained from the competitive chlorination studies of the CH_4/H_2 and C_2H_6/CH_4 reaction pairs using the $Cl + H_2$ reaction as the primary standard. Mean values for k_{CH_4}/k_{H_2} and $k_{CH_4}/k_{C_2H_6}$ of 0.31 exp(+830/T) and 0.23 exp(-1429/T), respectively, can be obtained from the data of Pritchard et al.[23] and Knox and Nelson[22] (for k_{CH_4}/k_{H_2}), and Knox[21], Pritchard et al.[24], and Lin et al.[15] (for $k_{C_2H_6}/k_{CH_4}$). Combining these ratios results in a value of 1.35 exp(+2259/T) for $k_{C_2H_6}/k_{H_2}$. As the value of k_{H_2} is still the subject of some controversy[26-28], the experimental ratio of $k_{C_2H_6}/k_{H_2}$ is combined with four different values of k_{H_2}, and the derived absolute rate coefficients are shown in Table IVB. The agreement between the derived and the measured Arrhenius expressions (and the k_{298} values) is quite good especially when the value used for k_{H_2} is that recommended by Watson[26] (prior to the data of Whytock et al.[12]) and CODATA[28], or that measured by Watson et al[13]. The Arrhenius expressions (and k_{298} values) obtained using either the NASA[27] or Whytock et al.[12] values for k_{H_2} are less satisfactory, although within the experimental uncertainties, in that the values of both A and k_{298} are much lower than experimentally measured in the direct studies.

While there is some scatter evident in the Arrhenius plot which could mask a small amount of curvature, there is no evidence of a curvature of the magnitude observed in the $Cl + CH_4$ reaction[12,16,17] over a similar temperature range. Consequently the results of the CH_4/C_2H_6 competitive chlorinations[15,21,24], where the difference in the E/R values of the $Cl + CH_4$ and $Cl + C_2H_6$ reactions is shown to be constant from ~ 200 - 600K, are incompatible with the results of the recent direct $Cl + CH_4$ and $Cl + C_2H_6$ studies which would predict that the difference in the E/R values would vary with temperature. The recent experimental E/R values determined for the $Cl + CH_4$ reaction at temperatures above 298 K range from

i.e., primary, secondary and tertiary. Consequently, the relative rate constant data reported by Pritchard et al.[24] is easily combined with the CODATA value of $k(C\ell + H_2)$ to yield the Arrhenius parameters and k_{298} values shown in Table V. In contrast, the Arrhenius parameters and k_{298} values which are shown in Table V and are derived from the data of Knox and Nelson[22] were calculated from the following more complex equations (expressed in units of cm^3 $molecule^{-1}$ s^{-1}):

$$k(C\ell + C_3H_8) = 6.81 \times 10^{-11} \exp(-76/T) + 4.78 \times 10^{-11} \exp(+85/T) \quad \text{(III)}$$

$$k(C\ell + n\text{-}C_4H_{10}) = 5.42 \times 10^{-11} \exp(+30/T) + 5.76 \times 10^{-11} \exp(+292/T) \quad \text{(IV)}$$

$$k(C\ell + iso\text{-}C_4H_{10}) = 7.97 \times 10^{-11} \exp(+15/T) + 1.10 \times 10^{-11} \exp(+417/T) \quad \text{(V)}$$

The value of $k(C\ell + C_2H_6)/k(C\ell + CH_4)$ used to derive the above equations was based on the data reported by Knox[21], but the value was that modified and reported by Lin et al.[15]. The Arrhenius parameters shown in Table V were derived for $C\ell + C_3H_8$ and $C\ell + n\text{-}C_4H_{10}$ from equations (III) and (IV) from 200 - 600 K and 298 - 600 K, respectively, to match the temperature ranges used in our study of these reactions.

It can be seen from Table V that the Arrhenius parameters and k_{298} values derived from the competitive chlorination studies are in excellent agreement with the absolute values obtained in this study. Equations (III-V), which were derived from the data of Knox and Nelson[22], indicate that reactions (2-4) should exhibit a non-linear Arrhenius behavior. Because the data base obtained in this study was limited, it was not possible to ascertain whether the $C\ell + C_3H_8$ and $C\ell + n\text{-}C_4H_{10}$ reactions exhibit any non-linear Arrhenius behavior. However, the rate constants obtained in this study confirm the trend of C-H reactivity deduced by Knox and Nelson[22], i.e., tertiary $\geq$ secondary > primary.

Table V

Absolute Rate Constant Data Calculated from the Competitive Chlorination Studies

Molecule	Parameter	Study		
		Reference (24)	Reference (22)	This Work
C_2H_6	A ($cm^3 molecule^{-1} s^{-1}$)	7.01 (-11)	6.13 (-11)	9.01 (-11)
	E/R (K)	76	96	133
	k (298K) ($cm^3 molecule^{-1} s^{-1}$)	5.43 (-11)	4.44 (-11)	5.67 (-11)
C_3H_8	A ($cm^3 molecule^{-1} s^{-1}$)	1.03 (-10)	1.12 (-10)	1.36 (-10)
	E/R (K)	-90	-13	-44
	k_{298} ($cm^3 molecule^{-1} s^{-1}$)	1.39 (-10)	1.16 (-10)	1.51 (-10)
$n\text{-}C_4H_{10}$	A ($cm^3 molecule^{-1} s^{-1}$)	-	8.44 (-11)	2.15 (-10)
	E/R (K)	-	-124	-12
	k_{298} ($cm^3 molecule^{-1} s^{-1}$)	-	2.13 (-10)	2.25 (-10)
$iso\text{-}C_4H_{10}$	k_{298} ($cm^3 molecule^{-1} s^{-1}$)	1.13 (-10)	1.28 (-10)	1.46 (-10)

Reference Reaction: $k(C\ell + H_2) = 4.7 \times 10^{-11} \exp(-2340/T)$. [26,28]

This explains why $k(C\ell + n\text{-}C_4H_{10}) > k(C\ell + iso\text{-}C_4H_{10}) \simeq k(C\ell + C_3H_8)$. Knox and Nelson[22] also reported that the activation energies decrease as the hydrocarbon becomes more complex, and that the E/R values reach limiting values of ~ 350 K for primary C-H, and ~ 150 K for secondary C-H bonds. Using the revised value for $k(C\ell + H_2)$ lowers the limiting E/R values to zero for primary C-H bonds, and to small negative (-200K) values for secondary C-H bonds. That the activation barrier for primary C-H bonds approaches zero as the complexity of the hydrocarbon increases seems more reasonable than it approaching an E/R value of ~ 350 K. The overall E/R values determined in this study are consistent with this conclusion.

Acknowledgements

We thank J. Linke for his indispensable glass blowing services, G. Tennant, M. Patapoff and W. Lattin for their expert assistance in constructing the experimental apparatus.

This paper presents the results of one phase of research carried out at the Jet Propulsion Laboratory, California Institute of Technology, under Contract No. NAS7-100, sponsored by the National Aeronautics and Space Administration.

REFERENCES

1. Rowland, F. S. and Molina, M. J., Rev. Geophys. Space Phys., 13, 1 (1975).
2. Westenberg, A. A., and de Haas, J., J. Chem. Phys., 48, 4405 (1968).
3. Benson, S. W., Cruickshank, F. R., and Shaw, R., Int. J. Chem. Kinetics, 1, 29 (1969).
4. Davis, D. D., Braun, W., and Bass, A. M., Int. J. Chem. Kinetics, 2, 101 (1970).
5. Watson, R. T., Machado, E. S., Schiff, R. L., Fischer, S., and Davis, D D., Proceedings of the 4th CIAP Conference, DOT-TSC-OST-75-38, Cambridge, MA, February (1975).
6. Lee, J. H., Michael, J. V., Payne, W. A., Stief, L. J., and Whytock, D. A., J. Chem. Soc. Faraday Trans. I 73, 1530 (1977).
7. Clyne, M. A. A., and Stedman, D. H., Trans. Faraday Soc., 62, 2164 (1966).
8. Spencer, J. E., and Glass, G. P., J. Phys. Chem., 79, 2329 (1975).
9. Ambidge, P. F., Bradley, J. N., and Whytock, D. A., J. Chem. Soc. Faraday Trans. I 72, 2143 (1976).
10. Leu, M. T. and DeMore, W. B., Chem. Phys. Lett., 41, 121 (1976).
11. Poulet, G., LeBras, G., and Combourieu, J., J. Chem. Phys., 71, 101 (1974).
12. Whytock, D. A., Lee, J. H., Michael, J. V., Payne, W. A., and Stief, L. J., J. Chem. Phys., 66, 2690 (1977).
13. Watson, R., Machado, G., Fischer, S., and Davis, D. D., J. Chem. Phys., 65, 2126 (1976).
14. Manning, R. G. and Kurylo, M. J., J. Phys. Chem., 81, 291 (1977).
15. Lin, C. L., Leu, M. T., and DeMore, W. B., J. Phys. Chem., 82, 1772 (1978).
16. Zahniser, M. S., Berquist, B. M. and Kaufman, F., Int. J. Chem. Kinetics, 10, 15 (1978).

17. Keyser, L. F., J. Chem. Phys., 69, 214 (1978).

18. Clyne, M. A. A. and Walker, R. F., J. Chem. Soc. Faraday Trans. I 69, 1547 (1973).

19. Michael, J. V., and Lee, J. H., Chem. Phys. Lett., 51, 303 (1977).

20. Poulet, G., Le Bras, G., and Combourieu, J., Proceedings of the WMO Meeting in Toronto, WMO #511, p. 289 (1978).

21. Knox, J. H., Chem. and Ind., 1631 (1955).

22. Knox, J. H. and Nelson, R. L., Trans. Faraday Soc., 55, 937 (1959).

23. Pritchard, H. O., Pyke, J. B., and Trotman-Dickenson, A. F., J. Am. Chem. Soc., 76, 1201 (1954).

24. Pritchard, H. O., Pyke, J. B., and Trotman-Dickenson, A. F., J. Am. Chem. Soc., 77, 2629 (1955).

25. Fettis, G. C. and Knox, J. H., Prog. React. Kinet., 2, 1 (1964).

26. Watson, R. T., J. Phys. Chem. Ref. Data, 6, 871 (1977).

27. (a) NASA Ref. Pub. #1010, "Chlorofluoromethanes and the Stratsophere," Chapter 1, R. D. Hudson, editor (1977); (b) JPL Publication 79-27, "Chemical Kinetic and Photochemical Data for Use in Stratospheric Modelling," Evaluation Number 2, NASA Panel for Data Evaluation.

28. "Evaluated Kinetic and Photochemical Data for Atmospheric Chemistry," CODATA Task Group on Chemical Kinetics. CODATA Bulletin #33; also in press, J. Phys. Chem. Ref. Data (1979).

29. Kaufman, F., Progress in Reaction Kinetics, Pergamon Press, Chapter 1, p. 1 (1961).

30. Howard, C. J., J. Phys. Chem., 83, 3 (1979).

31. Marrero, T. R., and Mason, E. A., J. Phys. Chem. Ref. Data, 1, 3 (1972).

32. Poirier, R. V., and Carr, Jr., R. W., J. Phys. Chem., 75, 1593 (1971).

33. Watson, R. T., Machado, E. S., Schiff, R. L., and Davis, D. D. Manuscript in preparation.

34. Watson, R. T., and Ray, G. Manuscript in preparation.